THEORETICAL INVESTIGATIONS OF EXPERIMENTAL GRAVITATION

Thesis by

Carlton Morris Caves

In Partial Fulfillment of the Requirements

for the Degree of

Doctor of Philosophy

California Institute of Technology

Pasadena, California

1979

(Submitted 1979 May 8)

ACKNOWLEDGEMENTS

This thesis has been made possible by a lot of hard work, by the support and encouragement of friends, colleagues, and associates, and by grants from generous public and private sources. It is appropriate that I acknowledge those people, groups, and institutions whose help and support have been particularly important.

The California Institute of Technology — and, in particular, its Division of Physics, Mathematics, and Astronomy — has provided a congenial atmosphere for research in physics. The Institute is an exciting and stimulating place to be, and it has the additional virtue that it is virtually free of the mindless bureaucracy which plagues many other universities. I have had fun at Caltech — perhaps too much fun given the amount of time I have managed to spend as a graduate student.

Kip Thorne's research group has been my "home" at Caltech for the last seven years. I hope Kip's group has benefited from my presence, because I have certainly benefited from my association with the group. For their help, advice, and encouragement, I thank all those people — grad students, post-docs, faculty, and staff — who have been associated with Kip's group during my years as a graduate student.

Three persons — Kip Thorne, Ron Drever, and Mark Zimmermann — have made particularly important contributions to my research.

Kip Thorne has been my thesis advisor, and he has been a good one. He has not bothered me when I wanted to work things out for myself, but he has been available when I needed help. He has allowed me to pursue my own interests, even when I am sure he thought that was not in my best interest. Perhaps most important, he has been a model of what a good theoretical

physicist should be. My interest in detection of gravitational radiation is a reflection of Kip's interest in the subject. In this I am not alone; the growing interest in gravitational radiation detection is due in large part to Kip's persistent and effective proselytizing for the development of gravitational wave astronomy.

Ron Drever has been a colleague and advisor for the last three years. Ron is like one of the active thermal pools at Yellowstone National Park; he is never quiescent, and he spouts ideas faster than they can be analyzed. In short, he is the cleverest experimenter I have ever met, and it has been a privilege and a pleasure for me to have been associated with him.

Mark Zimmermann has been a graduate student in Kip's group during most of my time at Caltech. I have bothered Mark with virtually every idea I have had at Caltech. Patiently he has listened to all of them, and just as patiently he has explained what was wrong with most of them.

I am particularly indebted to the technical typists — Jan Rasmussen, Gloria Laird, and Ruth Stratton — who typed the papers which make up this thesis. In the face of sometimes impossible demands they have been efficient, capable, and unperturbable. I am also grateful to Polly Grandmontagne for able general secretarial help.

My personal financial support has come from a variety of sources. I thank the National Science Foundation for providing a three-year NSF Predoctoral Fellowship, an anonymous donor for providing a one-year Feynman Fellowship, and the National Science Foundation and the National Aeronautics and Space Administration for providing (through research grants to Kip Thorne) a series of graduate research assistantships.

Many of my mornings in Pasadena have been jolted to a start by two sources of humor — Jack Smith's column in the Los Angeles Times and Al

Lohman and Roger Barkley's radio soap opera, "Light of my Life," on KFI. Jack and Al and Roger deserve a special thanks.

Finally I thank the Burger Continental (535 South Lake Avenue) for more delicious meals than I care to remember.

ABSTRACT

This thesis has two basic themes: the investigation of new experiments which can be used to test relativistic gravity, and the investigation of new technologies and new experimental techniques which can be applied to make gravitational wave astronomy a reality.

Advancing technology will soon make possible a new class of gravitation experiments: pure laboratory experiments with laboratory sources of non-Newtonian gravity and laboratory detectors. The key advance in technology is the development of resonant sensing systems with very low levels of dissipation. Chapter 1 considers three such systems (torque balances, dielectric monocrystals, and superconducting microwave resonators), and it proposes eight laboratory experiments which use these systems as detectors. For each experiment it describes the dominant sources of noise and the technology required.

The coupled electro-mechanical system consisting of a microwave cavity and its walls can serve as a gravitational radiation detector. A gravitational wave interacts with the walls, and the resulting motion induces transitions from a highly excited cavity mode to a nearly unexcited mode. Chapter 2 describes briefly a formalism for analyzing such a detector, and it proposes a particular design.

The monitoring of a quantum mechanical harmonic oscillator on which a classical force acts is important in a variety of high-precision experiments, such as the attempt to detect gravitational radiation. Chapter 3 reviews the standard techniques for monitoring the oscillator; and it introduces a new technique which, in principle, can determine the details of the force with arbitrary accuracy, despite the quantum properties of the oscillator.

The standard method for monitoring the oscillator is the "amplitude-

and-phase" method (position or momentum transducer with output fed through a linear amplifier). The accuracy obtainable by this method is limited by the uncertainty principle. To do better requires a measurement of the type which Braginsky has called "quantum nondemolition." A well-known quantum nondemolition technique is "quantum counting," which can detect an arbitrarily weak force, but which cannot provide good accuracy in determining its precise time-dependence. Chapter 3 considers extensively a new type of quantum nondemolition measurement — a "back-action-evading" measurement of the real part X_1 (or the imaginary part X_2) of the oscillator's complex amplitude. In principle X_1 can be measured arbitrarily quickly and arbitrarily accurately, and a sequence of such measurements can lead to an arbitrarily accurate monitoring of the classical force.

Chapter 3 describes explicit gedanken experiments which demonstrate that X_1 can be measured arbitrarily quickly and arbitrarily accurately, it considers approximate back-action-evading measurements, and it develops a theory of quantum nondemolition measurement for arbitrary quantum mechanical systems.

In Rosen's "bimetric" theory of gravity the (local) speed of gravitational radiation v_g is determined by the combined effects of cosmological boundary values and nearby concentrations of matter. It is possible for v_g to be less than the speed of light. Chapter 4 shows that emission of gravitational radiation prevents particles of nonzero rest mass from exceeding the speed of gravitational radiation. Observations of relativistic particles place limits on v_g and the cosmological boundary values today, and observations of synchrotron radiation from compact radio sources place limits on the cosmological boundary values in the past.

TABLE OF CONTENTS

INTRODUCTION

Recently I talked with my nephew, who lives in Madison, Wisconsin, on his third birthday. He surprised me when he abruptly began the conversation by asking, "Do you have any whales in California?" After a moment trying to figure out where that question had come from, I remembered that I had described to him, during a visit to Madison a couple of months earlier, the migration of the gray whale down the California coast. I then assured him that we do indeed have whales in California. We exchanged a few pleasantries about the peculiar way whales breathe, and he then terminated the conversation as abruptly as it had begun.

His parents have since reported to me that he still talks about the whales in California. Although he has never seen a whale, he is fascinated by their great size. They are the feature of California which has caught his attention. One hesitates to speculate about his vision of California; perhaps he sees a neighborhood not unlike his own in Madison, but with a whale in every backyard.

This three-year-old's vision of California is in some ways similar to the modern astrophysicist's view of the Universe. Observations over the last fifteen years have shown the Universe to be a far more violent place than had previously been thought. The astrophysicist today is confronted by a zoo of exceedingly luminous objects, such as quasars, compact radio sources, and BL Lac objects. In many of these objects the ultimate source of energy lies in a very small region at the center of the source. Ten years ago one scarcely dared suggest that this compact energy source might contain a massive black hole; today one scarcely dares suggest otherwise. Although the modern astrophysicist cannot with complete confidence say

that he has "seen" a black hole, he is fascinated by their strong gravitational field, which makes them natural candidates for supplying the enormous amounts of energy required to power quasars and other highly luminous objects. Black holes have certainly caught the attention of astrophysicists, and they have been incorporated into a new vision of the Universe — a Universe with a black hole at the center of every quasar and compact radio source.

One wonders how time will affect these two visions — the three-year-old's vision of a California thickly populated by whales and the astrophysicist's vision of a Universe thickly populated by massive black holes. Both the three-year-old and the astrophysicist will have to search for new information, which will almost certainly modify their respective visions. The three-year-old will easily obtain the necessary information as he grows older. The astrophysicist is likely to find his search more difficult; he cannot even say with certainty where or how he ought to look. Much, if not most, of his information will continue to come from observations in various parts of the electromagnetic spectrum. However, he may turn to experimental gravitation to provide additional, perhaps crucial, information. Indeed, information from experimental gravitation may help to resolve many of the puzzles of modern astrophysics.

Today the astrophysicist often encounters phenomena in which strong gravitational fields play an important role. Quasars and other highly luminous objects, perhaps powered by black holes, constitute one class of such phenomena. Other examples include the collapse of stars to form neutron stars and black holes; the interactions of a new-born neutron star or black hole with its environment; and the evolution of dense star clusters (globular clusters and galactic nuclei), which may lead to formation of a

black hole. Faced with describing these phenomena, the astrophysicist can anticipate that experimental gravitation will provide important information in two distinct, but related ways:

(i) Strong-field phenomena cannot be analyzed using Newton's theory of gravity. A relativistic theory of gravity must be used, and the theory chosen is almost always Einstein's general theory of relativity. Future experiments will test general relativity with increasing accuracy; and if those experiments confirm general relativity, they will increase the astrophysicist's confidence in using general relativity to analyze strong-field phenomena.

(ii) The catastrophic events which lead to formation of strong-field sources, and which may accompany subsequent interactions of the source with its environment, are usually veiled by surrounding matter. This obscuring veil prevents electromagnetic radiation, and perhaps even neutrinos, from escaping directly from the source. Thus no form of electromagnetic astronomy, nor even neutrino astronomy, can peer directly into the guts of these sources. Only gravitational waves escape unhindered. Future gravitational wave detectors will be able to monitor the details of these gravitational waves. By ripping away the veil surrounding strong-field sources, gravitational wave astronomy will provide information that cannot be obtained in any other way.

This thesis consists of four chapters, each of which is a paper which has been published or which has been submitted for publication. Each paper reports on a particular line of research which I have pursued (in two cases with collaborators). Thus each chapter is self-contained; each contains its own introductory material and its own footnotes, figures, and references. However, the four chapters are not unrelated. They are unified by their concern with the above two themes: the investigation of new experiments

which can probe more deeply into the nature of relativistic gravity, and the investigation of new technologies and new experimental techniques which can be applied to make gravitational wave astronomy a reality.

In this Introduction I give an overview of each of the four chapters. For each chapter I motivate the research described therein, give the main results of that research, and direct the reader to appropriate portions of each chapter where detailed analyses can be found. In addition, since two of the chapters (Chapters 1 and 3) involved collaborations with other authors, I describe briefly my particular contributions to those chapters.

* * * * *

Gravitation physicists are in some ways the paupers of physics. Unlike physicists in other fields, who are often overwhelmed by a wealth of experimental data, gravitation physicists have always been confronted by a dearth of data. For some this scarcity of experimental evidence is a blessing. Like a mendicant friar of medieval times, whose vow of poverty liberated his spirit to soar closer to God, these physicists find that the paucity of gravitation experiments liberates their theoretical flights of fancy to soar into realms completely detached from the mundane world of experiment. Other gravitation physicists react differently to their poverty-stricken condition. These physicists embark on self-help programs; they spend long (and usually fruitless) hours trying to dream up new experiments. Chapter 1 reports on one such self-help program — a search for laboratory experiments to test relativistic gravity.

Traditionally gravitation physicists have looked to astrophysical systems to provide the "laboratory" for their experiments. Unfortunately, most such systems are so complicated by nongravitational physics that a

"clean" test of gravitational effects is impossible. As a result, until recently almost all tests of relativistic gravity were restricted to one, reasonably clean "laboratory" — the solar system. A few years ago another potential relativity "laboratory" — the binary pulsar — was discovered. Although there remain some doubts about its "cleanness," it has already provided useful information: observations of the decrease of its orbital period provide indirect evidence for emission of gravitational radiation as predicted by general relativity (see reference 14 of Chapter 4).

Even these two "clean" systems have drawbacks. Nature does not design even its best laboratories with the needs of terrestrial gravitational experimenters in mind. The experimenter can do only those experiments which fortuitous astrophysical circumstances allow. How much nicer it would be to do experiments entirely in an earth-based or near-space laboratory, with both the source and detector of gravity under the control of the experimenter! Such purely laboratory experiments have been brought close to the realm of possibility by recent technological developments. The key advance has been the development of resonant detectors (harmonic oscillators) with very low levels of dissipation. Chapter 1 (Sec. II) discusses three such detectors: (i) torque-balance systems made, for example, from fused-quartz or sapphire fibers at temperatures $\lesssim 0.1\,^{\circ}K$; (ii) massive dielectric monocrystals at millidegree temperatures; and (iii) microwave resonators with superconducting mirrors.

One type of laboratory experiment looks for post-Newtonian gravitational effects. Typically such an experiment is designed as follows. A laboratory-size mass is set into motion (by rotation or vibration) so that it produces in its vicinity a "post-Newtonian gravitational field" (e.g., the Newtonian-type gravitational fields produced by kinetic energy or pressure, or the

magnetic-type gravitational fields produced by momentum). The motion of the source mass is modulated in such a way that the desired post-Newtonian signal drives resonantly the oscillations of the detector, and the experimenter monitors the resulting changes in the detector's motion.

Such experiments are no panacea. They can examine only certain types of post-Newtonian effects. For a typical laboratory source of gravity (size $L \lesssim 50$ cm, mass $M \lesssim 10^6$ g, rotational or vibrational velocity $v \lesssim 10^5$ cm-sec^{-1}), some post-Newtonian effects are completely negligible. For example, there is no hope of seeing nonlinear gravitational effects. The only post-Newtonian effects one can hope to see are the gravitational influences of velocity and stress. Post-Newtonian experiments are further constrained by the problem of "Newtonian noise." The Newtonian gravitational field of a laboratory source produces effects which are a priori much larger (usually by a factor $\sim c^2/v^2 \gtrsim 10^{11}$) than the largest post-Newtonian effects. Somehow one must design the experiment so that, at the detector frequency, Newtonian effects are smaller than the post-Newtonian signal. This requirement is a severe limitation on the possible experiments. The issue of what types of post-Newtonian effects can be measured in laboratory experiments, with particular attention to the Newtonian-noise problem, is discussed in Sec. III.A.

The bulk of Chapter 1 (Secs. IV-VI) is devoted to a description of eight laboratory experiments which have a chance of beating Newtonian noise. (Four of the experiments do not look for post-Newtonian effects; such experiments are not so seriously troubled by Newtonian noise.) For each of the experiments the dominant sources of noise are discussed. Particular attention is paid to the problem of thermal noise (Nyquist noise) in the detector and the stringent demands it places on the properties of the detector, and to the problem of isolating earth-based experiments from the

disturbing effects of seismic noise.

Chapter 1 is the result of a collaboration with Vladimir B. Braginsky and Kip S. Thorne. Braginsky and Thorne devised the experiments; I investigated their feasibility.

* * * * *

One of the resonant detectors considered in Chapter 1 is a microwave cavity with superconducting walls. The response of a microwave cavity to an arbitrary time-changing gravitational field is quite complicated: the gravitational field interacts directly with the electromagnetic field inside the cavity and with the cavity walls; and the electromagnetic field and the walls interact at the boundary between the two. I have developed a formalism to describe this complicated electro-mechanical system in the presence of a weak gravitational field. Chapter 2 briefly describes the formalism and then sketches an application of the formalism to analyze a gravitational wave detector which uses a microwave cavity.

Chapter 2 is only the tip of the iceberg as far as applications of this formalism go. The formalism can be used to analyze a variety of gravitation experiments, such as the one described in Sec. V of Chapter 1. However, its greatest utility may lie in its ability to analyze microwave cavities with moving walls. The formalism can be used to analyze a cavity whose walls move in some predetermined fashion. It can also be used to analyze the coupled system consisting of the electromagnetic field inside the cavity and the walls of the cavity; in this case the field and walls interact at the boundary between the two, the motion of the walls affecting the field and the field exerting a force on the walls.

I have not yet had time to write a detailed description of the formalism,

but I intend to do so. This future publication will also include applications of the formalism.

* * * * *

Chapter 3 forms the bulk of the thesis, and it contains what I believe are its most important results. It considers the problem of monitoring a weak, classical force which acts on a simple harmonic oscillator.

This problem arose in the context of attempts to detect gravitational radiation. One type of gravitational wave detector, which was used in the past and which is still being refined and improved for use in the future, is a mechanical resonant detector (Weber-type detector). In the past such detectors were usually massive cylinders of aluminum, but some future detectors will employ high-Q monocrystals of sapphire or silicon, or massive cylinders of niobium. A gravitational wave incident on the detector interacts with the fundamental mode of the detector (harmonic oscillator) and drives its oscillations. Theorists can estimate (with considerable uncertainty!) the size of gravitational wave bursts which sweep by the earth with reasonable frequency. These waves are highly classical (i.e., many gravitons pass through a square wavelength during the burst), but they are coupled so weakly to the detector that they deposit one, or even less than one, quantum in an initially unexcited detector. If the detector's oscillations are monitored using standard techniques, such waves can be detected barely, if at all — even in principle. It is here that the new techniques introduced in Chapter 3 come to the rescue. In principle they allow the gravitational waves to be monitored with arbitrary accuracy, no matter how weak they may be, so long as the monitoring is not so accurate as to reveal the quantum nature of the radiation itself.

The origin and resolution of this problem can be explained quite simply. (A more detailed version of the following argument is given in Sec. II.B.) A harmonic oscillator is characterized by its position x, momentum p, mass m, and angular frequency ω. Classically the state of the oscillator is specified by a point in a "phase plane" whose coordinates are x and $p/m\omega$ (see Fig. 1 of Chapter 3, p. 204). In the absence of forces this point rotates clockwise with angular velocity ω. An equivalent description uses coordinates X_1 and X_2 which rotate relative to the $(x,p/m\omega)$ coordinates:

$$X_1 = x\cos\omega t - (p/m\omega)\sin\omega t \quad ,$$

$$X_2 = x\sin\omega t + (p/m\omega)\cos\omega t \quad .$$

The quantity $X_1 + iX_2 = (x + ip/m\omega)\, e^{i\omega t}$ is the oscillator's complex amplitude. In the (X_1,X_2) phase plane the oscillator's state is specified classically by a point which is stationary in the absence of forces.

Quantum mechanically the oscillator's state cannot be a single point. The Heisenberg uncertainty principle, $\Delta x\,\Delta p/m\omega \geq \hbar/2m\omega$, forbids both x and p to be specified with no uncertainty. An equivalent uncertainty relation holds for X_1 and X_2: $\Delta X_1 \Delta X_2 \geq \hbar/2m\omega$. These uncertainty relations mean that the oscillator's sharp classical state is spread out into a fuzzy quantum mechanical "error box" with area $\geq \pi\hbar/2m\omega$ (see Fig. 1 of Chapter 3, p. 204).

The standard method of monitoring the oscillator is to couple it to a position transducer whose output is averaged over many oscillator periods in order to pick out the component of oscillation at frequency ω. This standard method attempts to determine both X_1 and X_2 with equal precision; equivalently, it attempts to determine both the amplitude and phase of the oscillator. The uncertainty principle implies that the best accuracy this "amplitude-and-phase" method can achieve is $\Delta X_1 = \Delta X_2 = (\hbar/2m\omega)^{1/2}$ — the "standard quantum limit" for amplitude-and-phase measurements. One can view

this standard limit as being produced by "back-action" noise from the measuring apparatus; during the measurement this noise perturbs X_1 and X_2 by equal amounts of order $(\hbar/2m\omega)^{1/2}$.

The amplitude-and-phase method can detect a classical force on the oscillator only if the force changes X_1 or X_2 by an amount $\gtrsim (\hbar/2m\omega)^{1/2}$ (see Sec. II.C). A force of this size would deposit approximately one quantum in an oscillator which begins in the ground state. For a gravitational wave detector with mass $m \simeq 10$ tons and frequency $\omega/2\pi \simeq 10^3$ Hz, the standard quantum limit is approximately 10^{-19} cm. To see a reasonable number of bursts, one must look out to the Virgo cluster of galaxies. These bursts, produced by stellar collapses, are predicted to change the complex amplitude of such a detector by about 10^{-19} cm. Thus these waves are at best only marginally observable by the amplitude-and-phase method.

The problem with amplitude-and-phase measurements can be illustrated in another way. Suppose a measurement of position $x = X_1$ at $t = 0$ is much more precise than the standard quantum limit. Then, immediately after the measurement, the oscillator's state is characterized by a long, thin error ellipse $[\Delta x << (\hbar/2m\omega)^{1/2} << \Delta p/m\omega$; see Fig. 3(a) of Chapter 3, p. 206]. As time passes the error ellipse rotates clockwise; as it rotates, the initial large uncertainty in p feeds back and forth between x and p. An amplitude-and-phase measurement, which averages over many rotations of the ellipse, will have accuracy much worse than the standard quantum limit, unless the initial error ellipse was a circle with radius $(\hbar/2m\omega)^{1/2}$.

One <u>can</u> maintain the precision of the initial measurement of x. However, to do so, one does not couple continuously to x; instead one monitors continuously the quantity that characterizes the thin dimension of the ellipse. That quantity is X_1. The crucial difference between coupling to x and

coupling to X_1 is the following: the error ellipse rotates in the $(x,p/m\omega)$ phase plane (initial uncertainty in p feeds onto x as time passes), but it remains at rest in the (X_1,X_2) phase plane (initial uncertainty in X_2 does not feed onto X_1).

Chapter 3 discusses and develops the basic idea of measuring X_1. There it is shown that measurements of X_1 can be arbitrarily quick and arbitrarily accurate in principle, that the measurements can be repeated as often as desired, and that a sequence of such measurements can lead to an arbitrarily accurate monitoring of a classical force (see Sec. II.E). In Chapter 3 measurements of X_1 are referred to as "back-action-evading" measurements, because a properly designed measurement allows X_1 to evade completely back-action noise from the measuring apparatus, at the expense of increasing the back-action on X_2.

Section III of Chapter 3 describes gedanken experiments which demonstrate that X_1 can be measured arbitrarily quickly and arbitrarily accurately. In these experiments the measuring apparatus must be coupled precisely to X_1. This precise coupling requires both a position transducer and a momentum transducer coupled to the oscillator. The couplings of the two transducers must be modulated sinusoidally, each with the appropriate phase; and the outputs of the two transducers must be added to produce a total output proportional to X_1. Designs for measuring apparatuses coupled precisely to X_1 are described in detail in Appendix B. For a given measurement time the strength of the coupling to X_1 determines the accuracy of the measurement; for arbitrarily strong coupling the measurement can be arbitrarily accurate. The momentum transducer is constructed by combining a velocity transducer with a negative capacitor or negative spring. Appendix A gives examples of negative capacitors and clarifies the role they play in a momentum transducer.

The modulated transducer couplings are provided by an external, classical generator. Appendix B demonstrates that a classical generator can be realized as a (quantum mechanical) harmonic oscillator excited in an arbitrarily energetic, coherent state, and it discusses the errors introduced when the generator is not completely classical. Appendix C analyzes in detail a sequence of measurements of X_1, including the "reduction of the wave function" at the end of each measurement; particular attention is paid to the behavior of X_1 and X_2 during a sequence.

One can avoid the use of two transducers by making "stroboscopic measurements" of X_1 (see Sec. II.F.2), in which one measures position (or momentum) at half-cycle intervals. Alternatively, one can make "continuous, single-transducer" measurements of X_1 (see Sec. II.F.3) by modulating appropriately the output of a single transducer (position or momentum), and then filtering the output to pick out the information about X_1 and to reject information about X_2. Continuous, single-transducer measurements are useful in the case of weak coupling. In this case long measurement times are required to achieve good accuracy, and continuous, single-transducer measurements are almost as good as perfectly coupled, two-transducer measurements. Appendix D gives a detailed quantum mechanical analysis of a simple type of continuous, single-transducer measurement.

The observables X_1 and X_2 are special observables for a harmonic oscillator. Section IV identifies the special features of X_1 and X_2 and generalizes those features to arbitrary quantum mechanical systems. The resulting special observables are called quantum nondemolition (QND) observables.

There are two different, but closely related ways to characterize a quantum nondemolition observable. The first characterization focuses on the uncertainties which are built into a quantum mechanical description of the

measured system. It characterizes a QND observable as one that can be measured repeatedly, with the result of each measurement being completely predictable from the result of an initial, precise measurement. For most observables one cannot make such a sequence of measurements. An initial, precise measurement produces huge uncertainties in observables which do not commute with the measured observable; in general, these uncertainties feed onto the measured observable as the system evolves, thereby ruining the accuracy of a subsequent measurement. To make repeated measurements whose results are completely predictable, one must measure an observable that does not become contaminated by uncertainties in noncommuting observables. Section IV.A uses this first characterization to define quantum nondemolition observables, and it derives from the definition the fundamental property of a QND observable: a system which begins in an eigenstate of a QND observable remains in an eigenstate of that observable.

The second characterization focuses on the quantum mechanical nature of the measuring apparatus. It characterizes a QND observable as one that can be completely shielded from the back-action noise of the measuring apparatus. Any observable can be free of <u>direct</u> back-action from the measuring apparatus, provided the interaction between the system and the measuring apparatus is designed properly (measured observable the only observable of the system which appears in the interaction Hamiltonian). However, for most observables the measuring apparatus will act back indirectly through observables which do not commute with the measured observable. Thus this second characterization is closely related to the first; the essential feature of both is that a QND observable is isolated from observables with which it does not commute. Section IV.B proves that any QND observable can be shielded from noise in the measuring apparatus, and it clarifies the relationship between the two

characterizations.

Chapter 3 is a paper written with four other authors — Kip S. Thorne, Ronald W. P. Drever, Vernon D. Sandberg, and Mark Zimmermann. Kip and I conceived the idea of measuring X_1 while under the stress of lunch at the Greasy (Chandler Dining Hall). Since that humble beginning the idea has been extensively elaborated by the five authors. Chapter 3 is the first of two papers reporting our results. (This first paper concentrates on issues of principle; the second will consider practical issues.) I have no qualms about associating my name with any part of the paper. However, three major parts of the paper — Section IV and Appendices C and D — are entirely my work. The ideas, the analysis, and the prose of these three parts are due to me.

* * * * *

Observations of ultrarelativistic particles might seem to have nothing to do with gravity, but in fact such observations can place strong constraints on some alternative theories of gravity — theories which allow the speed of gravitational radiation to differ from the speed of light. In such theories the speed of gravitational radiation is determined by the combined effects of the overall structure of the Universe and the presence of nearby concentrations of matter. It is possible for the speed of gravitational radiation to be less than the speed of light. A particle which exceeds the speed of gravitational radiation ought to emit a shock wave of gravitational Cherenkov radiation. In the absence of some small-scale structure to blur the shock front, the energy emitted ought to diverge, thus preventing particles from exceeding the speed of gravitational radiation. Observations of ultrarelativistic particles then place limits on the speed of gravitational radiation,

and these limits in turn constrain the theory's cosmological models.

Chapter 4 investigates these ideas in the context of Rosen's "bimetric theory" of gravity — a theory which can be made to agree with all solar system tests. Section 2 lays the foundation for analyzing the radiation emitted by weak-field systems in Rosen's theory. Section 3 analyzes the radiation emitted by particles moving at speeds near the speed of gravitational radiation. This analysis leads one to the tentative conclusion (tentative mainly because quantum corrections might cut off the radiation spectrum at high frequencies) that particles of nonzero rest mass cannot exceed the speed of gravitational radiation. Section 4 uses various observations to place limits on the speed of gravitational radiation today and in the past.

* * * * *

The new experiments and new experimental techniques discussed in this thesis will not be easy to implement. In particular, it is likely that many years of effort will be required to detect gravitational waves, and that some further years might be required to make gravitational wave detection a working tool of astronomy. The three-year-old, whose misimpression of California began this Introduction, will have corrected his misimpression long before gravitational waves are detected. As he grows up, developments in gravitational wave detection will proceed. Perhaps his generation of physics graduate students will be the first to reap the benefits of those developments — the first to participate in an exciting new era in which gravitational wave astronomy provides useful information about the nature of the Universe.

CHAPTER 1

LABORATORY EXPERIMENTS TO TEST RELATIVISTIC GRAVITY

This chapter is a paper by Vladimir B. Braginsky, Carlton M. Caves, and Kip S. Thorne. It was published in the 1977, April 15, issue of Physical Review D, volume 15, pages 2047-2068.

PHYSICAL REVIEW D VOLUME 15, NUMBER 8 15 APRIL 1977

Laboratory experiments to test relativistic gravity*

Vladimir B. Braginsky
Physics Faculty, Moscow State University, Moscow, U.S.S.R.

Carlton M. Caves† and Kip S. Thorne
California Institute of Technology, Pasadena, California 91125

(Received 3 January 1977)

Advancing technology will soon make possible a new class of gravitation experiments: pure laboratory experiments with laboratory sources of non-Newtonian gravity and laboratory detectors. This paper proposes seven such experiments; and for each one it describes, briefly, the dominant sources of noise and the technology required. Three experiments would utilize a high-Q torque balance as the detector. They include (i) an "Ampère-type" experiment to measure the gravitational spin-spin coupling of two rotating bodies, (ii) a search for time changes of the gravitation constant, and (iii) a measurement of the gravity produced by magnetic stresses and energy. Three experiments would utilize a high-Q dielectric crystal as the detector. They include (i) a "Faraday-type" experiment to measure the "electric-type" gravity produced by a time-changing flux of "magnetic-type" gravity, (ii) a search for "preferred-frame" and "preferred-orientation" effects in gravitational coupling, and (iii) a measurement of the gravitational field produced by protons moving in a storage ring at nearly the speed of light. One experiment would use a high-Q toroidal microwave cavity as detector to search for the dragging of inertial frames by a rotating body.

I. INTRODUCTION

Until now, almost all tests of relativistic gravity in the solar system have involved probes of the gravitational fields of the Sun, the Earth, or the Moon.[1] Such probes have included light deflection and quasar radio-wave deflection by the sun, the Shapiro time delay of radio signals passing near the Sun, perihelion shifts of planetary orbits, laser ranging to the Moon in search of the Nordtvedt effect, searches for sidereal periodicities in earth tides, gravitational red-shift in the earth's gravitational field, Eötvös-Dicke experiments in the fields of the Earth and Sun, and others.[2]

The purpose of this paper[3] is to point out that advancing technology will soon make possible a new class of experiments: pure laboratory experiments, with laboratory sources of post-Newtonian gravity and laboratory detectors. The laboratory may be earthbound, or it may be in an earth-orbiting satellite where background noise is much reduced. In either case, the experimenter's control over the source of gravity is the essential new feature in these experiments.

The key advance in technology that will make possible these new experiments is the development of sensing systems with very low levels of dissipation. In Sec. II we describe three such systems that could be used in gravitation experiments: torque-balance systems made, for example, from fused-quartz or sapphire fibers at temperatures $\lesssim 0.1\,^{\circ}\mathrm{K}$, massive dielectric monocrystals cooled to millidegree temperatures, and microwave resonators with superconducting walls. In Sec. III we briefly review the Nordtvedt-Will[4] parametrized-post-Newtonian (PPN) formalism for comparing gravitation experiments with theory, and the types of phenomena which occur in post-Newtonian gravity; we argue that because of "noise" from Newtonian gravity, the only post-Newtonian phenomena that look promising for laboratory measurement are magnetic-type gravitation and preferred-frame and preferred-orientation effects; and we present a truncated version of the PPN formalism specially suited to the analysis of magnetic-type gravity. Section IV describes four experiments which one might perform using a sensitive torque balance: (i) a gravitational "Ampère" experiment to measure the spin-spin gravitational coupling of two laboratory bodies ("magnetic-type" gravitational effect), (ii) a search for changes with time of the gravitational constant (non-post-Newtonian experiment), (iii) an improved-precision Eötvös experiment (non-post-Newtonian experiment), and (iv) a measurement of the gravity produced by magnetic stresses and energy (non-post-Newtonian experiment). Section V describes the use of a toroidal microwave resonator to measure the dragging of inertial frames by a rotating body ("magnetic-type" gravitational effect). Section VI describes three experiments that would use cooled dielectric monocrystals: (i) a gravitational "Faraday" experiment to measure the electric-type gravity produced by a time-varying flux of magnetic-type gravity, (ii) experiments to test for the existence of a preferred reference frame and preferred orientations in the universe, and (iii) an experiment to measure the gravitational force pro-

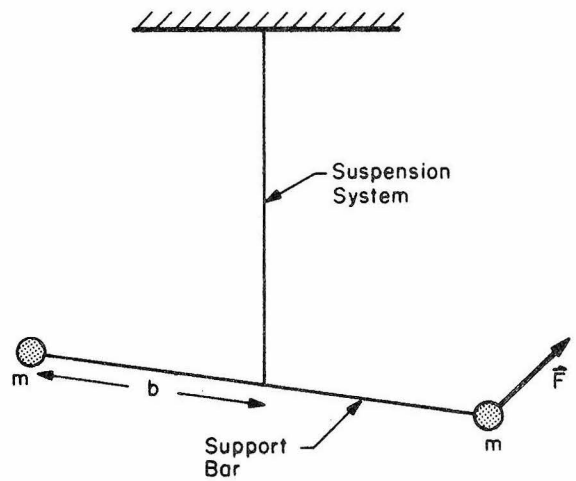

FIG. 1. A torsion oscillator with test masses m, on one of which there acts a post-Newtonian force F at right angles to the support bar. The suspension system could be a support fiber or an electric or magnetic support system with very high Q and very small restoring torque.

duced by particles moving at nearly the speed of light (non-post-Newtonian experiment).

II. SYSTEMS WITH VERY LOW DISSIPATION

A. Torsion oscillator

The typical source of a laboratory post-Newtonian gravitational field might be a mass $M \sim 10^5$ g with equatorial radius $R \sim 20$ cm, rotating with equatorial velocity $v \sim 5 \times 10^4$ cm/sec. Such a generator would produce post-Newtonian gravitational accelerations in its vicinity of magnitude

$$a_{PN} \equiv (F/m)_{PN} \simeq (G\tfrac{1}{5} M/R^2)(v/c)^2 \simeq 1 \times 10^{-17} \text{ cm/sec}^2 . \quad (2.1)$$

Here F is the force that acts on a sensor, and m is its mass.

One attractive type of sensor for such a small force is a torque balance (torsion oscillator) shown in idealized form in Fig. 1. In a post-Newtonian experiment one would modulate the source of gravity at the eigenperiod τ_0 of the oscillator, thereby producing after a time $\hat{\tau} \gg \tau_0$ (but $\hat{\tau} \ll \tau^*$ ≡ damping time of oscillator) a net change in the oscillation amplitude of the masses

$$(\Delta x_0)_{PN} = \frac{(F/m)_{PN}\, \tau_0 \hat{\tau}}{8\pi} \simeq 4 \times 10^{-9} \text{ cm if } \tau_0 \simeq 10^4 \text{ sec}, \ \hat{\tau} \simeq 10^6 \text{ sec}. \quad (2.2)$$

Such a displacement of a macroscopic mass ($m \simeq 30$ g) can be detected without serious difficulty by a variety of techniques (see Sec. 2 of the book by Braginsky and Manukin,[5] cited henceforth as BM).

The three most serious problems for a torque-balance sensor of post-Newtonian forces are fluctuational forces (Brownian noise) in the suspension system, time-varying gravity due to motion of nearby people, animals, and vehicles, and seismic "noise" at the eigenfrequency of the torque balance.

The fluctuational forces depend on the temperature T of the torque-producing suspension system, the amplitude damping time τ^* for torsion oscillations, the duration $\hat{\tau}$ over which the forces act ("measurement time"), and the mass m:

$$\left(\frac{F}{m}\right)_{\text{Brownian}} \simeq \left(\frac{16kT}{m\tau^*\hat{\tau}}\right)^{1/2} \simeq 1 \times 10^{-18} \text{ cm/sec}^2 \text{ if } m = 30 \text{ g}, \ T = 0.1\,^\circ\text{K}, \ \hat{\tau} = 10^6 \text{ sec}, \ \tau^* = 10^{13} \text{ sec}. \quad (2.3)$$

[Equation (2.3) is the Nyquist theorem in a form valid for $\tau_0 \ll \hat{\tau} \ll \tau^*$.] The parameters suggested here are all very reasonable from the viewpoint of present technology except the damping time $\tau^* = 10^{13}$ sec, which corresponds to a mechanical Q of

$$Q = \pi\tau^*/\tau_0 = 3 \times 10^9 \text{ for } \tau^* = 10^{13} \text{ sec}, \ \tau_0 = 10^4 \text{ sec}. \quad (2.4)$$

We expect that such damping times can be achieved within the next 2 to 5 years. Our reasons are these: (1) The present state-of-the-art result is $\tau^* \sim 10^{10}$ sec. An electrostatic suspension system constructed by Everitt, Fairbank, and their coworkers for use on board an Earth-orbiting spacecraft has its dominant damping produced by residual gas and is estimated to have $\tau^* \gtrsim 1 \times 10^{10}$ sec,[6] and the tungsten-wire suspension system used by Braginsky and Panov[7] in their 1971 room-temperature Eötvös experiment is believed to have had $\tau^* \sim 3 \times 10^9$ sec (though no attempt was made to measure it beyond setting the limit $\tau^* > 6 \times 10^7$ sec). (2) The suspension might be a fiber of fused quartz, for which losses decrease rapidly with decreasing temperature below $T \simeq 10\,^\circ$K, so that it is not unreasonable to expect $\tau^* \simeq 10^{13}$ sec at 0.1 °K. (3) One could use a

thin support fiber cut from a monocrystal of sapphire, for which (a) fundamental-mode oscillations of a 1 kg cylinder at $\omega_0 \simeq 10^5$ rad sec^{-1} show $Q \simeq 5 \times 10^9$ at 4.3 °K,[8] (b) losses again decrease rapidly with decreasing temperature, (c) losses decrease with decreasing frequency, (d) losses are lower for torsion oscillations than for the measured compressional oscillations, but (e) losses will be larger for a thin fiber than for a cylinder because of larger surface-area-to-volume ratio. (4) One could use a Meissner-effect suspension system for which the attainable Q should be roughly comparable to that in a superconducting microwave cavity at a given frequency ω_0 ($Q \sim 10^{10}$ to 10^{12} for present state of the art[9]), and for which the Q should increase with decreasing ω_0. (5) Damping due to residual gas in the vacuum chamber can readily be kept under control; the damping time for two spherical test masses m with a total projected area S being buffeted by gas molecules of mass μ, number density n, and temperature T would be

$$\tau^* \simeq \left(\frac{\pi}{2\mu k T}\right)^{1/2} \frac{3m}{2nS}$$

$$\simeq 1 \times 10^{13} \text{ sec} \quad \text{for } m = 30 \text{ g},\ S = 20 \text{ cm}^2,\ \mu = 7 \times 10^{-24} \text{ g},\ T = 1 \text{ °K},\ n = 1 \times 10^7 \text{ cm}^{-3} \text{ (pressure} = 10^{-12} \text{ torr)}. \tag{2.5}$$

Time-dependent gravity gradients due to the motion of nearby people, animals, and vehicles can be kept below the post-Newtonian signal by (i) using a torsion pendulum whose quadrupole and octupole coupling to gravity gradients is small, and (ii) performing the experiment in a well-isolated place, e.g., in a sealed, animal-free mine. With modest effort one could construct a torsion pendulum with the relevant quadrupole and octupole moments reduced from their usual values of $\sim mb^2$ and $\sim mb^3$, to $\sim 10^{-4} mb^2$ and $\sim 10^{-4} mb^3$, where m is the mass on each arm and b is the length of the arms. The torque-producing acceleration due to an object of mass M will be less than 10 percent of the post-Newtonian acceleration if the object is kept more distant than

$$r \gtrsim \max\left[\left(10^{-4}\frac{GMb}{0.1 a_{PN}}\frac{\tau_0}{\hat{\tau}}\right)^{1/3}, \left(\frac{GMb^3}{0.1 a_{PN}}\frac{\tau_0}{\hat{\tau}}\right)^{1/5}\right] \simeq \max\left[(100 \text{ m})\left(\frac{M}{10^3 \text{ kg}}\right)^{1/3},\ (40 \text{ m})\left(\frac{M}{10^3 \text{ kg}}\right)^{1/5}\right] \text{ for } b = 10 \text{ cm}. \tag{2.6}$$

The first and second terms represent the quadrupole and hexadecapole couplings, respectively, and the factor $\tau_0/\hat{\tau}$ is a bandwidth correction. Thus, for $M \lesssim 1000$ kg, an isolation radius of a few hundred meters is adequate.

Seismic "noise" (earth vibrations) at angular frequency $\omega_0 \simeq 2\pi/\tau_0$ in the bandwidth $\Delta\omega_0 \simeq 1/\hat{\tau}$ will produce accelerations of the torsion oscillator that could mask the post-Newtonian signal. Because of the low frequency of the torsion oscillator, these seismic accelerations cannot be removed by a passive filtering system. The seismic motions can be resolved into floor tilt, floor rotation, horizontal motion, and vertical motion. Tilt is a problem in the case of a fiber suspension system because it displaces the test masses relative to external, spatially varying force fields (electric, magnetic, gravitational), and thereby leads to time-varying torques. Floor rotation will cause angular accelerations of the experimental apparatus that directly mimic the post-Newtonian signal. In a perfect torsion oscillator with vanishing initial amplitude, horizontal and vertical motions would produce no torques; but in any real system such motions will couple to the oscillator through imperfections and through nonlinearities such as Coriolis and centrifugal forces.

The frequency region of interest, $\omega_0 \sim 10^{-3}$ rad/sec, lies above the frequencies of tides and below the frequencies of the Earth's normal modes. The data on Earth motions in this regime are not very reliable, and presumably the amplitude of the motions varies greatly from one location to another. If we characterize the stochastic component of the rotational, horizontal, and vertical motions by mean-square angular, strain, and acceleration amplitudes per unit angular bandwidth

$$J_\omega^{\text{rot}} \equiv \langle(\Delta\phi)^2\rangle/(\text{rad sec}^{-1}), \tag{2.7a}$$

$$J_\omega^{\text{hor}} \equiv \langle(\Delta l/l)^2\rangle/(\text{rad sec}^{-1}), \tag{2.7b}$$

$$J_\omega^{\text{vert}} \equiv \langle(\Delta g)^2\rangle/(\text{rad sec}^{-1}), \tag{2.7c}$$

then the observational data suggest, for quiet locations,[10,11]

$$J_\omega^{\text{hor}} \sim 4 \times 10^{-18} \text{ sec}(\omega/10^{-3} \text{ sec}^{-1})^{-3} \quad \text{for } 6 \times 10^{-6} \lesssim \omega \lesssim 6 \times 10^{-3} \text{ sec}^{-1} \tag{2.8a}$$

$$J_\omega^{\text{vert}} \sim 6 \times 10^{-12} \text{ sec}(\text{cm/sec}^2)^2(\omega/10^{-3} \text{ sec}^{-1})^{-2} \quad \text{for } 6 \times 10^{-5} \lesssim \omega \lesssim 6 \times 10^{-2} \text{ sec}^{-1}. \tag{2.8b}$$

There are no data on $J_\omega^{\rm rot}$, but it may be reasonable to assume

$$J_\omega^{\rm rot} \sim J_\omega^{\rm hor}. \tag{2.8c}$$

For the torsion oscillator of Fig. 1 the seismic rotations have the same effect as a sinusoidal force F acting on one of the masses m with amplitude

$$(F/m)_{\rm rot} = 2b\omega_0^2(2\pi J_\omega^{\rm rot}/\hat{\tau})^{1/2} \sim 1\times10^{-16}\ {\rm cm/sec^2} \quad \text{for } b\simeq 10\ {\rm cm},\ \hat{\tau}\simeq 10^6\ {\rm sec},\ \omega_0\simeq 10^{-3}\ {\rm sec^{-1}}. \tag{2.9a}$$

If $\mu_{\rm hor}$ is the dimensionless coupling parameter between horizontal accelerations at frequency ω_0 and torque accelerations F/m, then horizontal seismic motions produce the same effect as a sinusoidal torque acceleration

$$(F/m)_{\rm hor} = \mu_{\rm hor}(\lambda_0/2\pi)\omega_0^2(2\pi J_\omega^{\rm hor}/\hat{\tau})^{1/2} \sim 5\times10^{-10}\mu_{\rm hor}\ {\rm cm/sec^2} \quad \text{for } \lambda_0\simeq 6000\ {\rm km},\ \hat{\tau}\simeq 10^6\ {\rm sec},\ \omega_0\simeq 10^{-3}\ {\rm sec^{-1}}. \tag{2.9b}$$

Here λ_0 is a characteristic wavelength, and $\lambda_0/2\pi$ is a characteristic coherence length for the horizontal strains of Eq. (2.7b). Clearly λ_0 cannot be much larger than the radius of the Earth (the value chosen above) and it might be much smaller. If we similarly characterize the coupling to vertical seismic motions by a parameter $\mu_{\rm vert}$, then

$$(F/m)_{\rm vert} = \mu_{\rm vert}(2\pi J_\omega^{\rm vert}/\hat{\tau})^{1/2} \sim 6\times10^{-9}\mu_{\rm vert}\ {\rm cm/sec^2} \quad \text{for } \hat{\tau}\simeq 10^6\ {\rm sec},\ \omega_0\simeq 10^{-3}\ {\rm sec^{-1}}. \tag{2.9c}$$

These seismic effects appear to be huge compared to the tiny signal $(F/m)_{\rm PN}\simeq 10^{-17}$ cm/sec^2 that one wishes to measure. However, one might be able to circumvent them by very careful construction of the apparatus to achieve $\mu_{\rm hor}\sim\mu_{\rm vert}\sim 10^{-6}$, together with construction of an active antiseismic platform that reduces rotational, horizontal, and vertical motions by at least one, two, and three orders of magnitude, respectively. Tilt-induced torques might be circumvented by a combination of antiseismic platform, shielding of the torsion pendulum from external electric and magnetic fields, and adjustment of the distribution of gravitating mass in the nearby laboratory.

This discussion of seismic-induced torques is very incomplete. Any real torsion oscillator has a large number of mechanical degrees of freedom which can be excited by seismic noise, and which are coupled by nonlinearities, imperfections, and external force fields. To keep seismic-induced torques below the post-Newtonian signal, one must understand thoroughly the coupling of these degrees of freedom and bring it under control experimentally.

That one can circumvent seismic "noise" in principle follows from the fact that it is not a true noise, i.e., it is not a stochastically fluctuating force originating in a key element of the apparatus. However, its circumvention on Earth may prove so difficult in practice that one will seek the quieter environment of an Earth-orbiting laboratory.

B. Eigenvibrations of dielectric monocrystals

Accelerations at the laboratory post-Newtonian level, $(F/m)_{\rm PN}\simeq 1\times10^{-17}$ cm/sec^2, should also be measurable with massive ($m\sim 10^3$ to 10^5 g) dielectric monocrystals. Monocrystals of sapphire are particularly attractive, but quartz and others might also be suitable. In a post-Newtonian experiment one would modulate the source of gravity at an eigenperiod τ_0 of the crystal's vibrations, thereby producing after a time $\hat{\tau}\gg\tau_0$ (but $\hat{\tau}\ll\tau^*$ = damping time) a net change in the oscillation amplitude of the crystal

$$(\Delta x_0)_{\rm PN} \simeq \frac{(F/m)_{\rm PN}\tau_0\hat{\tau}}{4\pi} \simeq 5\times10^{-16}\ {\rm cm} \quad \text{for } \tau_0\simeq 6\times10^{-4}\ {\rm sec},\ \hat{\tau}\simeq 10^6\ {\rm sec}. \tag{2.10}$$

This amplitude change is far larger than that which will be measured ($\lesssim 10^{-17}$ cm) in the second-generation gravitational-wave antennas of the Fairbank-Hamilton group[12] and of the Braginsky group.[13] Moreover, the eigenfrequencies in the two experiments (post-Newtonian and gravitational-wave) are the same, but in the post-Newtonian experiment one can use a much longer time ($\hat{\tau}_{\rm PN}\simeq 10^6$ sec) to measure the amplitude change than in the gravitational-wave experiments ($\hat{\tau}_{\rm GW}<1$ sec). Thus, the measurement of the post-Newtonian amplitude changes should present no serious problems. For example, an electromagnetic-resonator sensor for displacements in which the inductance or capacitance is modulated by the crystal vibrations, would produce a fluctuational "back-action" force on the crystal itself of only (BM,[5] Sec. 5)

$$\left(\frac{F}{m}\right)_{\text{sensor, Brownian}} \simeq \frac{4}{\hat{\tau}}\left(\frac{kT_e\omega_0}{m\omega_e}\right)^{1/2}$$

$$\simeq 4\times 10^{-19}\ \text{cm/sec}^2 \quad \text{for } T_e \simeq 4\,^\circ\text{K},\ \omega_e \simeq 6\times 10^{10}\ \text{sec}^{-1},\ \omega_0 \simeq 10^4\ \text{sec}^{-1},\ m \simeq 10^4\ \text{g},\ \hat{\tau} \simeq 10^6\ \text{sec}. \tag{2.11}$$

Here T_e is the temperature of the electromagnetic sensor, ω_e is its angular frequency of oscillation, ω_0 is the angular eigenfrequency of the crystal, m is the mass of the crystal, and $\hat{\tau}$ is the measurement time. This back-action force is far smaller than the post-Newtonian force $(F/m)_{\text{PN}} \simeq 1\times 10^{-17}$ cm/sec^2.

Internal fluctuational forces in the crystal (Brownian-motion feeding of energy back and forth between various eigenmodes) have a magnitude governed by the crystal temperature T_0, the damping time $\tau^* = \tau_0 Q/\pi$ for crystal vibrations, the time of measurement $\hat{\tau}$, and the mass of the crystal m:

$$\left(\frac{F}{m}\right)_{\text{Brownian}} \simeq \left(\frac{8kT_0}{m\hat{\tau}\tau^*}\right)^{1/2}$$

$$\simeq 2\times 10^{-18}\ \text{cm/sec}^2 \quad \text{if } T_0 \simeq 10^{-3}\,^\circ\text{K},\ \tau^* \simeq 2\times 10^7\ \text{sec},\ m \simeq 10^4\ \text{g},\ \hat{\tau} \simeq 10^6\ \text{sec}. \tag{2.12}$$

This fluctuating force of 2×10^{-18} cm/sec^2 is adequately below the post-Newtonian level of 1×10^{-17} cm/sec^2. To achieve such a small fluctuating force we envision a 10 kg monocrystal of sapphire with an eigenperiod $\tau_0 \simeq 6\times 10^{-4}$ sec, cooled to a temperature $T_0 \sim 10^{-3}\,^\circ$K where its Q is $\gtrsim 1\times 10^{11}$, and a measurement time of $\hat{\tau} \simeq 10^6$ sec. Such an installation should be achievable within the next 2 or 3 years: (1) Monocrystals of sapphire with mass as large as 25 kg are now available commercially[14]; (2) Bagdasarov, Braginsky, and Mitrofanov[8] have achieved a Q of 5×10^9 for a 1-kg sapphire with $\omega_0 = 2.1\times 10^5$ sec^{-1} at $T_0 = 4.3\,^\circ$K; (3) the Q of this same sapphire (with no improvements in polishing or suspension) should rise rapidly with decreasing temperature (the measured increase between 77 °K and 4.3 °K was $Q \propto T_0^{-0.8}$); (4) more massive sapphires should have higher Q's (one expects $Q \propto \omega_0^{-1}$ roughly); (5) the theoretical Q for a pure, dislocation-free, impurity-free, perfectly polished, free-floating sapphire crystal is

$$Q \simeq (4C_p{}^2\rho)/\kappa T_0\alpha^2\omega_0$$

$$\sim 3\times 10^{15}(T_0/^\circ\text{K})^{-4}(\omega_0/10^4\ \text{sec}^{-1})^{-1} \quad \text{at } T \lesssim 10\,^\circ\text{K}, \tag{2.13}$$

where ρ is the density, C_p is the specific heat at constant pressure, κ is the thermal conductivity, and α is the thermal-expansion coefficient [BM,[5] Eq. (9.7)]; (6) cooling to millidegree temperatures can be achieved by adiabatic demagnetization of paramagnetic salts (the Fairbank-Hamilton group[15] plan to use this technique to cool a metal gravitational-wave antenna with mass $m \sim 5\times 10^6$ g to millidegree temperatures).

Seismic "noise" presents no serious problem for such a detector of gravitational forces. At its operating frequency ($\omega_0 \simeq 10^4$ sec^{-1}) and bandwidth ($\Delta\omega_0 \simeq 10^{-6}$ sec^{-1}) one can filter out the seismic noise. This feature makes such a detector much more attractive than the low-frequency ($\omega_0 \simeq 10^{-3}$ sec^{-1}) torsion oscillators of Sec. IIA.

C. Microwave resonator with superconducting mirrors

A third type of detector for post-Newtonian gravitational fields is a microwave resonator with superconducting mirrors, i.e., a superconducting cavity in which one excites electromagnetic traveling waves or standing waves. In such a detector the gravitational forces act on the electromagnetic waves, pushing them relative to the fixed walls of the cavity.

Because electromagnetic waves are not slow-motion entities (they do not have $v \ll c$), the "post-Newtonian acceleration" $a_{\text{PN}} \simeq (G\frac{1}{5}M/R^2)(v/c)^2 \simeq 1\times 10^{-17}$ cm/sec^2 is not a relevant concept in analyzing their response to gravity. In forthcoming papers, Caves[16] analyzes in detail the interaction of a microwave resonator with gravity, and in Sec. V of this paper we shall describe an experiment which one might hope to perform using a microwave resonator.[17]

The key features of superconducting microwave resonators, which make them attractive for gravitation experiments, are these: (i) the very low surface resistances of their walls, $R_s \sim 10^{-8}$ to 10^{-9} ohms,[9,18] which leads to near-perfect reflection of electromagnetic waves,

$$1 - \mathcal{R} = R_s/94\ \text{ohms}$$

$$\sim 10^{-10}\ \text{to}\ 10^{-11} \quad \text{for normal incidence}, \tag{2.14}$$

where $\mathcal{R}$ is the reflection coefficient; (ii) the resulting very high Q's of the resonators, $Q \sim 10^{10}$ to 10^{12} for cavities excited in low modes[9] (e.g.,

$Q = 5 \times 10^{11}$ for a TE_{011} mode with eigenfrequency 10.5 GHz, in a cylindrical niobium cavity with length and diameter 1.5 in. and temperature 1.3 °K)[19]; (iii) their high frequency stability, which has enabled Stein and Turneaure[20] to construct superconducting-cavity–stabilized-oscillator clocks (SCSO) with short-term stabilities $\Delta\omega/\omega \simeq 6 \times 10^{-16}$.

III. POST-NEWTONIAN GRAVITY IN THE LABORATORY

A. General remarks

In the theoretical discussion of many of our experiments (Secs. IV–VI) we shall use the Nordtvedt-Will parametrized-post-Newtonian (PPN) formalism.[4] In this formalism gravity is described by a general-relativistic-type metric accurate to post-Newtonian order. The metric contains eleven unknown, dimensionless constants called "PPN parameters" and denoted $\gamma, \beta, \alpha_1, \alpha_2, \alpha_3, \zeta_1, \zeta_2, \zeta_3, \zeta_4, \zeta_W, \eta$. Each "metric theory of gravity" (theory obeying the Einstein equivalence principle), when specialized to the post-Newtonian limit (low velocities and small stresses) is a special case of the PPN formalism corresponding to specific values of the PPN parameters. For general relativity $\gamma = \beta = 1$ and all other parameters vanish.

To conserve space we shall not write down the full PPN metric here; instead, we refer the reader to equations (39.32)–(39.34) and Box 39.5 of the book by Misner, Thorne, and Wheeler[2] (cited henceforth as MTW), and to Eq. (4) of Will's paper[4] where the parameter ζ_W is added to the formalism.

Table I contains, for future reference, a brief list of post-Newtonian gravitational phenomena and the PPN parameters which describe them. (For details see, e.g., Refs. 4 and 21.)

Consider a source of gravity with mass M, size L, internal density $\rho \simeq M/L^3$, internal energy density $\rho\Pi$, internal stresses p, internal strains s, velocity v of rotation or motion relative to center of mass, and velocity w of motion of center of mass relative to mean rest frame of the universe. For such a source the dimensionless magnitudes of post-Newtonian effects (fractional amounts by which post-Newtonian effects differ from Newtonian effects) are

$$GM/Lc^2,\ \Pi/c^2,\ p/\rho c^2,\ v^2/c^2,\ vw/c^2,\ w^2/c^2.$$

When the source of gravity is the Sun

TABLE I. Some post-Newtonian phenomena and their PPN parameters. For details see, e.g., Refs. 4 and 21.

Description of phenomenon	Parameters
1. Spatial curvature generated by rest mass, $\Delta g_{jk} \simeq 2c^{-2}\gamma U\delta_{jk}$	γ
2. Nonlinearities in superposition of Newtonian gravitational potentials, $\Delta g_{00} = -2c^{-2}\beta U^2$	β
3. Newtonian-type gravity (Δg_{00}) generated by gravitational energy ($4\beta_2\rho_0 U$)	$\beta_2 = \frac{1}{2}(\zeta_2 + 3\gamma - 2\beta + 1)$
4. Newtonian-type gravity (Δg_{00}) generated by kinetic energy ($4\beta_1\rho_0 v^2$)	$\beta_1 = \frac{1}{4}(\alpha_3 + \zeta_1 + 2\gamma + 2)$
5. The effect of anisotropies in kinetic energy ($\rho_0 v^2$ with $\vec{v}$ directed toward observer rather than transverse) on Newtonian-type gravity (Δg_{00})	ζ_1
6. Newtonian-type gravity (Δg_{00}) generated by internal energy ($2\beta_3\Pi\rho_0$)	$\beta_3 = \zeta_3 + 1$
7. Newtonian-type gravity (Δg_{00}) generated by isotropic part of stresses ($6\beta_4 p$)	$\beta_4 = \zeta_4 + \gamma$
8. The effect of anisotropies in stresses (stresses directed toward the observer vs transverse stresses) on Newtonian-type gravity (Δg_{00})	η
9. Magnetic-type gravity (g_{0j}) generated by momentum ($\Delta_1\rho_0\vec{v}$)	$\Delta_1 = \frac{1}{7}(\alpha_1 - \alpha_2 + \zeta_1 + 4\gamma + 3)$
10. The dependence of strength of momentum-generated gravity (g_{0j}) on direction of momentum (toward observer vs transverse)	$\Delta_2 = \alpha_2 - \zeta_1 + 1$
11. "Preferred-frame effects," i.e., the influence of matter's motion relative to universe on the gravity the matter generates	α_1, α_2, and α_3
12. "Preferred-orientation effects," i.e., the gravitational influence of the orientation of the experimental apparatus relative to the external universe	α_2, ζ_W
13. Breakdowns in global conservation laws for energy, momentum, and/or angular momentum	$\zeta_1 + 2\zeta_W, \zeta_2 - \zeta_W, \zeta_3, \zeta_4 + \frac{2}{3}\zeta_W, \alpha_1, \alpha_2, \alpha_3$

$$GM/Lc^2 \simeq \Pi/c^2 \simeq p/\rho c^2 \simeq 2\times 10^{-6},$$
$$v^2/c^2 \simeq 5\times 10^{-11},$$
$$vw/c^2 \simeq 5\times 10^{-9}, \qquad (3.1a)$$
$$w^2/c^2 \simeq 5\times 10^{-7}.$$

By contrast, a reasonable laboratory source of gravity has $\rho \simeq 10$ g/cm^3, $L \lesssim 50$ cm, $M \lesssim 10^6$ g, $v \lesssim 10^5$ cm/sec, $(p/\rho)^{1/2} \lesssim 10^5$ cm/sec, $s \lesssim 10^{-2}$, $w \lesssim 2\times 10^7$ cm/sec, so that at best

$$GM/Lc^2 \sim 1\times 10^{-24},$$
$$p/\rho c^2 \sim v^2/c^2 \sim 1\times 10^{-11},$$
$$\Pi/c^2 \simeq (v^2/c^2)s \sim 1\times 10^{-13}, \qquad (3.1b)$$
$$vw/c^2 \sim 2\times 10^{-9},$$
$$w^2/c^2 \sim 5\times 10^{-7}.$$

A comparison of the numbers in Eqs. (3.1b) and (3.1a) shows that laboratory experiments to probe nonlinear features of the gravitational field (dimensionless magnitude GM/Lc^2, PPN parameters β and β_2, items 2 and 3 of Table I) are hopeless. Similarly, laboratory measurements of the gravity produced by internal energy (dimensionless magnitude Π/c^2, PPN parameter β_3, item 6 of Table I) will be exceedingly difficult and perhaps impossible. However, there is hope for laboratory experiments which probe the gravitational influences of velocity and stress (dimensionless magnitudes v^2/c^2, vw/c^2, w^2/c^2, and $p/\rho c^2$, all PPN parameters except $\gamma, \beta, \beta_2, \beta_3$, items 4, 5, and 7–13 of Table I). Whether one can invent a laboratory experiment to measure spatial curvature (PPN parameter γ, item 1 of Table I) is not evident to us (see Sec. V B).

In any experiment one must separate cleanly the post-Newtonian effects from all influences of Newtonian gravitational fields. To achieve this one obviously must modulate the post-Newtonian gravitational fields in time, and guarantee that at the resulting frequency ω_{PN} of the post-Newtonian forces all Newtonian forces are negligible. This will be extremely difficult in general because, *a priori*, the Newtonian forces are larger than the post-Newtonian forces by $\sim c^2/v^2 \sim 10^{11}$; and special positioning of detectors (accuracy ~1 μm out of ~100 cm) and special orientations (accuracy ~0.3 arcsec) can typically reduce the Newtonian signal by only factors of ~1 μm/100 cm ~ 0.3 arcsec/90° ~ 10^{-6}. Clearly one must guarantee that Newtonian forces with the frequency ω_{PN} are sensitive only at second order or higher to errors in positions and orientations.

Two types of post-Newtonian effects are especially attractive from this "Newtonian-noise" viewpoint:

(1) *Preferred-frame and preferred-orientation effects.* They can be modulated by rotations of the entire laboratory apparatus relative to inertial space, i.e., relative to the locally preferred directions, induced by solar-system motion through the universe or by the mass distribution of the universe. In such rotations (produced either artifically or by rotation of the Earth) one can maintain with accuracy $\ll 10^{-6}$ the relative positions and orientations of various pieces of the experimental apparatus. Moreover, such rotations performed perfectly will selectively modulate the preferred-frame and preferred-orientation effects without modulating Newtonian effects. Examples of this will be given in Sec. VI B. Such experiments can measure the PPN parameters α_1, α_2, α_3, and ζ_w.

(2) *Magnetic-type gravitational effects*, i.e., effects associated with the g_{0j} metric components. These effects include the dragging of inertial frames by rotating bodies, Lens-Thirring gyroscope precession, gravitational accelerations produced by spin-spin interactions of rotating bodies, and gravitational accelerations due to spin-orbit coupling. The key property which distinguishes magnetic-type effects from all others is their sensitivity to the *direction* of rotation or motion of a laboratory source or detector. As source one could use a rapidly rotating, axially symmetric body and one could slowly modulate its angular velocity

$$\Omega = \Omega_0 \cos(\omega_{mod} t).$$

Magnetic-type gravitational effects are sensitive to the sign of Ω and therefore are modulated with angular frequency ω_{mod} and its harmonics $(2\omega_{mod}, 3\omega_{mod}, \ldots)$. Newtonian gravitational effects, and all the other "nonmagnetic" effects, are sensitive to Ω^2 (centrifugal distortions of rotating source, etc.) and therefore are modulated with angular frequency $2\omega_{mod}$ and its harmonics $(4\omega_{mod}, 6\omega_{mod}, \ldots)$. In an ideal experiment there is no Newtonian "noise" at the post-Newtonian frequency ω_{mod}. Examples of this will be given in Secs. IV A, V, and VI A. Such experiments are sensitive only to the parameter $\frac{7}{8}\Delta_1 + \frac{1}{8}\Delta_2 = \frac{1}{8}(\alpha_1 + 4\gamma + 4)$.[22]

For other post-Newtonian effects Newtonian noise might remain insurmountable in the near future. However, there are gravitational effects not encompassed by the post-Newtonian approximation which should be measurable by the technology described in this paper. These include (i) the equality of inertial and passive gravitational mass (Eötvös experiment, Sec. IV B), (ii) the time rate of change of the gravitation constant (Sec. IV C), (iii) the gravity produced by electromagnetic stresses (Sec. IV D), and (iv) the gravity produced

by particles that move with nearly the speed of light (Sec. VI C).

B. Formalism for analyzing magnetic-type gravity

In our discussion of experiments to analyze magnetic-type gravity we shall utilize a truncated and rewritten version of the PPN formalism. Our truncation consists of two steps: *First*, we delete from the formalism a number of phenomena that are already absent in general relativity, namely preferred-frame effects (set $w_j = 0$ in Chap. 39 of MTW), preferred-orientation effects (set $\zeta_w = 0$), and anomalies in g_{00} produced by anisotropies of stress and kinetic energy (set $\zeta = \eta = 0$). *Second*, we delete from the formalism all gravitational nonlinearities (set $\beta = \beta_2 = 0$), since there is no hope of measuring them in laboratory experiments, and we treat the Newtonian potential U formally as having magnitude

$$U/c^2 \sim (v/c)^4 \sim (p/\rho c^2)^2 \sim (\Pi/c^2)^2 \ll 1 \tag{3.2}$$

[cf. Eq. (3.1b)]. In rewriting the PPN formalism we replace the gravitational potentials U, Ψ, $\vec{V}$, and $\vec{W}$ of Chap. 39 of MTW by scalar and vector potentials

$$\Phi \equiv -(U + 2\Psi), \quad \vec{A} \equiv -\tfrac{7}{2}\Delta_1 \vec{V} - \tfrac{1}{2}\Delta_2 \vec{W}, \tag{3.3}$$

and we define an "electric-type" gravitational field $\vec{g}$ and a "magnetic-type" gravitational field $\vec{H}$ by

$$\vec{g} = -\vec{\nabla}\Phi - \frac{1}{c}\frac{\partial \vec{A}}{\partial t}, \quad \vec{H} = \vec{\nabla} \times \vec{A}. \tag{3.4}$$

Here the notation is that of flat-space 3-dimensional vector analysis, the coordinates (t, x, y, z) are those of the PPN coordinate frame of Chap. 39 of MTW, and we use cgs units rather than geometrized units.

In terms of the new notation $\Phi, \vec{A}, \vec{g}, \vec{H}$ the metric of spacetime, accurate to post-Newtonian order, becomes

$$\begin{aligned} g_{00} &= -c^2(1 + 2\Phi/c^2), \\ g_{0j} &= A_j/c, \\ g_{jk} &= \delta_{jk}(1 - 2\gamma\Phi/c^2) \end{aligned} \tag{3.5}$$

[cf. Eq. (39.32c) of MTW]. The source equation for the scalar field Φ is

$$\nabla^2\Phi = 4\pi G\rho_0(1 + 2\beta_1\vec{V}^2/c^2 + \beta_3\Pi/c^2 + 3\beta_4 p/\rho_0 c^2) \tag{3.6}$$

[Eqs. (39.34a, d) of MTW combined with Eq. (3.3) above]. The vector potential in the chosen PPN gauge has nonzero divergence

$$\vec{\nabla} \cdot \vec{A} = (-\tfrac{7}{2}\Delta_1 + \tfrac{1}{2}\Delta_2)\frac{1}{c}\frac{\partial \Phi}{\partial t} \tag{3.7a}$$

[Eqs. (3.3) above, and (39.27, (39.34b), and (39.15a) of MTW]. The Laplacian of the vector potential is

$$\nabla^2\vec{A} = (\tfrac{7}{2}\Delta_1 + \tfrac{1}{2}\Delta_2)4\pi G\rho_0\frac{\vec{v}}{c} + \Delta_2\frac{1}{c}\frac{\partial}{\partial t}\vec{\nabla}\Phi \tag{3.7b}$$

[Eqs. (3.3) above, and (39.27), (39.34b) of MTW]. By combining Eqs. (3.6) and (3.7) with definitions (3.4) of $\vec{g}$ and $\vec{H}$, and by making use of standard vector-analysis identities, one can derive the following Maxwell-type equations for the electric-type and magnetic-type gravitational fields:

$$\vec{\nabla} \cdot \vec{g} = -4\pi G\rho_0\left(1 + 2\beta_1\frac{\vec{V}^2}{c^2} + \beta_3\frac{\Pi}{c^2} + 3\beta_4\frac{p}{\rho_0 c^2}\right) + (\tfrac{7}{2}\Delta_1 - \tfrac{1}{2}\Delta_2)\frac{1}{c^2}\frac{\partial^2}{\partial t^2}\Phi, \tag{3.8a}$$

$$\vec{\nabla} \times \vec{g} = -\frac{1}{c}\frac{\partial \vec{H}}{\partial t}, \tag{3.8b}$$

$$\vec{\nabla} \cdot \vec{H} = 0, \tag{3.8c}$$

$$\vec{\nabla} \times \vec{H} = (\tfrac{7}{2}\Delta_1 + \tfrac{1}{2}\Delta_2)\left(-4\pi G\frac{\rho_0\vec{v}}{c} + \frac{1}{c}\frac{\partial}{\partial t}\vec{g}\right). \tag{3.8d}$$

Throughout these equations γ, β_1, β_3, β_4, Δ_1, and Δ_2 are PPN parameters, ρ_0 is the density of rest mass in the local rest frame of the matter, $\vec{v}$ is the ordinary (coordinate) velocity of the rest mass relative to the PPN coordinate frame, Π is specific internal energy, and p is pressure (see Chap. 39 of MTW).

When combined with the standard mathematics of general relativity truncated to post-Newtonian order, Eqs. (3.4)–(3.8) are a complete set of tools for analyzing the "near-zone" region of systems satisfying Eq. (3.2). For example a test mass, with 4-velocity $u^\alpha = dx^\alpha/d\tau$ and ordinary velocity $\vec{v} = d\vec{x}/dt = \vec{u}/u^0$, experiences a gravitational force $\vec{F}$ which one can derive from the geodesic equation. After some algebra that geodesic force reduces to the Lorentz-type expression

$$\frac{\vec{F}}{m} \equiv \frac{d\vec{u}}{dt} = \frac{d}{dt}(u^0\vec{v}) = u^0\left(\vec{g} + \frac{\vec{v} \times \vec{H}}{c} - \gamma\frac{\vec{V}^2}{c^2}\vec{\nabla}\Phi\right). \tag{3.9}$$

[In deriving this expression one must make the approximation $e^{2\gamma\Phi/c^2}(d/dt)(e^{-2\gamma\Phi/c^2}u^0\vec{v}) = (d/dt)(u^0\vec{v})$, an approximation which is valid for all conceivable laboratory-type experiments.] In this paper attention will focus on experiments where the detectors, like the sources, have velocities $|\vec{v}| \lesssim 1 \times 10^5$ cm/sec $\ll c$. Under these circumstances the gravitational force acting on a unit mass reduces to

$$\frac{\vec{F}}{m} = \left[1 + \tfrac{1}{2}(2\gamma + 1)\frac{\vec{V}^2}{c^2}\right]\vec{g} + \frac{\vec{v} \times \vec{H}}{c}. \tag{3.10}$$

Equations (3.4)–(3.10) express the law of laboratory, post-Newtonian physics in Maxwell-type language. An analogous formalism for weak-field general relativity has been used previously by Forward[23] in a discussion of conceivable gravitation experiments.

IV. EXPERIMENTS USING TORQUE BALANCES

In this section we describe several laboratory gravitation experiments which one might perform using a torque-balance detection system. Throughout we assume that the laboratory is earthbound, though one may prefer to perform the experiments in space to circumvent seismic "noise" (see Sec. IIA).

A. Gravitational Ampère experiment

One post-Newtonian experiment that may be feasible in the next few years is a gravitational analog of Ampère's experiment,[24] which demonstrated magnetic forces between current-carrying spiral-shaped wires. Such an experiment is of great theoretical interest because it detects magnetic-type gravitational forces. Magnetic-type gravity *must* exist according to general relativity and most (but not all) other relativistic theories of gravity, but nobody has ever detected such a force. Before describing our proposal for an Ampère-type experiment, we shall review previous ideas and efforts to search for magnetic-type gravity.

The Everitt-Fairbank gyroscope experiment[6] is designed to detect the magnetic-type gravitational torque produced on a gyroscope by the rotation of the Earth. Van Patten and Everitt[25] have proposed an experiment to measure the magnetic-type gravitational force which the Earth's rotation exerts on a satellite orbit. Chapman[26] has proposed an experiment to detect the magnetic-type force of the Earth's electric-type gravity acting on the orbital motion of spinning hoops (force proportional to orbital velocity $\vec{v}$ and angular momentum of hoop $\vec{S}$, spin-orbit coupling). None of these experiments (Everitt-Fairbank, Van Patten-Everitt, or Chapman) is of a "laboratory type" since they all rely on the Earth as the source of gravity. Also, all three experiments require expensive Earth-orbiting facilities.

Laboratory-type experiments to detect magnetic-type gravity have been suggested by a number of people,[27] but in all cases either the originator of the idea or his critics[28] have concluded that with state-of-the-art technology the experiment was not feasible.[29] The spin-spin coupling experiment described below looks more favorable thanks, primarily, to the high-Q technology of near-future torsion oscillators.

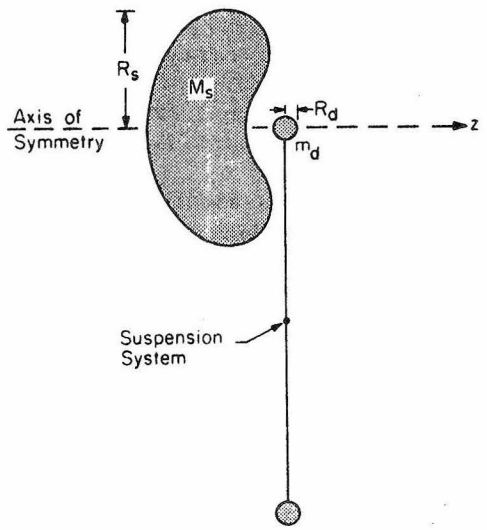

FIG. 2. Experimental configuration for a gravitational Ampère experiment (measurement of spin-spin coupling), as viewed from above. The source mass M_s and detector mass m_d both rotate about the source's axis of symmetry (z axis).

The experimental setup which we envision involves as source an axially symmetric body of mass M_s, density ρ_s, and outermost radius R_s, which rotates rigidly about its axis of symmetry (z axis of Fig. 2). The rotational angular velocity Ω_s is modulated at a frequency $\omega_0 \sim 10^{-3}$ sec^{-1}

$$\Omega_s = \Omega_0 \cos\omega_0 t \ . \tag{4.1}$$

The detector is a small sphere of mass m_d and radius R_d which is located on the z axis and rotates about that axis with constant angular velocity Ω_d. This detecting sphere is one mass of a torque-balance system of the type discussed in Sec. IIA (see Fig. 2). The frequency ω_0 of source modulation is chosen to coincide with the eigenfrequency of the torque balance. When the source is rotating in the same direction as the detector (i.e., when $\cos\omega_0 t > 0$), its magnetic-type gravitational force repels the detector; when the source rotates in the opposite direction, its magnetic-type force attracts the detector. This oscillating force on the detector [$\vec{F}/m_d = (\vec{v}/c) \times \vec{H}$ with $\vec{H}$ produced by the source and $\vec{F}$ integrated over the detector] is given by

$$\frac{F}{m_d} = (\tfrac{7}{8}\Delta_1 + \tfrac{1}{8}\Delta_2)\,\alpha G \rho_s R_d (\Omega_0 R_s)(\Omega_d R_d) c^{-2} \cos\omega_0 t \ ; \tag{4.2}$$

[cf. Eqs. (3.8c), (3.8d) with $\partial\vec{g}/\partial t$ negligibly small]. Here α is a dimensionless constant which depends on the precise shape of the source and location of the detector, but which is of order unity

if $M_s \sim \rho_s R_s^3$, $R_d \ll R_s$, and (source-detector separation) $= r \sim R_s$. One can compute α for any given source-detector configuration by applying the standard techniques of magnetostatics to Eqs. (3.8c), (3.8d). If the source is a sphere, then $\alpha(r/R_s)^4 = 96\pi/75 \simeq 4$.

The amplitude of the oscillating acceleration (4.2) is the quantity which enters into the torque-balance discussion of Sec. IIA. In general relativity ($\Delta_1 = \Delta_2 = 1$) it is

$$(F/m_d) \simeq 1 \times 10^{-17} \text{ cm/sec}^2 \quad \text{for } \rho_s = 8 \text{ g/cm}^3,\ R_d = 2 \text{ cm}, \qquad (4.3)$$
$$\Omega_0 R_s = \Omega_d R_d = 5 \times 10^4 \text{ cm/sec},\ \alpha = 4.$$

These parameters are reasonable for steel. The types of ceramics and fibers being developed for use on superflywheels[30] would have lower densities but higher maximum angular velocities, thereby yielding similar values of F/m; the chief advantage of such materials is that, because of their lower density, the Newtonian acceleration produced by the source is smaller than for steel, so that both types of Newtonian noise discussed below are reduced.

The considerations of Sec. IIA suggest that a torque system to detect the force (4.3) can be built, but that in an earthbound laboratory seismic noise will not be overcome easily.

Noise from Newtonian (electric-type) gravity should not be an insurmountable problem in the above experiment. The Newtonian gravitational field will be constant in time, except for small-amplitude modulations due to time-changing centrifugal deformation of the source sphere, and jitter in the source location.

The jittering displacement $\vec{\xi}(t)$ of the source's center of mass produces a jitter

$$(F/m)_N = -[(\vec{\xi}\cdot\nabla) - \tfrac{1}{2}(\vec{\xi}\cdot\nabla)^2 + \cdots] g_N \qquad (4.4)$$

in the Newtonian acceleration of the detector. Here g_N is the longitudinal component (z component) of the acceleration at the center of mass of the detector in the absence of jitter. Since the detector sits on the axis of symmetry of the source, $\partial_x g_N = \partial_y g_N = 0$. By appropriately shaping the source and positioning the detector one can also guarantee that $\partial_z g_N = 0$. This is approximately so for the configuration of Fig. 1. In this case

$$(F/m)_N = +\tfrac{1}{2}(\vec{\xi}\cdot\vec{\nabla})^2 g_N \simeq \tfrac{1}{2}(\xi/R_s)^2 (GM_s/R_s^2)$$
$$\simeq 1 \times 10^{-18} \text{ cm/sec}^2 \quad \text{for } \xi = 1 \times 10^{-5} \text{ cm},\ R_s = 30 \text{ cm},\ M_s = 3 \times 10^5 \text{ g}.$$

If a horizontal stability of $\xi \simeq 10^{-5}$ cm seems excessive, one can shape the source so that $\partial_z^2 g_N \ll g_N/R_s^2$ and then relax the constraint on ξ.

In an ideal experiment, with $\Omega_d \equiv \Omega_0 \cos\omega_0 t$, the centrifugal deformation of the source would oscillate with frequency $2\omega_0$ and would produce no Newtonian force whatsoever on the detector at frequency ω_0. But in any real experiment small deviations $\delta\Omega_0$ between amplitude of "positive" rotation and of "negative" rotation will produce a Newtonian signal at frequency ω_0:

$$\left(\frac{F}{m}\right)_N \simeq \Delta g_N \frac{\delta\Omega_0}{\Omega_0},$$

where Δg_N is twice the amplitude of centrifugal-flattening-induced oscillation of g_N at frequency $2\omega_0$. If one designs the source shape so that not only is $\partial_z g_N = 0$, but also $\Delta g_N \lesssim 10^{-6} GM_s/R_s^2$ for $\Omega_0 R_s \simeq 5 \times 10^4$ cm/sec,[31] then

$$\left(\frac{F}{m}\right)_N \simeq \frac{GM_s}{R_s^2} \times 10^{-6} \frac{\delta\Omega_0}{\Omega_0}$$
$$\simeq 2 \times 10^{-18} \text{ cm/sec}^2 \quad \text{for } \delta\Omega_0/\Omega_0 \simeq 1 \times 10^{-7}. \qquad (4.5)$$

Thus, a modulation precision of $\delta\Omega_0/\Omega_0 \simeq 10^{-7}$ is then adequate to keep the Newtonian signal well below the post-Newtonian signal. However, it may not be easy to design a source which has $\partial_z g_N$ and Δg_N as small as desired while still keeping the spin-spin coupling coefficient α reasonably large.

B. Improved Eötvös experiment

A torque-balance system and antiseismic platform of the type needed in the above experiment could also be used in three other gravitational experiments: a new high-precision Eötvös experiment, an experiment to search for time changes in the gravitation constant, and an experiment to measure the gravity produced by magnetic stresses.

An Eötvös experiment of the Dicke[32] type would search for periodic torques in the torsion balance due to rotation of the Earth relative to the Sun's gravitational field. The frequency of modulation, $\omega_0 \simeq 2\pi/(24 \text{ h}) \sim 10^{-4}$ sec^{-1} is a factor 10 lower than that contemplated for the Ampère experiment (see above and see Sec. IIA). As a result, seismic noise will present more serious difficulties here

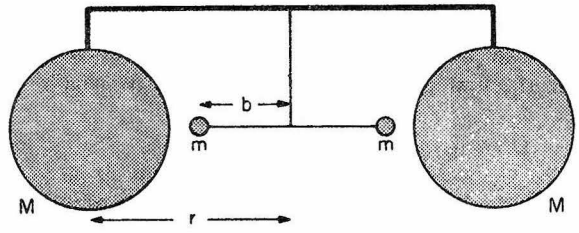

FIG. 3. Experimental configuration for measuring a time change of the gravitation constant.

than there, and we think it reasonable to aim for an acceleration sensitivity of $F/m \sim 10^{-14}$ or 10^{-15} cm/sec^2 rather than 10^{-17}. However, this sensitivity would yield a test of the weak-equivalence principle at the level

$$\frac{\delta g}{g} = \frac{a_1 - a_2}{a} \sim 10^{-14} \text{ or } 10^{-15}, \tag{4.6}$$

where a_1 is the acceleration of one material toward the Sun, a_2 is the acceleration of another material toward the Sun, and a is the mean acceleration toward the Sun. This is an improvement by a factor 100 to 1000 over the best present experiment,[7] but it is a factor 100 to 1000 worse than the 10^{-17} precision which one might expect for Eötvös experiments performed in Earth-orbiting laboratories.[33] At present, however, there is no strong theoretical motivation for performing an Eötvös experiment with precision 10^{-14}, 10^{-15}, or even 10^{-17}. The current accuracy[7] of 10^{-12} is adequate to check the gravitational coupling of all nongravitational forms of energy, including even weak-interaction energy,[34] and 10^{-17} is ten orders of magnitude too poor for checking the gravitational coupling of gravitational energy.[35] (The self-gravitational energy of a 10 g laboratory test mass is only $\sim 10^{-27}$ of its rest mass-energy.)

C. Time dependence of the gravitation constant

A search for time changes of the gravitation constant could be performed using the same type of installation as Eötvös[36] used for measuring the absolute value of the gravitation constant (see Fig. 3). The two large masses M produce, by their Newtonian gravity, a restoring torque that greatly exceeds the intrinsic torque of the torsion balance. The result is small-amplitude torsional oscillations with angular frequency

$$\omega = (\omega_g^2 + \omega_0^2)^{1/2} \simeq \omega_g[1 + \tfrac{1}{2}(\omega_0/\omega_g)^2], \tag{4.7a}$$

$$\omega_0 \lesssim 1 \times 10^{-4}\ \text{sec}^{-1}, \tag{4.7b}$$

where ω_0 is the intrinsic eigenfrequency of the gravity-free torque balance,

$$\omega_g = \left\{\frac{GM}{r^2 b}\left[\frac{r^3}{(r-b)^3} - \frac{r^3}{(r+b)^3}\right]\right\}^{1/2} \simeq 1 \times 10^{-3}\ \text{sec}^{-1}$$

$$\text{for } M \simeq 10^5 \text{ g},\ r \simeq 50 \text{ cm},\ b \simeq 25 \text{ cm}. \tag{4.7c}$$

If the gravitation constant changes with time there will be a corresponding time change of the oscillation frequency

$$\dot{\omega}/\omega \simeq \tfrac{1}{2}\dot{G}/G. \tag{4.8}$$

Changes in the dimensions r and b of the apparatus and in the intrinsic eigenfrequency ω_0 will also produce changes in ω ("noise"):

$$\dot{\omega}/\omega = -2.6(\dot{r}/r) + 1.1(\dot{b}/b) + (\omega_0/\omega)^2(\dot{\omega}_0/\omega_0) \quad \text{for } r = 2b. \tag{4.9}$$

Such changes can be induced by temperature fluctuations or material aging. One can probably keep them negligibly small by making the entire apparatus, including the torque-balance support system, out of monocrystal sapphire, by cooling the apparatus to $T \simeq 2$ °K where sapphire has a thermal-expansion coefficient $\alpha_T \simeq (5 \times 10^{-12}/\text{°K}) \times (T/2\ \text{°K})^{-3}$, and by maintaining the temperature constant to within $\Delta T \simeq 0.01$ °K so that thermal-expansion effects produce

$$\Delta\omega/\omega \simeq \tfrac{3}{2}\alpha_T\,\Delta T \simeq 1 \times 10^{-13}. \tag{4.10}$$

Whether such an installation would have negligible aging effects one cannot be sure; direct measurements of sapphire aging are needed. However, aging is likely to be far less than the $\dot{b}/b \sim 10^{-9}$/yr of quartz, since quartz has a far lower Debye temperature than sapphire (470 °K vs 1040 °K).

With such an installation it seems reasonable to measure ω to a precision $\Delta\omega/\omega \simeq 1 \times 10^{-12}$ by data collection for one week ($\simeq 100$ oscillation periods), and to thereby obtain during one month of measurements a limit on (or value for) $\dot{G}/G$ at the level $\sim 1 \times 10^{-12}$/month $\simeq 1 \times 10^{-11}$/yr. With greater effort one might even achieve 1×10^{-12}/yr. For comparison, Shapiro's monitoring of planetary orbits (the best current method of measuring $\dot{G}$) has given a limit of 1×10^{-10}/yr (Ref. 37) and may well achieve 1×10^{-11}/yr before the end of this decade. Most theories of gravity, but not general relativity, predict $\dot{G}/G$ in the range 10^{-12}/yr to 10^{-10}/yr.

D. Experiment to measure the gravity produced by magnetic fields

Although general relativity predicts that gravity should be produced by stress as well as by mass-energy (item 7 of Table I), at present there is no

experimental proof that this is so (the PPN parameter β_4 could be zero). Such a proof is particularly important for astrophysics because, according to general relativity, stress-produced gravity plays an important, perhaps crucial role in the maximum mass of neutron stars.[38]

A promising way to test whether and how much stress gravitates is to measure the gravity produced by a magnetic field. A magnetic field has the advantage that its stresses are equal to its energy density. In this section we describe briefly an experiment to measure magnetically-generated gravity.

Our experiment would make use of a DC magnetic field which is slowly turned on and off at the eigenfrequency ω_0 of a torque-balance detector. For example, one could set up a magnetic field of strength $B_0 \simeq 2\times 10^5$ G (the current state of the art) in a long cylindrical or toroidal pipe (inner diameter $b \simeq 10$ cm); and one could set up a torsion oscillator with one of its masses near the pipe. One would turn the magnetic field on an off at the eigenfrequency of the torsion oscillator, $\omega_0 \simeq 10^{-3}$ sec^{-1}, and watch to see whether gravity due to the oscillating magnetic stress energy produces a change in the amplitude and phase of the oscillator.

If only the energy of the magnetic field, and not its stress, were to gravitate, then the amplitude of the oscillating force would be

$$(F/m) \simeq 2(G/c^2)(B_0^2/8\pi)\pi b \simeq 7\times 10^{-18}\ \text{cm/sec}^2\,, \tag{4.11}$$

which is measurable with the techniques of Sec. IIA providing seismic noise can be controlled. On the other hand, in general-relativity theory the gravitational acceleration is produced by the energy density plus the trace of the stress tensor, which means that for the idealized case of an infinitely long pipe

$$(F/m) = 2(G/c^2)b^{-1}\left[\int (T^{00}+T^{jj})_{\text{mag}}\, 2\pi r\, dr + \int_{\text{walls of pipe}} T^{jj}\, 2\pi r\, dr\right].$$

The last term is the gravity produced by stresses that build up in the walls to counteract the magnetic pressure. Total stress balance, $T^{jk}{}_{,k}=0$, enables one to re-express this as

$$(F/m) = 2(G/c^2)b^{-1}\int_0^b (T^{00}+T^{zz})_{\text{mag}}\, 2\pi r\, dr = 0\,, \tag{4.12}$$

where $T^{zz} = -B^2/8\pi = -T^{00}$ is the longitudinal component of the stress. Thus, in general relativity there is no oscillating force, except the Newtonian "noise" associated with stress-induced changes $\delta\rho$ in the mass density ρ of the walls. Although

$$(F/m)_N = 2Gb^{-1}\int_{\text{walls}} \delta\rho\, 2\pi r\, dr = 0 \tag{4.13}$$

for idealized case of an infinitely long pipe, for any real solenoid the Newtonian "noise" will be nonzero.

The toughest part of this experiment would probably be designing and monitoring the pipe walls and the other laboratory-mass distributions, so as to keep the Newtonian noise negligible. It would probably help to rotate the pipe about its central axis with an angular velocity $\Omega \gg \omega_0$.

V. EXPERIMENTS USING MICROWAVE RESONATORS

A. The Davies frame-dragging experiment

Davies[39] has proposed an experiment, which might be performed in the 1980's or later, to measure the post-Newtonian "dragging of inertial frames" by the rotation of the Sun, and to thereby determine the Sun's total angular momentum. The technique is to send two electromagnetic signals around the Sun along the same path, but in opposite directions, and to measure the excess travel time for the signal which travels "against" the rotation compared with that which travels "with" the rotation. In this section we propose a laboratory variant of the Davies experiment.

The dragging of inertial frames, like spin-spin coupling, is a magnetic-type gravitational effect. It is most easily analyzed in terms of the vector potential $\vec{A}$ produced by the rotation of a gravitating body. Consider an axially symmetric body rotating rigidly about the z axis of a cylindrical coordinate system (t, r, z, ϕ). The body's velocity $\vec{v}$ is entirely in the ϕ direction,

$$v^{\phi} = \Omega_S = (\text{angular velocity of rotation})\,,$$
$$v^{\hat{\phi}} = \Omega_S r = (\text{physical component of velocity})\,. \tag{5.1}$$

In this case symmetry dictates that the vector potential $\vec{A}$ have only a ϕ component. The new notation

$$\Omega_D \equiv -c^{-1}A^{\phi} = -(rc)^{-1}A^{\hat{\phi}} \tag{5.2}$$

enables one to express in a simple form the influence of the vector potential A^{ϕ} on the metric [Eq. (3.5)]:

$$ds^2 = -c^2dt^2 + r^2(d\phi - \Omega_D dt)^2 + dz^2 + dr^2\,. \tag{5.3}$$

Equations (3.7b) with $\partial\Phi/\partial t = 0$, (5.1), and (5.2) give us the following expression for Ω_D:

$$\Omega_D(r,z) = (\tfrac{7}{8}\Delta_1 + \tfrac{1}{8}\Delta_2)\frac{4\Omega_S}{r}\int_{\text{source}} \frac{(G/c^2)\rho_0(r',z')r'^2\cos\phi' dr' d\phi' dz'}{[r^2+r'^2-2rr'\cos\phi'+(z-z')^2]^{1/2}}. \tag{5.4}$$

The quantity Ω_D is called "the angular velocity of dragging of inertial frames," or, sometimes, "the angular velocity of a locally nonrotating observer."[40] The reason for this name is evident from Eq. (5.3): Place two ideal light beams of infinitesimal wavelength in a thin toroidal waveguide (resonator) centered on the rotation axis of the source (Fig. 4). Adjust the angular velocity of rotation of the waveguide until the two beams require identically the same time for travel once around the guide. Equation (5.3), with $ds^2 = 0$ for the photon world lines, then guarantees that the waveguide must be rotating, relative to the coordinate system, and hence relative to inertial frames far from the gravitating source, with angular velocity $d\phi/dt = \Omega_D$. If instead the waveguide is kept at rest relative to distant inertial frames, the standing-wave pattern made by the two traveling waves in the guide will move relative to the guide with angular velocity Ω_D.

Although the above conclusions are deduced assuming waves that travel with the speed of light (geometric optics limit, wavelength of waves infinitesimal compared with circumference of waveguide), one can show[16] that they remain true for any standing-wave modes of any perfectly smooth, perfectly reflecting toroidal microwave resonator which surrounds the source and is at rest relative to distant inertial frames. The standing-wave pattern will always move relative to the resonator (waveguide) with angular velocity

$$\Omega_{SW} = \bar{\Omega}_D, \tag{5.5}$$

where $\bar{\Omega}_D$ is an appropriate average[16] of Ω_D over the interior of the resonator.

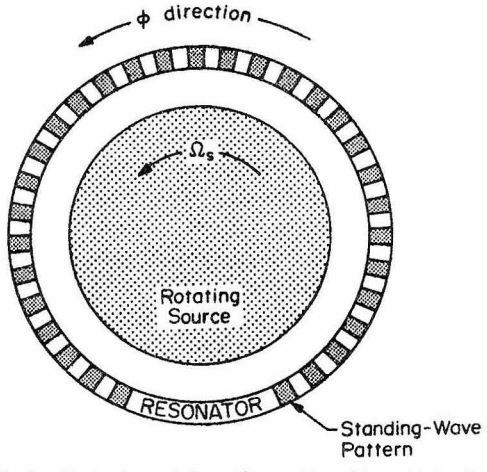

FIG. 4. Experimental configuration for measuring the dragging of inertial frames.

This motion of the standing-wave pattern can be regarded as due to a feeding of electromagnetic quanta from one normal mode, which has azimuthal dependence "$\cos m\phi$," to another normal mode with dependence "$\sin m\phi$." In an ideal resonator these two modes are degenerate and lossless, so the feeding proceeds smoothly. However, in any real resonator, wall imperfections split the degeneracy and induce losses, thereby producing normal modes which respond in a complicated manner to frame dragging. One of us (C.M.C.) analyzes that complicated response in another paper.[16] From his analysis it appears that the cleanest frame-dragging experiment might be one in which (i) one of the two (nearly degenerate) normal modes of the resonator is driven into *steady-state* excitation at its eigenfrequency $\omega_1 \simeq 10^{12}$ sec^{-1}, (ii) the angular velocity Ω_S of the rotating source of gravity, and hence also the frame-dragging angular velocity $\bar{\Omega}_D$, is modulated with frequency $\omega_{\text{mod}} = \omega_1 - \omega_2 =$ (frequency split between resonator's normal modes) $\gtrsim 10^{-5}$ sec^{-1}:

$$\bar{\Omega}_D = \bar{\Omega}_{D0}\cos(\omega_{\text{mod}} t), \tag{5.6}$$

(iii) the modulation of $\bar{\Omega}_D$ pumps electromagnetic quanta from the driven mode to the undriven mode, producing an angular oscillation of the standing-wave pattern in the resonator with frequency ω_{mod} and amplitude

$$\Delta\phi \simeq \bar{\Omega}_{D0}\tau^*/2, \tag{5.7}$$

where τ^* is the damping time of the normal modes. [Formula (5.7) can be derived either classically or quantum mechanically.]

If the rotating source of gravity has mass $M \simeq 5\times10^6$ g and equatorial radius $R \simeq 50$ cm, and if it rotates with equatorial velocity $\Omega_{S0}R \simeq 10^5$ cm/sec, then Eq. (5.4) gives

$$\bar{\Omega}_{D0} \simeq 0.5(GM/Rc^2)\Omega_{S0} \simeq 6\times10^{-21}\ \text{rad/sec}. \tag{5.8a}$$

It is conceivable that a damping time $\tau^* \simeq 10^5$ sec can be achieved with some years of technological effort (see below). If so, then the amplitude of standing-wave oscillation will be

$$\Delta\phi \simeq 3\times10^{-16}\ \text{rad}. \tag{5.8b}$$

One way to measure the oscillation effect would be this: Place a small "porthole" in the wall of the resonator at a location where the standing-wave intensity has its steepest gradient, and extract

signal from that hole at just such a rate as to modestly degrade the Q of the resonator (50% of photons extracted in one resonator damping time τ^* $\simeq 10^5$ sec). Then "$\sqrt{N}$" fluctuations in the signal extracted will lead to an uncertainty in the intensity oscillation amplitude of

$$(\Delta I/I)_{\text{noise}} = (\tfrac{1}{2}0.5\mathfrak{N}\hat{\tau}/\tau^*)^{-1/2}, \tag{5.9}$$

where $\mathfrak{N}$ is the total number of quanta in the resonator and $\hat{\tau} \gtrsim \tau^*$ is the measurement time. For comparison, the frame-dragging-induced intensity oscillation is

$$(\Delta I/I)_{\text{signal}} = I^{-1}(dI/d\phi)_{\max}\Delta\phi = (4\pi R/\lambda_e)\Delta\phi, \tag{5.10}$$

where $R \simeq 50$ cm is the radius of the cavity and λ_e is the azimuthal wavelength of the standing-wave pattern ($\lambda_e = 2\pi R/m$). Clearly we want λ_e as small as possible and $\mathfrak{N}$ as large as possible. The minimum λ_e and maximum magnetic field strength B_0 that one can put into a resonator without breaking the superconductivity of its walls are $\lambda_e \simeq 0.2$ cm, $B_0 \simeq 1000$ G. If the resonator has large radius R and small radius a, then the number of quanta is

$$\mathfrak{N} \simeq (2\pi^2 a^2 R)(B_0^2/8\pi)(hc/\lambda_e)^{-1}$$
$$\simeq 4\times 10^{24} \text{ for } a \simeq 10 \text{ cm}, R \simeq 50 \text{ cm}, \lambda_e \simeq 0.2 \text{ cm}, B_0 \simeq 1000 \text{ G } (4\times 10^9 \text{ erg of excitation energy}). \tag{5.11}$$

For these parameters the standing-wave oscillation (5.8b) corresponds to the transfer of approximately one quantum from the driven mode to the undriven mode during each damping time; and the measured signal and noise at the steepest gradient of the standing-wave pattern [Eqs. (5.10) and (5.9)] are

$$(\Delta I/I)_{\text{signal}} \simeq 1\times 10^{-12}, \quad (\Delta I/I)_{\text{noise}} \simeq 3\times 10^{-13} \tag{5.12}$$

for $\Delta\phi \simeq 3\times 10^{-16}$ rad, $\hat{\tau} \simeq 10^6$ sec, $\tau^* \simeq 10^5$ sec. Thus, the signal is detectable in one experiment of duration 10^6 sec $\simeq 2$ weeks. Of course, one can strengthen the signal by measuring for a longer time or performing a number of 2-week experiments.

The above parameters for the resonator (B_0 $\simeq 1000$ G, $\lambda_e \simeq 0.2$ cm, $R \simeq 50$ cm, $a \simeq 10$ cm, τ^* $\simeq 10^5$ sec) are rather extreme, but might be achievable with some years of developmental work. The main problem is the very long damping time τ^*, corresponding to a Q of

$$Q = \pi c\tau^*/\lambda_e \simeq 5\times 10^{16}. \tag{5.13}$$

One can make a very rough estimate of the achievable Q in terms of the reflection coefficient $\mathcal{R}$ for microwaves normally incident on the mirror walls:

$$Q \sim \frac{\pi R/\lambda_e}{1-\mathcal{R}} \simeq 5\times 10^{16} \text{ if } 1-\mathcal{R} \simeq 2\times 10^{-14}. \tag{5.14}$$

Reflection coefficients of $1-\mathcal{R} \sim 10^{-11}$ are the state of the art for the best superconducting cavities with $\lambda_e \simeq 1$ cm, excited in very low modes ($R \sim \lambda_e$) (see Sec. II C). Thus a Q as high as 5×10^{16} is not totally out of the question, but it will require major advances in superconducting technology.

Rather than using a closed toroidal cavity, it may be better to use an open electromagnetic resonator with several, e.g., six carefully shaped mirrors that bounce the beam from one to another to another around the rotating source of gravity. With appropriate mirror shapes and a sufficiently large Fresnel parameter, it should be possible to keep diffraction losses negligibly small.[41]

To keep the signal clean and big one needs very high relative-frequency stability between the driving oscillator (frequency ω_e) and the eigenfrequencies of the resonator (ω_1 and ω_2). Their relative phases must not drift substantially during the resonator damping time τ^*; i.e., their relative frequencies must remain stable to a precision

$$\Delta\omega/\omega \sim 1/\omega_1\tau^* \sim 1\times 10^{-17}. \tag{5.15}$$

For comparison, absolute-frequency stability of 6×10^{-16} has been achieved by Turneaure,[20] except for an extrapolatable drift which he is now trying to get rid of. Thus, the necessary oscillator stability might be achievable. However, unless one can devise a monitoring and feedback scheme to stabilize the eigenfrequencies of the resonator, the experiment will be impossible to perform.

Seismic noise would also be a very serious problem for this experiment. Any rotation of the cavity relative to nearby intertial frames will produce a counter-rotation of the standing-wave pattern relative to the cavity walls. The 24-h rotation of the Earth can be, and must be, counteracted by a rotation of the cavity relative to the laboratory. However, seismic-induced rotations will remain. At the eigenfrequency of the experiment ω_{mod}, and in its bandwidth $1/\hat{\tau}$, these rotations will drive an oscillation of the standing-wave pattern with amplitude

$$(\Delta\phi)^{\text{seismic}}_{\text{rot}} = \omega_{\text{mod}}\tau^*(2\pi J^{\text{rot}}_{\omega}/\hat{\tau})^{1/2}$$
$$\simeq (5\times10^{-10}\text{ rad})(\omega_{\text{mod}}/10^{-3}\text{ sec}^{-1})^{-1/2}\text{ for }\tau^*\simeq10^5\text{ sec},\ \hat{\tau}\simeq10^6\text{ sec} \quad (5.16)$$

[cf. Eqs. (2.7), (2.8), and (5.7)]. This amplitude is so large that it will swamp the signal (3×10^{-16} rad) unless some way is found to monitor and subtract it with high accuracy. Perhaps the best monitor technique would be to construct two toroidal resonators and attach them to each other rigidly, with one encircling the 1-m-diameter rotating mass and the other perhaps 1 m above that mass. The frame-dragging effect falls off roughly as $1/r^3$ [Eq. (5.4)], so in the upper resonator it would be roughly $\frac{1}{10}$ as large as in the lower resonator; whereas the rotation-induced effects should be the same in the two resonators. By subtracting the signals from the two resonators one should obtain the frame-dragging effect; and, as a check, one can verify that the signal's phase has the correct relationship to the modulation phase of the rotating mass.

Because of the need for a long damping time ($\tau^*\sim10^5$ sec), enormous relative-frequency stability ($\Delta\omega/\omega\sim10^{-17}$), and huge antiseismic compensation ($\sim10^6$), this experiment may well be the most difficult one described in our paper. Nevertheless, it may be worth pursuing for reasons of technological spinoff; the toroidal cavity needed for the experiment is essentially an electromagnetic gyroscope, and even if the desired precision of 10^{-15} rad/10^5 sec $\simeq10^{-20}$ rad/sec is never achieved, the more modest gyroscope produced by the effort could have technological uses.

B. "Light-deflection" experiment

At first sight it looks attractive to attempt a measurement of "light" deflection, and thereby of the PPN parameter γ, using a microwave resonator: Let an idealized beam of electromagnetic waves bounce back and forth inside an idealized, perfect, cylindrical microwave cavity of radius b. Place the cavity in a quadrupole gravitational field generated by masses M, as shown in Fig. 5. The gravitational force (light-deflection effect) will cause the orientation of the beam to oscillate with angular frequency

$$\Omega\simeq(1+\gamma)^{1/2}(GM/b^3)^{1/2}$$
$$\simeq10^{-3}\text{ sec}^{-1}\text{ for }M\simeq10^6\text{ g},\ b\simeq50\text{ cm}. \quad (5.17)$$

As indicated above [Eq. (5.14) and associated discussion], one can hope to maintain the beam in the cavity for a time $\hat{\tau}\gg10^{-3}$ sec, so the experiment looks promising.

Unfortunately, it is not. The simple light-deflection description is valid only so long as geometric optics is valid, i.e., only so long as the beam does not spread over the interior of the cavity, i.e., only for a time

$$\tau_{\max}\simeq\frac{b}{v_{\text{spread}}}\simeq\frac{b}{c\lambda/2\pi b}\simeq\frac{2\pi b^2}{c\lambda}$$
$$\simeq3\times10^{-6}\text{ sec for }b\simeq50\text{ cm},\ \lambda\simeq0.2\text{ cm}. \quad (5.18)$$

Over this period of time, no measurable effect can be built up. Over longer periods the only effect of the static quadrupole gravitational field is to produce a frequency splitting

$$\Delta\omega/\omega\simeq(1+\gamma)(GM/bc^2)\simeq10^{-24} \quad (5.19)$$

between various otherwise degenerate normal modes of the cavity, a splitting so small that it is hopeless to measure. [Note: the pendulum effect of Eq. (5.17) can be described in terms of mode splitting. For $\tau_{\max}=2\pi b^2/c\lambda\gtrsim1/\Omega\simeq(b^3/GM)^{1/2}$, the pendulum angular frequency satisfies $\Omega/\omega\lesssim GM/bc^2$; and therefore, it can be produced by superpositions of many normal modes with the gravitational splittings (5.19).]

Taking account of wave-packet spreading, i.e., using normal-mode analyses of the resonator, we have not been able to invent a viable experimental configuration which uses a microwave resonator to measure the PPN parameter γ.

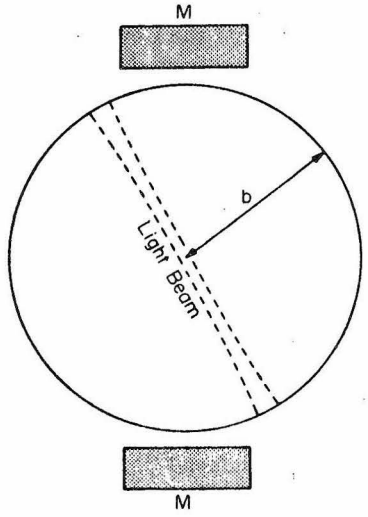

FIG. 5. Experimental configuration for an impossible measurement of the deflection of light.

VI. EXPERIMENTS USING MASSIVE DIELECTRIC CRYSTALS

The authors have previously suggested[3] that one might perform post-Newtonian experiments of the following type: Rapidly varying post-Newtonian and Newtonian accelerations are produced by a massive ($M \simeq 1 \times 10^5$ g), rotating or vibrating, nonsymmetrical body, e.g., a prolate spheroid of iron rotating end-over-end. The linear velocity of rotation would be $v \simeq 10^5$ cm/sec and the angular velocity $\omega \simeq 5 \times 10^3$ sec^{-1}; and the Newtonian and post-Newtonian fields would vary with $\omega_0 = 2\omega$ and its harmonics, i.e., with a period $\tau_0 \simeq 6 \times 10^{-4}$ sec. At typical locations near the source the Newtonian and post-Newtonian accelerations would have amplitudes

$$(F/m)_N \simeq 10^{-6} \text{ cm/sec}^2, \quad (F/m)_{PN} \simeq 10^{-17} \text{ cm/sec}^2. \tag{6.1}$$

These oscillating accelerations would be detected with a dielectric monocrystal (e.g., sapphire) in the manner of Sec. II B. It was our idea[3] to separate the post-Newtonian accelerations from the Newtonian "noise" by some suitable combination of the following: (1) careful choice of shape and orientation of source, and of location and orientation of detector so that the Newtonian acceleration would not couple to the normal mode of the detector being used, (2) modulation of the orientation of the detector with angular frequency ω_{mod} and with amplitude designed to move the post-Newtonian force on the normal mode to a frequency, e.g., $\omega_0 + \omega_{mod}$, at which there was no Newtonian force.

It seemed to us at first that with so many parameters free for adjustment it should be easy to invent viable experimental configurations. However, our expectations were naive: As noted in Sec. III A, the necessity to reduce the Newtonian signal by $\gtrsim 10^{12}$ means that the Newtonian signal produced by errors in typical parameters must be second order in all the errors, e.g.,

$$\frac{(F/m)_N}{10^{-6} \text{ cm/sec}^2} \sim \left(\frac{\text{error in location of detector}}{\text{size of apparatus}}\right)^2 + \left(\frac{\text{size of defects in source}}{\text{size of source}}\right)^2 + \cdots. \tag{6.2}$$

This places so many constraints on the experimental design that we have been able to invent only two apparently viable sets of post-Newtonian experiments that use a crystal detector: (i) gravitational "Faraday" experiments to detect the electric-type fields induced by time-changing magnetic-type gravity, and (ii) experiments to detect preferred-frame and preferred-orientation effects. These experiments are described below, along with (iii) a (non-post-Newtonian) experiment to measure the gravity of high-velocity particles using a crystal detector.

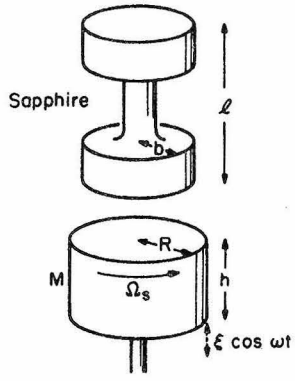

FIG. 6. Experimental configuration for detecting the gravitational analog of Faraday's law of induction.

A. Gravitational Faraday experiments

Equation (3.8b) implies that time-changing magnetic-type gravity $\vec{H}$ produces a gravitational "electromotive force" (EMF) in any ring of matter $\mathcal{C}$:

$$\oint_{\mathcal{C}} \vec{g} \cdot d\vec{l} = -\frac{1}{c}\frac{d}{dt}\int_S \vec{H} \cdot d\vec{S}. \tag{6.3}$$

Here S is any surface bounded by $\mathcal{C}$. This is the gravitational analog of Faraday's[42] law of induction.

As a special application of this law, consider a (nearly) nonrotating body at rest in a (nearly) homogeneous magnetic-type gravitational field. Let the field change by an amount $\Delta\vec{H}$. It is easy to show from Eq. (6.3) that this change will induce a change

$$\Delta\vec{\Omega} = -\tfrac{1}{2}c^{-1}\Delta\vec{H} \tag{6.4}$$

in the body's angular velocity.

The following analog of one of Faraday's original experiments[42] would seek to detect this gravitational Faraday effect: A cylinder of mass M, radius R, and height $h \lesssim R$ is set into uniform rotation with angular velocity Ω_s (see Fig. 6). This rotating cylinder is then moved up and down, along its rotation axis, with amplitude ξ and frequency ω. Coaxial with this source is an appropriately shaped, axially symmetric sapphire crystal, which is threaded by the source's magnetic-type gravitational field. The motion of the source produces an oscillating gravitational EMF [Eq. (6.3)] in the sapphire, and this EMF drives torsional oscillations of the crystal with eigenfrequency equal to the frequency ω of source motion. If the maximum radius b and height l of the sapphire are less than or of order the radius R of the source, then the driving force in the sapphire is

$$\frac{F}{m} \simeq \left(\frac{GM}{R^2}\right)\left(\frac{b}{R}\right)\left(\frac{l}{R}\right)\left(\frac{\Omega_s R}{c}\right)\left(\frac{\omega\xi}{c}\right)$$
$$\simeq 1\times 10^{-18}\ \text{cm/sec}^2 \text{ for } b\simeq l\simeq R\simeq h\simeq 10\ \text{cm},\ M\simeq 3\times 10^4\ \text{g},\ \xi\simeq 2\ \text{cm},\ \omega\simeq 500\ \text{sec}^{-1}, \quad (6.5)$$
$$\omega\xi\simeq 10^3\ \text{cm/sec},\ \Omega_s R\simeq 5\times 10^4\ \text{cm/sec}.$$

Brownian noise in the crystal can be kept well below this level if the crystal has $Q \gtrsim 10^{13}$ [$\tau^* \gtrsim 10^{10}$ sec, cf. Eq. (2.12)]. Seismic "noise" can be filtered out at the high frequency ($\nu \simeq 100$ Hz) of the crystal's oscillations. "Noise" from Newtonian-type gravity can be kept negligible if one can achieve a 10^{-7} perfection in the alignment and uniformity of crystal and generator. (Newtonian coupling requires imperfections of both generator and sensor, and it is proportional to the product of those imperfections.) This required perfection may be difficult to achieve, and it may also prove difficult to construct a sensor that measures the required amplitude change in the detector ($b\delta\phi \simeq 1\times 10^{-15}$ cm), without producing so much asymmetry on the detector that the Newtonian coupling of detector to generator becomes excessive.

In response to a preliminary version of this paper which contained no mention of any Faraday-type experiment, Ronald Drever (private communication) has suggested an experiment similar to this one. The key difference is that his generator would be a cylinder driven into torsional oscillations at the eigenfrequency of the crystal. To prevent breaking the generator one might have to keep its oscillation amplitude low enough that the post-Newtonian signal would be $F/m \simeq 10^{-19}$ cm/sec, rather than $F/m \simeq 10^{-18}$ cm/sec^2.

It might prove feasible to measure the induction effect [Eq. (6.4)] by a technique similar to the Everitt-Fairbank-Schiff gyroscope experiment.[6] One would place a nonrotating sphere in an Earth-orbiting satellite with polar orbit and search for an angular oscillation of the sphere about the Earth's polar axis. The oscillation would be relative to the distant stars, not relative to gyroscopes located in the satellite. The oscillation frequency would be twice the orbital frequency, and the amplitude would be

$$\Delta\phi \simeq \left(\frac{GM_E}{c^2R_E}\right)\frac{\Omega_E}{(GM_E/R_E{}^3)^{1/2}} \simeq 4\times 10^{-11}\ \text{rad}. \quad (6.6a)$$

Here M_E, R_E, and Ω_E are the mass, radius, and angular velocity of the Earth. The amplitude $\Delta\phi$ could be increased by using a high-Q resonant detector, e.g., a torsion oscillator of the type described in Sec. IIA with eigenfrequency twice the orbital frequency. For such an oscillator the Faraday-induced change in amplitude after a time $\hat{\tau}$ $\ll \tau^*$ = (damping time) would be

$$\delta(\Delta\phi) \simeq \frac{1}{2}\left(\frac{GM_E}{c^2R_E}\right)\Omega_E\hat{\tau} \simeq 5\times 10^{-8}\ \text{rad for } \hat{\tau}\simeq 10^6\ \text{sec}. \quad (6.6b)$$

It would be extremely difficult, but perhaps not impossible, to decouple such an oscillator from other sources of angular motion, e.g., aberration of the positions of reference stars.

Some day one might find a binary pulsar in which the induction effect is important. For a neutron star in a polar orbit of radius r around a maximally rotating Kerr black hole of mass M, the star's rotational angular velocity would be modulated with amplitude

$$\Delta\Omega \simeq \frac{c^3}{GM}\left(\frac{GM}{c^2r}\right)^3$$
$$\simeq 1\times 10^{-11}\ \text{sec}^{-1} \text{ if } M\simeq 3M_0 \text{ and } r\simeq 1\times 10^{11}\ \text{cm}. \quad (6.7)$$

This is too small to measure at present in the known binary pulsar,[43] but too small by only a factor 1000. In a binary pulsar with a 10^{10}-cm orbital radius the induction effect might be measurable, but we have not attempted to determine whether one could separate it cleanly from other effects.

B. Preferred-frame and preferred-orientation experiments

We turn now to experiments which would use sapphire crystals to search for preferred-frame and preferred-orientation effects (see Sec. III). The experimental configuration is shown schematically in Fig. 7(a): The source, perhaps a prolate spheroid of mass M and largest radius R, rotates around its shortest principal axis, the z axis, with angular velocity $\omega \simeq 6\times 10^{-3}$ sec^{-1}. The detector, a cylindrical monocrystal of length b, is placed near the source with its axis of symmetry on the z axis (coincident with the rotation axis of the source). The rotation of the Earth causes the entire experiment to rotate with angular velocity $\Omega \simeq 7\times 10^{-5}$ sec^{-1} relative to inertial space; and it might prove desirable to produce a more rapid rotation $\Omega \simeq 10^{-2}$ sec^{-1} by mounting the entire experiment on a rotating platform. Due to the motion of the solar system and galaxy, the laboratory moves with linear velocity $\vec{w}$ ($|\vec{w}| \sim 2\times 10^7$ cm/sec) relative to the mean rest frame of the universe.

The central regions of the galaxy, with mass $M_G \simeq 1\times 10^{11} M_0$, distance from Earth $R_G \simeq 10$ kpc, and direction from Earth $\vec{k}$, reach into the laboratory gravitationally to produce preferred-orientation effects.

Consider a particular element of mass $\rho d^3x'$ inside the source at location $\vec{x}'$. It moves relative to the center of mass of the detector with linear velocity

$$\vec{v} = (\text{velocity due to source rotation } \omega) + (\text{velocity due to platform rotation } \Omega). \quad (6.8)$$

At a point $\vec{x}$ inside the detector this mass element produces the following accelerations due to preferred-frame and preferred-orientation effects:

$$\left(\frac{\vec{F}}{m}\right)_{PN} = (-\Gamma^j_{00}\vec{e}_j)_{PN} = \frac{G\rho d^3x'}{c^2 r^2}\{-\alpha_2(\vec{w}\cdot\vec{n})\vec{v} + [(\tfrac{1}{2}\alpha_1 - \alpha_2)(\vec{v}\cdot\vec{n}) - \alpha_2(\vec{w}\cdot\vec{n})]\vec{w} - 2\zeta_W(GM_G/R_G)(\vec{k}\cdot\vec{n})\vec{k}$$
$$+ [3\alpha_2(\vec{v}\cdot\vec{n})(\vec{w}\cdot\vec{n}) + (\tfrac{1}{2}\alpha_1 - \alpha_2 - \alpha_3)(\vec{w}\cdot\vec{v})$$
$$+ \tfrac{1}{2}(\alpha_1 - \alpha_2 - \alpha_3)\vec{w}^2 + \tfrac{3}{2}\alpha_2(\vec{w}\cdot\vec{n})^2 + 2\zeta_W(GM_G/R_G) + 3\zeta_W(GM_G/R_G)(\vec{k}\cdot\vec{n})^2]\vec{n}\} \quad (6.9)$$

[cf. Eqs. (39.32b, c) of MTW[2] and Eq. (21) of Will's paper[4]]. Here r is the distance and $\vec{n}$ is the direction between source point and field point

$$r \equiv |\vec{x} - \vec{x}'|\,, \quad \vec{n} \equiv (\vec{x} - \vec{x}')/r\,,$$

$\alpha_1, \alpha_2, \alpha_3$ are preferred-frame PPN parameters, and ζ_W is the Whitehead preferred-location PPN parameter. Simple geometric considerations show that the force (6.9), integrated over all parts of the source and all parts of the detector, will couple to several different normal modes of the detector. By careful selection of the rotational angular velocity of the source ω, the experimenter can produce a resonant, secular driving of any one of those normal modes, and can thereby measure, or place experimental limits on, the combination of PPN parameters which couple to that mode.

As an example, consider the acceleration

$$(\vec{F}/m)_{PN} = (G\rho d^3x'/r^2c^2)[\tfrac{3}{2}\,\alpha_2(\vec{w}\cdot\vec{n})^2 + 3\zeta_W(GM_G/R_G)(\vec{k}\cdot\vec{n})^2]\vec{n}\,. \quad (6.10)$$

Geometric considerations show that it couples to the fundamental vibrational mode of the detector [Fig. 7(b)] with frequency

$$\omega_{PN} = 2(\omega \pm \Omega) \quad (6.11a)$$

and with amplitude

$$(F/m)_{PN} \simeq (\tfrac{1}{10}\,GM/R^2)(b/R)[\alpha_2\vec{w}^2/c^2 + 2\zeta_W(GM_G/R_G c^2)]$$
$$\simeq \left(1\times 10^{-12}\ \frac{\text{cm}}{\text{sec}^2}\right)\left[\alpha_2\left(\frac{\vec{w}}{2\times 10^7\ \text{cm/sec}}\right)^2 + 2\zeta_W\right] \text{ for } M \simeq 10^5 \text{ g and } R \simeq b \simeq 20 \text{ cm}\,. \quad (6.11b)$$

In the experiment feedback would be used on the source to keep ω_{PN} equal to the measured eigenfrequency ω_0 of the detector's fundamental mode, i.e., to keep the phase relations between the fundamental mode and the acceleration (6.10) constant to within $\delta\phi \lesssim 10^0$ over the time $\hat{\tau} \simeq 10^6$ sec of the measurement. The techniques of Sec. II B would be used to measure the influence of this post-Newtonian force on the amplitude of the detector's vibrations.

As a second example, consider the acceleration

$$(\vec{F}/m)_{PN} = (G\rho d^3x'/r^2c^2)(\tfrac{1}{2}\,\alpha_1 - \alpha_2 - \alpha_3)(\vec{v}\cdot\vec{w})\vec{n}\,. \quad (6.12)$$

Geometric considerations show that it couples to the $m = 1$ (dipole) normal mode of the detector shown in Fig. 7(c) with frequency

$$\omega_{PN} = 2\omega \pm \Omega \quad (6.13a)$$

and with amplitude

$$(F/m)_{PN} \simeq \tfrac{1}{10}\,(\tfrac{1}{2}\,\alpha_1 - \alpha_2 - \alpha_3)(GM/Rc^2)(b/R)\omega\,|\vec{w}\,|$$
$$\simeq (3\times 10^{-15}\ \text{cm/sec}^2)(\tfrac{1}{2}\,\alpha_1 - \alpha_2 - \alpha_3)\,|\vec{w}\,|/(2\times 10^7\ \text{cm/sec})$$
$$\text{for } M \simeq 10^5 \text{ g},\ R \simeq b \simeq 20 \text{ cm},\ R\omega \simeq 10^5 \text{ cm/sec}. \quad (6.13b)$$

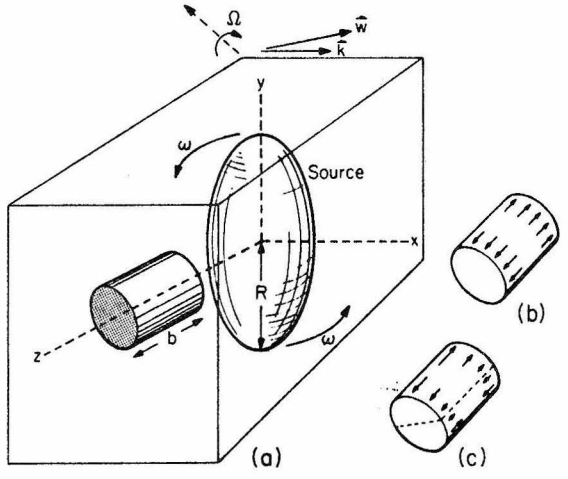

FIG. 7. (a) Experimental configuration for a set of preferred-frame experiments. (b) Motions of the detector excited in its fundamental mode; the type of excitation produced by the preferred-frame forces of Eq. (6.10). (c) Motions of the detector excited in a dipole mode; the type of excitation produced by the preferred-frame force of Eq. (6.12).

Newtonian "noise" is not a serious problem for these experiments. If the apparatus were perfectly constructed and aligned, there would be no Newtonian coupling whatsoever to either the fundamental mode or the dipole mode [Figs. 7(b), 7(c)] of the detector. Imperfections will lead to a coupling with amplitude and frequency

$$(F/m)_N \lesssim 10^{-12}\ \text{cm/sec}^2, \quad \omega_N = 2\omega . \tag{6.14}$$

If the Ω rotation is produced by the Earth's rotation, there is no way to get any remotely significant Newtonian signal at the post-Newtonian frequencies (6.11a), (6.13a). If the apparatus is placed on a rotating platform, there will be some Newtonian signal at ω_{PN}, owing to deformations of the source caused by gravitational fields of objects in the external, non-Ω-rotating laboratory. However, simple estimates show that this Newtonian signal is far below the accuracy $F/m \simeq 3\times 10^{-16}$ cm/sec^2 that one might hope to achieve in the experiment.

From such experiments, performed with various orientations of the apparatus, one could hope to achieve limits of

$$\left|\alpha_2\left(\frac{\vec{w}}{200\ \text{km/sec}}\right)^2 + 2\zeta_w\right| \lesssim 3\times 10^{-6},$$
$$\left|\tfrac{1}{2}\alpha_1 - \alpha_2 - \alpha_3\right| \frac{|\vec{w}|}{200\ \text{km/sec}} \lesssim 1\times 10^{-3}, \tag{6.15}$$

or, conceivably, positive measurements in violation of general relativity. It is worth noting that α_1, α_2, α_3, and ζ_w are known from previous experiments[44] to lie in the ranges

$$|\alpha_1| \lesssim 0.07, \quad |\alpha_2| \lesssim 0.002,$$
$$|\alpha_3| \lesssim 2\times 10^{-5}, \quad |\zeta_w| \lesssim 0.001, \tag{6.16}$$

assuming that $|\vec{w}| \simeq 200$ km/sec. Consequently, the above two variants of the experiment can be regarded as new, improved measurements of α_1, α_2, and ζ_w.

The "magnetic-type" experiments described in Secs. IV A and V A are aimed at measuring

$$\tfrac{7}{8}\Delta_1 + \tfrac{1}{8}\Delta_2 = 4\gamma + 4 + \alpha_1 . \tag{6.17}$$

γ is known to be unity to within $\simeq 2$ percent[45] and will likely be determined to within $\simeq 0.3$ percent by time-delay measurements on the Viking spacecraft. Consequently, the magnetic-type experiments, like one of the above preferred-frame experiments, are attempts to measure α_1. The preferred-frame experiment should be much easier to perform than the magnetic-type experiments, and can place a much tighter limit on α_1 ($\lesssim 0.001$ vs $\lesssim 0.3$). Thus, if one believed that the PPN formalism embodied all possibilities for post-Newtonian gravity (which we do *not*), then one would put one's efforts into the preferred-frame experiment. On the other hand, if one wants to "see" magnetic-type gravitational forces for the first time in history, one will prefer the more difficult magnetic-type experiments.

C. Gravity at high velocities

Consider a point particle of mass m_0 which flies past a stationary observer with velocity v and impact parameter b. If gravity is a spin-two classical field as described by general relativity, the particle's gravity will give the observer an impulse

$$J_2 \equiv \int_{-\infty}^{+\infty}\left(\frac{F}{m}\right)dt = \frac{2Gm_0}{\gamma v b}\,(1+2\gamma^2 v^2/c^2), \tag{6.18}$$

where $\gamma \equiv (1-v^2/c^2)^{-1/2}$. If gravity were an attractive spin-one field (analog of electromagnetism, Exercise 7.2 of MTW[2]), the impulse would be

$$J_1 \equiv \int_{-\infty}^{+\infty}\left(\frac{F}{m}\right)dt = \frac{2Gm_0}{vb}, \tag{6.19}$$

and if gravity were a spin-zero field (scalar field, Exercise 7.1 of MTW[2]), the impulse would be

$$J_0 \equiv \int_{-\infty}^{+\infty}\left(\frac{F}{m}\right)dt = \frac{2Gm_0}{\gamma v b}. \tag{6.20}$$

At low velocities the impulses are indistinguishable, but for $\gamma \gg 1$ they are very different—$J_2 : J_1 : J_0 = 2\gamma^2 : \gamma : 1$. There may be other ways of theorizing about the γ dependence of the impulse, but these

elementary considerations already show that it is of some interest.

It may be possible to test the γ dependence using as a source protons that circulate around a storage ring, and as a detector a monocrystal of sapphire sitting just outside the beam pipe. In such an experiment one would bunch the protons so they all fly past the crystal during a time interval Δt short compared to the crystal's eigenperiod τ_0; and one would adjust τ_0 to equal the proton circuit time in the storage ring,

$$\tau_0 = \mathcal{C}/c = (3\times 10^{-6}\ \text{sec})(\mathcal{C}/1\ \text{km}), \tag{6.21}$$

where $\mathcal{C} \equiv$ ring circumference. Then the gravitational acceleration would occur over and over again at the same phase of the crystal oscillation and (hopefully) would produce a measurable change in the crystal's amplitude and phase.

If I is the total beam current in the ring, e is the proton charge, and b is the distance from the center of the beam pipe to the crystal, then the time-averaged gravitational acceleration is

$$(F/m)_{\text{avg}} \equiv (1/\tau_0)\int_0^{\tau_0} (F/m)dt = (I/e)J$$
$$= \frac{2G(m_p/e)I}{\gamma v b}\,(1+2\gamma^2 v^2/c^2) \quad \text{for general relativity}$$
$$\simeq 1\times 10^{-19}\ \text{cm/sec}^2 \quad \text{for } \gamma m_p c^2 \simeq 1000\ \text{GeV},\ I\simeq 10\ \text{A},\ b\simeq 10\ \text{cm}. \tag{6.22}$$

This time-averaged acceleration, hitting impulsively at fixed phase, will produce the same long-term amplitude change in the crystal as a sinusoidal acceleration of amplitude

$$(F/m)_{\text{eff}} = 2(F/m)_{\text{avg}} = 2\times 10^{-19}\ \text{cm/sec}^2 \tag{6.23}$$

for above parameters. For comparison, the intersecting storage rings now operating at CERN have $\gamma m_p c^2 \simeq 30$ GeV, $I\simeq 20$ A, $\mathcal{C}\simeq 1$ km, the POPAE storage rings proposed for Fermilab would have $\gamma m_p c^2 \simeq 1000$ GeV, $I\simeq 5$ A, $\mathcal{C}\simeq 5.5$ km, and the ISABELLE storage rings proposed for Brookhaven would have $\gamma m_p c^2 \simeq 200$ GeV, $I\simeq 10$ A, $\mathcal{C}\simeq 2.7$ km. Thus, an experiment with $(F/m)_{\text{eff}} \simeq 1\times 10^{-19}$ cm/sec^2 does not seem unreasonable; and it may be possible to operate the storage rings at somewhat higher beam currents, thereby strengthening the signal.

This experiment would face serious, but perhaps surmountable problems from fluctuational forces in the crystal [Eq. (2.12)] and back-action forces of the sensor on the crystal [Eq. (2.11)]. For the POPAE design parameters with a 10-A current rather than 5 A, the signal strength and crystal eigenfrequency are $(F/m)_{\text{eff}} \simeq 2\times 10^{-19}$ cm/sec^2, $\omega_0 = 2\pi c/\mathcal{C} \simeq 3.4\times 10^5$ sec^{-1}. A sapphire crystal with this ω_0 would have length $b\simeq 10$ cm, and with a radius $a\simeq 10$ cm, its mass would be $m\simeq 10^4$ g. To keep the internal fluctuational forces below 5×10^{-20} cm/sec^2 during a measurement time $\hat{\tau}\simeq 3\times 10^6$ sec at a crystal temperature $T_0 \simeq 1\times 10^{-3}$ °K, one must achieve a crystal damping time of $\tau^* \simeq 1\times 10^{10}$ sec [Eq. (2.12)]. This corresponds to $Q = \pi\tau^*/\tau_0 \simeq 2\times 10^{15}$. Such a Q is easily compatible with theoretical limits on sapphire crystals [cf. Eq. 2.13]; however, several years of crystal development and experimentation are needed before one can know how hard it will be to achieve such a Q in practice.

For the above parameters and for the sensor described by Eq. (2.11), the fluctuational back-action force of the sensor on the crystal would be $F/m \simeq 7\times 10^{-19}$ cm/sec^2. This is a factor 3 larger than the signal. Thus, unless a substantial improvement in beam current were achieved, thereby raising the signal substantially, one would have to devise a sensor better than that of Eq. (2.11). That one can do so, at least in principle (but just barely), without resorting to "quantum nondemolition techniques,"[46] is evident from the following: The signal $(F/m)_{\text{eff}} \simeq 2\times 10^{-19}$ cm/sec^2 produces an amplitude change in the crystal

$$\Delta x_0 = \tfrac{1}{2}(F/m)_{\text{eff}}\,\hat{\tau}/\omega_0 \simeq 9\times 10^{-19}\ \text{cm} \tag{6.24}$$

which satisfies the constraint for "quantum-demolition" sensors[47]

$$\tfrac{1}{2} m(\omega_0 \Delta x_0)^2/(\hbar\omega_0) \simeq 1.3 > 1. \tag{6.25}$$

These stringent requirements on the Q of the crystal and the performance of the sensor would be much alleviated (i) if there existed storage rings of circumference $\mathcal{C} \gg 5$ km (thus permitting lower ω_0 and larger m for the crystal), or (ii) if a ring with $\mathcal{C}\simeq 5$ km could achieve a beam current $I \gg 10$ A.

It appears to us that this experiment need not encounter serious problems with Newtonian gravitational noise due to flexing of the beam tube as the protons pass and other motions of macroscopic masses. Nor should electromagnetic forces of the passing protons be a problem if the crystal is reasonably shielded.

However, a very serious problem is the bombardment of the crystal by particles produced in collisions of the proton beam with residual gas in the beam tube. The most serious effect of such particles might be heating of the crystal with consequent degradation of the Q of its fundamental mode. To circumvent this one would have to continually remove thermal energy from the crystal, perhaps through a wire by which it is suspended. Also serious might be the damage of the crystal by particles passing through it, and direct excitation of its fundamental mode. It is impossible to assess these effects reliably without experimental tests. Our crude estimates suggest that with reasonable amounts of shielding one *might* prevent them from seriously degrading the experiment; but we would not be surprised if they were so serious as to make this experiment even more difficult than the Davies frame-dragging experiment (Sec. V A).

VII. CONCLUSIONS

None of the experiments described in this paper would be easy to perform. They all stretch the limits of current technology. However, most of them are close to those limits, and may turn out to be within those limits if the experimenter is sufficiently clever and dedicated. We suggest that now is the time for experimenters to begin work on detailed feasibility studies and design studies for these experiments, and for others that use similar technology.

ACKNOWLEDGMENTS

For helpful discussions we thank John Dick, David Douglass, Ronald Drever, Richard Feynman, and John Turneaure.

REFERENCES AND FOOTNOTES

*This paper draws upon work which was supported in part by the Ministry of Higher Education, U.S.S.R., and upon work supported in part by the National Aeronautics and Space Administration under Contract No. NGR-05-002-256 and the National Science Foundation under Grant No. AST75-01398 A01.

†Work supported in part by a National Science Foundation Predoctoral Fellowship and a Feynman Fellowship.

[1]An important exception involving laboratory generators of gravity and laboratory detectors was the experiment to test the equality of active and passive gravitational mass by L. B. Kreuzer, Phys. Rev. 169, 1007 (1968).

[2]For details and references see, e.g., Chap. 40 of C. W. Misner, K. S. Thorne, and J. A. Wheeler, *Gravitation* (Freeman, San Francisco, 1973), cited henceforth as MTW.

[3]Preliminary versions of the material in this paper have been presented at meetings of the American Physical Society: see V. B. Braginsky, C. M. Caves, and K. S. Thorne, Bull. Am. Phys. Soc. 20, 98 (1975); 20, 1488 (1975).

[4]C. M. Will and K. Nordtvedt, Jr., Astrophys. J. 177, 757 (1972); Chap. 39 of MTW (Ref. 2); and C. M. Will, Astrophys. J. 185, 31 (1973).

[5]V. B. Braginsky and A. B. Manukin, *Measurement of Small Forces in Physical Experiments: Techniques and Fundamental Limitations* (Nauka, Moscow, 1974) (English translation in preparation by Univ. of Chicago Press).

[6]C. W. F. Everitt, in *Experimental Gravitation, Proceedings of Course 56 of the International School of Physics "Enrico Fermi,"* edited by B. Bertotti (Academic, New York, 1974), p. 331. See especially Eq. (26) and associated discussion; and note that the damping time is independent of the spin velocity of the ball.

[7]V. B. Braginsky and V. I. Panov, Zh. Eksp. Teor. Fiz. 61, 873 (1971) [Sov. Phys.—JETP 34, 463 (1972)].

[8]Kh. S. Bagdasarov, V. B. Braginsky, and V. P. Mitrofonov, results reported at International Symposium on Experimental Gravitation, Pavia, Italy, 1976 (unpublished); for earlier results see paper by the same authors in Kristallografiya 19, 883 (1974) [Sov. Phys.—Crystallogr. 19, 549 (1975)].

[9]H. Pfister, Cryogenics 16, 17 (1976).

[10]$J_\omega^{\rm hor}$ comes from Fig. 1 of J. Berger and J. Levine, J. Geophys. Res. 79, 1210 (1974).

[11]$J_\omega^{\rm vert}$ comes from the following references: Fig. 1 of R. J. Warburton, C. Beaumont, and J. M. Goodkind, Geophys. J. R. Astron. Soc. 43, 707 (1975); Fig. 2 of J. Weber and J. V. Larson, J. Geophys. Res. 71, 6005 (1966); and the ambient spectrum of Figs. 3 and 4 of B. Block, J. Dratler, Jr., and R. D. Moore, Nature (London) 226, 343 (1970).

[12]H. Paik, in *Experimental Gravitation, Proceedings of Course 56 of the International School of Physics "Enrico Fermi"* (Ref. 6), p. 515.

[13]V. B. Braginsky, in *Gravitational Radiation and Gravitational Collapse, IAU Symposium No. 64,* edited by C. Morette-DeWitt (Reidel, Dordrecht, 1974); also, V. B. Braginsky, in *Proceedings of the International School of Cosmology and Gravitation, Course 4: Gravitational Waves,* edited by J. Weber (Plenum, New York, to be published).

[14]See, e.g., F. Schmid and D. J. Viechnicki, Solid State Technol. 16, 45 (1973).

[15]W. M. Fairbank, S. P. Boughn, H. Paik, M. S. McAshan, J. E. Opfer, R. C. Taber, W. O. Hamilton, B. Pipes, T. Bernat, and J. M. Reynolds, in *Experimental Gravitation, Proceedings of Course 56 of the International School of Physics "Enrico Fermi"* (Ref. 6), p. 294.

[16]C. M. Caves, papers in preparation.

[17]See also K. S. Thorne and V. B. Braginsky, Astrophys. J. Lett. 204, L1 (1976) for a brief discussion of the use of superconducting-cavity stabilized oscillators as clocks in Doppler-tracking searches for gravitational waves.

[18]See, e.g., J. P. Turneaure, in *Proceedings of the 8th International Conference on High Energy Accelerators* (CERN, Geneva, 1971), p. 51.

[19]M. A. Allen, Z. D. Farkas, H. A. Hogg, E. W. Hoyt, and P. B. Wilson, IEEE Trans. Nucl. Sci. 18, 168 (1971).

[20]S. R. Stein and J. P. Turneaure, IEEE Proc. 63, 1249 (1975).

[21]C. M. Will, in *Experimental Gravitation Proceedings of Course 56 of the International School of Physics "Enrico Fermi"* (Ref. 6), p. 1; D. L. Lee, A. P. Lightman, and W.-T. Ni, Phys. Rev. D 10, 1685 (1974).

[22]This fact follows from Eq. (39.27) of MTW (Ref. 2).

[23]R. L. Forward, Proc. IRE 49, 892 (1961); see also references cited therein.

[24]In a series of experiments performed in 1820, Ampère explored the magnetic interactions of electric currents. Ampère described his results in readings presented to the Académie Royale des Sciences on September 18 and 25, 1820 [A.-M. Ampère Ann. Chim. Phys. 15, pp. 59–76, 177–208 (1820); English translations of portions of these papers can be found in R. A. R. Tricker, *Early Electrodynamics: The First Law of Circulation* (Pergamon, New York, 1965)]. In addition to his famous experiment investigating the magnetic forces between parallel conductors, Ampère also demonstrated that two current-carrying spiral-shaped wires attract and repel each other like permanent magnets.

[25]R. A. Van Patten and C. W. F. Everitt, Phys. Rev. Lett. 36, 629 (1976).

[26]P. K. Chapman, paper presented at the 26th Congress of the International Astronautical Federation, Lisbon, 1975 (unpublished).

[27]W. W. Salisbury, Nature (London) 224, 783 (1969); E. Frehland, Nature (London) 230, 11 (1971); J. Jaffe, Gen. Relativ. Gravit. 6, 49 (1975).

[28]R. F. O'Connell and S. N. Rasband, Nature (London) 232, 193 (1971); Jaffe, Ref. 27.

[29]An exception is an unpublished proposal by S. N. Rasband, 1974, for an experiment to measure the gravitational spin-spin force using a monocrystal of sapphire as a detector. This experiment might conceivably be performable, but it looks much less promising to us than the experiments described in Secs. IV A and VI A of this paper.

[30]See, e.g., R. F. Post and S. F. Post, Sci. Am. 229, 17 (1973); also D. W. Rabenhorst, Applied Physics Laboratory, Johns Hopkins Univ., papers presented at various engineering meetings (unpublished).

[31]One can readily construct an idealized example of such a source using two thin rings.

[32]P. G. Roll, R. Krotkov, and R. H. Dicke, Ann. Phys. (N.Y.) 26, 442 (1964).

[33]P. W. Worden, Jr. and C. W. F. Everitt, in *Experimental Gravitation, Proceedings of Course 56 of the International School of Physics "Enrico Fermi"* (Ref. 6), p. 381.

[34]M. P. Haugan and C. M. Will, Phys. Rev. Lett. 37, 1 (1976).

[35]The coupling of gravitational energy has been checked using as test masses the Earth and Moon (Nordtvedt effect) by J. G. Williams *et al.*, Phys. Rev. Lett. 36, 551 (1976); and by I. I. Shapiro, C. C. Counselmann III, and R. W. King, *ibid.* 36, 555 (1976).

[36]R. von Eötvös, Ann. Phys. Chem. 59, 354 (1896).

[37]I. I. Shapiro, result reported in Washington, D.C. meeting of American Association for the Advancement of Science, 1976 (unpublished). For earlier results from the same type of experiment, see I. I. Shapiro, W. B. Smith, M. E. Ash, R. P. Ingalls, and G. H. Pettingill, Phys. Rev. Lett. 26, 27 (1971).

[38]See, e.g., the discussion of "self-regeneration" of pressure on p. 605 of MTW; also see R. V. Wagoner and R. C. Malone, Astrophys. J. Lett. 189, L75 (1974).

[39]R. W. Davies, in *Experimental Gravitation, Proceedings of Course 56 of the International School of Physics "Enrico Fermi"* (Ref. 6), p. 331.

[40]J. M. Bardeen, Astrophys. J. 162, 71 (1970). The relevant part of this reference is summarized in Exercise 33.3 of MTW.

[41]See, e.g., G. Birnbaum, *Optical Masers* (Academic, New York, 1964), Chap. 6.

[42]M. Faraday, Phil. Trans. (1832), p. 125.

[43]J. H. Taylor, R. A. Hulse, L. A. Fowler, G. E. Gullahorn, and J. M. Rankin, Astrophys. J. Lett. 206, L53 (1976).

[44]K. Nordtvedt, Jr. and C. M. Will, Astrophys. J. 177, 775 (1972); M. G. Rochester and D. E. Smylie, J. Geophys. Res. 79, 4948 (1974); R. J. Warburton and J. M. Goodkind, Astrophys. J. 208, 881 (1976).

[45]E. B. Fomalant and R. A. Sramek, Phys. Rev. Lett. 36, 1475 (1976).

[46]V. B. Braginsky and Yu. I. Vorontsov, Usp. Fiz. Nauk. 114, 41 (1974) [Sov. Phys.—Usp. 17, 644 (1975)]; also V. B. Braginsky, Yu. I. Vorontsov, and V. D. Krivchenkov, Zh. Eksp. Teor. Fiz. 68, 55 (1975) [Sov. Phys.—JETP 41, 28 (1975)].

[47]See, e.g., R. Giffard, Phys. Rev. D 14, 2478 (1976); or Eq. (3.17) of V. B. Braginsky, *Physics Experiments with Test Bodies* (Nauka, Moscow, 1970), English translation published as Report No. NASA-TT F762, available from National Technical Information Service, Springfield, Virginia.

CHAPTER 2

MICROWAVE CAVITY GRAVITATIONAL RADIATION DETECTORS

This chapter is a paper which appeared in the 1979, January 1, issue of Physics Letters, volume 80B, pages 323-326. It is reproduced here with the permission of the publisher, North-Holland Publishing Company, Amsterdam.

Volume 80B, number 3 PHYSICS LETTERS 1 January 1979

MICROWAVE CAVITY GRAVITATIONAL RADIATION DETECTORS ☆

Carlton M. CAVES
W.K. Kellogg Radiation Laboratory, California Institute of Technology, Pasadena, CA 91125, USA

Received 26 September 1978

The coupled electro–mechanical system consisting of a microwave cavity and its walls can serve as a gravitational radiation detector. A gravitational wave interacts with the walls, and the resulting motion induces transitions from a highly excited cavity mode to a nearly unexcited mode.

Microwave cavities with superconducting walls may have a variety of applications as detectors of non-newtonian gravitational fields. The response of a microwave cavity to a time-changing gravitational field is quite complicated. Both the electromagnetic field in the cavity and the cavity walls interact directly with the gravitational field; in addition, the electromagnetic field and walls interact with one another at the boundary between the two.

I have developed a formalism for analyzing this complicated electro–mechanical system in the presence of a weak gravitational field. A previous paper [1] sketched an application of the formalism to a proposed experiment to measure dragging of inertial frames. This letter presents results of applying the formalism to microwave cavities designed to detect gravitational radiation. Subsequent papers [2] will give details of the formalism and of its various applications.

In 1971 Braginsky and Menskii [3] suggested using microwave cavities to detect high-frequency gravitational waves ($\nu \sim$ (cavity's fundamental mode frequency)). I have analyzed their high-frequency detectors and have also found new designs for, and developed the theory of, detectors designed to operate at much lower frequencies. After the first formal (but unpublished) write-up of my analysis [4], I became aware that Pegoraro et al. [5] had arrived at some similar designs for low-frequency detectors.

☆ Supported in part by the National Aeronautics and Space Administration (NGR 05-002-256 and a grant from PACE) and by a Feynman Fellowship.

Both high- and low-frequency microwave cavity detectors operate in essentially the same way. A gravitational wave incident on the cavity couples its electromagnetic modes and thereby induces transitions between modes. The coupling is due to the *direct interaction* of the electromagnetic field with the wave and to an *indirect interaction* in which the wave interacts directly with the cavity walls, whose resulting motion couples the electromagnetic modes. In the simplest detectors, the cavity is designed so that two of its modes are strongly coupled by the gravitational wave. One of these two modes (mode 1) is driven into steady-state oscillation at its eigenfrequency; initially the other mode (mode 2) is nearly unexcited. A passing gravitational wave with Fourier components near the splitting frequency between the two modes "pumps" quanta from mode 1 to mode 2, and the wave is detected by monitoring the resulting excitation of mode 2.

Focus attention now and for the remainder of this letter on low-frequency detectors – those designed to operate at frequencies much lower than the cavity's fundamental mode frequency. Since the wave's characteristic wavelength is much larger than the cavity's dimensions, it is convenient to describe the wave in Fermi-normal ("physical") coordinates [6]. In these coordinates the motion of the cavity walls is described by the local displacement vector ξ, which is governed by the usual equations for an elastic medium subject to a tidal force produced by the gravitational wave and to stresses at its boundary produced by the electromagnetic field.

However, analysis of the electromagnetic field in these

coordinates is complicated because the boundary of the cavity is moving. To handle this difficulty [2], one transforms to new coordinates in which the boundary is at rest, and one chooses the new coordinates so that they differ from the old coordinates only in a small region near the boundary. In the new coordinates one uses the artifice of writing the curved-space, generally-covariant Maxwell equations in a form which is identical to the flat-space Maxwell equations for a moving, anisotropic medium [7]. With the Maxwell equations recast in this form and with the boundary at rest, the boundary conditions are the familiar ones. All information about the interaction of the electromagnetic field with the gravitational wave is contained in the "dielectric tensor" $\boldsymbol{\varepsilon}$ and the "velocity" $\boldsymbol{g}$ of the (fictitious) moving medium. At linear order in the gravitational wave amplitude, $\boldsymbol{\varepsilon}$ and $\boldsymbol{g}$ split cleanly into terms representing the direct and indirect interactions. The indirect interaction terms are proportional to the physical displacement of the cavity boundary; the direct interaction terms are smaller by a factor ~ (cavity dimension/gravitational wave wavelength)^2 and can be neglected for low-frequency detectors.

The recast Maxwell equations and the mechanical equations can be decomposed into normal-mode equations. The Coulomb-gauge vector potential is expanded in terms of the cavity's normalized electromagnetic eigenmodes A_n: $A = \Sigma_n c_n A_n$ ($\int A_n \cdot A_m \, dV = \delta_{nm}$); and the local displacement vector is expanded in terms of the walls' normalized mechanical eigenmodes $\boldsymbol{\xi}_\alpha$: $\boldsymbol{\xi} = \Sigma_\alpha d_\alpha \boldsymbol{\xi}_\alpha$ ($M^{-1} \int \rho \boldsymbol{\xi}_\alpha \cdot \boldsymbol{\xi}_\beta \, dV = \delta_{\alpha\beta}$, where ρ and M are the density and mass of the walls). The result is a set of coupled equations for the normal-mode coordinates c_n and d_α in the absence of dissipation [2].

In the case of interest, mode 1 is highly excited at its eigenfrequency by an external source ($c_1 = \mathrm{Re}(A e^{i\omega_1 t})$; (total energy in mode 1) = $U_1 = \omega_1^2 |A|^2/8\pi$), and mode 2 is strongly coupled to mode 1 by wall motion. Typically, only one mechanical mode (α = m) couples strongly to the gravitational wave and, at the same time, produces displacements of the cavity boundary which strongly couple the two electromagnetic modes. Neglecting all other electromagnetic and mechanical modes, one obtains equations for c_2 and d_m in the presence of a highly excited mode 1. With addition of empirical damping terms and neglect of high-frequency stresses on the walls, these equations become

$$\ddot{c}_2 + 2\beta \dot{c}_2 + \omega_2^2 c_2 = \omega_1^2 c_1 d_m \mathcal{L}^{-1}, \tag{1a}$$

$$\ddot{d}_m + 2\beta_m \dot{d}_m + \omega_m^2 d_m = (\omega_1^2/4\pi M) c_1 c_2 \mathcal{L}^{-1} + f_m . \tag{1b}$$

Here ω_1 and ω_2 are the angular eigenfrequencies of modes 1 and 2 when the cavity is *fixed* in the shape it has after it is distorted by the time-averaged stresses produced by the field in mode 1; ω_m is the angular eigenfrequency of the mechanical mode; $\mathcal{L}^{-1}$ is a field-wall "matrix element" given by

$$\mathcal{L}^{-1} \equiv \int_S (T_2 \cdot T_1 - A_2 \cdot A_1)(\boldsymbol{\xi}_m \cdot d\boldsymbol{a}),$$

where $T_n \equiv \omega_n^{-1} \nabla \times A_n$ and $d\boldsymbol{a}$ is the outward-directed surface element of the cavity boundary; and

$$f_m \equiv -M^{-1} \int \rho (\xi_m)^j R_{0j0k} x^k \, dV,$$

where the R_{0j0k} are the "electric" components of the wave's Riemann tensor. The terms in eqs. (1) involving $\mathcal{L}^{-1}$ represent the coupling of modes 1 and 2 by wall motion (eq. (1a)) and the force exerted on the wall by the electromagnetic field (eq. (1b)); f_m represents the coupling of the mechanical mode to the gravitational wave.

It is convenient to introduce a dimensionless complex quantity μ defined by $c_2 = \mathrm{Re}(\mu A e^{i\omega_1 t})$. The Green function solution for μ is

$$\mu(t) = \int_0^t g(t, t') f_m(t') \, dt' ,$$

where

$$g(t, t') = \frac{i\omega_1}{2\mathcal{L}} \sum_{j=1}^{4} \frac{\delta_j + \omega_{21} - i\beta}{\Pi_{k \neq j} (\delta_j - \delta_k)} \, e^{i\delta_j (t - t')}, \tag{2}$$

for $t \geqslant t'$. Here $\omega_{21} \equiv \omega_2 - \omega_1$, and the δ's are the roots of the quartic equation

$$(\delta^2 - \omega_m^2 - 2i\beta_m \delta)(\delta^2 - \omega_{21}^2 - 2i\beta\delta) = \omega_1 \omega_{21} \mathcal{L}^{-2} (U_1/2M). \tag{3}$$

The real parts of the δ's give the detector's operating frequencies.

The δ's change as the field in mode 1 is turned on.

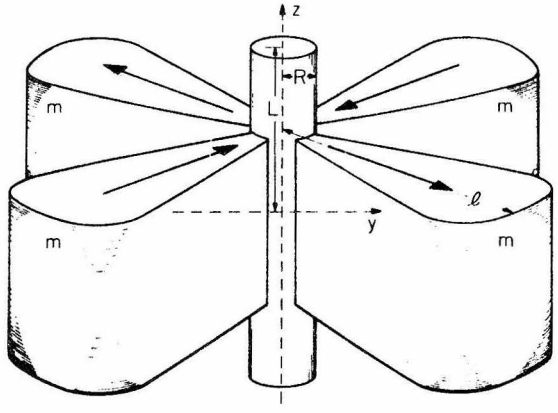

Fig. 1. Diagram of microwave cavity detector described in text.

For large fields, they can differ substantially from their zero-field values. Unless the entire system is designed carefully, one or more of the δ's may have a large and negative imaginary part; and mode 2 will be unstable. This instability can be avoided by suitably arranging the mass in the cavity walls and by suitably choosing the cavity's zero-field shape.

One possible design for such a detector is shown in fig. 1. The microwave cavity is nearly cylindrical with radius $R \approx 10$ cm and length $2L \approx 500$ cm. The microwave modes are the two $TE_{1,1,1}$ modes with angular frequency $\omega_1 \approx 6 \times 10^9$ rad s^{-1}; for a perfect cylinder these two modes are degenerate. The magnetic field lies principally in the z-direction; in mode 1 it has a "cos φ" azimuthal dependence, and in mode 2 a "sin φ" dependence – where φ is measured from the x-axis. Mode 1 is driven to a magnetic field strength ≈ 750 G, which corresponds to total energy $U_1 \approx 9 \times 10^8$ erg and number of quanta $N_1 \approx 10^{26}$. Almost all the mass in the cavity walls is in four lobes – each of the mass $m \approx 10^6$ g – which extend a distance $l \approx 500$ cm from the axis of the cavity at angles midway between the x- and y-axes. The relevant mechanical mode is the one whose motion is indicated by the large arrows in fig. 1; its angular frequency is $\omega_m \approx 10^3$ rad s^{-1}. The zero-field shape of the cavity is chosen so that $\delta_1 \approx 3.3\omega_m + 3i\beta$, $\delta_2 \approx 2.8\omega_m - 2i\beta$, $\delta_3 = -\delta_2^*$, and $\delta_4 = -\delta_1^*$ ((operating frequency) ≈ 500 Hz)[‡1].

[‡1] Mode 2 is unstable on time scales of order the electromagnetic damping time [$\mathrm{Im}(\delta_2) \approx -2\beta$]. This weak instability is of no concern for measurements made on much shorter time scales; it can be eliminated by using "artificial damping".

The lobes have been placed so that they couple strongly to a gravitational wave with "cross" polarization propagating along the axis of the microwave cavity and so that the resulting motion of the walls strongly couples the electromagnetic modes ($\mathcal{L} \sim R$). Such a wave, with dimensionless amplitude h, characteristic time $\tau_g \approx \delta_1^{-1}$, and duration $\hat{\tau}$, changes the amplitude of μ by an amount

$$|\Delta\mu_0| \approx (1/6)h(\omega_1\hat{\tau})\,(l/R)\,(\hat{\tau}/\tau_g) \approx 3 \times 10^{-13},$$

for $h \approx 2 \times 10^{-21}$ and $\hat{\tau} \approx 3\tau_g \approx 10^{-3}$ s. This sensitivity goal is comparable to the most optimistic design goals for 1 km baseline laser systems and third-generation bar antennas.

To detect the wave, one must be able to monitor this small change in c_2. For example, one might probe the magnetic field in mode 2 using a small wire loop whose output is fed into a standard linear amplifier Such a linear system attempts to measure c_2 as a function of time, which means measuring both c_2 and $\dot{c}_2$; the uncertainty principle ($(\Delta c_2)\,(\Delta\dot{c}_2) \geqslant 2\pi\hbar$) guarantees that the system cannot determine μ with greater precision than $|\Delta\mu| \geqslant (2N_1)^{-1/2} \approx 6 \times 10^{-14}$. This limit is small enough that a standard linear system, provided it is nearly quantum-limited, can detect the desired change in c_2. It should be noted that systems which do not attempt to measure both c_2 and $\dot{c}_2$ (quantum-nondemolition systems [8]) can, in principle, achieve greater precision.

Another serious problem is Nyquist noise (thermal fluctuations) in the cavity walls. To achieve a signal-to-noise ratio of 5 for an integration time $\approx \hat{\tau}$ requires

$$h \gtrsim 10\,(\tau_g^2/l)\,(8kT_m/M\tau_m^*\hat{\tau})^{1/2} \approx 2 \times 10^{-21},$$

for wall temperature $T_m \approx 3 \times 10^{-3}$ K and mechanical damping time $\tau_m^* = \beta_m^{-1} \approx 2 \times 10^3$ s, which corresponds to a mechanical $Q \approx 10^6$. The mass, wall temperature, and mechanical Q assumed here are similar to those projected for third-generation aluminum-bar antennas. Thermal fluctuations in mode 2 itself produce, after a time $\approx \hat{\tau}$, a root-mean-square change in μ of

$$|\Delta\mu| \approx [(2kT_e/U_1)\,(\hat{\tau}/\tau^*)]^{1/2} \approx 2 \times 10^{-14},$$

for electromagnetic temperature $T_e \approx 4$ K and damping time $\tau^* = \beta^{-1} \approx 3$ s. The corresponding electromagnetic

$Q \approx 10^{10}$ has been attained and exceeded in small superconducting cavities excited in a fundamental mode [9]. This discussion of Nyquist noise assumes that one can couple to mode 2 strongly enough to measure the small change in c_2 in a time $\approx \hat{\tau}$. If a longer integration time is required, Nyquist noise will be a more serious problem.

It should not be difficult to design low-frequency microwave cavity detectors which operate over a wide range of frequencies as detectors of either pulsed or CW radiation. For example, by changing its zero-field shape and mechanical eigenfrequency, the detector described here can be modified to operate at lower frequencies ($\nu \sim$ 10–100 Hz). Another possible design consists of two long cavities at right angles, weakly coupled and excited in a high-frequency mode in which the two cavities oscillate in phase. A gravitational wave propagating in the direction perpendicular to the plane of the cavities induces transitions into a mode in which the two cavities oscillate out of phase. Alternatively, one could omit the weak coupling and operate the two cavities as a Fabry–Perot interferometer. This design has been suggested by Pegoraro et al. [5] to detect CW radiation from known binary star systems; however, Nyquist noise in the walls and seismic noise (earth vibrations) would pose severe problems for such an attempt. Operated as a detector of pulses in the same frequency band as the detector described here, this design would have comparable sensitivity.

Although I have referred to these coupled electro–mechanical systems as microwave cavity detectors, they can also be regarded as purely mechanical detectors with a particular kind of electromagnetic transducer. Viewed in this way, they are similar to Braginsky's [10] proposal to instrument a bar detector with a microwave cavity transducer. In the Braginsky scheme a small microwave cavity, which narrows at one place to a small gap, sits on the end of the bar; the cavity's fundamental mode is excited off-resonance, and movement of the wall at the gap induces on-resonance excitation of the same mode. The main distinguishing features of the design considered here are that the cavity is much larger, the coupling to wall motion occurs over virtually the entire cavity boundary, and – perhaps most important – the signal to be detected appears in a mode which is spatially distinct from the highly excited mode. This last feature may be very important in reducing contamination due to the large field in mode 1 when one attempts to monitor the very weak field in mode 2.

For helpful suggestions I thank R.W. P. Drever, K.S. Thorne, and M. Zimmermann.

References

[1] V.B. Braginsky, C.M. Caves and K.S. Thorne, Phys. Rev. D15 (1977) 2047.
[2] C.M. Caves, papers in preparation.
[3] V.B. Braginsky and M.B. Menskii, Pis'ma Zh. Eksp. Teor. Fiz. 13 (1971) 585 [Sov. Phys. JETP Lett. 13 (1971) 417].
[4] C.M. Caves, in: K.S. Thorne's August, 1977 research proposal to NASA for renewal of research grant NGR 05-002-256 on Experimental tests of gravitation theories.
[5] F. Pegoraro, E. Picasso and L.A. Radicati, J. Phys. A, to be published.
[6] F.K. Manasse and C.W. Misner, J. Math. Phys. 4 (1963) 735.
[7] A.M. Volkov, A.A. Izmest'ev and G.V. Skrotskii, Zh. Eksp. Teor. Fiz. 59 (1970) 1254 [Sov. Phys. JETP 32 (1971) 636].
[8] K.S. Thorne, R.W.P. Drever, C.M. Caves, M. Zimmermann and V.D. Sandberg, Phys. Rev. Lett. 40 (1978) 667.
[9] H. Pfister, Cryogenics 16 (1976) 17.
[10] V.B. Braginsky and A.B. Manukin, Measurement of weak forces in physics experiments, ed. D.H. Douglass (Univ. of Chicago Press, Chicago, 1977) p. 11.

CHAPTER 3

ON THE MEASUREMENT OF A WEAK CLASSICAL FORCE COUPLED TO A QUANTUM MECHANICAL OSCILLATOR

This chapter is a paper by Carlton M. Caves, Kip S. Thorne, Ronald W. P. Drever, Vernon D. Sandberg, and Mark Zimmermann. It has been submitted for publication to Reviews of Modern Physics. The paper is the first part of a two-part treatise dealing with the question of making "quantum nondemolition" measurements of harmonic oscillators. Part One (this chapter) concentrates on issues of principle; Part Two will consider issues of practice. The research reported in this chapter was supported in part by the National Aeronautics and Space Administration [NGR 05-002-256 and a grant from PACE] and by the National Science Foundation [AST76-80801 A02].

I. INTRODUCTION

Consider a very classical incoming signal — i.e., a signal carried by a boson field with occupation number (number of quanta per quantum mechanical state) huge compared to unity. The signal is coupled weakly to a (quantum mechanical) harmonic oscillator — so weakly in fact that, if the oscillator is initially unexcited, the signal can deposit into it an average of only a few quanta per cycle; perhaps even much less than one. The objective is to measure the incoming signal by monitoring some aspect of the oscillator's motion. Question: With what accuracy can the signal be measured? Answer: With arbitrary accuracy, in principle. So long as one concerns oneself only with limitations imposed by nonrelativistic quantum mechanics, and so long as the signal is arbitrarily classical, then no matter how weak may be the coupling of the signal to the oscillator, it can be measured arbitrarily accurately.

However, to obtain good accuracy when the coupling is weak, one must not monitor the oscillator's state using currently standard methods. Those methods ask the oscillator "What is your amplitude and phase of oscillation?" — and because amplitude and phase are noncommuting observables, the uncertainty principle forbids a precise answer. For such "amplitude-and-phase" methods the amplitude error, expressed in terms of the number of oscillator quanta N, must exceed $(\Delta N)_{min} = (N + \frac{1}{4})^{\frac{1}{2}}$; the phase error (for large N) must exceed $(\Delta\psi)_{min} = \frac{1}{2} N^{-\frac{1}{2}}$ (Serber and Townes, 1960; Braginsky, 1970; Giffard, 1976). These errors prevent accurate measurement of the incoming signal, and prevent any measurement at all in the case of weak signals.

To measure the signal more accurately, one must ask the oscillator for less information about itself — "less is more"![1] Specifically, one must ask the oscillator for the value of only one observable, and it must be an observable whose future values are precisely predictable (in the absence of forces) from the result of an initial, precise measurement. The signal is then detected by the changes it produces in the values of this observable.

A well-known technique of this type is "quantum counting." This technique asks the oscillator, "How many quanta N do you have in yourself? — But don't tell me anything about your phase." In principle the query can be repeated over and over again, and the answers can be completely precise and predictable (no uncertainty!) in the absence of external forces. When $N \gg 1$, quantum counting can reveal, in principle, an incoming signal far weaker than those detectable by the "amplitude-and-phase" method. However, it cannot detect signals so weak as to change N by less than unity; and for strong signals, it cannot measure the signal strength more precisely than a factor ~ 3 (cf. Sec. II.D below).

Recently the authors of this article have proposed new methods of measurement (Thorne et al., 1978,1979). In these methods one says to the oscillator, "What is the real part of your complex amplitude? — But don't tell me anything about the imaginary part." In principle the query can be repeated as often as desired, the answers can come through with arbitrary accuracy, and they can lead to an arbitrarily accurate monitoring of an arbitrarily weak, classical incoming signal. We call such measurements "back-action-evading" because they permit the real part of the complex amplitude to evade the back-action forces of the measuring apparatus (at the price of increasing the back-action forces on the imaginary part of the amplitude).[2]

The problem of measuring classical signals with a weakly coupled

oscillator arises in a variety of contexts — e.g., in experiments to detect gravitational radiation; in the reception of long-wavelength electromagnetic waves using antennas that are very small compared to a wavelength; in experiments to test general relativity (e.g., Eötvös experiments); in gravimeters, gravity gradiometers, accelerometers, gyroscopic devices (inertial navigators, gyrocompasses, guidance systems); and elsewhere. In most of these areas quantum mechanical properties of the oscillator are not an issue at present or even in the near future; but they may become an issue in the more distant future — and, equally importantly, the back-action-evading methods of measurement described in this paper may improve the signal-to-noise ratio even in the classical regime.

The task of detecting gravitational waves was the immediate motivation for our interest in quantum mechanical oscillators as detectors of classical signals. A long-range goal is to detect millisecond-duration bursts of gravitational waves from supernovae at a sufficient distance (the Virgo cluster of galaxies) to guarantee several events per year (see, e.g., Thorne, 1978 or Epstein and Clark, 1979). Bursts from that distance are predicted to have a quantum mechanical occupation number $n \sim 10^{75}$ for states with the wave vector inside the solid angle, $\Delta\Omega \sim 10^{-38}$ steradians, subtended at Earth by the source (cf. Eqs. 6-8 of Thorne et al., 1979). The occupation number averaged over all states in the roughly 45-degree beam width of the antenna is $\bar{n} \sim 10^{37}$. This is also the mean number of gravitons that interact with the antenna during one cycle as the wave burst passes. Clearly, the force of these gravitons on the antenna should be highly classical. Unfortunately, a resonant-bar antenna of mass m couples so weakly to these waves that they can change the number of phonons in its fundamental mode by only $\delta N \lesssim 0.4\ (N + \frac{1}{2})^{\frac{1}{2}}\ (m/10\ \text{tons})$ (cf. Thorne, 1978) — a change so small that with standard "amplitude-and-phase" methods of measurement, the uncertainty

principle prevents detection. The 1979 gravitational-wave detectors will be several orders of magnitude away from this limit, but the limit might be reached in 5 or 10 years.

A Russian experimenter, Vladimir Braginsky, called attention to this problem in 1974 in a series of lectures at American centers for experimental relativity (Stanford, LSU, MIT, Princeton, and Caltech; see Braginsky, 1977). Braginsky and Vorontsov (1974) proposed circumventing the problem by replacing amplitude-and-phase methods with "phonon counting." It did not, and does not, seem practical to count the phonons directly. Instead one might, Braginsky and Vorontsov suggested, couple the bar to a microwave cavity, thereby converting phonons into microwave quanta; measure the number of microwave quanta; and thereby monitor changes in the number of phonons in the bar. Braginsky and Vorontsov (1974) proposed a specific method of measuring the number of microwave quanta; see also Braginsky, Vorontsov, and Krivchenkov (1975). Three years later Unruh (1977, 1978) proved that this Braginsky-Vorontsov method is flawed; and Braginsky, Vorontsov, and Khalili (1977) found the flaw in their original, unpublished analysis. However, in these same papers Unruh (1977, 1978) and Braginsky et al. (1977) proposed new methods of measuring the number of microwave quanta — methods that still look viable in principle.

Unfortunately, any quantum-counting technique at acoustical or microwave frequencies, including the new Unruh and Braginsky techniques, may be extremely difficult to implement in practice. This is because, to avoid perturbing the number of quanta $\hat{N}$ while measuring it, one must construct an interaction Hamiltonian that commutes with $\hat{N}$; such a Hamiltonian must be quadratic (or quartic or ...) in the amplitude of the oscillator; and at these frequencies it is extremely difficult to construct quadratic couplings with negligible linear admixtures. For this reason we think that a linearly

coupled "back-action-evading" measurement is more promising, for gravitational-wave detection, than phonon counting.

Braginsky has used the phrase "quantum nondemolition" to describe a measurement which, in principle, can be made time after time on a single system, giving always the same precise result in the absence of external forces (signals). Quantum counting can be done accurately and predictably in either a demolition or a nondemolition mode: The Unruh-Braginsky phonon-counting methods are nondemolition in the limit that one takes arbitrarily long to perform a measurement; photon counting with X-ray proportional counters is demolition. Our proposed back-action-evading measurements of the real part of the complex amplitude are nondemolition in principle. For further discussion of the phrase "quantum nondemolition" see Secs. II.E and IV below.

This paper serves two purposes: First, it reviews those aspects of the measurement of classical signals with a quantum mechanical oscillator which we think are important (i) for a conceptual understanding of the subject, and (ii) for the future development of the subject. Second, it presents in detail our own new ideas on back-action-evading measurements of oscillators. This paper does not attempt a review of efforts to detect gravitational waves. For that topic see, instead, Tyson and Giffard (1978), Braginsky and Rudenko (1978), or Douglass and Braginsky (1979).

This paper is Part One of a two-part treatise. Part One deals with issues of principle; Part Two (Paper II) deals with practical realizations of back-action-evading measurements. The two Parts rely very little on each other. It should be easy to read one without reading the other, but it may not be easy to wade through either one.

This paper consists of three major sections. In Sec. II we discuss measurements of a quantum mechanical oscillator from a somewhat formal, mathematical point of view. Section II.A gives examples of the types of oscillators, both mechanical and electromagnetic, that we consider; it motivates our neglect of fluctuations due to Nyquist forces; and it introduces a single, unified mathematical description of the various oscillators. Section II.B derives and discusses the constraints that the Heisenberg uncertainty principle places on measurements of an oscillator; and it introduces the three types of measurement which we consider: amplitude-and-phase measurements, quantum-counting measurements, and back-action-evading measurements. These three types of measurement are then analyzed, each in turn, in Secs. II.C, D, E, with emphasis on the accuracy with which each type of measurement can monitor a classical force. Section II.F presents and discusses several different interaction Hamiltonians which could be used in back-action-evading measurements of the real part of the complex amplitude. (Practical realizations of these Hamiltonians are discussed in Paper II.) Section II.G discusses the zero-frequency limit of back-action-evading measurements — i.e., back-action-evading measurements of "free masses."

In Sec. III we describe gedanken experiments of the back-action-evading type in which, in principle, one can measure the real part of the complex amplitude arbitrarily quickly and accurately. Section III.A deals with measurements of free masses; Sec. III.B with measurements of harmonic oscillators. Much of the detailed discussion of these gedanken experiments is relegated to Appendices A-C.

In Sec. IV we use the results of preceding sections as a foundation for a general discussion of "quantum nondemolition measurements" in nonrelativistic quantum theory.

II. FORMAL DISCUSSION OF MEASUREMENTS OF HARMONIC OSCILLATORS

A. Mathematical Description of the Oscillator

The oscillators that we study are macroscopic in size. An example is the fundamental mode of mechanical oscillation of a monocrystal of sapphire with mass M ~ 100 kg. Such crystals, cooled to a few millidegrees, might be used 5 to 10 years hence as third-generation resonant-bar detectors for gravitational waves (cf. Braginsky, 1974; and the lectures by Braginsky, Douglass, and Weber in Bertotti, 1977). Such a crystal contains ~ 3×10^{27} atoms, and therefore its mechanical oscillations have ~ $3 \times (3 \times 10^{27})$ degrees of freedom. The fundamental mode is one of those degrees of freedom, and it is almost completely decoupled from all the others. The strength of its coupling to other modes is quantified by its "Q" — which is the number of radians of oscillation required for its energy to decrease by a factor 1/e (due to "friction" against the other modes), from an initial energy far above thermal. A Q of 4.2×10^9 has been achieved with a small, doubly convex quartz lens at 2 °K by Smagin (1974); a Q of 5×10^9 has been achieved for a 1 kg sapphire crystal at 4.3 °K by Bagdasarov et al. (1977); a Q of 2×10^9 has been achieved with a 4.9 kg silicon crystal at 3.5 °K by McGuigan et al. (1978); and it is not unreasonable to hope for Q ~ 10^{13} at a temperature of a few millidegrees.

The coupling to other modes produces not only friction; it also produces fluctuating forces ("Nyquist forces") which cause the amplitude of the fundamental mode to random walk. In thermal equilibrium the mean number of phonons in the fundamental mode is $\bar{N} = kT/\hbar\omega \sim 10^4$ for $T \sim 0.003$ °K and $\omega/2\pi \sim 5000$ Hz. In a time interval $\Delta t \ll Q/\omega$ the number of phonons random walks by $\Delta N \sim \bar{N}(2\omega\Delta t/Q)^{\frac{1}{2}}$. Hence, a change of unity requires a mean time of $\Delta t \sim Q/(2\omega\bar{N}^2) \sim 1$ sec if $Q \sim 10^{13}$. This is very long compared to the 0.2 millisecond period of the fundamental mode — so long, in fact, that for

such a crystal Nyquist forces should be totally negligible compared to noise and quantum mechanical uncertainties in the device that measures the crystal's oscillations.

An obvious second example of a macroscopic oscillator is an electrical LC circuit.

A third example is a normal mode of electromagnetic oscillation of a microwave cavity with superconducting walls. Such cavities are being used as displacement sensors for resonant-bar gravitational-wave detectors (Braginsky, Panov et al., 1977), and they have been proposed as the fundamental element in a new type of gravitational-wave detector (Braginsky, Grishchuk et al., 1973; Grishchuk and Sazhin, 1975; Pegoraro, Picasso, and Radicati, 1978; Caves, 1979) and in other gravity experiments (Braginsky, Caves, and Thorne, 1977). The normal modes of such a cavity have Q's of $\sim 10^{11}$ to 10^{12} (Pfister, 1976; Allen et al., 1971) — high enough that for some purposes one can ignore thermal (Nyquist) fluctuations in the electromagnetic field.

Nyquist forces not only are negligible in some contexts of interest; they are also irrelevant to the issues of principle which this paper addresses. Therefore, we shall ignore them until Paper II — i.e., we shall assume that the one mode of interest can be treated as a harmonic oscillator which couples only to (i) the weak classical signal which we seek to measure, and (ii) our measuring system.

The oscillator is characterized by its canonical coordinate $\hat{x}$ and momentum $\hat{p}$, which are Hermitian operators (observables); and by its mass m and angular frequency ω. If the oscillator is the fundamental mode of a resonant bar, we shall normalize $\hat{x}$ to equal the displacement from equilibrium of the end of the bar. Then m will be roughly half the mass of the bar; and, when the bar is decoupled from the measuring apparatus, $\hat{p}$ will be approximately the momentum of the right half of the bar relative to its center. If the oscillator is an LC circuit, we shall normalize $\hat{x}$ to equal the charge on

the capacitor. Then m will be the inductance, and $\hat{p}$ will be the magnetic flux in the inductor. If the oscillator is a normal mode of a microwave cavity, we shall normalize m to equal unity. Then $\hat{x}$ can be $(V/4\pi\omega^2)^{\frac{1}{2}} \times$ (mean magnetic field in cavity), and $\hat{p}$ can be $(V/4\pi)^{\frac{1}{2}} \times$ (mean electric field in cavity), where V is the cavity volume.

No matter what the nature of the oscillator may be, its coordinate and momentum have the commutator

$$[\hat{x},\hat{p}] = i\hbar \; ; \tag{2.1}$$

its Hamiltonian is

$$\hat{H}_o \equiv \hat{p}^2/2m + \tfrac{1}{2} m\omega^2 \hat{x}^2 \; ; \tag{2.2}$$

its creation and annihilation operators are

$$\hat{a}^\dagger = \left(\frac{m\omega}{2\hbar}\right)^{\frac{1}{2}} \left(\hat{x} - i\,\frac{\hat{p}}{m\omega}\right), \qquad \hat{a} = \left(\frac{m\omega}{2\hbar}\right)^{\frac{1}{2}} \left(\hat{x} + i\,\frac{\hat{p}}{m\omega}\right) ; \tag{2.3}$$

and the operator representing the number of quanta is

$$\hat{N} = \hat{a}^\dagger\hat{a} = \hat{H}_o/\hbar\omega - \tfrac{1}{2} \; . \tag{2.4}$$

In addition to these standard operators, which one finds in most quantum mechanics textbooks, it is useful to introduce the quantities

$$\hat{X}_1(\hat{x},\hat{p},t) \equiv \hat{x} \cos \omega t - (\hat{p}/m\omega) \sin \omega t \; , \tag{2.5a}$$

$$\hat{X}_2(\hat{x},\hat{p},t) \equiv \hat{x} \sin \omega t + (\hat{p}/m\omega) \cos \omega t \; . \tag{2.5b}$$

It is straightforward to show that

$$\hat{x} + i\hat{p}/m\omega = (\hat{X}_1 + i\hat{X}_2)\, e^{-i\omega t} \; . \tag{2.6}$$

Thus, $\hat{X}_1 + i\hat{X}_2$ is the quantum mechanical analogue of the oscillator's classical "complex amplitude." As in the classical limit, so also in the Heisenberg picture of quantum mechanics, $\hat{X}_1$ and $\hat{X}_2$ are conserved in the absence of interactions with the outside world:

$$\frac{d\hat{X}_j}{dt} = \frac{\partial \hat{X}_j}{\partial t} - \frac{i}{\hbar}[\hat{X}_j, \hat{H}_o] = 0. \tag{2.7}$$

$\hat{X}_1$ and $\hat{X}_2$ are Hermitian operators and are therefore observables. One can show that they, and linear combinations of them with constant coefficients, are the only conserved observables that are linear functions of $\hat{x}$ and $\hat{p}$. Notice that $\hat{X}_1$ and $\hat{X}_2$ have explicit time dependence (Eqs. 2.5). In this they differ from all the other observables considered above ($\hat{x}$, $\hat{p}$, $\hat{H}_o$, $\hat{N}$) and from most, but not all, observables that one encounters in quantum theory.

B. The Uncertainty Principle and Ways to Measure the Oscillator

In classical theory it is possible to measure the oscillator's complex amplitude $X \equiv X_1 + iX_2$ with complete precision. Not so in quantum theory. Equations (2.1) and (2.5) imply that $\hat{X}_1$ and $\hat{X}_2$ do not commute:

$$[\hat{X}_1, \hat{X}_2] = i\hbar/m\omega \ . \tag{2.8}$$

Therefore, the variances of $\hat{X}_1$ and $\hat{X}_2$ in any oscillator state must satisfy

$$\Delta X_1 \, \Delta X_2 \geq \frac{1}{2} \left| \langle [\hat{X}_1, \hat{X}_2] \rangle \right| = \hbar/2m\omega \ , \tag{2.9a}$$

which is the complex-amplitude analogue of the Heisenberg uncertainty principle for position and momentum:

$$\Delta x \, \Delta p \geq \hbar/2. \tag{2.9b}$$

One can think of x and $p/m\omega$ as Cartesian coordinates in a phase plane (we divide by $m\omega$ to make both coordinates have dimensions of length). Then X_1 and X_2 are Cartesian coordinates that rotate clockwise with angular velocity ω relative to the $(x, p/m\omega)$ coordinates (cf. Eqs. 2.5 and 2.6). The uncertainty relations $\Delta X_1 \Delta X_2 \geq \hbar/2m\omega$, $\Delta x \Delta p/m\omega \geq \hbar/2m\omega$ are equivalent manifestations of the fact that any quantum mechanical state is characterized by an "error box" in the phase plane with area at least $\pi\hbar/2m\omega$; see Fig. 1.

The standard method for measuring the motion of a macroscopic oscillator is to couple it to a canonical-coordinate (x) transducer whose output is proportional to x, and to feed the output into an amplifier. Figure 2 shows a simple example where the oscillator is an LC circuit (part a, to left of dashed line). In this example, x is the charge on the capacitor, p is the flux through the inductor, no transducer is needed, and the amplifier (part b) produces an output voltage $A \cdot Q$ proportional to the total charge Q that flows through it ("zero-impedance charge amplifier"). The amplifier necessarily is noisy. As a minimum, it has noise due to uncertainty-principle constraints on its internal dynamical variables. If this is its only noise, it is called an "ideal amplifier." Viewed non-quantum-mechanically, the noise is of two types: (i) a stochastically fluctuating noise current $I_n(t) \equiv dQ_n/dt$ which, in the case of Fig. 2, gets superimposed on the amplifier's input [so $V_{out} = A \cdot (x + Q_n)$]; and (ii) a noise voltage $V_n(t)$ which, in Fig. 2, produces a driving force on the oscillator and thereby changes its momentum ($\dot{p} = L\ddot{x} = V_n$).

It is useful to distinguish two types of measurements that can be made with such a system: "quick measurements" and "amplitude-and-phase measurements."

In a quick measurement one reads out the amplifier output in a time τ short compared to the oscillator period ($\omega\tau \ll 1$; "broad-band amplifier"). From the output one infers the instantaneous coordinate x of the oscillator to within a precision, for the example in Fig. 2,

$$\delta x_o \simeq (S_Q/2\tau)^{\frac{1}{2}} . \tag{2.10a}$$

Here S_Q is the spectral density of the amplifier's noise charge $Q_n(t) \equiv \int I_n dt$, and $1/2\tau$ is the bandwidth of the measurement. During this measurement the amplifier's "back-action" noise voltage $V_n(t)$ kicks the oscillator, producing an unpredictable momentum change:

$$\delta p_o = \int V_n dt \simeq (S_V/2\tau)^{\frac{1}{2}}\, \tau/2, \tag{2.10b}$$

where S_V is the spectral density of the noise voltage $V_n(t)$.[3] The Heisenberg uncertainty principle places the constraint

$$(S_V\, S_Q)^{\frac{1}{2}} \geq 2\hbar \tag{2.11}$$

on the noise performance of any zero-impedance charge amplifier (cf. Weber, 1959; Heffner, 1962; Eq. 3.7 below). Thus, even with an ideal amplifier, a quick measurement produces an uncertainty product

$$\delta x_o \cdot \delta p_o \simeq \tfrac{1}{4} (S_V\, S_Q)^{\frac{1}{2}} \geq \hbar/2 . \tag{2.12}$$

This simple example illustrates how the Heisenberg uncertainty principle is enforced in any quick measurement of precision δx_o: Back-action forces from the measuring system always perturb the oscillator's momentum by an amount $\delta p_o \gtrsim (\hbar/2)(1/\delta x_o)$.

A quick measurement produces an uncertainty error box which, for $\delta x_o \ll \delta p_o/m\omega$, is a long thin ellipse in the phase plane (Fig. 3a). As time

passes, the oscillator's "system point" rotates clockwise in the phase plane:

$$x + ip/m\omega = (X_1 + iX_2)e^{-i\omega t}, \qquad X_1 + iX_2 = \text{constant} \tag{2.13}$$

(Eqs. 2.6 and 2.7), and thus its error box also rotates clockwise; see Fig. 3a. As a result, if one tries to predict the outcome of a second quick measurement of x, the error in the prediction oscillates in time between δx_o and $\delta p_o/m\omega \geq (\hbar/2m\omega)(1/\delta x_o)$:

$$\delta x(t) = [(\delta x_o)^2 \cos^2\omega t + (\delta p_o/m\omega)^2 \sin^2\omega t]^{\frac{1}{2}} . \tag{2.14}$$

If one wants the maximum of these oscillations to be as small an error as possible, one must arrange for the error box to be round and to have the minimum allowed radius $\delta x_o = \delta p_o/m\omega = \delta X_1 = \delta X_2 = (\hbar/2m\omega)^{\frac{1}{2}}$. An ideal measurement with these uncertainties will necessarily drive the oscillator into a quantum mechanical "coherent state" — i.e., a state with a minimum-uncertainty Gaussian wave packet that undergoes classical, oscillatory motion without spreading; see, e.g., Merzbacher (1970).

Turn now from "quick measurements" to "amplitude-and-phase measurements." In such measurements one uses an amplifier that amplifies only a narrow band of frequencies $\Delta\omega \ll \omega$ centered on the oscillator frequency ω. Such an amplifier produces a sinusoidal output with complex amplitude $(V_1 + iV_2) = A \cdot (\bar{X}_1 + i\bar{X}_2)$, where $\bar{X}_1 + i\bar{X}_2$ is a time average of the oscillator's amplitude (averaging time $\tau = \pi/\Delta\omega \gg 1/\omega$). The accuracy of the measurement is constrained by the amplifier's superimposed noise (Q_n in Fig. 2), and by its back-action noise (V_n in Fig. 2). These noises affect the measurement amplitudes $\bar{X}_1$ and $\bar{X}_2$ equally (neither phase is preferred), producing the following probable error when S_V/S_Q is optimized:

$$\delta\bar{X}_1 = \delta\bar{X}_2 \simeq \left[\frac{\frac{1}{2}(S_V S_Q)^{\frac{1}{2}}}{2m\omega}\right]^{\frac{1}{2}} \geq \left(\frac{\hbar}{2m\omega}\right)^{\frac{1}{2}} . \tag{2.15}$$

In the complex-amplitude plane (phase plane) the error box is round; see Fig. 3b. We call such measurements "amplitude-and-phase" because they attempt to determine both the oscillator's absolute amplitude $|X| \equiv |X_1 + iX_2| = (X_1^2 + X_2^2)^{\frac{1}{2}}$ (or equivalently its energy or number of quanta), and its phase[4] $\psi \equiv \tan^{-1}(X_2/X_1)$.

An "ideal" amplitude-and-phase measurement (one with the minimum possible noise) will drive the oscillator into a quantum mechanical coherent state with a round error box of radius $\Delta x = \Delta p/m\omega = \Delta X_1 = \Delta X_2 = (\hbar/2m\omega)^{\frac{1}{2}}$. Moreover, for such an ideal measurement the probability distribution of the measured values of X_1 and X_2 is a two-dimensional Gaussian, centered on the expectation value $(\langle\hat{X}_1\rangle, \langle\hat{X}_2\rangle)$ of $\hat{X}_1$ and $\hat{X}_2$ with variances $\Delta X_1 = \Delta X_2 = (\hbar/2m\omega)^{\frac{1}{2}}$. From the measured values of X_1 and X_2, one can infer the oscillator's number of quanta and its phase. It is easy to verify from the Gaussian distribution that the expected value of the inferred number of quanta is $N = (m\omega/2\hbar)(\langle\hat{X}_1\rangle^2 + \langle\hat{X}_2\rangle^2)$, and the variance is $\Delta N = (N + \frac{1}{4})^{\frac{1}{2}}$. For large N the expected value of the inferred phase is $\psi = \tan^{-1}(\langle X_2\rangle/\langle X_1\rangle)$, and the variance is $\Delta\psi = \frac{1}{2}N^{-\frac{1}{2}}$. These variances associated with a coherent state are the minimum possible errors obtainable by the amplitude-and-phase method.

Henceforth, we shall call these minimum errors the "standard quantum limits" for amplitude-and-phase measurements:

$$\left.\begin{array}{l}\text{Standard}\\ \text{Quantum}\\ \text{Limits}\end{array}\right\} \quad \begin{array}{l}\Delta x = \Delta p/m\omega = \Delta X_1 = \Delta X_2 = (\hbar/2m\omega)^{\frac{1}{2}},\\ \Delta N = (N + \frac{1}{4})^{\frac{1}{2}} \quad , \quad \Delta\psi = \frac{1}{2}N^{-\frac{1}{2}} \quad \text{for} \quad N \gg 1.\end{array} \tag{2.16}$$

The fact that these are the very best measurement precisions achievable by the amplitude-and-phase method was first discovered, in the context of

mechanical oscillators and gravitational-wave detection, by Braginsky (1970), and was first proved with generality by Giffard (1976). However, these amplitude-and-phase limits have long been known in the field of quantum electronics; see, e.g., Serber and Townes (1960).

For a mechanical oscillator of the type to be used in gravitational-wave detection ($m \lesssim 10$ tons, $\omega/2\pi \simeq 1000$ Hz), the standard quantum limit is $\Delta X_j = (\hbar/2m\omega)^{\frac{1}{2}} \gtrsim 1 \times 10^{-19}$ cm. This is slightly larger than the amplitude changes one expects from a gravitational wave burst due to a supernova explosion in the Virgo cluster of galaxies. Thus, amplitude-and-phase measurements of resonant-bar antennas do not look promising for gravitational-wave astronomy (Braginsky, 1977; cf. Sec. I of this paper).

"Quantum counting" is an alternative method of measuring a harmonic oscillator. An ideal quantum counter can measure the number operator $\hat{N}$ of the oscillator with complete precision, and can give repeatedly the same result for a sequence of measurements of $\hat{N}$ if no external forces are acting on the oscillator. Equations (2.4) and (2.5) imply

$$\hat{N} = \tfrac{1}{2}(m\omega/\hbar)(\hat{X}_1^2 + \hat{X}_2^2) - \tfrac{1}{2} . \qquad (2.17)$$

Hence, a measurement of $\hat{N}$ is equivalent to a measurement of the absolute amplitude $|X| = (X_1^2 + X_2^2)^{\frac{1}{2}}$ of the oscillator. Such a measurement, with complete precision, must leave the phase $\psi = \tan^{-1}(X_2/X_1)$ completely undetermined. In the phase plane the error box for such a measurement is an annulus (Fig. 3c). If one attributes to this error annulus a thickness corresponding to $\delta N = 1$, then its area is $4\pi(\hbar/2m\omega)$ — i.e., four times the minimum allowable area.

Quantum counters with high efficiency (high precision) are common devices for photons of optical frequency and higher — e.g., photo-diodes, and X-ray

proportional counters. These counters are all demolition devices; they destroy the photons they count. For photons at infrared frequencies and below, and for phonons at acoustical frequencies, quantum counters with reasonable efficiency are not yet available. Unruh (1977, 1978) and Braginsky, Vorontsov, and Khalili (1977) have suggested designs of nondemolition devices for measuring the number of photons in a microwave cavity; and Braginsky and Vorontsov (1974) have proposed that one couple such a cavity to a resonant bar thereby converting bar phonons into cavity photons, measure the number of cavity photons, and thereby monitor changes in the number of bar phonons.

Recently the authors (Thorne et al., 1978, 1979) have proposed yet another method of measuring an oscillator: a "back-action-evading" measurement of the real part of the complex amplitude, X_1 (or, if one prefers, of the imaginary part X_2). In this method one measures X_1 with high precision; and in the process, in accordance with the uncertainty principle (2.9a), one perturbs X_2 by a large amount. In other words, the measuring apparatus is carefully designed so its back-action force drives X_2, leaving X_1 largely unscathed; and because X_1 and X_2 are separately conserved, the resulting large uncertainty in X_2 does not feed back onto X_1 as the oscillator evolves. This means that a sequence of high-precision back-action-evading measurements can give the same result for X_1 time and time again.

The error box for a back-action-evading measurement is a long, thin ellipse (Fig. 3d), and it becomes a vertical line ($\Delta X_1 = 0$, $\Delta X_2 = \infty$) in the limit of a "perfect measurement." It is instructive to compare the back-action-evading error box (Fig. 3d) with the error box for a quick, high-precision measurement of x (Fig. 3a). If a first measurement is made at $t = 0$, when $x = X_1$, the subsequent error boxes are qualitatively the same. As the oscillator evolves, these error boxes remain fixed in the (X_1, X_2) coordinate system (X_1 and X_2 are conserved); but they rotate as seen in the $(x, p/m\omega)$ coordinate system.

It is this simple fact which makes possible a sequence of arbitrarily accurate measurements of X_1 all giving the same result, and forbids a similar sequence of arbitrarily accurate measurements of x.

In the next three subsections we compute, for three types of measurements (amplitude-and-phase, quantum counting, and back-action-evading), the maximum precision with which one can monitor a weak, classical force F(t) that drives the oscillator.

C. Monitoring a Force by the Amplitude-And-Phase Method

Let an oscillator be driven by a weak classical force F(t), so that its Hamiltonian is

$$\hat{H} = \hat{H}_o - \hat{x}F(t); \qquad \hat{H}_o = (\text{expression 2.2}) \quad . \tag{2.18}$$

The classical nature of the force is embodied in the fact that F is a real function of time t rather than an operator. The unitary evolution operator $\hat{U}(t, t_0)$, which governs the evolution of the state vector in the Schrödinger picture, satisfies

$$i\hbar d\hat{U}/dt = \hat{H}(t)\ \hat{U} \quad , \qquad \hat{U}(t_0, t_0) = 1 \quad . \tag{2.19}$$

It is straightforward, using the techniques of §15.9 of Merzbacher (1970), to show that

$$\hat{U}(t, t_0) = \exp[-i(t - t_0)\ \hat{H}_o/\hbar]\ \exp[-i\beta + \alpha\hat{a}^\dagger - \alpha^*\hat{a}] \ , \tag{2.20a}$$

where

$$\alpha(t,t_0) = (2m\omega\hbar)^{-1/2} \int_{t_0}^{t} F(t')i \exp[+i\omega(t' - t_0)]\, dt' \quad , \tag{2.20b}$$

$$\beta(t,t_0) = \int_{t_0}^{t} \frac{1}{2} i(\alpha^*\dot{\alpha} - \alpha\dot{\alpha}^*)\, dt' \quad . \tag{2.20c}$$

Here a dot denotes a time derivative; $\hat{a}$ and $\hat{a}^\dagger$ are the oscillator's annihilation and creation operators (Eq. 2.3); and a star (*) denotes complex conjugation. Notice that α is complex, but β is real. The effect of the force on the oscillator is characterized by the dimensionless quantity α. It will play an important role below.

Now suppose that the oscillator is being studied by a sequence of "amplitude-and-phase" measurements, each of duration $\tau \gtrsim 1/\omega$. How large must the driving force be to produce a measurable change in the oscillator's complex amplitude? Classically the change in complex amplitude during the time τ is

$$\delta(X_1 + iX_2) = \int_0^\tau [F(t')/m\omega]\, ie^{i\omega t'}\, dt'$$

$$= (2\hbar/m\omega)^{\frac{1}{2}}\, \alpha(\tau,0). \tag{2.21}$$

This change is measurable if its absolute magnitude exceeds the diameter of the error box $2(\hbar/2m\omega)^{\frac{1}{2}}$ (standard quantum limit) — i.e., if

$$|\alpha(\tau,0)| \gtrsim 1 \quad \text{"Standard quantum limit."} \tag{2.22a}$$

Note that $|\alpha(\tau,0)|$ has the physical meaning

$$|\alpha(\tau,0)|^2 = \frac{1}{\hbar\omega} \cdot \left[\begin{array}{l}\text{total energy that the force } F(t) \text{ would deposit}\\ \text{in a classical oscillator during time } \tau, \text{ if}\\ \text{the oscillator were initially unexcited}\end{array}\right]$$

$$= \left[\begin{array}{l}\text{the mean number of quanta that the force would}\\ \text{deposit in a quantum mechanical oscillator, if}\\ \text{the oscillator were initially in its ground state}\end{array}\right] . \quad (2.22b)$$

A fully quantum mechanical derivation of the measurability criterion (2.22a) proceeds as follows. Assume that a previous, ideal amplitude-and-phase measurement has left the oscillator in a coherent state (Merzbacher, 1970) at time t = 0:

$$|\psi(0)\rangle = \exp(-\frac{1}{2}|\rho|^2 + \rho\hat{a}^\dagger)|0\rangle , \quad (2.23)$$

where ρ is a complex number and $|0\rangle$ is the ground state. This coherent state has

$$\langle\hat{X}_1 + i\hat{X}_2\rangle = (2\hbar/m\omega)^{1/2}\rho ,$$

$$\Delta X_1 = \Delta X_2 = (\hbar/2m\omega)^{1/2} . \quad (2.24)$$

Then in the Schrödinger picture the oscillator's state at time τ is $|\psi(\tau)\rangle = \hat{U}(\tau,0)|\psi(0)\rangle$, which by virtue of Eqs. (2.23), (2.20a), and the commutator $[\hat{a},\hat{a}^\dagger] = 1$ is

$$|\psi(\tau)\rangle = \exp[-i\tau\hat{H}_o/\hbar]\exp[-i\beta + \frac{1}{2}(\alpha\rho^* - \alpha^*\rho)] \times$$

$$\times \exp[-\frac{1}{2}|\alpha + \rho|^2 + (\alpha+\rho)\hat{a}^\dagger]|0\rangle . \quad (2.25)$$

Here $\alpha = \alpha(\tau,0)$ and $\beta = \beta(\tau,0)$ are given by Eqs. (2.20b,c). This final state, like the initial, is coherent. It has $\langle\hat{X}_1 + i\hat{X}_2\rangle = (2\hbar/m\omega)^{1/2}(\rho + \alpha)$ and $\Delta X_1 = \Delta X_2 = (\hbar/2m\omega)^{1/2}$. Thus, the force F(t) displaces the center of the oscillator's uncertainty circle by

$$\delta\langle \hat{X}_1 + i\hat{X}_2 \rangle = (2\hbar/m\omega)^{1/2}\, \alpha(\tau,0) = \int_0^\tau [F(t')/m\omega]\, ie^{i\omega t'}\, dt' \quad , \quad (2.21')$$

while leaving the size of the error circle unchanged. As expected, this displacement is the same as that derived classically (Eq. 2.21); and because the error circle does not change size, the minimum measurable force (Eq. 2.22a) is also the same. This minimum measurable force has been derived and discussed in the context of gravitation experiments by Braginsky (1970), and with much greater generality by Giffard (1976); see also a recent, very elegant treatment by Hollenhorst (1979).

One might have thought that by a sequence of n measurements one could determine the center of the error circle with accuracy $(\hbar/2m\omega)^{1/2}\,(1/n)^{1/2}$, and thereby could measure a force $(1/n)^{1/2}$ smaller than Eq. (2.22a). This is not the case because each measurement of precision $(\hbar/2m\omega)^{1/2}$ perturbs the location of the error box by an amount $\gtrsim (\hbar/2m\omega)^{1/2}$. Viewed heuristically, a sequence of n measurements produces a "$\sqrt{n}$" random walk of the error box location that cancels the usual "$1/\sqrt{n}$" improvement of measurement accuracy.

D. Monitoring a Force by the Quantum-Counting Method

Next consider quantum-counting measurements of an oscillator on which a classical force is acting. Assume that at time t = 0 a precise measurement of the number of quanta puts the oscillator into an energy eigenstate $|N\rangle$ with N quanta. Then in the Schrödinger picture the oscillator's state evolves to $|\psi(\tau)\rangle = \hat{U}(\tau,0)|N\rangle$ during the time interval τ. From Eq. (2.20a), the commutation relation $[\hat{a},\hat{a}^\dagger] = 1$, and the raising and lowering relations $\hat{a}^\dagger|N\rangle = (N+1)^{1/2}\,|N+1\rangle$, $\hat{a}|N\rangle = N^{1/2}\,|N-1\rangle$, one can derive the probability $P(N \to N';\tau)$ that in the time interval τ the number of quanta changes

from N to N':

$$P(N \to N';\tau) \equiv |\langle N'|\hat{U}(\tau,0)|N\rangle|^2$$

$$= \frac{r!}{s!}\left[L_r^{(s-r)}(|\alpha|^2)\right]^2 |\alpha|^{2(s-r)}\, e^{-|\alpha|^2} \quad , \tag{2.26}$$

where $s \equiv \max(N,N')$, $r \equiv \min(N,N')$, and $L_r^{(n)}(x)$ is the generalized Laguerre polynomial.

The probability that the force has induced any change at all is

$$1 - P(N \to N;\tau) = 1 - e^{-|\alpha|^2}\left[L_N(|\alpha|^2)\right]^2$$

$$= 1 - e^{-|\alpha|^2}(1 - N|\alpha|^2 + \tfrac{1}{4}N(N-1)|\alpha|^4 - \ldots)^2 \quad . \tag{2.27}$$

This probability is significant if and only if $|\alpha|^2 \gtrsim (N+1)^{-1}$, i.e.,

$$|\alpha(\tau,0)| \gtrsim (N+1)^{-1/2} \quad . \tag{2.28}$$

This is the criterion for measurability of the force by quantum-counting techniques. It has been derived and discussed by Braginsky (1970) and by Braginsky and Vorontsov (1974); see also the elegant recent treatment by Hollenhorst (1979).

A semiclassical derivation of criterion (2.28) proceeds as follows: Orient the axes of the complex frequency plane so the (unknowable) phase of the initial state is $\psi = 0$; then the initial energy is $E = \frac{1}{2}m\omega^2 X_1^2$; the initial number of quanta is $N = E/\hbar\omega - \frac{1}{2} = \frac{1}{2}[(m\omega/\hbar)X_1^2 - 1]$; the force-induced change in N is $\delta N = (m\omega/\hbar)X_1\delta X_1 = [(2N+1)(m\omega/\hbar)]^{1/2}\delta X_1$, where $\delta(X_1 + iX_2)$ is given by the classical expression (2.21) except for an unknowable phase; to within a factor of order unity, which is fixed by the unknowable phase, $\delta X_1 \simeq (\hbar/m\omega)^{\frac{1}{2}}|\alpha(\tau,0)|$; the criterion of measurability,

$\delta N \gtrsim 1$, then comes out to be (2.28), to within a factor of order unity.

Criterion (2.28) implies that, no matter how weak the force F may be, and no matter how short the time interval τ between measurements may be, one can detect the force by preparing the oscillator in a sufficiently energetic initial state (state of sufficiently large N).

When F is large enough to be measured (criterion 2.28 satisfied), then the probability distribution (2.26) is not narrowly peaked. Even under the best of circumstances it can reveal $|\int_0^\tau F(t')\, e^{i\omega t'}\, dt'| = (2m\omega\hbar)^{1/2}\, |\alpha(\tau,0)|$ only to within a multiplicative factor of ~ 3 at the 90% confidence level; cf. Fig. 4. This is far from enough information to permit reconstruction of F(t).

On the other hand, if one had an infinite number of oscillators all coupled to the same classical force (e.g., to a gravitational wave), and all excited to sufficiently high energies, then from the statistics of quantum-counting measurements one could compute the probability distribution (2.26), and from it one could infer $|\alpha(t_2,t_1)|^2$ for any desired t_1 and t_2. Equivalently one could infer $|\int_{t_1}^{t_2} F(t')\, e^{i\omega t'}\, dt'|^2$ — which is sufficient to reveal all details of F(t) except an overall, time-independent sign.

E. Monitoring a Force by the Back-Action-Evading Method

Turn next to our proposed "back-action-evading" method of measuring the $\hat{X}_1$ of an oscillator on which a classical force acts.

In principle, nonrelativistic quantum theory permits $\hat{X}_1$ to be measured "arbitrarily quickly and arbitrarily accurately."[5] By this we mean that,

if the oscillator begins the measurement in a near-eigenstate of $\hat{X}_1$, then the measurement can determine the eigenvalue with arbitrary accuracy for any measurement time, no matter how short. We also mean that, regardless of the initial state of the oscillator, the measurement can leave the oscillator in a state arbitrarily close to an eigenstate of $\hat{X}_1$ whose eigenvalue is the measured value ("measurement of the first kind"; Pauli, 1958, and footnote 6 later in this article).

Such an "arbitrarily quick and accurate" measurement can be achieved by a measuring system which satisfies two requirements: (i) the measuring apparatus must be coupled precisely to $\hat{X}_1$ — i.e., it must be coupled to $\hat{X}_1$ and to no other observable of the oscillator; and (ii) the coupling between the measuring apparatus and the oscillator must be arbitrarily strong.[6] When requirement (i) is satisfied, $\hat{X}_1$ is completely shielded from noise in the measuring apparatus; then the arbitrarily strong coupling of requirement (ii) can lead to arbitrarily good accuracy for any measurement time, no matter how short. (The crucial property of $\hat{X}_1$ — that it is completely shielded from the measuring apparatus when requirement (i) is satisfied — is a general property of "quantum nondemolition observables"; for a precise definition of "quantum nondemolition observable" and a proof of this property, see Sec. IV.)

A skeptic will mistrust this justification of our claim that $\hat{X}_1$ can be measured arbitrarily quickly and accurately. He might worry about the perfection with which one can achieve the time-dependent coupling (Sec. II.F below) required for a measurement of $\hat{X}_1$, or he might not believe that $\hat{X}_1$ can be isolated from the measuring apparatus. To alleviate such worries, we describe in Sec. III.B a gedanken experiment which shows that arbitrarily quick and accurate measurements can be made.

Of course in practice there are limits to the quickness and precision with which $\hat{X}_1$ can be measured — limits imposed by the strengths of real materials, voltage breakdown in capacitors, etc. In Paper II we discuss some of these practical issues. Until then, however, we restrict attention to limits of principle which are imposed by nonrelativistic quantum mechanics. In this context the crucial point is that, whereas the uncertainty principle of nonrelativistic quantum theory places severe restrictions on the accuracy of amplitude-and-phase measurements, it places no restriction whatsoever on the speed or accuracy of measurements of $\hat{X}_1$.

We now compute the precision with which one can monitor a classical force $F(t)$ by back-action-evading measurements of $\hat{X}_1$. Our computation is carried out in the Heisenberg picture. Suppose that an initial precise measurement of $\hat{X}_1$, at time $t = t_0$, gives a value ξ_0 and leaves the oscillator in the corresponding eigenstate $|\xi_0\rangle$ of $\hat{X}_1$. (The spectrum of $\hat{X}_1$, like the spectra of $\hat{x}$ and $\hat{p}$, is continuous; thus ξ_0 can be any real number.) As time passes the state of the oscillator remains fixed in the Heisenberg picture, $|\psi(t)\rangle \equiv |\xi_0\rangle$; but $\hat{X}_1$ evolves:

$$\frac{d\hat{X}_1}{dt} = -\frac{i}{\hbar}[\hat{X}_1, \hat{H}] + \frac{\partial \hat{X}_1}{\partial t} = -\frac{F(t)}{m\omega}\sin\omega t \qquad (2.29)$$

(Eqs. 2.18, 2.2, 2.5a, 2.1). Integrating this equation, we obtain

$$\hat{X}_1(t) = \hat{X}_1(t_0) - \int_{t_0}^{t} [F(t')/m\omega]\sin(\omega t')\,dt' \quad . \qquad (2.30)$$

Because $|\psi(t)\rangle = |\xi_0\rangle$ is an eigenstate of $\hat{X}_1(t_0)$, and because $\int_{t_0}^{t} [F(t')/m\omega]\sin(\omega t')\,dt'$ is a real number, $|\psi(t)\rangle$ is also an eigenstate of $\hat{X}_1(t)$ with eigenvalue

$$\xi(t,t_0) = \xi_0 - \int_{t_0}^{t} [F(t')/m\omega] \sin(\omega t')\, dt' \quad . \tag{2.31}$$

A precise measurement of $\hat{X}_1(t)$ at time t must then yield this eigenvalue $\xi(t,t_0)$ and must leave the state of the oscillator unchanged (except for overall phase).

This remarkable fact — that even when a classical force is acting, successive perfect measurements of $\hat{X}_1$ leave the oscillator's state unchanged — means that perfect measurements of $\hat{X}_1$ are "quantum nondemolition" in a stronger sense than quantum-counting measurements can ever be. In the quantum-counting case the classical force drives the oscillator away from eigenstates of the measured operator $\hat{N}$, and a subsequent perfect measurement then "demolishes" the oscillator's evolved state — i.e., it "reduces the wave function" back into an eigenstate of $\hat{N}$. Perfect quantum-counting experiments are truly nondemolition only in the absence of an external driving force.

By a sequence of arbitrarily quick and accurate back-action-evading measurements of $\hat{X}_1$ one can monitor, in principle, the precise time evolution of the oscillator's eigenvalue $\xi(t,t_0)$ (Eq. 2.31); and from $\xi(t,t_0)$ one can compute the precise time evolution of the driving force (signal):

$$F(t) = -(m\omega d\xi/dt)/(\sin \omega t) \quad . \tag{2.32}$$

Of course, in the realistic case of imperfect measurements, the inferred $F(t)$ will be highly inaccurate at times $t \simeq n\pi/\omega$, when $\sin \omega t \simeq 0$. However, when the force is produced by a classical field (e.g., a gravitational or electromagnetic wave) whose wavelength is long compared to the size of the measuring apparatus, one can couple two different oscillators to F. On the

first oscillator one can measure $\hat{X}_1$ getting $\xi(t,t_0)$, and on the second one can measure $\hat{X}_2$ getting $\zeta(t,t_0) \equiv \zeta_0 + \int_{t_0}^{t} [F(t')/m\omega] \cos(\omega t')\, dt'$. One can infer $F(t)$ independently from the two measurements, and the accuracies of the two methods will be complementary: The second is good at $t = n\pi/\omega$ when the first is bad; the first is good at $t = (n + \frac{1}{2})\pi/\omega$ when the second is bad.

This technique of measuring $\hat{X}_1$ on one oscillator and $\hat{X}_2$ on another completely circumvents the uncertainty principle. In the complex amplitude plane the vertical error line associated with $\hat{X}_1$ (first oscillator), and the horizontal error line associated with $\hat{X}_2$ (second oscillator), intersect in a point. This point moves, under the action of $F(t)$, in precisely the same manner as the system point of a single classical oscillator driven by $F(t)$; see Fig. 5.

That measurements of $\hat{X}_1$ can reveal all details of $F(t)$, while quantum-counting measurements cannot, is intimately connected with the fact that measurements of $\hat{X}_1$ are quantum nondemolition even in the presence of a classical force while quantum-counting measurements are not. For further discussion see Sec. IV.

Of course, in practice there are limits to the accuracy with which back-action evasion can monitor an external force $F(t)$. The most serious limits arise from Nyquist noise in the oscillator, and from constraints on the strength of coupling of real transducers to the oscillator — constraints due to the finite strengths of real materials, voltage breakdown in real capacitors, and superconducting breakdown in real circuits; see Paper II. Less serious in practice, but important in principle, are limits due to special relativistic effects,[5] and a limit due to the quantum mechanical properties of any real external force.

The latter limit, which we shall call the "real quantum limit," arises when one is monitoring the external force F so accurately that one discovers it is not classical, but rather is being produced by a boson system with a finite occupation number per quantum mechanical state. The magnitude of this real quantum limit on the force F is a function of the strength of coupling of the boson system to the oscillator: The weaker the coupling, the smaller will be the magnitude of the force at which the system's quantum properties are felt. We can quantify the coupling as follows: Consider all quantum states associated with the driving force (e.g., if the force is a broad-band electromagnetic or gravitational wave, consider all states in the beam pattern of the antenna with frequencies ω in range $\Delta\omega \sim \omega$). Let $\bar{n}_{SQL}$ be the average occupation number of these states when the force is just strong enough to be detectable in one cycle by amplitude-and-phase methods (force at level of "standard quantum limit," Eqs. 2.16 and 2.22a). Then $\bar{n}_{SQL}$ characterizes the strength of coupling of the oscillator to the boson system. In the special case of an antenna for electromagnetic or gravitational waves, one can show that

$$\bar{n}_{SQL} \simeq \lambda\!\!\!^{-2}/\sigma_o$$
$$\simeq 10^{38} \text{ for resonant-bar gravitational-wave antennas,} \qquad (2.33)$$

(cf. Sec. I). Here $\lambda\!\!\!^{-} = c/\omega$ is the reduced wavelength of the waves and σ_o is the cross section of the antenna (equal to $\omega^{-1}\int\sigma(\omega')d\omega'$ where the integral is over the antenna's resonance and $\sigma(\omega')$ is the cross section at frequency ω'; cf. Chapter 37 of Misner, Thorne, and Wheeler, 1973).

The real quantum limit for measurements that last one cycle is reached at a level that is smaller than the standard quantum limit by $(1/\bar{n}_{SQL})^{\frac{1}{2}}$:

$$\left.\begin{array}{l}\text{Real}\\ \text{Quantum}\\ \text{Limit}\end{array}\right\} \quad \begin{array}{l} \Delta X_1 \simeq \left(\frac{\hbar}{2m\omega}\right)^{\frac{1}{2}} \left(\frac{1}{\bar{n}_{SQL}}\right)^{\frac{1}{2}} , \\ |\alpha(\frac{2\pi}{\omega}, 0)| \simeq (1/\bar{n}_{SQL})^{\frac{1}{2}} . \end{array} \tag{2.34}$$

If one were monitoring the force F(t) by back-action-evading techniques at this level of accuracy, one's measurements would be sensitive to zero-point (vacuum) fluctuations in the system that produces the force F.

Henceforth, as previously, we shall ignore these issues and shall regard the force F(t) as truly classical ($\bar{n}_{SQL} = \infty$).

F. Interaction Hamiltonians for Back-Action-Evading Measurements of X_1

1. Continuous, Two-Transducer Measurements

A back-action-evading measurement of $\hat{X}_1$ is made by (i) coupling the oscillator to a measuring apparatus which produces an output large enough to be essentially classical, (ii) reading out the output of the measuring apparatus, and (iii) inferring a value for X_1 from that output. The coupling of the oscillator to the measuring apparatus is embodied, mathematically, in the "interaction part" of the Hamiltonian, $\hat{H}_I$. To prevent back-action of the measuring apparatus on $\hat{X}_1$ it is necessary that $\hat{H}_I$ commute with $\hat{X}_1$. To make the measurement of very small X_1's experimentally feasible, it is advantageous to use a linear coupling of the measuring apparatus to the oscillator's position and momentum. These constraints of linear coupling and commutation with $\hat{X}_1$ force $\hat{H}_I$ to have the form

$$\hat{H}_I = K\hat{X}_1\hat{Q} = K[\hat{x}\cos\omega t - (\hat{p}/m\omega)\sin\omega t]\,\hat{Q}\ . \tag{2.35}$$

Here K is a "coupling constant" that may be time-dependent, and $\hat{Q}$ is an operator (observable) of the measuring apparatus. ($\hat{Q}$ commutes with all the oscillator observables.) The total Hamiltonian for the coupled system consisting of the oscillator, the measuring apparatus, and the classical driving force has the form

$$\hat{H} = \hat{H}_o(\text{Eq. 2.2}) - F(t)\,\hat{x} + \hat{H}_I(\text{Eq. 2.35}) + \hat{H}_M\ . \tag{2.36}$$

Here $\hat{H}_M$ is the Hamiltonian of the measuring apparatus — i.e., it is the part of the Hamiltonian that depends only on measuring apparatus observables.

When K is time-independent, the interaction Hamiltonian (2.35) can be realized as follows: One couples the oscillator to a coordinate (x) transducer, and one sinusoidally modulates the transducer output at the frequency ω of the oscillator; one also couples the oscillator to a momentum (p) transducer and modulates its output sinusoidally with a phase which leads that of the coordinate transducer by a quarter cycle; one adds the two outputs and sends the sum into an amplifier. (The sinusoidal modulations must be produced by a classical signal generator — e.g., another oscillator with the same frequency as the primary oscillator, vibrating in a large-amplitude coherent state.) Specific designs for this type of measuring apparatus will be described in Appendix B of this paper, and in Paper II. In Sec. III.B we shall see that, if the coupling constant K is made arbitrarily large, then in principle the measurement of $\hat{X}_1$ can be made arbitrarily quickly and arbitrarily accurately.

We shall characterize such measurements as "continuous, two-transducer measurements."

2. Stroboscopic Measurements

If one is willing to make measurements only twice per cycle, then one can avoid the necessity for both coordinate and momentum transducers. In particular, if one pulses on the coupling at times $t = n\pi/\omega$, so $K = K_o\delta(\sin \omega t)$, then the interaction Hamiltonian (2.35) becomes

$$\hat{H}_I = K_o \cos \omega t \ \delta(\sin \omega t)\ \hat{x}\hat{Q} = \frac{K_o}{\omega}\hat{x}\hat{Q}\sum_n (-1)^n \delta(t - \frac{n\pi}{\omega}), \qquad (2.37a)$$

which requires only a coordinate transducer for its realization. [The factor $(-1)^n$, i.e., the sign change in the coupling between even and odd pulses, compensates for the sign change in the relation between $\hat{x}$ and $\hat{X}_1$: $\hat{X}_1 = (-1)^n \hat{x}$.]

If one pulses on the coupling at $t = (n + \frac{1}{2})\pi/\omega$, then

$$\hat{H}_I = (K_o/m\omega)\,[-\sin\omega t\ \ \delta(\cos\omega t)]\,\hat{p}\hat{Q}\ , \tag{2.37b}$$

which requires only a momentum transducer. The possibility of such pulsed measurements was discovered independently and simultaneously by Zimmermann in our research group (see Thorne et al., 1978), and by Braginsky, Vorontsov, and Khalili (1978) in Moscow. Braginsky et al. call such measurements "stroboscopic."

Stroboscopic measurements with the interaction Hamiltonian (2.37a) can be described semiclassically as follows: One measures the oscillator's coordinate $x = X_1$ at $t = 0$, obtaining a precise value ξ_0 and in the process giving the momentum a huge, unknowable, uncertainty-principle kick. The kick causes x to evolve in an unknown way. However, because the oscillator's period is independent of its amplitude, after precisely a half cycle x must be precisely equal to $-\xi_0$ in the absence of an external force, or equal to

$$-\xi(\pi/\omega,0) = -\left\{\xi_0 - \int_0^{\pi/\omega} [F(t')/m\omega]\,\sin\omega t'\ dt'\right\} \tag{2.38}$$

in the presence of a classical force F (cf. Eq. 2.31). At $t = \pi/\omega$ a second pulsed measurement is made, giving precisely this value for $x = -X_1$, and again kicking the momentum by a huge, unknowable amount. Subsequent pulsed measurements at $t = n\pi/\omega$ give values

$$x = (-1)^n\,\xi(n\pi/\omega,0) = (-1)^n\left\{\xi_0 - \int_0^{n\pi/\omega} [F(t')/m\omega]\,\sin\omega t'\,dt'\right\}, \tag{2.39}$$

which are unaffected by the unknown kick of each measurement.

In the Schrödinger picture of quantum mechanics these stroboscopic

measurements are described as follows: A precise measurement of $\hat{x}$ at $t=0$ gives the value ξ_0 and collapses the oscillator's wave function $\psi(x,0)$ into an arbitrarily narrow function peaked at ξ_0 —i.e., $\psi(x,0) \simeq [\delta(x-\xi_0)]^{\frac{1}{2}}$. Immediately after the measurement the wave function $\psi(x,t)$ spreads out over all space; but as t approaches π/ω, ψ gathers itself into an arbitrarily narrow function again, now centered on $x = -\xi(\pi/\omega,0)$ (Eq. 2.38). A precise measurement of $\hat{x}$ at this time gives this precise value and leaves the oscillator's state unchanged except for phase (no collapse of wave function; quantum nondemolition measurement). Just before each subsequent measurement ($t = n\pi/\omega$) the wave function again collects itself into an arbitrarily narrow function, and a perfect nondemolition measurement can again be made.

In practice, of course, no measurement can be made perfectly. The following simple argument reveals the limit of accuracy for stroboscopic measurements which require a finite time $2\Delta t$, or which are made at times that differ by Δt from precise half-cycle timing. (A more rigorous calculation gives the same limit.) Let σ be the precision of such a measurement at $t \simeq 0$. Then immediately after the measurement the oscillator's wave function must have variances $\Delta x_0 = \sigma$, $\Delta p_0 \geq \hbar/2\sigma$. The next measurement will have optimal accuracy only if the first measurement has put the wave function into a minimum-uncertainty wave packet ($\Delta p_0 = \hbar/2\sigma$). Then, as time passes the variances of $\hat{x}$ and $\hat{p}$ feed each other so that, at the time $t = (\pi/\omega \pm \Delta t)$ of the next measurement,

$$\Delta x = [(\Delta x_0)^2 \cos^2 \omega t + (\Delta p_0/m\omega)^2 \sin^2 \omega t]^{\frac{1}{2}}$$

$$= [\sigma^2 + (\hbar \Delta t/2m\sigma)^2]^{\frac{1}{2}} \quad \text{for} \quad \Delta t \ll \pi/\omega. \tag{2.40}$$

This is the minimum possible uncertainty for the next measurement. It is minimized (optimal strategy!) by setting $\sigma = (\hbar \Delta t/2m)^{\frac{1}{2}}$, which gives

$$\Delta x_1 = \Delta x = [(\hbar/m\omega)(\omega \Delta t)]^{\frac{1}{2}} \tag{2.41}$$

for the best possible accuracy of stroboscopic measurements with timing imperfections Δt. This result has been derived independently by Thorne et al. (1978) and by Braginsky, Vorontsov, and Khalili (1978).

3. Continuous, Single-Transducer Measurements

Return now to continuous measurements. The more rapidly one seeks to measure, the larger must be the coupling constant K. This fact will be quantified in Eq. (3.21) below and in Paper II. In many situations, practical considerations will force K to be so small that measurements of the desired accuracy will require a time τ far longer than one cycle. In such cases, as in stroboscopic measurements, one can avoid the use of two transducers. For example, one can construct an interaction Hamiltonian of the form

$$\hat{H}_I = K\hat{Q}\hat{x} \cos \omega t = \tfrac{1}{2}K\hat{Q}(\hat{X}_1 + \hat{X}_1 \cos 2\omega t + \hat{X}_2 \sin 2\omega t) ; \tag{2.42a}$$

or

$$\hat{H}_I = (K/m\omega)\, \hat{Q}\hat{p} \sin \omega t = -\tfrac{1}{2}K\hat{Q}(\hat{X}_1 - \hat{X}_1 \cos 2\omega t - \hat{X}_2 \sin 2\omega t); \tag{2.42b}$$

cf. Eq. (2.6). The first of these is achieved by a coordinate transducer with sinusoidally modulated output; the second, by a momentum transducer with modulated output. Measurements with such Hamiltonians we shall call "continuous, single-transducer measurements."

In such single-transducer measurements, the apparatus which follows the transducer must average over a time $\tau \gg 2\pi/\omega$ in producing its output — i.e., it must contain a "low-pass filter" with high-frequency cutoff at $\omega_{max} \simeq \pi/\tau \ll \omega$. Then the sinusoidal output due to the sinusoidal terms in $\hat{H}_I$ (Eqs. 2.42) will average away to near zero. To free $\hat{X}_1$ from back-action forces of the measuring apparatus, one must ensure that the back-action forces have negligible Fourier components at frequency 2ω. This

can be arranged, for example, by placing a low-pass filter between the transducer and the subsequent apparatus. See Paper II for full details.

Such a continuous, single-transducer back-action-evading measurement is similar to a lock-in amplifier. In the lock-in amplifier a slowly changing signal S is given an initial "carrier" modulation, $S \cdot \cos \omega t$, before it acquires (through amplification and other signal processing) a noise N. The noisy signal $S \cos \omega t + N$ is then subjected to "phase-sensitive detection" — i.e., it is multiplied by $\cos \omega t$ and then is sent through a low-pass filter to give a signal $\frac{1}{2} S$ which is nearly free of the noise N. By contrast, in our back-action-evading measurement of an oscillator, the oscillator itself provides the initial modulation of the "signal" X_1 to produce a "carrier" $x = X_1 \cos \omega t + X_2 \sin \omega t$ — which then enters the signal-processing apparatus through a transducer. The subsequent modulation and filtering of the carrier are identical to the phase-sensitive detection of the lock-in amplifier, except for this key difference: In the lock-in amplifier the phase-sensitive detection follows amplification, and its purpose is to remove from the signal the noise inserted during signal processing; in our back-action-evading measurement the phase-sensitive detection precedes amplification, and its purpose is to make one's measurement insensitive to the noisy back-action of the amplifier on the oscillator, which was the source of the initial modulation. (For comments on the related issue of the similarity between our back-action-evading measurements and the operation of a degenerate parametric amplifier, see footnote 2.)

The modulation in our single-transducer interaction Hamiltonian (2.42) need not be sinusoidal, nor need it be at the oscillator frequency. A variety of other types of modulation will do the job — if they are accompanied by appropriate filters placed between the transducer and the subsequent

apparatus. For details see Paper II; for a semi-practical example see Thorne et al. (1979).

In Appendix D we show that continuous, single-transducer, back-action-evading measurements with averaging times $\tau \gg 2\pi/\omega$ are capable of accuracies at least as good as

$$\Delta X_1 \simeq (\hbar/2m\omega)^{\frac{1}{2}} (1/\omega\tau)^{\frac{1}{2}} ; \tag{2.43}$$

and perhaps with cleverness one can do better. (Appendix D is best read after Sec. III and Appendix C.) Paper II discusses practical limitations on modulated measurements — including limitations due to finite strength of coupling K.

Continuous, single-transducer, back-action-evading measurements of $\hat{X}_1$ are analogous to the single-transducer quantum-counting measurements proposed by Unruh (1977, 1978) and by Braginsky, Vorontsov, and Khalili (1977). The Unruh-Braginsky interaction Hamiltonian has the form

$$\hat{H}_I = K\hat{Q}\hat{x}^2 = \tfrac{1}{2} K\hat{Q}[(2\hbar/m\omega)(\hat{N} + \tfrac{1}{2}) + (\hat{X}_1^2 - \hat{X}_2^2) \cos 2\omega t + (\hat{X}_1\hat{X}_2 + \hat{X}_2\hat{X}_1) \sin 2\omega t] \tag{2.44}$$

(cf. Eqs. 2.17 and 2.5), which is analogous to our (2.42); and they measure $\hat{N}$ by averaging over a time $\tau \gg 2\pi/\omega$.

G. The Zero-Frequency Limit of Back-Action-Evading Measurements

In the limit $\omega \to 0$ a mechanical oscillator becomes a "free mass," and the real and imaginary parts of the complex amplitude become

$$\hat{X}_1 = \hat{x} - (\hat{p}/m)\, t \ ; \qquad m\omega\, \hat{X}_2 = \hat{p} \ . \tag{2.45}$$

For a free mass these quantities, $\hat{p}$ and $\hat{x} - (\hat{p}/m)\,t$, are conserved in the absence of external forces; and one can monitor a classical external force by "back-action-evading measurements" of either of these quantities.

To measure $\hat{p}$ requires only a momentum transducer — i.e., a transducer whose interaction Hamiltonian is

$$\hat{H}_I = K\hat{p}\hat{Q} \ . \tag{2.46}$$

To measure $\hat{X}_1$ requires both a position transducer and momentum transducer

$$\hat{H}_I = K\hat{X}_1\hat{Q} = K\hat{x}\hat{Q} - K\hat{p}\hat{Q}t/m \ . \tag{2.47}$$

As in the case of a harmonic oscillator, so also for a free mass, a measurement of $\hat{X}_1$ or $\hat{p} = m\omega\,\hat{X}_2$ can be arbitrarily quick and arbitrarily accurate in principle (so long as one ignores issues of strengths of materials, relativistic effects, etc.). This we demonstrate in the next section.

III. GEDANKEN EXPERIMENTS FOR ARBITRARILY QUICK AND ACCURATE BACK-ACTION-EVADING MEASUREMENTS OF X_1 OR X_2

In this section we describe and analyze gedanken experiments by which, in principle, one can measure arbitrarily quickly and accurately (i) the momentum $\hat{p} = \lim_{\omega \to 0} (m\omega\hat{X}_2)$ of a free mass, and (ii) the real part $\hat{X}_1$ of the complex amplitude of a harmonic oscillator. Throughout this section, as above, the phrase "in principle one can measure arbitrarily quickly and accurately" implicitly contains the caveat "within the framework of non-relativistic quantum mechanics and ignoring constraints due to strengths of materials, voltage breakdown in capacitors, relativistic effects, etc." Consequently, in this section and related appendices we shall, without further comment or shame, take limits in which sizes of capacitors go to infinity, energies in electromagnetic frequency generators (clocks) go to infinity, etc. To alleviate queasiness caused by this cavalier approach, we shall administer a strong dose of practical constraints in Paper II.

In this section we shall first (§A) discuss measurements of free masses, and then (§B) measurements of oscillators.

A. Measurements of a Free Mass

1. The Standard Quantum Limit

Gedanken experiments described in the literature suggest a possible limit

$$(\Delta F)_{\min} \simeq (m\hbar/\tau^3)^{\frac{1}{2}} \qquad \text{"standard quantum limit"} \tag{3.1}$$

on the accuracy with which one can measure a weak classical force F acting on a free mass m, with a measurement of duration τ.

This "standard quantum limit" is correct and unavoidable (Braginsky and Vorontsov, 1974) if one tries to study F by measurements of the mass's position (analog of "amplitude and phase" method for an oscillator; cf. Eqs. 3.1 and 2.22). An initial position measurement of precision Δx_i produces, by the position-momentum uncertainty relation, a variance $\Delta p \geq \Delta p_{min} = \hbar/2\Delta x_i$ in the mass's initial momentum, which in turn produces the following variance of position after a time τ :

$$\Delta x(\tau) \geq \left[(\Delta x_i)^2 + (\Delta p_{min}/m)^2\tau^2\right]^{\frac{1}{2}} = \left[(\Delta x_i)^2 + (\hbar\tau/2m\Delta x_i)^2\right]^{\frac{1}{2}} \geq (\hbar\tau/m)^{\frac{1}{2}} \quad (3.2)$$

("standard quantum limit for free-mass position"). In this same time τ a constant force F produces a change of position $\delta x = \frac{1}{2}(F/m)\tau^2$. Comparing the signal δx with the noise (3.2), we obtain the standard quantum limit (3.1) on the force F, to within a factor 2. A laser-interferometer detector for gravitational waves is an example of a system which studies weak classical forces by position measurements, and which is therefore subject to the constraint (3.1); see, e.g., Drever et al. (1977). For laser detectors this constraint is a serious potential problem at low gravitational-wave frequencies, $f \lesssim 1$ Hz.

Another measuring system that is subject to the constraint (3.1) is a "velocity sensor." By "velocity sensor" we mean a measuring system in which, viewed classically, the velocity $\dot{x}$ of the mass m produces an emf in a circuit, and the effects of that emf are measured using a voltage or current or charge amplifier. An idealized, simple-minded version of such a sensor is shown in Fig. 6a. For that sensor or any "velocity sensor," the Lagrangian of the entire system, with amplifier disconnected, has the form

$$\mathcal{L} = \tfrac{1}{2}m\dot{x}^2 + \tfrac{1}{2}L\dot{Q}^2 - \frac{1}{2C}Q^2 - Km\dot{x}Q + Fx \quad . \quad (3.3)$$

Here F is the force on m, which one seeks to measure; Q is the charge that has flowed onto the upper plate of the capacitance C; $\dot{Q}$ is the current in the circuit; and for the system of Fig. 6a the coupling constant is $K = aB/mc$, where a is the height of the magnetic-field region, B is the field strength, and c is the speed of light. The generalized momenta of this system are

$$p = \partial\mathcal{L}/\partial\dot{x} = m(\dot{x} - KQ), \qquad \Pi = \partial\mathcal{L}/\partial\dot{Q} = L\dot{Q} \; ; \tag{3.4}$$

and the Hamiltonian $H = p\dot{x} + \Pi\dot{Q} - \mathcal{L}$, after quantization, is

$$\hat{H} = \frac{\hat{p}^2}{2m} + \frac{\hat{\Pi}^2}{2L} + \tfrac{1}{2}\left(mK^2 + \frac{1}{C}\right)\hat{Q}^2 + K\hat{p}\hat{Q} - F\hat{x} \; . \tag{3.5}$$

Notice that <u>the velocity coupling $-Km\dot{x}Q$ in the Lagrangian is equivalent to a momentum coupling $K\hat{p}\hat{Q}$ in the Hamiltonian plus a capacitance $C_K \equiv 1/mK^2$ in the readout circuit</u>. It is the capacitance C_K which prevents such a velocity sensor even in principle from monitoring the momentum p and force F with arbitrary speed and accuracy.

A semiclassical derivation of the quantum limit (3.1) for such a velocity sensor proceeds as follows: If the mass is initially in an eigenstate (or near eigenstate) of $\hat{p}$ with eigenvalue p_o, then the form (3.5) of the Hamiltonian guarantees it will remain in an eigenstate of $\hat{p}$ but with eigenvalue $p(t) = p_o + Ft$. (Here F is assumed constant, for simplicity.) Figure 6b is then an equivalent circuit for the measuring apparatus. Simple analysis of this circuit, with voltage amplifier included, shows that the output $\tilde{V}_a$ of the amplifier at frequency f is

$$\tilde{V}_a = A(f)\left\{\frac{-K\tilde{p} + \tilde{I}_n[-i2\pi fL + 1/(-i2\pi fC_K)]}{1 + C/C_K - (2\pi f)^2 CL} + \tilde{V}_n\right\} . \tag{3.6a}$$

Here a tilde denotes a Fourier transform, and for simplicity we have assumed that the amplifier has infinite input impedance and that initially there is zero charge on the capacitor and zero current through the inductor. For a quick measurement of

duration τ (frequency and bandwidth $f \sim \Delta f \sim 1/2\tau$), the signal-to-noise ratio is optimized by setting $C = L = 0$; then

$$SNR \sim \frac{K(p_o + F\tau/2)}{\left\{\left[S_V(f) + S_I(f)/(2\pi f C_K)^2\right] \Delta f\right\}^{\frac{1}{2}}} . \qquad (3.6b)$$

Here $S_V(f)$ is the spectral density of the amplifier's voltage noise V_n and $S_I(f)$ is the spectral density of its current noise I_n. The Heisenberg uncertainty principle constrains the noise temperature of the amplifier to be $T_n \geq 2\pi\hbar f/k \ln 2$ (Weber, 1959; Heffner, 1962) which, by virtue of Eq. (12.33) of Robinson (1974), is equivalent to the constraint

$$S_V(f)\, S_I(f) \gtrsim (4\pi\hbar f)^2 \qquad (3.7)$$

(cf. Eq. 2.11). The ratio S_V/S_I can be adjusted by preceding the amplifier with a transformer. The optimal SNR occurs when $S_V/S_I = 1/(2\pi f C_K)^2$, which — together with $f \sim \Delta f \sim 1/2\tau$ — gives

$$(SNR)_{opt} \sim \left(\frac{C_K \tau}{\hbar}\right)^{\frac{1}{2}} K(p_o + F\tau/2). \qquad (3.8)$$

Since $C_K = 1/mK^2$, this optimal SNR does not improve as $K \to \infty$. In fact, independent of K the minimum detectable force (SNR $\simeq$ 1) is the "standard quantum limit" (3.1). For the case of a charge or current amplifier in series with the circuit (and for optimization of the circuit impedances to $C = \infty$, $L = 0$), a similar analysis gives the same limit.

Wagoner, Will, and Paik (1978) have proposed a design for a free-mass gravitational-wave detector which makes use of a velocity sensor. Their technique for coupling the circuit to the mass is essentially equivalent to the technique shown in Figure 6a, but is a more practical variant of it. Their Lagrangian has the standard velocity-sensor form (3.3); and therefore, its performance can <u>never</u> exceed the "standard quantum limit" (3.1).

2. Momentum Sensors Can Be Arbitrarily Quick and Accurate

From a velocity sensor such as that in Fig. 6 one can construct a momentum sensor by inserting into the circuit a capacitor with negative capacitance, $-C_K = -1/mK^2$. A negative capacitor is not a common electronic component. Nevertheless, such capacitors can exist in principle, and in principle their internal noise can be made negligible; see Appendix A for details.

The momentum sensing system, which one obtains from the velocity sensor of Eq. (3.3) by inserting the negative capacitance $-C_K = -1/mK^2$, has the Lagrangian

$$\mathcal{L} = \tfrac{1}{2} m\dot{x}^2 + \tfrac{1}{2} L\dot{Q}^2 + \left(\frac{mK^2}{2} - \frac{1}{2C}\right) Q^2 - Km\dot{x}Q + Fx. \tag{3.9}$$

Its velocities and momenta are related by (3.4); and its quantized Hamiltonian is (3.5) with negative capacitance inserted:

$$\hat{H} = \frac{\hat{p}^2}{2m} + \frac{\hat{\Pi}^2}{2L} + \frac{1}{2C}\hat{Q}^2 + K\hat{p}\hat{Q} - F\hat{x}\ . \tag{3.10}$$

In principle the positive capacitance C and the inductance L can be adjusted to whatever values one wishes.

Such a measuring system can make arbitrarily quick and accurate measurements of $\hat{p}$, and of the classical force F which drives $\hat{p}$. One way to see this is by a semiclassical voltage-amplifier analysis of the type sketched in Eqs. (3.6)-(3.8). Another way is by a fully quantum mechanical analysis corresponding to the case of a charge or current amplifier in series with the circuit (which now has $C = \infty$), rather than a voltage amplifier in parallel. In this analysis we leave the amplifier out of the circuit initially; we let the circuit evolve freely until a reasonably strong current is flowing;

and we then insert our amplifier and quickly measure that current, or measure the charge on the infinite capacitor C. The free evolution of the system is governed by the Heisenberg equations for the Hamiltonian (3.10):

$$\begin{aligned} d\hat{x}/dt &= \hat{p}/m + K\hat{Q} \ , \\ d\hat{p}/dt &= F \ , \\ d\hat{Q}/dt &= \hat{\Pi}/L \ , \\ d\hat{\Pi}/dt &= -K\,\hat{p} \ . \end{aligned} \tag{3.11}$$

These Heisenberg equations are easily integrated to give

$$\begin{aligned} \hat{p}(t) &= \hat{p}(0) + Ft \ , \\ \hat{\Pi}(t) &= \hat{\Pi}(0) - K[\hat{p}(0)t + \tfrac{1}{2} Ft^2], \\ \hat{Q}(t) &= \hat{Q}(0) + (1/L)[\hat{\Pi}(0)t - \tfrac{1}{2} K\hat{p}(0)t^2 - \tfrac{1}{6} KFt^3] \ , \\ \hat{x}(t) &= \hat{x}(0) + \hat{p}(0)t + \frac{1}{2} Ft^2 + K\hat{Q}(0)t + (K/L)[\tfrac{1}{2} \hat{\Pi}(0)t^2 - \tfrac{1}{6} K\hat{p}(0)t^3 - \frac{1}{24} KFt^4]. \end{aligned} \tag{3.12}$$

From these integrals we can infer the following. If the circuit is initially (at t = 0) prepared in a Gaussian wave-packet state with

$$\begin{aligned} &\langle \hat{\Pi}(0) \rangle = \langle \hat{Q}(0) \rangle = 0, \\ &\Delta\Pi(0) = (L\hbar/2\tau)^{\frac{1}{2}}, \qquad \Delta Q(0) = (\hbar\tau/2L)^{\frac{1}{2}} \ , \end{aligned} \tag{3.13}$$

and if the "free mass" is initially in a near-eigenstate of $\hat{p}$ with eigenvalue p_o, then after time τ has elapsed the expectation values and variances of the circuit variables are

$$\begin{aligned} &\langle \hat{\Pi}(\tau) \rangle = -K(p_o\tau + \tfrac{1}{2} F\tau^2), \qquad \Delta\Pi(\tau) = (L\hbar/2\tau)^{\frac{1}{2}} \ , \\ &\langle \hat{Q}(\tau) \rangle = -(K/L)(\tfrac{1}{2} p_o\tau^2 + \frac{1}{6} F\tau^3), \qquad \Delta Q(\tau) = (\hbar\tau/L)^{\frac{1}{2}} \ . \end{aligned} \tag{3.14}$$

At time τ we go into the circuit, disconnect it from the transducer if we wish, and measure either $\hat{\Pi}$ (the flux in the inductor), or $\hat{\Pi}/L$ (the current in the circuit), or $\hat{Q}$ (the charge on the infinite capacitor). With appropriately designed amplifiers, in principle we can make one or another of these measurements to within the variances (3.14), in a time $\lesssim \tau$. [This can be verified using the standard quantum limit on the noise performances of amplifiers. Note, moreover, that the precisions desired, $\delta\Pi \sim (L\hbar/2\tau)^{1/2}$ and $\delta Q \sim (\hbar\tau/L)^{1/2}$, are sufficiently modest that the uncertainty principle $\delta\Pi\,\delta Q \geq \hbar/2$ even permits us to make the $\hat{\Pi}$ and $\hat{Q}$ measurements simultaneously!] From the measured value of $\hat{\Pi}$ or $\hat{\Pi}/L$ or $\hat{Q}$ we can infer p_o, in the absence of an external force F, to within probable error

$$\delta p_o \sim \frac{\Delta Q(\tau)}{\partial \langle \hat{Q}(\tau) \rangle / \partial p_o} \sim \frac{\Delta \Pi(\tau)}{\partial \langle \hat{\Pi}(\tau) \rangle / \partial p_o}$$

$$\sim (L\hbar/K^2\tau^3)^{1/2} \quad ; \tag{3.15a}$$

or, if p_o is known to this precision from previous measurements, we can infer the external force F to within probable error

$$\delta F \sim (L\hbar/K^2\tau^5)^{1/2} \quad . \tag{3.15b}$$

Equations (3.15) reveal that, no matter how quick (τ) the entire experiment must be, we can make the coupling constant K large enough in principle to produce any desired accuracy for our inferred values of the "free-mass" momentum p_o and force F.

The above argument is similar to the one by which Aharanov and Bohm (1961, 1964) refute a common misinterpretation of the energy-time uncertainty relation; cf. footnote 6. The Aharanov-Bohm argument has been criticized by Fock (1962) because it involves turning the coupling constant K on and off at

$t = 0$ and $t = \tau$, so that the mass m will be truly free of all coupling before and after the experiment. Fock suspects that the turn-on and turn-off cannot be done with the required precision. We, like Aharanov and Bohm (1964), disagree with Fock — but Fock's worries and our disagreement are irrelevant to the present analysis, because our objective here is merely to measure the momentum p_o and force F with arbitrary accuracy, and that can be done without any time changes in the coupling constant K.

B. Measurements of a Harmonic Oscillator

We now return to our discussion of harmonic oscillators, and present a gedanken experiment which shows that the $\hat{X}_1$ of an oscillator can be measured arbitrarily quickly and accurately, in principle. In this section we shall describe our gedanken experiment in somewhat abstract terms — focusing attention on the dynamical variables of the system and measuring apparatus, on the Hamiltonian which governs their evolution, and on a mathematical sketch of the measurement process and its potential accuracy. In Appendix B we describe apparatus which, in principle, could give a physical realization of the experiment; and in Appendix C we present a full mathematical analysis of the measurement process, complete with "reduction of the wave function" and repetitive measurements.

The oscillator to be measured is described by the variables of Eqs. (2.1)-(2.5), including coordinate $\hat{x}$, momentum $\hat{p}$, complex amplitude $\hat{X}_1 + i\hat{X}_2$, frequency ω, and mass m.

The measuring apparatus consists of three parts: a "generator," which provides energy for and regulates the sinusoidal coupling of the interaction Hamiltonian; a "meter," which is coupled to $\hat{X}_1$ by the generator; and a "readout system" for studying the $\hat{X}_1$-induced motion of the meter.

The generator is a quantum mechanical oscillator, which has precisely the same frequency ω as the oscillator being measured. Before the measurement, the generator is prepared in a coherent state of arbitrarily large amplitude. As is discussed in Appendix B.1.c, this means that the generator can be treated classically, and that it is not loaded by the experimental apparatus — and, consequently, that it produces perfect "cos ωt" and "sin ωt" terms in the Hamiltonian.

The meter is a one-dimensional quantum mechanical "free mass," with generalized coordinate $\hat{Q}$, generalized momentum $\hat{\Pi}$, and generalized mass L. The coupling of the meter to the oscillator's $\hat{X}_1$ will be so strong that a tiny change δX_1 will make Q "swing" by an amount large compared to the width of its wave packet (cf. Eqs. 3.19 below). This swinging can then be observed with a classical readout system — i.e., we can put the "quantum-classical cut" of our analysis between the meter and the readout system, thereby avoiding the necessity to describe the readout system quantum mechanically; see discussion in Appendix C.

The total Hamiltonian for the coupled system, excluding the readout, is

$$\hat{H} = \hat{H}_o + \hat{H}_M + \hat{H}_I, \tag{3.16a}$$

$$\hat{H}_o = \hat{p}^2/2m + \tfrac{1}{2} m\omega^2\hat{x}^2, \tag{3.16b}$$

$$\hat{H}_M = \hat{\Pi}^2/2L, \tag{3.16c}$$

$$\hat{H}_I = K(\hat{x}\cos\omega t - \frac{\hat{p}}{m\omega}\sin\omega t)\hat{Q} = K\hat{X}_1\hat{Q}\ . \tag{3.16d}$$

Here $\hat{H}_o$ is the Hamiltonian of the free oscillator, $\hat{H}_M$ is the Hamiltonian of the meter,[7] and $\hat{H}_I$ is the interaction Hamiltonian for the oscillator coupled, via the classical generator ("cos ωt" and "sin ωt" terms), to the

meter. In the Heisenberg picture of quantum mechanics the state of the system is constant, and the observables $\hat{X}_1 = \hat{x} \cos \omega t - (\hat{p}/m\omega) \sin \omega t$, $\hat{X}_2 = \hat{x} \sin \omega t + (\hat{p}/m\omega) \cos \omega t$, $\hat{Q}$, and $\hat{\Pi}$ evolve in accordance with the Heisenberg equations

$$d\hat{X}_1/dt = 0 \quad , \tag{3.17a}$$

$$d\hat{X}_2/dt = -(K/m\omega)\hat{Q} \quad , \tag{3.17b}$$

$$d\hat{Q}/dt = \hat{\Pi}/L \quad , \tag{3.17c}$$

$$d\hat{\Pi}/dt = -K\hat{X}_1 \quad . \tag{3.17d}$$

These are algebraically identical to the classical Hamiltonian equations of the system. Note that $\hat{X}_1$ is completely unaffected by the coupling to the measuring apparatus.

We presume that at time $t = t_0$, before the measurement begins, the oscillator is in a state (perhaps pure; perhaps mixed) with probability distribution $\mathcal{P}(X_1)$ whose expectation value is $\langle \hat{X}_1(t_0) \rangle = \xi_o$ and whose variance is $\Delta X_1(t_0) = \Sigma$. At $t = t_0$ the meter is prepared in a pure Gaussian wave-packet state with $\langle \hat{Q}(t_0) \rangle = \langle \hat{\Pi}(t_0) \rangle = 0$, $\Delta Q(t_0) = (\hbar\tau/2L)^{1/2}$, $\Delta\Pi(t_0) = (\hbar L/2\tau)^{1/2}$, where τ is the duration of the planned measurement. These variances are chosen to minimize the variance of $\hat{Q}$ after a time τ. The preparation of the meter can be done either with the oscillator-meter coupling turned on (in which case K = constant before, during, and after the entire experiment), or with the coupling turned off ($K = 0$ for $t < t_0$, $K = \text{const}$ for $t_0 < t < t_0 + \tau$). The probability distribution $\mathcal{P}(X_1)$ is left unaffected by the physical manipulations of Q and Π involved in the preparation; cf. Eq. (3.17a).

After preparation of the meter, the system is allowed to evolve freely (Eqs. 3.17) for a time τ. During this interval $\hat{X}_1$ is conserved, and the evolution of $\hat{Q}$ is given by

$$\hat{Q}(t) = \hat{Q}(t_0) + \frac{\hat{\Pi}(t_0)}{L}(t-t_0) - \frac{K\hat{X}_1}{2L}(t-t_0)^2 \quad . \tag{3.18}$$

The interaction produces a strong correlation between the states of the oscillator and meter: At time $t_1 = t_0 + \tau$ the meter's mean coordinate gets displaced to

$$\langle\hat{Q}(t_1)\rangle = -(K\tau^2/2L)\,\xi_o \tag{3.19a}$$

(cf. Eq. 3.18), while its variance grows to

$$\Delta Q(t_1) = [(\hbar\tau/L) + (K\tau^2/2L)^2\Sigma^2]^{1/2} \quad . \tag{3.19b}$$

At time t_1 the readout system "reads out" a value Q_m for the meter coordinate, where Q_m is likely to lie somewhere in the range $\langle\hat{Q}(t_1)\rangle \pm$ (a few) $\times\, \Delta Q(t_1)$. (This readout can be done leaving the coupling K on, or turning it off, as one wishes; it makes no difference.) Using formula (3.19a) the experimenter infers from Q_m a value

$$\xi_m = -(2L/K\tau^2)\,Q_m \tag{3.20a}$$

for X_1. In a set of measurements on an ensemble of identical systems, the mean of this inferred value is ξ_o, and its variance is

$$\Delta\xi_m = (2L/K\tau^2)\Delta Q(t_1) = (\Sigma^2 + 4\hbar L/K^2\tau^3)^{1/2} \quad . \tag{3.20b}$$

Of course, as (3.20b) shows, one cannot determine ξ_o accurately if the probability distribution $\mathcal{P}(X_1)$ has a large spread; however, if $\mathcal{P}(X_1)$ is highly peaked about ξ_o [$\Sigma << (4\hbar L/K^2\tau^3)^{1/2}$], the measurement can determine ξ_o with a probable error

$$\Delta\xi_m \simeq (4\hbar L/K^2\tau^3)^{1/2} \quad . \tag{3.21}$$

No matter how small the measurement time τ may be, by choosing K^2/L large enough one can make the measurement error $\Delta\xi_m$ as small as one wishes. [Note that this remains true even if the readout of Q is much less accurate than $(\hbar\tau/L)^{\frac{1}{2}}$; see analysis in Appendix C.7.] The measurements can be "arbitrarily quick and arbitrarily accurate."

If a weak, classical force is driving the oscillator (term $-\hat{x}\,F(t)$ added to the Hamiltonian; cf. Eq. 2.18), then during the time τ the expectation value of $\hat{X}_1$ changes by an amount

$$\delta\xi = -\int_{t_0}^{t_1} [F(t')/m\omega] \sin\omega t'\, dt' \tag{3.22}$$

(cf. Eq. 2.31); and the meter's mean coordinate gets displaced to

$$\langle\hat{Q}(t_1)\rangle = -(K\tau^2/2L)(\xi_o + \mathcal{F}) \quad , \tag{3.23a}$$

$$\mathcal{F} \equiv -(2/\tau^2)\int_{t_0}^{t_1} dt' \int_{t_0}^{t'} dt'' \int_{t_0}^{t''} dt'''\,[F(t''')/m\omega]\sin\omega t''' \quad , \tag{3.23b}$$

while the variance of $\hat{Q}(t_1)$ is still given by (3.19b). For measurement times short enough that $F(t)\sin\omega t$ is nearly constant during the measurement, $\mathcal{F} \simeq (1/3)\delta\xi \simeq -(\tau/3)[F(t_0)/m\omega]\sin\omega t_0$. If ξ_o is known from previous measurements to within the error (3.21), a measurement of $\hat{Q}$ at time t_1 allows one to determine $\mathcal{F}$ (or $\delta\xi$) with accuracy

$$\Delta\mathcal{F} \sim (\hbar L/K^2\tau^3)^{1/2} \quad . \tag{3.24}$$

Such a measurement permits one (in principle) to monitor the force F arbitrarily quickly and accurately, in the limit as τ and $(\hbar L/K^2\tau^5)^{1/2}$ are made arbitrarily small.

The preceding analysis is rigorous, but it is far from complete. In Appendix C we present a more detailed analysis; in particular, we analyze a

sequence of measurements of X_1, including the "reduction of the wave function" at the end of each measurement. This more detailed analysis allows us to investigate the behavior of X_1 and X_2 during a sequence of measurements. The most important results concern X_2. We show that a "feedback force" on the meter can keep the expectation value of $\hat{X}_2$ close to zero. However, the variance of $\hat{X}_2$ inevitably increases during a sequence, and the increase is proportional to the square root of the number of measurements. Practical implications of this "random walk of X_2" are discussed in Paper II.

IV. FORMAL DISCUSSION OF QUANTUM NONDEMOLITION MEASUREMENT[8]

In this section we shall distill from our analysis of oscillators and free masses the essence of "quantum nondemolition measurement" and label that essence using the formal and precise language of nonrelativistic quantum mechanics. The final product may be unpalatable to the practical-minded reader, but we hope it will clarify the fundamental principles underlying "nondemolition measurement."

A. Definition of Quantum Nondemolition Measurement and Its Implications

Our investigation of quantum nondemolition measurement was stimulated by the desire to monitor a classical force acting on a harmonic oscillator with better accuracy than can be obtained using standard "amplitude-and-phase" techniques. Braginsky (1970), and later Giffard (1976), had pointed out the limitations of the standard techniques (see Sec. II.C), and Braginsky and Vorontsov (1974) had proposed overcoming these limitations by making what they called "quantum nondemolition measurements." In such a measurement one monitors a single observable of the oscillator, and it must be an ob-

servable that can be measured over and over again with the result of each measurement being completely determined (in the absence of a classical force) by the result of an initial, precise measurement. The force is detected by changes it produces in this sequence of precisely predictable values.

The key feature of such a nondemolition measurement is repeatability — once is not enough! If one can couple strongly enough to a physical system, then any of its observables can be measured (in principle) with arbitrary precision at a particular instant. (This is the content of a controversial general "theorem" in nonrelativistic quantum theory; see discussion in footnote 6). Such a precise measurement "localizes" the system at the measured value of the observable. An initial, precise measurement can be regarded as preparing the system in a state with a nearly definite value of the measured observable. The goal of a subsequent measurement is to determine this value. However, the initial, precise measurement inevitably produces huge uncertainties in observables that do not commute with the measured observable, and in general, these uncertainties "feed back" into the measured observable as the system evolves. Consequently, the result of a subsequent measurement is uncertain. If one wishes to make repeated precise measurements whose results are completely predictable (no uncertainty!), one must measure an observable that does not become contaminated by uncertainties in other, noncommuting observables.

It is easy to formulate a general condition for making such a sequence of completely predictable measurements: The system being measured must be in an eigenstate of the measured observable at the time of each measurement. Then the result of each measurement is exactly equal to the eigenvalue at the time of the measurement, and immediately after the measurement the system is left in the same eigenstate ("measurement of the first kind"; cf. footnote 6).

This condition clarifies the nature of nondemolition measurement and, at the same time, makes it clear that what is not being demolished is the state of the system; it is left unchanged by each measurement except for an unknown (and irrelevant) phase factor.

To formalize these ideas, consider an arbitrary quantum mechanical system with free Hamiltonian $\hat{H}_o$. The objective is to measure an observable $\hat{A}$ of this system. ($\hat{A}$ is a Hermitian operator; it may have explicit time-dependence). For a resonant-bar gravitational wave detector, the system would be the fundamental mode of the bar, which can be idealized as a simple harmonic oscillator; and $\hat{A}$ might be the number of quanta in the oscillator or the real part of the oscillator's complex amplitude. For such a detector, one measures $\hat{A}$ in order to monitor the classical force on the oscillator produced by a gravitational wave; to allow for that possibility here, we include in the Hamiltonian a term $\hat{D}F(t)$, where $\hat{D}$ is some observable of the system and $F(t)$ is the "classical force." To insure that $\hat{A}$ responds to $F(t)$, we require $[\hat{A},\hat{D}] \neq 0$.

In order to measure $\hat{A}$, one must couple the system to a measuring apparatus. The details of the system's interaction with the measuring apparatus are described by the interaction Hamiltonian $\hat{H}_I$, which contains all terms in the Hamiltonian that depend on variables of both the system and the measuring apparatus. The total Hamiltonian — including the system, its coupling to the "classical force," and the measuring apparatus — has the form

$$\hat{H} = \hat{H}_o + \hat{D}F(t) + \hat{H}_I + \hat{H}_M \ , \tag{4.1}$$

where $\hat{H}_M$ is the Hamiltonian of the measuring apparatus — i.e., that part of the Hamiltonian which depends only on measuring apparatus variables (cf. Eq. 2.36).

We now define a quantum nondemolition (QND) measurement of $\hat{A}$ as a sequence of precise measurements of $\hat{A}$ such that the result of each measurement (after the first) is completely predictable (in the absence of a classical force) from the result of the preceding measurement. If an observable can be measured this way (in principle), we call it a quantum nondemolition observable.

This definition can be used to derive a condition for a QND observable—a condition most easily formulated by ignoring the details of the interaction with the measuring apparatus. This is not to say that these details are unimportant: For example, the strength of the coupling between the system and measuring apparatus determines how quickly a given measurement precision can be achieved (see Sec. III). However, the fundamental limits on the predictability of a sequence of measurements of $\hat{A}$ are determined not by the interaction with the measuring apparatus, but by uncertainties (variances of observables) which are built into a quantum mechanical description of the free evolution of the system. Of course, the interaction with the measuring apparatus, if chosen poorly, can ruin a QND measurement by increasing the variance of the measured observable; however, as we demonstrate in Sec. IV.B, the interaction need not degrade the measurement at all in principle. Therefore, for the remainder of this subsection, we ignore the interaction term in the Hamiltonian; we simply assume that there is a way to measure $\hat{A}$ with arbitrary precision at any instant (infinitely strong coupling!) and that such a measurement leaves the system in an eigenstate of $\hat{A}$ whose eigenvalue is the measured value ("measurement of the first kind"; cf. footnote 6). We also ignore, for the moment, the classical force.

We now consider a sequence of measurements of $\hat{A}$. The analysis proceeds most smoothly in the Heisenberg picture of quantum mechanics, which we use

throughout the rest of this subsection. The initial measurement is made at time t_0, and we assume that the experimenter has no control over the state of the system before this initial measurement. (This may be a bad assumption; see discussion in Sec. IV.C.) The normalized eigenstates of $\hat{A}(t_0)$ are denoted by $|A,\alpha\rangle$, where $\hat{A}(t_0)|A,\alpha\rangle = A|A,\alpha\rangle$ and where α labels the states in any degenerate subspaces of $\hat{A}(t_0)$.

The result of the initial measurement is one of the eigenvalues A_0 of $\hat{A}(t_0)$, and the state of the system immediately after the measurement is an eigenstate of $\hat{A}(t_0)$ with this eigenvalue: $|\Psi(t_0)\rangle = \sum_\alpha c_\alpha |A_0,\alpha\rangle$, where the c_α's are arbitrary (subject to normalization) constants. In the interval before the next measurement the system evolves freely, and in the Heisenberg picture the state of the system does not change: $|\Psi(t)\rangle = |\Psi(t_0)\rangle$. If a second measurement at $t = t_1$ is to yield a completely predictable result, then all of the states $|A_0,\alpha\rangle$ must be eigenstates of $\hat{A}(t_1)$ with the same eigenvalue, although the new eigenvalue need not equal A_0. Hence, one obtains the requirement

$$\hat{A}(t_1)|A_0,\alpha\rangle = f_1(A_0)|A_0,\alpha\rangle \quad , \quad \text{for all } \alpha \quad , \tag{4.2}$$

where f_1 is an arbitrary real-valued function. Equation (4.2) guarantees that the result of a measurement at $t = t_1$ will be $f_1(A_0)$, because $|\Psi(t_0)\rangle$ will be an eigenstate of $\hat{A}(t_1)$ with eigenvalue $f_1(A_0)$ for arbitrary c_α's.

By assumption, the result of the initial measurement can be any of the eigenvalues of $\hat{A}(t_0)$. Thus Eq. (4.2) must hold for all values of A_0, and $\hat{A}(t_1)$ must satisfy the operator equation $\hat{A}(t_1) = f_1[\hat{A}(t_0)]$.[9] In a sequence of measurements a similar operator equation must hold at each step in the sequence. Therefore, one obtains the following set of requirements for a QND observable that is to be measured at times $t = t_0,\cdots,t_n$:

$$\hat{A}(t_k) = f_k[\hat{A}(t_0)] , \qquad \text{for } k = 1,\cdots,n , \tag{4.3}$$

where each f_k is some real-valued function. These formal constraints on the free evolution of $\hat{A}$ in the Heisenberg picture embody the fundamental principle of QND measurement: If the system begins in an eigenstate of $\hat{A}$, its free evolution must leave it in an eigenstate of $\hat{A}$ at the time of each measurement. The conditions (4.3) for a QND observable were given previously by the authors (Thorne et al., 1978).

One is usually interested in making QND measurements at arbitrary times or continuously. Then Eq. (4.3) must hold for all times:

$$\hat{A}(t) = f[\hat{A}(t_0);t,t_0] . \tag{4.4}$$

An observable that satisfies Eq. (4.4) we call a continuous QND observable. An observable that satisfies Eq. (4.3) only at carefully selected times we call a stroboscopic QND observable. Examples of stroboscopic QND observables are the position and momentum of a harmonic oscillator (stroboscopic measurement; see Sec. II.F.2). Because of their importance, we restrict our attention to continuous QND observables for the rest of this section.

The simplest way to satisfy Eq. (4.4) is to choose an observable which is conserved in the absence of interactions with the external world:

$$0 = \frac{d\hat{A}}{dt} = -\frac{i}{\hbar}[\hat{A},\hat{H}_o] + \frac{\partial \hat{A}}{\partial t} . \tag{4.5}$$

For example, the continuous QND observables we have considered for a harmonic oscillator—$\hat{X}_1$, $\hat{X}_2$, and $\hat{N}$—are conserved. Note that the free Hamiltonian $\hat{H}_o$ is always a QND observable (provided $\partial \hat{H}_o/\partial t = 0$).

It is harder to find nontrivial examples of nonconserved continuous QND observables. One system which has such observables is a mass m on a "negative spring"—i.e., a mass with Hamiltonian $\hat{H}_o = \hat{p}^2/2m - \frac{1}{2} m\omega^2 \hat{x}^2$. For

such a system the observables $\hat{x} \pm (\hat{p}/m\omega)$ are QND observables, but they are not conserved.

It is useful to note here an important commutation property satisfied by any continuous QND observable $\hat{A}$:

$$[\hat{A}(t),\hat{A}(t')] = 0 \quad , \quad \text{for all times } t \text{ and } t' \, . \tag{4.6}$$

This property follows immediately from the QND condition (4.4). Equivalent to (4.6) is the statement that $\hat{A}$ commutes with all its derivatives—i.e.,

$$0 = \left[\hat{A}, \frac{d^n \hat{A}}{dt^n} \right] = \left[\hat{A}, \sum_{\ell=0}^{n} \left(-\frac{i}{\hbar} \right)^{n-\ell} \binom{n}{\ell} \left[\frac{\partial^\ell \hat{A}}{\partial t^\ell} , \hat{H}_o \right]^{(n-\ell)} \right] , \tag{4.7}$$

$$\text{for } n = 1, 2, 3, \ldots ,$$

where

$$[\hat{C},\hat{D}]^{(n)} \equiv \begin{cases} \hat{C} & , \quad n = 0 \\ \Big[\Big[\ldots \Big[[\hat{C},\hat{D}],\underbrace{\hat{D}}\Big], \ldots \Big], \hat{D} \Big] & , \quad n = 1, 2, 3, \ldots \end{cases} \tag{4.8}$$

$$n \ \hat{D}\text{'s}$$

The latter equality in Eq. (4.7) can be obtained (provided $\partial \hat{H}_o / \partial t = 0$) by using the operator equations of motion in the Heisenberg picture.

Unruh (1979) has recently considered the problem of nondemolition measurement. He discusses many of the issues considered in this section, but from a somewhat different point of view. He has proposed that Eq. (4.7) (or, equivalently, Eq. 4.6) be used to characterize QND observables. [Actually, Unruh considers only observables with no explicit time-dependence—a serious restriction which rules out such very important observables as the $\hat{X}_1$ of an oscillator. Because of this restriction, Unruh's quantum nondemolition condition is

$$[\hat{A},[\hat{A},\hat{H}_o]^{(n)}] = 0 \ , \quad \text{for } n = 1,2,3,\ldots , \tag{4.7'}$$

which is the specialization of (4.7) to the case $\partial\hat{A}/\partial t = 0$.]

The motivation for Unruh's definition is discussed in Sec. IV.B, but for now it is important to note that, although Eq. (4.7) is an immediate consequence of the QND condition (4.4), the implication cannot be reversed. The observables satisfying Eq. (4.7) constitute a more general class than the QND observables; we call such observables generalized (continuous) QND observables.

Examples of observables which satisfy Eq. (4.7), but not Eq. (4.4), can be obtained by considering a system suggested by Unruh (1979): a charged particle (charge e, mass m) moving in a uniform magnetic field $\vec{B} = B_o\vec{e}_z$ and an electric field $\vec{E} = (eB_o^2/8m)\vec{\nabla}(x^2 + y^2 - 2z^2)$. If the vector potential is chosen to be $\vec{A} = \frac{1}{2} B_o(-y\vec{e}_x + x\vec{e}_y)$, then $\hat{p}_x$ and $\hat{p}_y$ (x- and y-components of the particle's canonical momentum) form a pair of generalized QND observables, but they do not satisfy the QND criterion (4.4). [For this system the observables $\hat{x} - (\hat{p}_x/m)t$ and $\hat{y} - (\hat{p}_y/m)t$ form another pair of generalized QND observables.]

Any generalized QND observable $\hat{A}$ does obey an evolution constraint similar to the QND constraint (4.4). Successive differentiation of Eq. (4.7) shows that all derivatives of $\hat{A}$ mutually commute, and a Taylor expansion of $\hat{A}$ about some initial time t_0 shows that the free evolution of $\hat{A}$ must have the form

$$\hat{A}(t) = f[\hat{A}(t_0);\hat{B}_1,\cdots,\hat{B}_n;t,t_0] \ , \tag{4.9}$$

where the Hermitian operators $\hat{B}_i$ commute with one another and with $\hat{A}(t_0)$. In writing (4.9), it is assumed that none of the operators $\hat{B}_i$ can be written as a function of $\hat{A}(t_0)$ and the other $\hat{B}_i$'s; otherwise, the functional dependence of $\hat{A}(t)$ could be simplified. Note that if $\hat{A}(t_0)$ has no degeneracies, the

only operators which commute with it are functions of itself; hence, a non-degenerate generalized QND observable is automatically a QND observable.

Generalized QND observables can be compared most tellingly with QND observables by using Eq. (4.9). The key difference is the following: A system which begins in any eigenstate of a QND observable remains in an eigenstate of that observable; this is true for a generalized QND observable only if the initial eigenstate is a simultaneous eigenstate of $\hat{A}(t_0)$ and the $\hat{B}_i$'s. An equivalent manifestation of this difference is that, in a sequence of measurements of a generalized QND observable, the result of a given measurement cannot be predicted solely from the result of the preceding measurement. However, it can be predicted from the results of several preceding measurements — enough to specify the values of $\hat{A}(t_0)$ and each of the $\hat{B}_i$'s. In practice generalized QND observables may prove to be as useful as QND observables, but the distinction between the two must be kept in mind.

Having defined QND measurement, we now consider its application to the problem of monitoring a classical force F(t). The procedure for monitoring F(t) is to make a sequence of measurements of a QND observable and to detect the force by the changes it produces in the precisely predictable values which would be measured in the absence of the force.

One would like to do more than simply "detect" the force: Ideally, one would like to monitor its time-dependence with arbitrary accuracy; and if the force is arbitrarily classical, there is no reason in principle why one cannot do so. In fact, a sequence of measurements of the observable $\hat{A}$ can reveal with arbitrary accuracy the time evolution of F(t) if and only if the following conditions are satisfied: (i) The measuring apparatus and its coupling to the measured system ($\hat{H}_M$ and $\hat{H}_I$ of Eq. 4.1) must be chosen so as to produce instantaneous and arbitrarily precise measurements of $\hat{A}$ (see Sec.

IV.B below). (ii) The measurements must be made at arbitrarily closely-spaced times. (iii) The result of the (k+1)'th measurement at time t_k must be uniquely determined by the result of the initial measurement at time t_0 plus the time history F(t') of the force between t_0 and t_k. This is possible if and only if $\hat{A}$ is a continuous QND observable in the presence of the driving force F (Eq. 4.4):

$$\hat{A}(t) = f[\hat{A}(t_0);F(t');t,t_0] \quad \text{for} \quad t_0 < t' < t \ , \tag{4.10a}$$

where $\hat{A}(t)$ is the Heisenberg-picture evolution of $\hat{A}$ under the action of $\hat{H} = \hat{H}_o + \hat{D}F$. Here f is a function of $\hat{A}(t_0)$, t, and t_0, and is a functional of F(t'). (iv) From the time history of the measured values of $\hat{A}(t)$ one must be able to compute uniquely the time history of F(t). The measured values will be

$$A(t) = f[A_0;F(t');t,t_0] \ ,$$

where A_0 is the (arbitrary) eigenvalue of $\hat{A}(t_0)$ obtained in the first measurement. Thus condition (iv) is equivalent to the demand that

$$\begin{aligned} A(t) \equiv f[A_0;F(t');t,t_0] \ & \text{must be a uniquely invertible} \\ & \text{functional of } F(t'), \text{ for every eigenvalue } A_0 \text{ that is} \\ & \text{a possible result of the first measurement of } \hat{A}(t_0). \end{aligned} \tag{4.10b}$$

Of these conditions only Eqs. (4.10a,b) are constraints on the choice $\hat{A}$ of the observable to be measured. Thus, for a given system and a given coupling to the classical force F (i.e., for given $\hat{H} = \hat{H}_o + \hat{D}F$), conditions (4.10) are necessary and sufficient to permit in principle measurements of $\hat{A}$ that reveal with arbitrary accuracy the time evolution of F(t). To such an observable $\hat{A}$ we shall give the name "QNDF". Because a QNDF observable is QND in the presence of the force F, it will necessarily satisfy Eq. (4.6) — $[\hat{A}(t),\hat{A}(t')] = 0$ — and also the first equality of Eq. (4.7). These

same two equations are also satisfied by "generalized QNDF observables" -- i.e., observables for which the functional f of Eqs. (4.10) depends also on a set of mutually commuting Hermitian operators $\hat{B}_i$ which all commute with $\hat{A}(t_0)$.

The distinction between QND and QNDF observables arose earlier in comparing quantum-counting measurements and measurements of $\hat{X}_1$ as ways of monitoring a force acting on a harmonic oscillator (see Sec. II.D, E). Measurements of $\hat{X}_1$ can be used to monitor an arbitrarily weak force F(t) with arbitrary accuracy, in principle; quantum counting can "detect" an arbitrarily weak force, but it cannot provide good accuracy in monitoring the force's precise time-dependence. The fundamental reason for this difference is that $\hat{X}_1$ is a QNDF observable, while $\hat{N}$ is not.

In his recent treatment of nondemolition measurement Unruh (1979) has also drawn attention to the important distinction between QND and QNDF observables (QNDR and QNDD, respectively, in his notation).

B. Interaction with the Measuring Apparatus

Up to now we have neglected the details of the measuring apparatus which is actually used to measure a QND observable $\hat{A}$. We now rectify this omission. Our main concern is to demonstrate our earlier assertion that the interaction between the system and the measuring apparatus need not degrade the quality of a QND measurement at all, in principle. The analysis in this subsection is restricted to continuous observables, but it can easily be modified to handle stroboscopic observables.

In a real experiment the measuring apparatus consists of a series of components. Each component is coupled to the preceding component, and only the first stage in the series directly "contacts" the system.

Fortunately, we need not concern ourselves with this entire complicated structure; its complexities can remain buried in the measuring apparatus Hamiltonian $\hat{H}_M$. We need only consider the first stage of the measuring apparatus and its interaction with the system — an interaction whose mathematical manifestation is the interaction Hamiltonian $\hat{H}_I$.

The measuring apparatus must actually respond to $\hat{A}$, and this demand means that $\hat{H}_I$ must depend on $\hat{A}$ and on one or more variables of the first stage of the measuring apparatus. In addition, the measuring apparatus ought not to respond to observables of the system other than $\hat{A}$, and this desire means that $\hat{A}$ ought to be the only observable of the system appearing in $\hat{H}_I$. The simplest interaction Hamiltonian of this form is

$$\hat{H}_I = K \hat{A} \hat{Q} , \tag{4.11}$$

where $\hat{Q}$ is some observable of the measuring apparatus and K is a coupling constant. This is the type of interaction Hamiltonian which was used in Secs. II.F.1 and III.B to analyze continuous measurements of $\hat{X}_1$.

If $\hat{A}$ contains <u>explicit</u> time-dependence, the coupling between the system and the measuring apparatus must be modulated so as to supply the proper time-dependence in $\hat{H}_I$. The modulation must be provided by an external, <u>classical</u> "clock." Unruh (1979) has pointed out that any "clock" is an inherently quantum mechanical device whose quantum properties cannot be ignored <u>a priori</u>; however, the "clock" can always be excited into a highly energetic, essentially classical state, where uncertainties due to its quantum mechanical nature are unimportant. This issue is discussed in the context of measurements of $\hat{X}_1$ in Appendix B.1.c.

We now turn to the main concern of this subsection — to demonstrate the following fundamental property of QND observables. <u>The evolution of a continuous QND observable $\hat{A}$ (in the Heisenberg picture) is completely unaffected</u>

by the interaction with the measuring apparatus (in the absence of a classical force), provided that $\hat{A}$ is the only observable of the system which appears in the interaction Hamiltonian.[10] The proof of this property relies on only one feature of $\hat{A}$ — that it satisfies Eq. (4.6) in the absence of the interaction with the measuring apparatus. Thus the property holds for generalized QND observables, and for QNDF observables even in the presence of the classical force.

Proving the property is not difficult, but it is sufficiently important that it is worthwhile to sketch the proof in some detail. We consider the case of a QND observable in the absence of a classical force, and we now let $\hat{A}$ denote the QND observable in the Schrödinger picture. The total Hamiltonian, now considered to be written in the Schrödinger picture, is given by Eq. (4.1) with the classical-force term deleted. We let $\hat{U}_o(t,t_0)$, $\hat{U}_M(t,t_0)$, and $\hat{U}(t,t_0)$ be the unitary time-development operators for $\hat{H}_o$, $\hat{H}_M$, and $\hat{H}$, respectively (cf. Eq. 2.19). The assumption about the nature of the interaction means that $\hat{H}_I$ has the form

$$\hat{H}_I = \hat{H}_I[\hat{A}(t);\hat{Q}_1,\cdots,\hat{Q}_n;t] \quad , \tag{4.12}$$

where the operators $\hat{Q}_i$ are observables of the measuring apparatus.

The two operators of interest are the interaction-picture and Heisenberg-picture forms of the QND observable:

$$\hat{A}_I(t) \equiv \hat{U}_o^\dagger(t,t_0)\ \hat{A}(t)\hat{U}_o(t,t_0) \quad , \tag{4.13a}$$

$$\hat{A}_H(t) \equiv \hat{U}^\dagger(t,t_0)\ \hat{A}(t)\hat{U}(t,t_0) \quad . \tag{4.13b}$$

The interaction-picture operator $\hat{A}_I(t)$ gives the evolution of the QND observable in the absence of the interaction with the measuring apparatus; thus it is the operator which satisfies the QND condition (4.4) and which, in particular, also satisfies Eq. (4.6). The Heisenberg-picture operator $\hat{A}_H(t)$

gives the evolution of the QND observable in the presence of the measuring apparatus. The object of the proof is to show that $\hat{A}_H(t) = \hat{A}_I(t)$.

The operators $\hat{A}_I(t)$ and $\hat{A}_H(t)$ are related by

$$\hat{A}_H(t) = \hat{\mathcal{U}}^\dagger(t,t_0)\, \hat{A}_I(t)\, \hat{\mathcal{U}}(t,t_0) \quad . \tag{4.14}$$

Here $\hat{\mathcal{U}}(t,t_0) = \hat{U}_o^\dagger(t,t_0)\, \hat{U}_M^\dagger(t,t_0)\, \hat{U}(t,t_0)$ satisfies the equation

$$i\hbar \frac{d\hat{\mathcal{U}}(t,t_0)}{dt} = \hat{\mathcal{H}}_I(t)\, \hat{\mathcal{U}}(t,t_0) \quad , \qquad \hat{\mathcal{U}}(t_0,t_0) = 1 \quad , \tag{4.15}$$

where

$$\hat{\mathcal{H}}_I(t) \equiv \hat{H}_I[\hat{A}_I(t);\ (\hat{Q}_1)_I(t),\cdots,(\hat{Q}_n)_I(t);t] \quad , \tag{4.16a}$$

$$(\hat{Q}_i)_I(t) \equiv \hat{U}_M^\dagger(t,t_0)\, \hat{Q}_i \hat{U}_M(t,t_0) \quad . \tag{4.16b}$$

The solution for $\hat{\mathcal{U}}(t,t_0)$ can be written as

$$\hat{\mathcal{U}}(t,t_0) = \mathbf{T} \exp\left[-\frac{i}{\hbar}\int_{t_0}^{t} \hat{\mathcal{H}}_I(t')dt'\right] \quad , \tag{4.17}$$

where $\mathbf{T}$ means that all products are time-ordered (see e.g., Sec. 18.7 of Merzbacher, 1970). The fact that $\hat{A}_I(t)$ satisfies Eq. (4.6) guarantees that $[\hat{A}_I(t),\hat{\mathcal{U}}(t,t_0)] = 0$, which with Eq. (4.14) implies that $\hat{A}_H(t) = \hat{A}_I(t)$. As claimed, the QND observable is completely isolated from the measuring apparatus. A trivial extension of this argument proves the result for QNDF observables in the presence of the classical force.

The meaning of this fundamental property should be emphasized. The property says that the evolution of a QND observable, calculated using the equations of motion in the Heisenberg picture, is unaffected by interaction with the measuring apparatus. This means that the expectation value and variance of $\hat{A}$ evolve during a measurement exactly as they would have had the

measuring apparatus been disconnected. "Noise" in the measuring apparatus does not feed back onto $\hat{A}$ and increase its variance. However, a complete description of a measurement requires more than just a calculation of the quantum mechanical evolution: At some time the measurement must end, the quantum mechanical evolution equations must be suspended, and the quantum state of the coupled system and measuring apparatus must be "reduced" to be consistent with the results of the measurement.

If the system begins the measurement in an eigenstate of $\hat{A}$, it remains in an eigenstate of $\hat{A}$ throughout the measurement, and the "reduction of the wave function" leaves it in the same eigenstate. This is an immediate consequence of the above fundamental property. However, in any real measurement the probability distribution of $\hat{A}$ has some variance, and at the time of "reduction" the expectation value of $\hat{A}$ "jumps" a distance which can be as large as the variance. In this sense the measuring apparatus does affect the QND observable. However, these "jumps" are a consequence of the fact that the measuring apparatus is not making absolutely precise measurements; they do not affect our conclusion that <u>in principle</u> the measuring apparatus need not degrade the predictability of a sequence of measurements of $\hat{A}$. For a detailed analysis of this issue in the context of measurements of $\hat{X}_1$, see Appendix C.

It is now clear why the details of the interaction with the measuring apparatus could be ignored in Sec. IV.A. There we assumed infinitely strong coupling so that precise measurements could be made instantaneously. For a realistic interaction, the coupling strength is finite, and a certain amount of time is required to achieve a desired measurement precision. However, no matter what the coupling strength may be and how long the measurement may last,

a QND observable is completely unaffected by the coupling to the measuring apparatus if $\hat{H}_I$ has the required form. Indeed, for any measurement time one can achieve any desired accuracy by making the coupling strength large enough — i.e., the measurements can be arbitrarily quick and arbitrary accurate. Of course, it may be difficult in practice to design an interaction which is sensitive only to $\hat{A}$; and if other observables of the system appear in $\hat{H}_I$, the time a measurement can take before it disturbs $\hat{A}$ significantly may be limited.

It is interesting to note here that if the right kind of interaction can be designed, a QND observable is isolated not only from "quantum noise" but also from "classical noise" in the measuring apparatus (thermal noise in resistors, shot noise in amplifiers, etc.). In this sense any QND measurement is a "back-action-evading" measurement, because the measured observable evades the back-action noise from the measuring apparatus.

As mentioned earlier, Unruh (1979) has proposed that Eq. (4.7') be used to characterize nondemolition measurement. He considers only observables with no explicit time dependence, he assumes an interaction Hamiltonian of the form (4.11), and he characterizes nondemolition measurement by the demand that the measured observable be completely isolated from the measuring apparatus. As we have shown, any generalized QND observable meets this demand. Thus it is not surprising that Unruh's QND condition is Eq. (4.7') — the condition for a generalized QND observable with no explicit time dependence.

C. Comments and Caveats

The discussion of nondemolition measurement in this section has been presented in the formal language of nonrelativistic quantum mechanics, and the description of the measurement process has been highly idealized. The

reader can be forgiven for asking whether these idealized descriptions have anything to do with real experiments. We think so, and the best evidence for our affirmative answer is in Paper II, where specific, practical schemes for making nondemolition measurements on harmonic oscillators and free masses are discussed. All of these practical schemes are founded firmly on the fundamental principles outlined in this section. Perhaps the best thing we can do here is to indicate in a very general way the relevance of these fundamental principles to real experiments.

The objective of this section was to develop a simple, unambiguous criterion for identifying those observables of any system which, in principle, can be measured repeatedly with no uncertainty in the results. The QND condition (4.3) provides that criterion. Given this criterion, the experimenter faces a clear-cut choice. If he chooses to measure an observable other than a QND observable, he knows that, as he improves the precision of his measurements, he will eventually run "smack-dab" into an impenetrable barrier — impenetrable because it is constructed from quantum mechanical uncertainties dictated by the uncertainty principle. On the other hand, if he chooses to measure a QND observable, he knows that nonrelativistic quantum mechanics erects no such barrier. The real value of the principles outlined in this section is that they do this job of clarifying what quantum mechanics allows.

Once the QND observables of a given system have been identified, the experimenter has a variety of options. If he is ambitious, he might try to design a measuring device which couples nearly exactly to a particular QND observable, as in continuous measurements of X_1 (see Sec. II.F.1). This task might prove to be quite difficult, so the experimenter might rein in his ambition and choose instead to design a measuring device which couples

to the QND observable only in a time-averaged sense, as in single-sensor, back-action-evading measurements of X_1 (see Sec. II.F.3 and Paper II). The essential point is that all these options flow from the fundamental principles of nondemolition measurement.

Powerful, simple, clear-cut—these are words that describe the QND condition (4.3). Yet these virtues are purchased at the expense of certain assumptions about the measurement process, and under some circumstances these assumptions may make the QND condition too restrictive. Despite our belief in the utility of the QND condition, it is important to register here a couple of caveats which warn against using it carelessly.

Caveat 1. The definition of QND measurement is formulated in terms of arbitrarily precise measurements. No real experiment can achieve such perfect measurements, so the QND criterion (4.3) is always more stringent than necessary. The virtue of QND observables is that, for any desired measurement accuracy, a QND observable can do the job in principle; the caveat is that it may be possible to find an observable other than a QND observable which can also do the job.

Caveat 2. The strict operator constraint (4.3) follows from Eq. (4.2) only if one assumes that the experimenter has no control over the state of the system before the initial measurement. In most experiments this is not the case; the experimenter usually prepares the system in some way before beginning his measurements. The second caveat is that, if the experimenter does have some control over the possible initial states of the system, the QND condition (4.3) need only hold in the subspace of states which the system can actually occupy. For a simple system such as a harmonic oscillator this caveat is probably unimportant, but for more complicated systems it

may make a difference.

If these caveats are kept in mind, the experimenter should be able to apply the QND condition to arbitrary systems. He can then face the experimental future free from uncertainty — about quantum mechanical uncertainties.

APPENDIX A

CAPACITORS WITH NEGATIVE CAPACITANCE

In the text of this paper one occasionally encounters the concept of a capacitor with negative capacitance. The physical structure of such a capacitor and the details of its noise are discussed in this Appendix.

We present three models for such a capacitor. The first utilizes a mechanical spring. It will please theorists because it can be analyzed fully quantum mechanically, but it will annoy experimenters because it may not be realizable in practice. The second and third will please experimenters because they are constructed from standard electronic components; but they will annoy theorists because one (the third) functions as a negative capacitor only over a very narrow band of frequencies, and the other (the second) uses an amplifier whose internal structure is unspecified and gives a noise performance not as good as that of the first model.

In Sec. 1 we present our first "spring-based" model capacitor; in Sec. 2 we show that in principle it can function perfectly, introducing absolutely zero noise into the gedanken experiments of Sec. III of the text; and in Sec. 3 we present several alternative viewpoints about the nature and role of this negative capacitor. In Sec. 4 we present our second, "amplifier-based" model capacitor; we derive an expression for the spectral density of its voltage noise; and we show that its noise is too great to do the job required in Sec. III. In Sec. 5 we present our third, "narrow-band" negative capacitor — which also cannot do the job required in the gedanken experiments of Sec. III, unless one alters them by inserting a frequency upconversion.

1. A Spring-Based Negative Capacitor

Our first "spring-based" model capacitor is shown in Fig. 7(a). It consists of three parallel plates with arbitrarily large areas. The top and bottom plates are rigidly fixed. The middle plate has negligible mass, and

is free to move in response to the combined action of springs (total spring constant k) and electrostatic forces. Two batteries produce a potential difference $2V_0$ and an electric field V_0/D between the outer plates. When a charge + Q moves onto the central plate from terminal A, the central plate gets pulled adiabatically upward a distance $z = V_0 Q/kD$; and terminal A thereby acquires a potential $(-V_0^2/kD^2)Q$ relative to terminal B. Thus, the system functions as a capacitor with negative capacitance, $-C_N$, where

$$C_N \equiv kD^2/V_0^2. \tag{A.1}$$

(The charge $Q_{max} = \pm kD^2/V_0$, which is sufficient to drive the central plate into contact with the upper or lower plate, can be made arbitrarily large in principle while holding C_N fixed.)

This capacitor has two possible sources of noise: noise in the batteries, and noise in dynamical motions of the central plate.

The battery noise can be made zero in principle. Figure 7(b) shows a model for a noiseless DC battery. It consists of two parallel plates with finite separation D', infinitely large areas $\mathcal{A}'$ and charges $\pm Q'$, and finite surface densities of charge, $\sigma' = \pm Q'/\mathcal{A}' \equiv \pm V_0/4\pi D'$. Any finite charge Q that flows through terminals A' and B' produces zero fractional change in the plate charges ($Q/Q' = 0$ since $Q' = \infty$), and therefore produces zero change in the battery voltage V_0. (Here, as throughout this paper, we ignore relativistic effects such as speed-of-light limitations on how fast the electrons can redistribute themselves on the plates near the terminals.)

Dynamical motions of the central plate of our capacitor are a delicate issue. We shall analyze them with care, first giving a heuristic semi-classical analysis and then (in Sec. 2) giving a fully quantum mechanical analysis. In our analysis initially we make the area $\mathcal{A}$ of the capacitor plates finite but large; the capacitance $C_0 \equiv 2(\mathcal{A}/4\pi D)$ of the central

plate relative to the outer plates, finite but large; and the mass μ of the central plate, finite but tiny. The motion of the central plate is described by the dynamical variable $z(t) \equiv$ (height above central position); the charge that sits on the central plate is denoted by the dynamical variable $Q(t)$. The entire system shown in Fig. 7(a) is then described classically by the Lagrangian

$$\mathcal{L} = \tfrac{1}{2}\mu\dot{z}^2 - \tfrac{1}{2}kz^2 + \frac{V_0}{D}Qz + \frac{Q^2z^2}{2C_0D^2} - \frac{Q^2}{2C_0} \quad . \tag{A.2}$$

This Lagrangian serves two purposes: (i) its Euler-Lagrange equations $\delta\mathcal{L}/\delta z = 0$ describe the motion of the central plate; and (ii) the voltage of terminal A relative to terminal B is given by

$$V_A - V_B = -\partial\mathcal{L}/\partial Q. \tag{A.3}$$

We now simplify our Lagrangian by making the plates infinitely large ($C_0 \to \infty$); we replace V_0/D by $(k/C_N)^{\frac{1}{2}}$ (cf. Eq. A.1); and we make the replacement

$$k = \mu\Omega^2, \tag{A.4}$$

where Ω is the very high natural frequency of oscillation of the central plate. The Lagrangian then reads

$$\mathcal{L} = \tfrac{1}{2}\mu\dot{z}^2 - \tfrac{1}{2}\mu\Omega^2z^2 + (\mu\Omega^2/C_N)^{\frac{1}{2}}Qz; \tag{A.5}$$

and the Euler-Lagrange equation of z becomes

$$\ddot{z} + \Omega^2 z = (\Omega^2/\mu C_N)^{\frac{1}{2}}Q. \tag{A.6}$$

We assume that Ω is extremely large compared to the rate at which Q changes. Then the central plate moves nearly adiabatically in response to changes of Q:

$$z = (\mu\Omega^2C_N)^{-\frac{1}{2}}Q + z_{na} + z_{f\ell} \ . \tag{A.7}$$

Here we include a correction term z_{na} to account for nonadiabatic effects due to finite Ω:

$$z_{na}/z \to 0 \quad \text{as} \quad \Omega \to \infty; \tag{A.8}$$

and we include a term $z_{f\ell}$ to account semiclassically for fluctuations of the central plate demanded by quantum theory.

The voltage drop between terminals A and B, as computed from Eqs. (A.3), (A.5), (A.7), is

$$\begin{aligned} V_A - V_B &= - (\mu\Omega^2/C_N)^{\frac{1}{2}} z \\ &= - Q/C_N + V_{na} + V_{f\ell} \ . \end{aligned} \tag{A.9a}$$

The first term is that for a perfect negative capacitor. The second, nonadiabatic term vanishes in the limit $\Omega \to \infty$:

$$V_{na}/(V_A - V_B) = z_{na}/z \to 0 \quad \text{as} \quad \Omega \to \infty. \tag{A.9b}$$

In the following section we shall show rigorously that, for the gedanken experiments of Sec. III, the quantum fluctuations $V_{f\ell}$ produce no charge flow in the circuit, $Q_{f\ell} \to 0$, in the adiabatic limit $\Omega \to \infty$. The following argument explains, heuristically, why this is so: The zero-point oscillations of the central plate have a magnitude

$$|z_{f\ell}| \sim (\hbar/\mu\Omega)^{\frac{1}{2}} \ , \tag{A.10}$$

corresponding to an energy $\frac{1}{2}\hbar\Omega$. These produce a fluctuating voltage

$$|V_{f\ell}| = (\mu\Omega^2/C_N)^{\frac{1}{2}} \, |z_{f\ell}| \sim (\hbar\Omega/C_N)^{\frac{1}{2}} \ . \tag{A.9c}$$

The characteristic frequency Ω of these fluctuations is far higher than the natural frequencies of the circuit to which our negative capacitor is hooked up. Therefore, these fluctuations have great difficulty driving oscillations

of the circuit:

$$Q_{f\ell} \propto [(\text{natural frequencies})/\Omega]^2 V_{f\ell}$$
$$\propto \Omega^{-3/2} \to 0 \quad \text{as} \quad \Omega \to \infty . \tag{A.11}$$

In summary, our heuristic argument shows that the model negative capacitor of Fig. 7 functions perfectly (no noise) in the gedanken experiments of Sec. III. However, this is so only in the idealized limits that (i) the area of the capacitor's plates is infinite ($\mathcal{A} \to \infty$, $C_0 \to \infty$); (ii) the natural oscillation frequency of its central plate is infinite ($\Omega^2 = k/\mu \to \infty$); and (iii) one ignores relativistic corrections, issues of strengths of materials, etc.

2. Gedanken Experiment to Measure the Momentum of a Free Mass

We now sketch a fully quantum mechanical analysis of one of the gedanken experiments of Sec. III, replacing the ideal negative capacitance of Sec. III by the spring-based model negative capacitance of Fig. 7 (a). The gedanken experiment we choose is the measurement of the momentum of a free mass (Sec. III.A.2). The reader can perform a similar calculation for the gedanken experiment to measure the X_1 of an oscillator (Sec. III.B). The result will be the same: In the adiabatic limit $\Omega \to \infty$, the negative capacitor produces zero noise.

The physical setup of our momentum-measuring experiment is that of Fig. 6a with (i) the noisy amplifier (dashed part) removed; (ii) the capacitance C set to infinity; and (iii) our negative capacitor (Fig. 7) inserted at the location of the dotted arrow. The Lagrangian of everything except the negative capacitor is Eq. (3.3); the contribution of the negative capacitor is Eq. (A.5); and the value of the negative capacitance which we require to

convert our velocity sensor into a momentum sensor is

$$-C_N = -1/mK^2. \tag{A.12}$$

(See sentence preceding Eq. 3.9.) The total Lagrangian then becomes

$$\begin{aligned}\mathcal{L} &= \tfrac{1}{2} m\dot{x}^2 + \tfrac{1}{2} L\dot{Q}^2 - Km\dot{x}Q + Fx \\ &\quad + \tfrac{1}{2}\mu\dot{z}^2 - \tfrac{1}{2}\mu\Omega^2 z^2 + (m\mu K^2\Omega^2)^{\frac{1}{2}} Qz.\end{aligned} \tag{A.13}$$

We shall see that, in the limit $\Omega \to \infty$, this Lagrangian gives the same quantum mechanical results for the measurement of the momentum $\hat{p}$, and force F, as did the Lagrangian (3.9) which contained a perfect negative capacitor $-C_N = -1/mK^2$.

The canonical momenta for the Lagrangian (A.13) are

$$\begin{aligned} p &= \partial\mathcal{L}/\partial\dot{x} = m\dot{x} - KmQ, \\ \Pi &= \partial\mathcal{L}/\partial\dot{Q} = L\dot{Q}, \\ \pi &= \partial\mathcal{L}/\partial\dot{z} = \mu\dot{z}. \end{aligned} \tag{A.14}$$

The Hamiltonian $H = p\dot{x} + \Pi\dot{Q} + \pi\dot{z} - \mathcal{L}$, after quantization, is

$$\begin{aligned}\hat{H} &= \frac{\hat{p}^2}{2m} + \left(\frac{\hat{\Pi}^2}{2L} + \tfrac{1}{2} mK^2\hat{Q}^2\right) + \left(\frac{\hat{\pi}^2}{2\mu} + \tfrac{1}{2}\mu\Omega^2\hat{z}^2\right) \\ &\quad - F\hat{x} + K\hat{p}\hat{Q} - (m\mu K^2\Omega^2)^{\frac{1}{2}}\hat{Q}\hat{z}.\end{aligned} \tag{A.15}$$

This Hamiltonian will give the same results, when $\Omega \to \infty$, as did the Hamiltonian (3.10) with a perfect negative capacitor.

The Heisenberg equations for the Hamiltonian (A.15) are

$$
\begin{aligned}
d\hat{p}/dt &= F \quad , \\
d\hat{x}/dt &= \hat{p}/m + K\hat{Q} \quad , \\
d\hat{\pi}/dt &= -\mu\Omega^2\hat{z} + (m\mu K^2\Omega^2)^{\frac{1}{2}}\,\hat{Q} \quad , \\
d\hat{z}/dt &= \hat{\pi}/\mu \quad , \\
d\hat{\Pi}/dt &= -K\hat{p} - mK^2\hat{Q} + (m\mu K^2\Omega^2)^{\frac{1}{2}}\,\hat{z} \quad , \\
d\hat{Q}/dt &= \hat{\Pi}/L .
\end{aligned}
\tag{A.16}
$$

These equations describe coupled, driven harmonic oscillators. They can be decoupled by the change of variables

$$
\begin{aligned}
\hat{y}_1 &= \hat{Q} + [(m\mu)^{\frac{1}{2}}K/L\Omega]\,\hat{z} \quad , \\
\hat{y}_2 &= \hat{z} - [(m/\mu)^{\frac{1}{2}}K/\Omega]\,\hat{Q} \quad .
\end{aligned}
\tag{A.17}
$$

Here $\hat{y}_1$ has eigenfrequency zero, and in the adiabatic limit ($\Omega \to \infty$) it becomes $\hat{Q}$; $\hat{y}_2$ has eigenfrequency

$$\sigma \equiv (\Omega^2 + mK^2/L)^{\frac{1}{2}} \quad , \tag{A.18}$$

and in the adiabatic limit it becomes $\hat{z}$. By changing variables to $\hat{y}_1$, $\hat{y}_2$, then solving the Heisenberg equations, and then rewriting the solution in terms of $\hat{Q}$ and $\hat{z}$ we obtain

$$\hat{p}(t) = \hat{p}_o + Ft, \tag{A.19a}$$

$$\hat{Q}(t) = \left(\frac{\Omega}{\sigma}\right)^2 \left\{ \left[\hat{Q}_o + \frac{(m\mu)^{\frac{1}{2}} K}{L\Omega} \hat{z}_o \right] + \left[\frac{\hat{\Pi}_o}{L} + \frac{(m\mu)^{\frac{1}{2}} K}{L\Omega} \frac{\hat{\pi}_o}{\mu} \right] t \right.$$

$$+ \left[\frac{mK^2}{L\Omega^2} \hat{Q}_o - \frac{(m\mu)^{\frac{1}{2}} K}{L\Omega} \hat{z}_o \right] \cos \sigma t + \left[\frac{mK^2}{L\Omega^2} \frac{\hat{\Pi}_o}{L} - \frac{(m\mu)^{\frac{1}{2}} K}{L\Omega} \frac{\hat{\pi}_o}{\mu} \right] \frac{\sin \sigma t}{\sigma}$$

$$- \frac{K}{L} \left[\tfrac{1}{2} \hat{p}_o t^2 + \frac{1}{6} F t^3 \right]$$

$$\left. - \frac{K}{L} \frac{mK^2}{L\Omega^2} \left[\frac{\hat{p}_o}{\sigma^2} (1 - \cos \sigma t) + \frac{F}{\sigma^2} \left(t - \frac{\sin \sigma t}{\sigma} \right) \right] \right\} , \qquad \text{(A.19b)}$$

$$\hat{z}(t) = \left(\frac{\Omega}{\sigma}\right)^2 \left\{ \left[\hat{z}_o - \frac{(m/\mu)^{\frac{1}{2}} K}{\Omega} \hat{Q}_o \right] \cos \sigma t + \left[\frac{\hat{\pi}_o}{\mu} - \frac{(m/\mu)^{\frac{1}{2}} K}{\Omega} \frac{\hat{\Pi}_o}{L} \right] \frac{\sin \sigma t}{\sigma} \right.$$

$$+ \left[\frac{mK^2}{L\Omega^2} \hat{z}_o + \frac{(m/\mu)^{\frac{1}{2}} K}{\Omega} \hat{Q}_o \right] + \left[\frac{mK^2}{L\Omega^2} \frac{\hat{\pi}_o}{\mu} + \frac{(m/\mu)^{\frac{1}{2}} K}{\Omega} \frac{\hat{\Pi}_o}{L} \right] t$$

$$\left. + \frac{(m/\mu)^{\frac{1}{2}} K^2}{L\Omega} \left[\frac{\hat{p}_o}{\sigma^2} (1 - \cos \sigma t) + \frac{F}{\sigma^2} \left(t - \frac{\sin \sigma t}{\sigma} \right) - \tfrac{1}{2} \hat{p}_o t^2 - \frac{1}{6} F t^3 \right] \right\} .$$

(A.19c)

The remaining variables can easily be computed from these using the Heisenberg equations (A.16). In these solutions a subscript "o" means the value at $t = 0$:

$$\hat{p}_o \equiv \hat{p}(0), \quad \hat{Q}_o \equiv \hat{Q}(0), \text{ etc.} \qquad \text{(A.20)}$$

The solution (A.19b) for $\hat{Q}(t)$ illustrates, fully quantum mechanically, the phenomena sketched semiclassically in the last section: (i) In the exact

adiabatic limit $\Omega \to \infty$, the charge $\hat{Q}(t)$ that flows in the circuit is identical to that obtained with a perfect, noiseless negative capacitor (compare Eqs. A.19b and 3.12). (ii) When Ω is finite but $\Omega \gg (mK^2/L)^{\frac{1}{2}}$ = (natural frequency of circuit without negative capacitor), there are corrections in $\hat{Q}(t)$ due to nonadiabatic behavior; but these corrections vanish as $\Omega \to \infty$.

Quantum mechanical fluctuations in $\hat{Q}(t)$ show up when one computes the variance $\Delta Q(t) = \langle(\hat{Q} - \langle\hat{Q}\rangle)^2\rangle^{\frac{1}{2}}$ in terms of the variances at time $t = 0$. Because $\hat{Q}(t)$ reduces to the "perfect-capacitor" form (Eq. 3.12) when $\Omega \to \infty$, we are guaranteed that $\Delta Q(t)$ will reduce to the perfect-capacitor variance (Eq. 3.14) when $\Omega \to \infty$. Thus, in the adiabatic limit, quantum fluctuations of the central plate have no effect on the charge $\langle\hat{Q}(t)\rangle$ that flows, or on its variance $\Delta Q(t)$. Our negative capacitor does its job perfectly and noiselessly.

3. Alternative Viewpoints on the Spring-Based Negative Capacitor

We have argued in the text (Sec.III.A.2) that, in monitoring the motion of a mechanical system, a momentum sensor is equivalent to a velocity sensor plus a negative capacitor. Similarly (Appendix B.2), in monitoring an electromagnetic system, a sensor for generalized momentum is equivalent to a sensor for generalized velocity plus a negative spring.

In designing practical variants of such sensors, it may be useful to keep in mind several different viewpoints about negative capacitors and negative springs. One viewpoint is that embodied in the phrases "capacitor with negative capacitance" and "spring with negative spring constant." Two other viewpoints are presented in this section.

Our second viewpoint on negative capacitors is this (the extension to negative springs should be obvious): A velocity sensor is equivalent to

a momentum sensor plus a restoring force in the sensor's circuit (term $\frac{1}{2} mK^2\hat{Q}^2$ in the Hamiltonian of Eq. 3.5). The stronger is the coupling of the velocity sensor to the mechanical mass (coupling constant K), the stronger is the restoring force in the sensor's circuit. If one wishes to measure the mechanical momentum more accurately than the standard quantum limit, one must make K so strong that the restoring force causes the circuit to oscillate through several cycles during the measurement time τ. Because of these oscillations, the effects of the driving signal (voltage -Kp) do not accumulate monotonically in the circuit. Consequently, the signal-to-noise ratio is debilitated, and the measurement cannot beat the standard quantum limit (cf. Eq. 3.8). To rectify the situation one must modify the sensing circuit so that it contains a low-frequency ($f \lesssim 1/\tau$) normal mode in which the signal can accumulate monotonically. Our so-called "spring-based negative capacitor" accomplishes just this. It gives the readout circuit two dynamical degrees of freedom instead of one; and when it is properly tuned to the rest of the sensor ($kD^2/V_0^2 = 1/mK^2$; Eqs. A.1 and A.12), one of the degrees of freedom ($\hat{y}_1 = \hat{Q} + [(m\mu)^{\frac{1}{2}} K/L\Omega]\hat{z}$) has zero eigenfrequency. The signal builds up monotonically in this degree of freedom giving, in principle, an arbitrarily large signal-to-noise ratio.

Our third viewpoint on negative capacitors builds on this second viewpoint. When our "spring-based negative capacitor" is included in the sensor, then the sensor circuit has two normal modes. It is essential that one of the normal modes have a low enough eigenfrequency, $f \lesssim 1/\tau$, for the signal to accumulate monotonically. However, it is <u>not</u> essential that the other normal mode have such a high eigenfrequency that it decouples from the rest of the system ($\Omega \to \infty$; adiabatic limit; situation assumed in all previous discussion). For example, we might let Ω, the natural frequency of

the central plate in the "negative capacitor," be of order $(mK^2/L)^{\frac{1}{2}}$, the natural frequency of the circuit in the absence of the negative capacitor:

$$\Omega \simeq (mK^2/L)^{\frac{1}{2}} \quad . \tag{A.21}$$

Then, it turns out, the mechanical motion of the central plate, $\hat{z}(t)$, is influenced sufficiently by the zero-frequency normal mode, $\hat{y}_1(t)$, that one can read out from that motion the signal contained in $y_1(t)$. More specifically, for the gedanken experiment of Sec. III.A.2, with initial conditions

$$\langle \hat{\Pi}_o \rangle = \langle \hat{Q}_o \rangle = \langle \hat{\pi}_o \rangle = \langle \hat{z}_o \rangle = 0, \qquad \langle \hat{p}_o \rangle = p_o \ ,$$

$$\Delta\Pi_o = (\hbar L/2\tau)^{\frac{1}{2}} \ , \ \Delta Q_o = (\hbar\tau/2L)^{\frac{1}{2}}, \tag{A.22}$$

$$\Delta\pi_o = (\hbar\mu/2\tau)^{\frac{1}{2}} \ , \ \Delta z_o = (\hbar\tau/2\mu)^{\frac{1}{2}}, \quad \Delta p_o = 0,$$

no correlations of above variables,

the expectation value and variance of the central plate's position at time τ are (Eq. A.19c)

$$\langle \hat{z}(\tau) \rangle = -\tfrac{1}{2}\left(\frac{\Omega}{\sigma}\right)^2 \frac{(m/\mu)^{\frac{1}{2}}K^2}{L\Omega} p_o\tau^2 \left[1 + O\left(\frac{1}{\Omega^2\tau^2}\right)\right] \quad , \tag{A.23a}$$

$$\Delta z(\tau) \simeq \left(\frac{\Omega}{\sigma}\right)^2 \left(\frac{\hbar\tau}{\mu}\right)^{\frac{1}{2}} \left[1 + O\left(\frac{1}{\Omega^2\tau^2}\right)\right] \quad . \tag{A.23b}$$

Here use has been made of Eq. (A.21), and for simplicity the classical driving force has been omitted ($F = 0$). One can attach a pointer with a scale to the central plate, and in principle one can read out $z(\tau)$ from that pointer with probable error $\Delta z(\tau)$. From the result one can infer the free-mass momentum p_o to within probable error

$$\delta p_o = \frac{\Delta z(\tau)}{\partial \langle \hat{z}(\tau) \rangle / \partial p_o} \simeq \left(\frac{\hbar L}{K^2 \tau^3} \right)^{\frac{1}{2}} \cdot \left[1 + O\left(\frac{L}{mK^2 \tau^2} \right) \right] \quad , \tag{A.24}$$

where again Eq. (A.21) has been used. For a given τ, if the coupling is stronger than $K^2 = L/m\tau^2$, then the measurement can be more accurate than the standard quantum limit [$\delta p_o < (\hbar m/\tau)^{\frac{1}{2}}$]; and if $K \to \infty$, then the measurement can be arbitrarily accurate.

In this variant of the experiment the "spring-based negative capacitor" functions as a readout device ("charge meter") which is carefully tuned ($kD^2/V_0^2 = 1/mK^2$; Eqs. A.1 and A.12) to the rest of the sensing circuit. The pointer attached to the central plate gets displaced by an amount $\langle \hat{z}(\tau) \rangle$, which is proportional to the charge that has flowed onto the central plate — and thence proportional to the momentum p_o of the free mass. A person adopting this "third viewpoint" should realize that the careful tuning ($kD^2/V_0^2 = 1/mK^2$) is required to produce a zero-frequency mode in which the signal can accumulate ("viewpoint two"), but he need not be aware that his charge meter is functioning, in effect, like a negative capacitor ("viewpoint one").[11]

4. An Amplifier-Based Negative Capacitor

Figure 8(a) shows a model negative capacitor constructed from standard electronic components, including a voltage amplifier with infinite input impedance. The amplifier has arbitrarily large amplification at all frequencies of interest, and its equivalent voltage and current noise sources $V_n(t)$ and $I_n(t)$ have spectral densities constrained by the quantum limit

$$S_V(f)\, S_I(f) \geq (4\pi\hbar f)^2 \tag{A.25}$$

(Heffner, 1962; Eq. 3.7 of this paper). (For simplicity we assume zero correlation between the voltage and current noises.) The capacitors C_1 and C_2 act as a voltage divider. When a voltage V is applied to A, the amplifier forces a negative charge $-C_0(C_1/C_2)V$ to flow in at terminal A and onto the capacitor C_0. Thus, the system exhibits a negative capacitance $-C_N$ given by

$$C_N = C_0(C_1/C_2) \quad . \tag{A.26}$$

It is straightforward to show that the voltage-current relation for this device is

$$\tilde{V} = \frac{\tilde{I}}{i\,2\pi f\, C_N} - \tilde{V}_n \left(1 + \frac{C_2}{C_1}\right) + \frac{\tilde{I}_n}{i\,2\pi f}\left(\frac{1}{C_N} + \frac{1}{C_1}\right) \quad , \tag{A.27}$$

where a tilde denotes Fourier transform at frequency f $\left[\tilde{A}(f) = \int_{-\infty}^{\infty} A(t)\, e^{i2\pi ft} dt\right]$. This is identical to the voltage-current relation for the "Thevenin equivalent circuit" of Fig. 7(b). The voltage noise source for that circuit, $V_N(t)$, has spectral density which we can read off Eq. (A.27):

$$S_{V_N}(f) = \left(1 + \frac{C_2}{C_1}\right)^2 S_V(f) + \frac{S_I(f)}{(2\pi f)^2}\left(\frac{1}{C_N} + \frac{1}{C_1}\right)^2 \quad . \tag{A.28}$$

This noise is minimized for fixed C_N by setting $C_1/C_2 \to \infty$, $C_1/C_N \to \infty$, and by impedance-matching the amplifier so that $S_I/S_V = (2\pi f\, C_N)^2$. (In principle the impedance-matching can be achieved at any chosen frequency by a transformer that immediately precedes the amplifier input.) Then the spectral density of the equivalent noise source V_N becomes

$$S_{V_N} = \frac{(S_V S_I)^{1/2}}{\pi f\, C_N} \quad . \tag{A.29}$$

The quantum limit (A.25) for the amplifier then implies

$$S_{V_N} \gtrsim 4\hbar/C_N \ . \tag{A.30}$$

This is the very best noise performance that the model negative capacitor of Fig. 8 can possibly achieve. It is instructive to compare this noise, which has a white spectrum, with that of our spring-based model for a negative capacitor (Eq. A.9c), which is concentrated at the very high frequency Ω .

Unfortunately, the noise performance (A.30) is too poor to permit use of this negative capacitor in the "arbitrarily quick and accurate" gedanken experiments of Sec. III. For example, in the momentum measuring experiment of Sec. III.A.2 we require $C_N = 1/mK^2$, where m is the mass of the "free mass" being measured, and K is the coupling constant in the transducer. In "DC" measurements of duration τ our model capacitor would superimpose on the transducer output a fluctuating voltage with variance

$$\Delta V_N \simeq \left(S_{V_N} \frac{1}{2\tau}\right)^{1/2} \gtrsim \left(\frac{2\hbar}{C_N \tau}\right)^{1/2} = K\left(\frac{2\hbar m}{\tau}\right)^{1/2} \ . \tag{A.31}$$

For comparison, the signal voltage produced by the transducer is $V_s = -Kp$ (cf. Eq. 3.11 with $V_s = d\Pi/dt$), where p is the momentum to be measured. Evidently the voltage noise V_N of the negative capacitor produces an uncertainty

$$\delta p \simeq (2\hbar m/\tau)^{1/2} \tag{A.32a}$$

in one's measurement of p, and a corresponding uncertainty

$$\delta F \simeq \delta p/\tau \simeq (2\hbar m/\tau^3)^{1/2} \tag{A.32b}$$

in one's knowledge of any classical force acting on the free mass. These uncertainties are equal to the standard quantum limit for a free mass. Thus, the noise of our second negative capacitor [Fig. 8(a)] is too great to permit its use in measurements designed to beat the standard quantum limit.

5. A Narrow-Band Negative Capacitor

When one is performing measurements in a narrow band of angular frequencies $\Delta\omega$ around a high "carrier" frequency Ω, one can use an inductor as a negative capacitor. Aside from fractional corrections of order $\Delta\omega/\Omega$, an inductor with inductance $L \equiv (\Omega^2 C_N)^{-1}$ has the same impedance in this band as a negative capacitor $-C_N$:

$$Z = -i\,2\pi f\,L = \frac{1}{-i\,2\pi f(-C_N)}\left[1 + O\left(\frac{\Delta\omega}{\Omega}\right)\right] \quad . \tag{A.33}$$

In principle such a "narrow-band" negative capacitor can be noiseless.

The "arbitrarily quick and accurate" gedanken experiments of Sec. III require a negative capacitor that operates over a broad band of frequencies, $0 < f \lesssim 1/2\tau$. Thus, an inductor cannot do the required job. However, one can invent a more complicated version of those gedanken experiments, in which, for a measurement of the momentum of a free mass, the output of the velocity transducer is multiplied by $\cos \Omega t$ with $\Omega >> 1/\tau$. Similarly, for a measurement of the X_1 of an oscillator, the outputs of both the coordinate and velocity transducers can be multiplied by $\cos \Omega t$. Then the readout is at frequencies $\simeq \Omega$ in the band $\Delta\omega \simeq \pi/\tau$, and a narrow-band negative capacitor (i.e., an inductor) does an adequate job of converting the velocity transducer into a momentum transducer. Such a measurement can determine the momentum of a free mass with accuracy $\delta p_o \simeq (\Omega\tau)^{-1/2}\,(\hbar m/\tau)^{1/2}$, or the X_1 of an oscillator with accuracy $\delta X_1 \simeq (\omega\tau)^{-1/2}\,(\Omega\tau)^{-1/2}\,(\hbar/2m\omega)^{1/2}$. This trick of "upconversion" of the signal to a carrier frequency Ω is discussed in detail in Paper II.

APPENDIX B

PHYSICAL REALIZATIONS OF THE HAMILTONIAN (3.16) FOR ARBITRARILY QUICK AND ACCURATE MEASUREMENTS OF X_1

In this Appendix we describe gedanken apparatus by which, in principle, one could make the "arbitrarily quick and accurate" measurements of X_1 described abstractly in Sec. III.B. Our objective is not to describe practical apparatus for real experiments. (Practical issues are discussed in Paper II.) Rather, we seek to demonstrate, in the manner of a mathematician proving a theorem, that in principle there can exist apparatus governed precisely by the Hamiltonian of Sec. III.B (Eq. 3.16).

Section 1 of this Appendix describes apparatus for measuring a mechanical oscillator, and discusses the relationship between classical generators to be used in that apparatus and quantum mechanical generators. Section 2 describes apparatus for an electromagnetic oscillator.

1. Mechanical Oscillator

a) Physical Description

Figure 9 shows a physical realization of the coupled oscillator and measuring apparatus which were described abstractly in Sec. III.B. In this figure our mechanical oscillator is drawn with very thick lines. It consists of a mass (stippled square) coupled by a spring to a rigid wall.

Our electromagnetic generator circuit is drawn with lines of medium thickness. It is an LC circuit with a single lumped inductance L_g and with total capacitance C_g split up among three capacitors in series — two at the top of the diagram; the third at the lower right. This generator will be excited into a highly classical, coherent state, thereby producing voltages proportional to cos ωt across its capacitors, and a current proportional to

- sin ωt through its inductor. These voltages and this current will provide the sinusoidal couplings for our position and momentum transducers.

The meter of Sec. III.B (a circuit with self-inductance L but no net capacitance) and the transducers which couple the meter to the mechanical oscillator are drawn with thin lines. The position transducer is the three-plate balanced capacitor labeled C_o in the upper part of Fig. 9. The outer plates will be biased with voltages $\pm$ (constant)·cos ωt by the generator's capacitors $3C_g$; and as a result the central plate, which is attached rigidly to the oscillator, will acquire a voltage proportional to x cos ωt. The momentum transducer consists of two parts: a velocity transducer [mutual inductance Mx between L and L_g which, because of the generator current $I_g \propto$ sin ωt through L_g, will produce a voltage across L that is proportional to $d(x \sin \omega t)/dt = \dot{x} \sin \omega t + \omega x \cos \omega t$]; and a complicated system of compensating capacitors which convert the velocity transducer into a momentum transducer [net output voltage proportional to $(p/m\omega)\sin \omega t + x \cos \omega t$]. We adjust the relative strengths of the couplings in our position and momentum transducers so that the total signal voltage in the meter (thin-line circuit of Fig. 9) is $K\cdot[x \cos \omega t - (p/m\omega)\sin \omega t] \equiv K\cdot X_1$.

The readout system measures the total charge Q that the signal voltage KX_1 has driven through the meter circuit. In the limit of very strong coupling, we can put the quantum/classical cut between the meter and the readout system, and we can forego any detailed mathematical description of the readout system; cf. Sec. III.B and Appendix C.2.

b) Derivation of the Hamiltonian

Initially we analyze the system of Fig. 9 in the Lagrangian formalism of classical mechanics; then we compute the Hamiltonian and quantize it.

In the Lagrangian formalism the mechanical oscillator is characterized by its mass m, frequency ω, and time-dependent position $x(t)$. The electromagnetic generator, which produces the sinusoidal couplings, is characterized by its total capacitance C_g and inductance L_g, and by the current $\dot{Q}(t) \equiv dQ/dt$ which flows in it. The eigenfrequency of the generator is identical to that of the mechanical oscillator:

$$L_g C_g = 1/\omega^2 \quad . \tag{B.1}$$

The meter is characterized by its self-inductance L and its current $\dot{Q}(t) = dQ/dt$.

From the constant K, which characterizes the coupling of the oscillator to the meter, and from the mass m and frequency ω of the oscillator, we can construct a characteric length scale s:

$$s \equiv m\omega^2/K^2 \quad . \tag{B.2a}$$

We shall choose the generator's capacitance C_g to be huge compared with s, and we shall introduce the small dimensionless parameter

$$\varepsilon \equiv s/3C_g \quad . \tag{B.2b}$$

Before each measurement the generator, regarded quantum mechanically, will be excited into a coherent state with

$$\langle \hat{Q} \rangle = Q_o \cos \omega t \ , \qquad \Delta Q = (\hbar/2L_g \omega)^{1/2} \ , \tag{B.3a}$$

$$Q_o \equiv Ks^2/\varepsilon^{3/2} \quad . \tag{B.3b}$$

The mean number of quanta in the generator, $\langle \hat{N} \rangle \equiv N_o$, and the fractional width of its wave packet will then be

$$\langle \hat{N} \rangle = N_o = \frac{\mathcal{Q}_o^2/2C_g}{\hbar\omega} = \frac{3}{2}\frac{m(\omega s)^2}{\varepsilon^2 \hbar\omega} \quad , \tag{B.3c}$$

$$\Delta\mathcal{Q}/\mathcal{Q}_o = \frac{1}{2} N_o^{-1/2} \quad . \tag{B.3d}$$

In the limit $\varepsilon \to 0$, the generator will contain an infinite number of quanta, $N_o \to \infty$, and it will become fully classical, $\Delta\mathcal{Q}/\mathcal{Q}_o \to 0$. We shall keep ε finite but small in our analysis, until we have obtained our Hamiltonian. Then (Sec. c below) we shall take $\varepsilon \to 0$, thereby bringing our Hamiltonian into the form (Eq. 3.16) studied in Sec. III.B and Appendix C.

We now construct the Lagrangian for our system, choosing the magnitudes of various parameters along the way so that in the limit $\varepsilon \to 0$ the corresponding Hamiltonian will reduce to (3.16).

The mechanical oscillator (thick lines in Fig. 9) has the familiar Lagrangian

$$\mathcal{L}_o = \frac{1}{2} m\dot{x}^2 - \frac{1}{2} m\omega^2 x^2 \quad . \tag{B.4}$$

The generator's inductance L_g is fixed in inertial space. The meter's inductance L is partly attached to the mechanical oscillator, and partly attached to inertial space — with the details of the attachments designed to produce a mutual inductance between L and L_g which is proportional to the oscillator's displacement x. The proportionality constant M is chosen to be

$$M = \varepsilon^{3/2} (\omega s)^{-2} \quad . \tag{B.5}$$

The resulting Lagrangian associated with the inductances is

$$\mathcal{L}_i = \frac{1}{2} L\dot{Q}^2 + \frac{1}{2} L_g \dot{\mathcal{Q}}^2 + Mx\dot{Q}\dot{\mathcal{Q}} \tag{B.6a}$$

$$= \frac{1}{2} L\dot{Q}^2 + \frac{1}{2} L_g \dot{\mathcal{Q}}^2 + Kx(\dot{Q}/\omega)(\dot{\mathcal{Q}}/\omega\mathcal{Q}_o) \quad . \tag{B.6b}$$

Consider next the circuitry above the mechanical oscillator in Fig. 9 — i.e., the position transducer, plus two-thirds of the generator's capacitance. The two capacitors labeled $3C_g$ are fixed in inertial space, as are the outside two plates of the capacitor C_o. The central plate of C_o is rigidly attached to the mechanical oscillator, so that its separations from the outside plates are $\frac{1}{2} D_o \pm x$. We define C_o to be the capacitance between the outside plates at a moment when there is no charge on the central plate ($Q = 0$). We set

$$C_o \equiv s/\varepsilon^{3/4} , \qquad D_o \equiv s/\varepsilon^{1/2} \tag{B.7}$$

so that in the limit $\varepsilon \to 0$, (i) the plate separation D_o gets arbitrarily large, leaving plenty of room for the oscillator to move, and (ii) the linear size of the plates, $(D_o C_o)^{1/2} \propto \varepsilon^{-5/8}$, gets far larger than their separation, $D_o \propto \varepsilon^{-1/2}$. The total energy in the capacitors, expressed in terms of Q, $\mathcal{Q}$, and x, is equal to minus the Lagrangian, $-\mathcal{L}_c$, of the capacitors. A straightforward computation gives

$$\mathcal{L}_c = - \frac{\mathcal{Q}^2}{3C_g(1 + 2C_o/3C_g)} - \frac{Q^2}{8C_o}\left[1 + \frac{2C_o}{3C_g} - \frac{4(x/D_o)^2}{1 + 2C_o/3C_g}\right] - \frac{2\mathcal{Q}Qx/D_o}{3C_g(1 + 2C_o/3C_g)} . \tag{B.8a}$$

By using Eqs. (B.7), (B.2b), and (B.3b), and discarding all contributions to $\mathcal{L}_c$ which vanish in the limit $\varepsilon \to 0$, we bring this into the form

$$\mathcal{L}_c = - \frac{\mathcal{Q}^2}{3C_g(1 + 2\varepsilon^{1/4})} - 2KxQ\left(\frac{\mathcal{Q}}{\mathcal{Q}_o}\right) . \tag{B.8b}$$

(Eqs. B.2 and B.3 imply $Q_o^2/C_g \propto 1/\varepsilon^2$, which forces us to keep $\varepsilon^{1/4}$ correction in B.8b).

The mutual inductance of Eq. (B.6) produces a time-dependent velocity coupling. As in Sec. III.A.2, so also here, a negative capacitor is needed to convert this velocity coupling into a pure momentum coupling — but now the negative capacitance must be time-dependent. It is achieved by the compensating capacitors at the bottom of Fig. 9 . These include (i) a constant negative capacitance -s, which has the internal structure discussed in Appendix A.1 and which contributes

$$\mathcal{L}_s = + \frac{1}{2} Q^2/s \qquad (B.9)$$

to the Lagrangian; and (ii) the variable positive capacitor "C_1". The left plate of C_1 is fixed in inertial space and the right plate of C_1 is attached rigidly by an insulator to the movable left plate of the generator's capacitor "$3C_g$" — which in turn is attached by insulated springs (total spring constant k) to the right plate of $3C_g$. This arrangement enables the generator to modulate the plate separation of C_1 and thereby modulate its capacitance. The total mass of the movable plates is vanishingly small (eigenfrequency of vibration infinitely large) so that, like the central plate of the model negative capacitor in Fig. 7a, they move adiabatically and they inject zero noise into the electrical system. When no charge is on the capacitors, the movable plates have position y = 0 and the capacitances are $3C_g$ and C_1. When charges $\mathcal{Q}$ and Q are applied, the equilibrium position is

$$y = \frac{1}{k}\left(\frac{\mathcal{Q}^2}{6C_gD_g} - \frac{Q^2}{2C_1D_1}\right) . \qquad (B.10)$$

We set

$$k = \frac{1}{2}\,\varepsilon^{-3/2}\,m\omega^2 \quad , \qquad D_g = \varepsilon^{-5/8}\,s \quad , \qquad C_1 = \varepsilon^{-1/8}\,s \quad ,$$

$$D_1 = \varepsilon^{1/4}\,s \quad , \tag{B.11}$$

so that in the limit $\varepsilon \to 0$ the plates' linear sizes become large compared to their equilibrium separations and large compared to their displaced separations:

$$\frac{D_g}{(C_g D_g)^{1/2}} \to 0 \ , \quad \frac{(D_g - y)}{(C_g D_g)^{1/2}} \to 0 \ , \quad \frac{D_1}{(C_1 D_1)^{1/2}} \to 0 \ , \quad \frac{D_1 + y}{(C_1 D_1)^{1/2}} \to 0 \ .$$

A straightforward computation gives for the Lagrangian of these two variable capacitors (equal to minus the energy in the springs and capacitors)

$$\mathcal{L}_{vc} = -\frac{Q^2}{6C_g}\left(1 - \frac{1}{12}\,\frac{Q^2}{kC_g D_g^2}\right) - \frac{Q^2}{2C_1}\left(1 - \frac{1}{4}\,\frac{Q^2}{kC_1 D_1^2}\right)$$

$$- \frac{1}{12}\,\frac{Q^2 Q^2}{kC_1 D_1 C_g D_g} \ . \tag{B.12a}$$

Using Eqs. (B.11), (B.2), and (B.3b), and discarding terms in $\mathcal{L}_{vc}$ that vanish when $\varepsilon \to 0$, we bring this into the form

$$\mathcal{L}_{vc} = -\frac{Q^2}{6C_g}\left[1 - \frac{1}{2}\,\varepsilon^{3/4}\left(\frac{Q}{Q_o}\right)^2\right] - \frac{Q^2}{2s}\left(\frac{Q}{Q_o}\right)^2 \ . \tag{B.12b}$$

(The $\varepsilon^{3/4}$ correction must be kept here because $Q_o^{\,2}/C_g \propto 1/\varepsilon^2$.)

The total Lagrangian is the sum of Eqs. (B.4), (B.6b), (B.8b), (B.9), and (B.12b):

$$\mathcal{L} = \frac{1}{2}\,m\dot{x}^2 - \frac{1}{2}\,m\omega^2 x^2 + \frac{1}{2}\,L_g\dot{Q}^2 - \frac{Q^2}{2C_g}\left[\frac{1 + (2/3)\varepsilon^{1/4}}{1 + 2\varepsilon^{1/4}} - \frac{1}{6}\,\varepsilon^{3/4}\left(\frac{Q}{Q_o}\right)^2\right]$$

$$+ \frac{1}{2}\,L\dot{Q}^2 + \frac{Q^2}{2s}\left[1 - \left(\frac{Q}{Q_o}\right)^2\right] - 2KxQ\left(\frac{Q}{Q_o}\right) + Kx\left(\frac{\dot{Q}}{\omega}\right)\left(\frac{\dot{Q}}{\omega Q_o}\right) \ . \tag{B.13}$$

The terms multiplying $-\mathcal{Q}^2/2C_g$ produce only a slight renormalization of the generator frequency and a slight anharmonicity in its oscillations — and these effects vanish in the limit $\varepsilon \to 0$. Therefore we may discard these terms, thereby bringing our Lagrangian into the form

$$\mathcal{L} = \frac{1}{2} m\dot{x}^2 - \frac{1}{2} m\omega^2 x^2 + \frac{1}{2} L_g \dot{\mathcal{Q}}^2 - \frac{\mathcal{Q}^2}{2C_g} + \frac{1}{2} L\dot{Q}^2 + \frac{Q^2}{2s}\left[1 - \left(\frac{\mathcal{Q}}{\mathcal{Q}_o}\right)^2\right]$$

$$- 2KxQ\left(\frac{\mathcal{Q}}{\mathcal{Q}_o}\right) + Kx\left(\frac{\dot{Q}}{\omega}\right)\left(\frac{\dot{\mathcal{Q}}}{\omega\mathcal{Q}_o}\right) \quad . \tag{B.14}$$

A slightly prettier form can be obtained by the change of generator coordinate

$$\mathcal{Q}_{old} = \mathcal{Q}_{new} - \frac{K}{\mathcal{Q}_o L_g \omega^2} xQ \tag{B.15}$$

— a change which becomes $\mathcal{Q}_{old} = \mathcal{Q}_{new}$ in the limit $\varepsilon \to 0$ ($\mathcal{Q}_o/C_g \to \infty$). By making this change of coordinate, and by discarding terms in $\mathcal{L}$ which vanish as $\varepsilon \to 0$, we bring our Lagrangian into the final form

$$\mathcal{L} = \frac{1}{2} m\dot{x}^2 - \frac{1}{2} m\omega^2 x^2 + \frac{1}{2} L_g \dot{\mathcal{Q}}^2 - \frac{\mathcal{Q}^2}{2C_g} + \frac{1}{2} L\dot{Q}^2 + \frac{Q^2}{2s}\left[1 - \left(\frac{\mathcal{Q}}{\mathcal{Q}_o}\right)^2\right]$$

$$-KQ\left[x\left(\frac{\mathcal{Q}}{\mathcal{Q}_o}\right) + \frac{\dot{x}}{\omega}\left(\frac{\dot{\mathcal{Q}}}{\omega\mathcal{Q}_o}\right)\right] \quad . \tag{B.16}$$

We next introduce the generalized momenta

$$p = \frac{\partial\mathcal{L}}{\partial\dot{x}} = m\dot{x} - \frac{KQ}{\omega}\left(\frac{\dot{\mathcal{Q}}}{\omega\mathcal{Q}_o}\right), \quad \Pi = \frac{\partial\mathcal{L}}{\partial\dot{Q}} = L\dot{Q} \ , \quad \mathcal{J} = \frac{\partial\mathcal{L}}{\partial\dot{\mathcal{Q}}} = L_g\dot{\mathcal{Q}} - \frac{KQ\dot{x}}{\omega^2\mathcal{Q}_o} \ , \tag{B.17}$$

compute the Hamiltonian $H = p\dot{x} + \Pi\dot{Q} + \mathcal{J}\dot{\mathcal{Q}} - \mathcal{L}$, discard terms that vanish as $\varepsilon \to 0$, and quantize. The result is

$$\hat{H} = \frac{\hat{p}^2}{2m} + \frac{1}{2}m\omega^2\hat{x}^2 + \frac{\hat{\Pi}^2}{2L} + \frac{\hat{Q}^2}{2s}\left[\left(\frac{\hat{\mathcal{J}}}{L_g\omega\mathcal{Q}_o}\right)^2 + \left(\frac{\hat{\mathcal{Q}}}{\mathcal{Q}_o}\right)^2 - 1\right]$$
$$+ \frac{\hat{\mathcal{J}}^2}{2L_g} + \frac{\hat{\mathcal{Q}}^2}{2C_g} + K\hat{Q}\left(\hat{x}\frac{\hat{\mathcal{Q}}}{\mathcal{Q}_o} + \frac{\hat{p}}{m\omega}\frac{\hat{\mathcal{J}}}{L_g\omega\mathcal{Q}_o}\right) . \qquad \text{(B.18)}$$

c) Quantum Generator Compared with Classical Generator

Equation (B.18) is the Hamiltonian of our oscillator plus measuring apparatus, with the generator treated quantum mechanically. W. G. Unruh (1979) has pointed out the importance of treating the generator quantum mechanically rather than classically in any fully rigorous analysis of measurements of X_1, and he was the first person to write down the Hamiltonian (B.18) for such a fully rigorous analysis.

We now show that the quantum generator can be replaced, in principle, by a classical generator without loss of accuracy in our analysis — thereby justifying our use of classical generators throughout the text of this paper. Specifically, before any measurements begin the quantum generator is prepared in the coherent state (B.3), which has a mean number of quanta N_o, and has

$$\frac{\langle\hat{\mathcal{Q}}\rangle}{\mathcal{Q}_o} = \cos\omega t \ , \qquad \frac{\langle\hat{\mathcal{J}}\rangle}{L_g\omega\mathcal{Q}_o} = -\sin\omega t \ ,$$

$$\frac{\Delta\mathcal{Q}}{\mathcal{Q}_o} = \frac{\Delta\mathcal{J}}{L_g\omega\mathcal{Q}_o} = \frac{1}{2N_o^{1/2}} \ ,$$

$$\left\langle\frac{\hat{\mathcal{J}}^2}{2L_g} + \frac{\hat{\mathcal{Q}}^2}{2C_g}\right\rangle = (N_o + \tfrac{1}{2})\hbar\omega \ , \qquad \text{(B.19)}$$

$$\left\langle\left(\frac{\hat{\mathcal{J}}}{L_g\omega\mathcal{Q}_o}\right)^2 + \left(\frac{\hat{\mathcal{Q}}}{\mathcal{Q}_o}\right)^2 - 1\right\rangle = \frac{1}{2N_o} \ ,$$

$$\Delta\left[\left(\frac{\mathcal{J}}{L_g\omega\mathcal{Q}_o}\right)^2 + \left(\frac{\mathcal{Q}}{\mathcal{Q}_o}\right)^2 - 1\right] = \frac{1}{N_o^{1/2}} \ .$$

Comparison of Eqs. (B.19) and (B.18) shows that, in the limit $N_o \to \infty$ (i.e., $\varepsilon \to 0$), the generator behaves completely classically and is not loaded at all

by the rest of the system — i.e., it is governed by the uncoupled Hamiltonian

$$\hat{H}_g = \frac{\hat{\mathcal{J}}^2}{2L_g} + \frac{\hat{Q}^2}{2C_g} \quad ; \tag{B.20}$$

and it always remains in the infinitely-sharply-peaked coherent state of (B.19). The Hamiltonian for the rest of the system, when $N_o \to \infty$, is obtained by removing the decoupled generator Hamiltonian (B.20) from (B.18), and by replacing $\hat{Q}/Q_o$ and $\hat{\mathcal{J}}/L_g\omega Q_o$ by their sharp classical values, cos ωt and - sin ωt. The result,

$$\hat{H} = \frac{\hat{p}^2}{2m} + \frac{1}{2} m\omega^2\hat{x}^2 + \frac{\hat{\Pi}^2}{2L} + K\hat{Q}(\hat{x} \cos \omega t - \frac{\hat{p}}{m\omega} \sin \omega t) \quad , \tag{B.21}$$

is identical to the Hamiltonian (3.16) with classical generator, which was analyzed in Sec. III.B of the text.

Suppose that the generator is not fully classical, i.e., that N_o is finite. Then to what extent will a measurement of $\hat{X}_1$ be marred by quantum fluctuations in the generator and by loading of the generator by the experimental apparatus? The answer, when the exact Hamiltonian has the form (B.18), can be computed by a perturbation-theory analysis of the gedanken experiment of Sec. III.B. Such a computation reveals the following, for the case where one wishes to measure $\hat{X}_1$ with accuracy better than the standard quantum limit, $(\hbar/2m\omega)^{1/2}$, and with measurement time τ:
Let μ be the fractional distance below the standard quantum limit which the experiment could achieve with a perfect, classical generator:

$$\mu \equiv \left(\frac{4\hbar L}{K^2\tau^3}\right)^{1/2} \left(\frac{1}{\hbar/2m\omega}\right)^{1/2} = \left(\frac{8mL\omega}{K^2\tau^3}\right)^{1/2} \tag{B.22}$$

(cf. Eq. 3.21); if the probability distribution of $\hat{X}_1$ before the experiment begins is peaked about a value ξ_o near zero, with halfwidth $\Sigma = \alpha(\hbar/2m\omega)^{1/2}$

where $\alpha \lesssim \mu$, then the measurement (i) can determine ξ_o with a probable error

$$\Delta\xi_m \simeq \mu\left(\frac{\hbar}{2m\omega}\right)^{1/2}\left[1+\frac{\alpha^2}{\mu^2}+\text{terms of order}\left(\frac{1}{\mu^4(\omega\tau)^2N_o},\frac{1}{\mu^4(\omega\tau)N_o},\frac{1}{\mu^2\alpha^2N_o}\right)\right]^{1/2}, \tag{B.23a}$$

and (ii) increases the variance of $\hat{X}_1$ to

$$\Delta X_1 \simeq \alpha\left(\frac{\hbar}{2m\omega}\right)^{1/2}\left[1+\text{terms of order}\left(\frac{1}{\mu^4(\omega\tau)N_o},\frac{1}{\mu^2\alpha^2N_o}\right)\right]^{1/2}. \tag{B.23b}$$

Evidently the quantum properties of the generator cause neligible error in the experiment if the generator is excited in a coherent state with mean number of quanta

$$\langle\hat{N}\rangle \equiv N_o \gg \max\left\{\frac{1}{\mu^4(\omega\tau)^2}\ ,\ \frac{1}{\mu^2\alpha^2}\right\}. \tag{B.24}$$

Note that for measurements near the standard quantum limit ($\mu \sim \alpha \sim 1$) in times not much shorter than one cycle ($\omega\tau \gtrsim 1$), the generator does not need to be highly excited.

Unruh (1979) has pointed out that one can design a quantum mechanical generator which is protected entirely from loading (back action) by the experimental apparatus, even when the level of generator excitation is finite. To achieve such a "loading-free" generator one uses not a harmonic oscillator ($\hat{H}_g = \hat{p}^2/2L_g + \hat{Q}^2/2C_g$; $[\hat{Q},\hat{p}] = i\hbar$), but rather the following system with two dynamical degrees of freedom:

$$\hat{H}_g = \frac{\hat{p}^2}{2L_g} + \frac{1}{2}L_g\omega^2\hat{Q}^2 - \frac{\hat{q}\hat{p}}{L_g} + L_g\omega^2\,\hat{j}\hat{Q}, \tag{B.25a}$$

$$[\hat{q},\hat{Q}] = i\hbar\ ,\quad [\hat{j},\hat{p}] = i\hbar\ ,\quad \text{all other commutators vanish.} \tag{B.25b}$$

Equation (B.25a) is the Hamiltonian of a charged particle in a suitable constant magnetic field with a quadrupole electric field to cancel the quadratic

$\hat{j}^2$ and $\hat{q}^2$ terms in the magnetic Hamiltonian [cf. the example between Eqs. (4.7') and (4.9), with the change of notation $m \to 1/(L_g\omega^2)$, $\frac{1}{2}eB_o \to 1/(L_g\omega)$, $\hat{x} \to \hat{q}$, $\hat{p}_x \to \hat{Q}$, $\hat{y} \to L_g\omega\hat{j}$, $\hat{p}_y \to \hat{\mathcal{J}}/L_g\omega$]. If such a generator is used in our gedanken experiment (replace $\hat{\mathcal{J}}^2/2L_g + \hat{Q}^2/2C_g$ in B.18 by B.25a), the resulting Heisenberg equations for $\hat{\mathcal{J}}$ and $\hat{Q}$ will be precisely those of a free harmonic oscillator:

$$d\hat{\mathcal{J}}/dt = -L_g\omega^2\hat{Q} \quad , \qquad d\hat{Q}/dt = \hat{\mathcal{J}}/L_g \quad . \tag{B.26}$$

This shows the complete absence of loading of Unruh's generator by our experiment, independent of the state of the generator. However, quantum fluctuations are still present in Unruh's generator and can affect the experiment — unless one puts Unruh's generator into a state with arbitrarily small variances of $\hat{Q}$ and $\hat{\mathcal{J}}$ (possible because $[\hat{Q},\hat{\mathcal{J}}] = 0$). Such a special state,

$$\langle\hat{Q}\rangle = Q_o\cos\omega t \quad , \quad \langle\hat{\mathcal{J}}\rangle = -L_g\omega Q_o\sin\omega t \quad , \quad \Delta\mathcal{J} = L_g\omega\Delta Q = \text{const} \to 0, \tag{B.27}$$

is the analog of the arbitrarily energetic coherent state ($Q_o \to \infty$) which our generator requires in order to avoid quantum fluctuations. Our generator's coherent state has an arbitrarily large expectation value and variance for its energy:

$$\langle\hat{H}_g\rangle = (N_o + \tfrac{1}{2})\hbar\omega \to \infty \quad , \quad \Delta H_g = N_o^{1/2}\hbar\omega = (Q_o/2\Delta Q)\hbar\omega \to \infty \quad . \tag{B.28a}$$

Unruh's special state (B.27), in principle, can have a finite mean energy $\langle\hat{H}_g\rangle$; but its energy variance is arbitrarily large and, in fact, for given Q_o and ΔQ is of the same magnitude as our variance:

$$\Delta H_g \Delta Q \geq \frac{1}{2}|\langle[\hat{Q},\hat{H}_g]\rangle| = \frac{\hbar}{2L_g}\,|\langle\hat{\mathcal{J}}\rangle| = \frac{1}{2}\hbar\omega Q_o|\sin\omega t| \quad ,$$

$$\Delta H_g \Delta \mathcal{J} \geq \frac{1}{2}|\langle[\hat{\mathcal{J}},\hat{H}_g]\rangle| = \frac{1}{2}\hbar L_g\omega^2|\langle\hat{Q}\rangle| = \frac{1}{2}\hbar\omega(L_g\omega Q_o)|\cos\omega t| \quad ,$$

whence

$$\Delta H_g \geq 2^{-1/2}(Q_o/2\Delta Q)\hbar\omega \to \infty \quad . \tag{B.28b}$$

Unruh's generator (charged-particle system described by Eq. B.25) was mentioned in Sec. IV.A as an illustration of the concept of a "generalized QND observable." The observables $\hat{Q}$ and $\hat{\mathcal{J}}$ are a pair of such observables, and it is precisely this fact that allows Unruh's generator to avoid back action (loading) from the experiment.

Unruh's generator is important because it shows that in principle one can design a generator which is completely free of back action. However, it is not clear how one could realize physically the desired coupling of Unruh's generator to our experiment.

2. Electromagnetic Oscillator

We now turn to a physical realization of the Hamiltonian (3.16) for the case of an electromagnetic oscillator. Such a realization was given in our Physical Review Letter (Thorne et al., 1978) and is reproduced with minor changes in Fig. 10.

The oscillator whose X_1 is to be measured is an "LC circuit" consisting of the two coils (total self-inductance m) near the bottom of Fig. 10, and the four capacitor plates A, A', B, B' near the top. The oscillator is coupled, via coordinate (charge x) and momentum (magnetic flux p) transducers to a torsion pendulum (vertical central rod in Fig. 10, and paraphernalia attached to it). The coupling produces a torque $-KX_1$ on the torsion pendulum, causing it to swing through an angle Q. The coupling to

$X_1 = x \cos \omega t - (p/m\omega) \sin \omega t$ requires a sinusoidal voltage $V_o(t) \propto \cos \omega t$ in the coordinate (charge x) transducer, and a sinusoidal current $I_o(t) \propto \sin \omega t$ in the momentum (magnetic flux p) transducer. The sinusoidal voltage and current are produced by an electromagnetic generator analogous to that in the preceding section, which is excited into an arbitrarily energetic, coherent state. As sketched in the last section, this generator produces a perfect, classical output. For simplicity we here ignore its details and replace it by ideal, classical voltage and current sources $V_o(t)$ and $I_o(t)$.

We now describe the gedanken apparatus in greater detail. The LC oscillator (coils m and capacitor A-B-A'-B' in Fig. 10) is described mathematically by the charge x on plate A, the current $\dot{x}$ that flows through the coils, the total self-inductance m of the coils, the total capacitance C between plates A and A' (via B, B', and the zero-impedance voltage source connecting them), and the eigenfrequency $\omega = (1/mC)^{1/2}$ of the circuit's oscillations. The coordinate (charge x) transducer consists of plates B and B', to which are applied a sinusoidal voltage difference $V_o \equiv -(b/a)\, K \cos \omega t$, and which are mechanically attached to the torsion pendulum. This voltage, together with the oscillator's charge x, produces a torque $\Gamma = -Kx \cos \omega t - (K^2/m\omega^2)\, Q \cos^2 \omega t$ on the pendulum. The velocity (current) transducer consists of the thin wire loop at the bottom of Fig. 10, through which a sinusoidal current $I_o \equiv (K/M\omega) \sin \omega t$ is driven. The loop is attached to the central rod so that its mutual inductance with the oscillator, MQ, is proportional to the angular displacement Q of the torsion pendulum. Current in the oscillator produces a torque $\Gamma = K(\dot{x}/\omega) \sin \omega t$ on the pendulum. The torsion pendulum (consisting of the central rod and paraphernalia attached to it and the torsion fiber that suspends it) is characterized by its moment of inertia L, torsional

spring constant $L\Omega^2$, natural frequency (in the absence of couplings) Ω, and generalized coordinate (equal to angular displacement) Q.

The complete apparatus — LC oscillator plus transducers plus torsion pendulum — is described by the classical Lagrangian

$$\mathcal{L} = \tfrac{1}{2} m (\dot{x}^2 - \omega^2 x^2) + \tfrac{1}{2} L (\dot{Q}^2 - \Omega^2 Q^2) - \tfrac{1}{2} (K^2/m\omega^2) (Q^2 \cos^2 \omega t) - K [x \cos \omega t - (\dot{x}/\omega) \sin \omega t] Q \quad . \tag{B.29}$$

The generalized momenta of the oscillator and pendulum are $p = \partial\mathcal{L}/\partial\dot{x} = m\dot{x} + (K/\omega)(\sin \omega t)Q$ and $\Pi = \partial L/\partial\dot{Q} = L\dot{Q}$; and the Hamiltonian, after quantization, is

$$\hat{H} = \hat{p}^2/2m + \tfrac{1}{2} m\omega^2 \hat{x}^2 + K\hat{X}_1\hat{Q} + \hat{\Pi}^2/2L + \tfrac{1}{2} L \bar{\Omega}^2 Q^2 \quad . \tag{B.30}$$

Here the eigenfrequency $\bar{\Omega}$ of the pendulum is shifted from its natural value Ω by coupling to the coordinate and momentum sensors:

$$\bar{\Omega}^2 = \Omega^2 + K^2/m\omega^2 L \quad . \tag{B.31}$$

The frequency renormalization (B.31) comes from two sources: First, the velocity (current) transducer used in the apparatus is equivalent to a momentum [$p = m\dot{x} + (KQ/\omega) \sin \omega t$] transducer plus a positive spring on the torsion pendulum with spring constant $(K^2/m\omega^2) \sin^2 \omega t$. (This is the analog, for measurements of electromagnetic oscillators, of our "velocity sensor equals momentum sensor plus positive capacitance" in Secs. III.A.2 and III.B.) Second, the "concentric-tin-can" shape of our capacitor-plus coordinate-transducer (Fig. 10) is carefully designed to produce on the torsion pendulum a restoring torque with spring constant $(K^2/m\omega^2) \cos^2 \omega t$.

This was done so that the net renormalization of the pendulum's eigenfrequency would be time independent.

The Hamiltonian (B.30) will have the desired form (Eq. 3.16) for a quick and accurate measurement of $\hat{X}_1$, if we set $\bar{\Omega}^2 = 0$. This requires that the natural eigenfrequency Ω of the torsion pendulum be imaginary

$$\Omega^2 = -K^2/m\omega^2 L \quad , \tag{B.32}$$

i.e., that the pendulum possess a noiseless spring with negative spring constant $-K^2/m\omega^2$. This negative spring is the analog of the negative capacitors needed in the preceding section; cf. also footnote 11 in Appendix A. Figure 11 shows an idealized example of such a noiseless, negative spring.

APPENDIX C

ARBITRARILY QUICK AND ACCURATE BACK-ACTION-EVADING MEASUREMENTS OF X_1: A DETAILED QUANTUM MECHANICAL ANALYSIS[12]

1. Overview

This Appendix builds upon and expands the discussion given in Sec. III.B; the objective is to give a detailed quantum mechanical analysis of a sequence of measurements of the X_1 of a harmonic oscillator. The analysis is exact quantum mechanically, and it should satisfy a theorist's desire for rigor. However, this rigor is purchased at the price of a highly idealized description of the measurement process, and this idealization may make an experimenter uneasy. He may prefer the more realistic, but semiclassical, measurement analyses given in Paper II.

Presenting two different analyses to appeal to two different constituencies may seem more like politics than physics, but we plead principle as well as pragmatism for the practice. We give an exact quantum mechanical analysis of a simple, idealized version of a real measurement. We then ask whether a semiclassical treatment of a similar, simple system gives the same results. If it does, we gain the confidence to apply semiclassical techniques to complicated, realistic measuring systems — systems so complex that an exact quantum mechanical treatment would be exceedingly difficult.

The key word in this Appendix is sequence. Section III.B of the body of this paper described apparatus for measuring X_1 and analyzed a single measurement of X_1 using this apparatus. The analysis proceeded by calculating the free evolution of the coupled oscillator-meter system (Eqs. 3.17-3.19), and it demonstrated that X_1 can be measured arbitrarily quickly and arbitrarily

accurately (Eq. 3.21). In this Appendix we string together a sequence of measurements of the type considered in Sec. III.B. To analyze the sequence, we must do more than just calculate the free quantum mechanical evolution of the system; we must also have a rule for carrying the quantum state from one measurement to the next. That rule is the "reduction of the wave function" at the end of each measurement (see Eq. C.28 below). Free evolution and reduction of the wave function — together these two allow us to follow changes in the state of the oscillator from measurement to measurement, and with this knowledge we can investigate the behavior of the oscillator during a sequence of measurements.

One important issue is the question of how X_1 changes during a sequence. Two results of our analysis bear on this issue. The first is that between measurements the expectation value of $\hat{X}_1$ can change, with the expected change always less than or equal to the variance of $\hat{X}_1$. The second is that the variance of $\hat{X}_1$ always decreases from one measurement to the next, for the type of measurement we analyze. Putting these two results together, we show that the expected change in the expectation value of $\hat{X}_1$ during a sequence of measurements is approximately the variance of $\hat{X}_1$ before the initial measurement.

Another, perhaps more important, issue is the question of how X_2 changes. In each measurement of the type in Sec. III.B, the expectation value of $\hat{X}_2$ receives a large "kick" because the meter coordinate $\hat{Q}$ gets displaced a large distance from zero (cf. Eqs. 3.17-3.19). These kicks accumulate from one measurement to the next, and the expectation value of $\hat{X}_2$ runs away. However, these "expectation-value kicks" are essentially classical and predictable, so one might think that the resulting "classical runaway of X_2" could be avoided by applying a "feedback force" to the meter — a force whose purpose is to keep the meter coordinate close to zero. We investigate this

issue using a model for the feedback, and we show that feedback can indeed keep the expectation value of $\hat{X}_2$ from running away. However, only part of each kick is classical. The feedback, no matter how good it may be, cannot eliminate the huge, unpredictable, quantum mechanical kick given X_2 by each precise measurement of X_1 — a kick whose size is determined by the uncertainty principle (2.9a). One might expect these "uncertainty principle kicks" to add randomly, thereby causing X_2 to random walk. We verify the existence of this "random walk of X_2" by showing that, during a sequence of measurements, the variance of $\hat{X}_2$ increases as the square root of the number of measurements.

We choose to ignore the classical driving force $F(t)$ in this Appendix. Its effect on the oscillator could be included in the analysis. However, Sec. III.B has already shown that the classical force can be measured arbitrarily quickly and arbitrarily accurately. In addition, the classical force is irrelevant to the issues addressed in this Appendix. Its inclusion would only complicate the analysis without adding any new insights.

2. Description of the Measuring Apparatus

We now turn our attention to a detailed description of the measurement process. We begin by describing the physical system, which is nearly the same as that in Sec. III.B. The oscillator to be measured is characterized by the variables of Eqs. (2.1)-(2.5), including coordinate $\hat{x}$, momentum $\hat{p}$, complex amplitude $\hat{X}_1+i\hat{X}_2$, mass m, and frequency ω. The oscillator is coupled to a measuring apparatus which consists of three parts: a generator, a meter, and a readout system. The generator provides the sinusoidal coupling in the interaction Hamiltonian. The meter is a one-dimensional quantum mechanical "free mass" with generalized coordinate $\hat{Q}$, generalized momentum $\hat{\Pi}$, and generalized mass L; the meter is coupled by the generator to $\hat{X}_1$ of the

oscillator. The readout system is coupled to the meter in such a way that at designated moments of time it "reads out" a value for the meter's coordinate Q and that at all times during each measurement it applies a constant "feedback force" to the meter. The feedback force is included to prevent the classical runaway of X_2.

Of the three parts of the measuring apparatus, only the meter will be treated quantum mechanically. As is discussed in Appendix B.1, the generator can be treated classically if, before the initial measurement in the sequence, it is prepared in a coherent state of arbitrarily large amplitude. Then the generator is completely unloaded by its coupling to the rest of the system, and it produces perfect "cos ωt" and "sin ωt" terms in the Hamiltonian.

The readout system will also be treated classically — i.e., we place the "quantum-classical cut" of our analysis between the meter and the readout system. This choice is legitimate if inclusion of all or part of the readout system in the quantum mechanical analysis would not substantially degrade the calculated accuracy of the measurement. For example, the readout system can in principle be a device which is so strongly coupled to the meter that it makes arbitrarily precise, essentially instantaneous measurements of the meter coordinate (see discussion in footnote 6). This is the model we shall adopt. Then a "readout" of Q by the readout system is described as follows: The readout system determines a value for the meter coordinate Q at a particular instant, thereby localizing the meter precisely at the measured value; formally this means that the quantum state of the oscillator-meter system is "reduced" to an eigenstate of $\hat{Q}$ whose eigenvalue is the measured value (see Eq. C.28 below).

In practice the readout system will not make infinitely precise measurements of the meter coordinate. We shall consider the case of a finite-precision readout system in Sec. 7 of this Appendix, where we sketch

a density-matrix analysis of a sequence of measurements of X_1.

Finally, we also treat the feedback force classically.

3. Foundations for the Analysis

The Hamiltonian for the coupled oscillator-meter system has the form (3.16) with the addition of a term describing the feedback force:

$$\hat{H} = \hat{H}_o + \hat{H}_M + \hat{H}_I \quad , \tag{C.1a}$$

$$\hat{H}_o = \hat{p}^2/2m + \tfrac{1}{2} m\omega^2 \hat{x}^2 \quad , \tag{C.1b}$$

$$\hat{H}_M = \hat{\Pi}^2/2L \quad , \tag{C.1c}$$

$$\hat{H}_I = K(\hat{X}_1 - \alpha)\hat{Q} \quad . \tag{C.1d}$$

Here $\hat{H}_o$ is the Hamiltonian of the free oscillator, $\hat{H}_M$ is the Hamiltonian of the meter, and K is a coupling constant. The interaction Hamiltonian $\hat{H}_I$ consists of two terms: a term $K\hat{X}_1\hat{Q}$ which describes the coupling of the oscillator to the meter via the classical generator, and a term $-K\alpha\hat{Q}$ which describes the classical feedback force on the meter. The size of the feedback force is determined by the parameter α ("force" = $K\alpha$). The feedback is under the control of the experimenter; in general, α will change from measurement to measurement in the sequence. Designs for physical systems which are governed in principle by the Hamiltonian (C.1) are considered in Appendix B. Here we do not concern ourselves with any specific physical system. The Hamiltonian (C.1) is the starting point of the analysis, which applies to any system governed by that Hamiltonian.

The analysis in Sec. III.B uses the Heisenberg picture. It is the most convenient picture for calculating the evolution of the expectation value

and variance of $\hat{Q}$ (Eqs. 3.19), and those are the only results really necessary for that analysis. In this Appendix we work exclusively in the Schrödinger picture. This is not because the Heisenberg picture could not be used; rather, it is because the Schrödinger picture is more convenient and more natural for analyzing a sequence of measurements. In particular, the reduction of the wave function can be handled more easily in the Schrödinger picture.

In the Heisenberg picture the complex amplitude of a free harmonic oscillator is conserved (Eq. 2.7). In the Schrödinger picture the operators $\hat{X}_1$ and $\hat{X}_2$ are time-dependent, and whenever it is necessary, we shall indicate explicitly the time at which they are evaluated:

$$\hat{X}_1(t) = \hat{x} \cos \omega t - (\hat{p}/m\omega) \sin \omega t, \tag{C.2a}$$

$$\hat{X}_2(t) = \hat{x} \sin \omega t + (\hat{p}/m\omega) \cos \omega t. \tag{C.2b}$$

The corresponding Heisenberg operators for a free harmonic oscillator are given by $(\hat{X}_j)_H(t) \equiv \hat{U}_o^\dagger(t,t_0)\, \hat{X}_j(t)\, \hat{U}_o(t,t_0)$, where $\hat{U}_o$ is the time-development operator for the free oscillator:

$$\hat{U}_o(t,t_0) = e^{-i(t - t_0)\hat{H}_o/\hbar} . \tag{C.3}$$

Hence, conservation of the complex amplitude of a free oscillator translates into the following identity in the Schrödinger picture:

$$\hat{X}_j(t) \equiv \hat{U}_o(t,t_0)\, \hat{X}_j(t_0)\, \hat{U}_o^\dagger(t,t_0) . \tag{C.4}$$

Equation (C.4) holds for arbitrary times t and t_0.

In the Schrödinger picture the information about the state vector $|\psi(t)\rangle$ of the coupled oscillator-meter system is conveniently expressed in terms of an evolving "wave function," which is defined by projecting $|\psi(t)\rangle$

onto appropriate basis states. For the meter the choice of basis states is obvious. Since we are interested in the behavior of the meter coordinate, we choose the eigenstates $|Q\rangle$ of $\hat{Q}$ with delta-function normalization:

$$\hat{Q}|Q\rangle = Q|Q\rangle \quad ; \quad \langle Q|Q'\rangle = \delta(Q-Q') \ . \tag{C.5}$$

For the oscillator the most convenient basis states are eigenstates of $\hat{X}_1(t)$. To define such states we begin with the delta-function normalized eigenstates $|\xi,0\rangle$ of $\hat{X}_1(0) = \hat{x}$:

$$\hat{X}_1(0)|\xi,0\rangle = \xi|\xi,0\rangle \quad ; \quad \langle\xi,0|\xi',0\rangle = \delta(\xi-\xi'). \tag{C.6}$$

We then define new states

$$|\xi,t\rangle \equiv \hat{U}_o(t,0)|\xi,0\rangle \ . \tag{C.7}$$

These new states have delta-function normalization, and as one shows using Eq. (C.4), they are also the desired eigenstates of $\hat{X}_1(t)$:

$$\hat{X}_1(t)|\xi,t\rangle = \xi|\xi,t\rangle \quad ; \quad \langle\xi,t|\xi',t\rangle = \delta(\xi-\xi'). \tag{C.8}$$

An important property of these states is that

$$|\xi,t\rangle = \hat{U}_o(t,t_0)|\xi,t_0\rangle \ . \tag{C.9}$$

A complete set of states for the oscillator-meter system can be obtained by taking the tensor product of the states $|\xi,t\rangle$ and $|Q\rangle$:

$$|\xi,Q;t\rangle \equiv |\xi,t\rangle \otimes |Q\rangle \ . \tag{C.10}$$

Given this complete set, we can define a wave function corresponding to the state vector $|\psi(t)\rangle$ by

$$\psi(\xi,Q;t) \equiv \langle\xi,Q;t|\psi(t)\rangle \ . \tag{C.11}$$

The wave function has the usual interpretation: $|\psi(\xi,Q;t)|^2 d\xi dQ$ is the probability at time t of simultaneously finding the meter coordinate between Q and Q + dQ and the oscillator with X_1 between ξ and $\xi + d\xi$.

In the Schrödinger picture the evolution of the state vector $|\psi(t)\rangle$ is determined by the unitary time-development operator $\hat{U}(t,t_0)$ [not to be confused with $\hat{U}_o(t,t_0)$] — i.e.,

$$|\psi(t)\rangle = \hat{U}(t,t_0)|\psi(t_0)\rangle \quad , \tag{C.12a}$$

where $\hat{U}(t,t_0)$ satisfies the Schrödinger equation

$$i\hbar\, d\hat{U}(t,t_0)/dt = \hat{H}(t)\, \hat{U}(t,t_0) \quad , \qquad \hat{U}(t_0,t_0) = 1 \; . \tag{C.12b}$$

For the Hamiltonian (C.1), the solution for $\hat{U}(t,t_0)$ can be obtained using the techniques employed to solve for the time-development operator of a forced harmonic oscillator (Eqs. 2.20). We omit the details and simply give the solution:

$$\hat{U}(t,t_0) = \hat{U}_o(t,t_0)\, \exp\left\{ -\frac{i}{\hbar}(t-t_0)^3 \frac{K^2[\hat{X}_1(t_0) - \alpha]^2}{6L} \right\} \times$$
$$\times \exp\left\{ -\frac{i}{\hbar}(t-t_0)\, K[\hat{X}_1(t_0) - \alpha]\hat{Q} \right\} \times$$
$$\times \exp\left\{ \frac{i}{\hbar}(t-t_0)^2 \frac{K[\hat{X}_1(t_0) - \alpha]}{2L} \hat{\Pi} \right\} \hat{U}_M(t,t_0) \quad , \tag{C.13}$$

where

$$\hat{U}_M(t,t_0) = e^{-i(t-t_0)\hat{H}_M/\hbar} \tag{C.14}$$

is the time-development operator for the meter Hamiltonian.

The abstract operator equations (C.12) and (C.13) governing the evolution of the state vector can be translated into an equivalent equation for

the evolution of the wave function. In the case of interest to us the oscillator and meter are in states $|\chi\rangle$ and $|\Phi\rangle$, respectively, at time t_0; the corresponding wave functions are $\chi(\xi) \equiv \langle \xi, t_0 | \chi \rangle$ and $\Phi(Q) \equiv \langle Q | \Phi \rangle$. The initial state vector is $|\psi(t_0)\rangle = |\chi\rangle \otimes |\Phi\rangle$, with associated wave function $\psi(\xi,Q;t_0) = \chi(\xi)\Phi(Q)$. Since $e^{-ia\hat{\Pi}/\hbar}$ is the displacement operator for the meter (see, e.g., Sec. 14.7 of Merzbacher, 1970), it is easy to show that

$$e^{-i\nu[\hat{X}_1(t_0) - \alpha]\hat{\Pi}/\hbar} |\xi,Q;t_0\rangle = |\xi,Q+\nu(\xi-\alpha);t_0\rangle \quad , \tag{C.15}$$

where ν is any real number. Using Eqs. (C.5), (C.8)-(C.13), and (C.15), one can derive the following equation for the evolution of the wave function:

$$\psi(\xi,Q;t) = \exp\left[-\frac{i}{\hbar}(t-t_0)^3 \frac{K^2(\xi-\alpha)^2}{6L}\right] \times \exp\left[-\frac{i}{\hbar}(t-t_0) K(\xi-\alpha)Q\right] \times$$

$$\times \chi(\xi)\ \Phi_{free}\left(Q + (t-t_0)^2 \frac{K(\xi-\alpha)}{2L}, t\right) \quad . \tag{C.16a}$$

Here $\Phi_{free}(Q,t)$ is the wave function which gives the evolution of a "free mass" whose initial state is $|\Phi\rangle$, i.e.,

$$\Phi_{free}(Q,t) \equiv \int dQ'\, \mathcal{K}_{free}(Q,Q';t,t_0)\ \Phi(Q') \quad , \tag{C.16b}$$

where

$$\mathcal{K}_{free}(Q,Q';t,t_0) \equiv \langle Q | \hat{U}_M(t,t_0) | Q' \rangle \tag{C.16c}$$

is the kernel of the free-mass Schrödinger equation. The explicit form of $\mathcal{K}_{free}$ is given in many standard quantum mechanics text books; see, e.g., Eq. (8.91) of Merzbacher (1970).

The wave function (C.16) shows particularly clearly the effect of the interaction on the meter. The probability distribution of the meter coordinate at time t is

$$P(Q) = \int |\Psi(\xi,Q;t)|^2 d\xi = \int P(Q|\xi)|\chi(\xi)|^2 d\xi \quad , \tag{C.17a}$$

$$P(Q|\xi) \equiv \left|\Phi_{\text{free}}\left(Q + (t-t_0)^2 \frac{K(\xi-\alpha)}{2L}, t\right)\right|^2 \quad . \tag{C.17b}$$

Here $P(Q|\xi)$ can be regarded as a conditional probability distribution — i.e., the probability distribution of Q given that $X_1 = \xi$. The important feature of $P(Q|\xi)$ is this: It has the same shape as the probability distribution for a "free mass," but it is displaced a distance $-K(\xi-\alpha)(t-t_0)^2/2L$ — precisely the displacement produced by a classical force $-K(\xi-\alpha)$.

4. Analysis of a Single Measurement

We are now ready to analyze a single measurement in detail — the first task in constructing a sequence of measurements. For generality we let the particular measurement under consideration be the n^{th} in the sequence. The measurement process can be described in general terms as follows. Before the n^{th} measurement the meter is prepared in an appropriate initial state, and the oscillator is in some state left over from the preceding measurement. At time t_{n-1} the interaction is turned on, and the oscillator and meter are allowed to interact freely for a time τ. At time $t_n = t_{n-1} + \tau$ the interaction is turned off, the readout system makes an infinitely precise "measurement" of the meter coordinate, and the wave function is reduced. (We shall call this precise "measurement" of Q a "readout" to avoid confusion with the "measurement of X_1" which lasts from t_{n-1} to t_n.) The reduction of the wave

function is the link that connects this measurement to the next one. It allows us to identify the state of the oscillator after the measurement--a state which becomes the initial oscillator state for the next measurement.

Two aspects of this process deserve special attention. The first is that the oscillator-meter coupling is on only during the interval from t_{n-1} to t_n: The interaction is turned on abruptly at time t_{n-1} and turned off abruptly at time t_n (functional form of K for n^{th} measurement: $K = 0$ for $t < t_{n-1}$ and $t > t_n$, $K = \text{constant} \neq 0$ for $t_{n-1} < t < t_n$). The step-function form of K is not the important issue; less abrupt forms for K could be used without changing the results significantly. The important point is that preparation of the meter is done with the interaction turned off. In a real experiment one would probably leave the interaction on while the meter is prepared. One could do so without affecting X_1, because X_1 is completely isolated from the meter; however, X_2 would be affected (cf. Eqs. 3.17). Since one of our objectives is to investigate the behavior of X_2, we choose to prepare the meter with the interaction turned off. Then X_2 is unaffected by meter preparation. Indeed, while the interaction is turned off, the oscillator's X_1-wave-function is constant.

The second important aspect is that we regard each measurement in the sequence as beginning at the instant when a readout terminates the preceding measurement. This is purely a matter of convenience. If the reader wishes to insert a time interval between measurements to allow for meter preparation or any other activity, she can do so. Our results will not be affected, because the oscillator's X_1-wave-function is constant while the interaction is turned off.

All quantities characteristic of the time interval $t_{n-1} \leq t < t_n$ will be denoted by a subscript n-1 --e.g., state vector $|\psi_{n-1}(t)\rangle$, wave function

$\psi_{n-1}(\xi,Q;t)$, feedback parameter α_{n-1}. The values measured at time t_n will be denoted by a subscript n.

We now consider in turn each of the four components of the n^{th} measurement: specification of the initial state, free evolution of the coupled oscillator-meter, readout of the meter coordinate, and reduction of the wave function.

At time t_{n-1} the oscillator is in some state $|\chi_{n-1}\rangle$ with wave function $\chi_{n-1}(\xi) = \langle\xi,t_{n-1}|\chi\rangle$; except for the first measurement, this state is left over from the previous measurement. The associated expectation value and variance of $\hat{X}_1(t_{n-1})$ we denote $\langle X_1\rangle_{n-1}$ and $(\Delta X_1)_{n-1}$; similarly, for $\hat{X}_2(t_{n-1})$, $\langle X_2\rangle_{n-1}$ and $(\Delta X_2)_{n-1}$. The meter is prepared in a Gaussian (minimum-uncertainty) wave-packet state $|\Phi\rangle$ with wave function

$$\Phi(Q) = [2\pi(\Delta Q)_o^2]^{-1/4} \exp[-Q^2/4(\Delta Q)_o^2] \quad . \tag{C.18}$$

This state has $\langle\hat{Q}\rangle = \langle\hat{\Pi}\rangle = 0$. We choose the variances $(\Delta Q)_o = (\hbar\tau/2L)^{1/2}$, $(\Delta\Pi)_o = (\hbar L/2\tau)^{1/2}$ — a choice which minimizes the variance of $\hat{Q}$ at time t_n. The initial state vector is $|\psi_{n-1}(t_{n-1})\rangle = |\chi_{n-1}\rangle \otimes |\Phi\rangle$, with wave function $\psi_{n-1}(\xi,Q;t_{n-1}) = \chi_{n-1}(\xi)\ \Phi(Q)$. Finally, the experimenter must also choose a value α_{n-1} for the feedback parameter.

The interaction is turned on at time t_{n-1}, and the coupled oscillator-meter evolves freely for a time τ. The evolution of the wave function during this interval can be obtained by specializing Eqs. (C.16) to quantities characteristic of the n^{th} measurement. Integration of Eq. (C.16b) using the particular form (C.18) for $\Phi(Q)$ yields

$$\Phi_{free}(Q,t) = [2\pi(\Delta Q)_o^2]^{-1/4} \left(1+i\,\frac{u}{\tau}\right)^{-1/2} \exp\left[-\frac{Q^2}{4(\Delta Q)_o^2}\left(1+i\,\frac{u}{\tau}\right)^{-1}\right], \tag{C.19}$$

where $u \equiv t-t_{n-1}$. The effect of the interaction is to produce a strong correlation between the states of the meter and oscillator: At time $t_n = t_{n-1}+\tau$ the expectation value of the meter coordinate gets displaced to

$$\langle\hat{Q}\rangle(t_n) = -(K\tau^2/2L)(\langle X_1\rangle_{n-1} - \alpha_{n-1}) \quad , \tag{C.20a}$$

and its variance becomes

$$\Delta Q(t_n) = \left[(\cancel{\hbar}\tau/L) + (K\tau^2/2L)^2(\Delta X_1)^2_{n-1}\right]^{1/2} \quad . \tag{C.20b}$$

Equations (C.20) can be calculated directly from the probability distribution of the meter coordinate (Eqs. C.17 and C.19) or, perhaps more easily, from a Heisenberg-picture analysis of the free evolution of the oscillator-meter system (cf. Eqs. 3.17-3.19).

At time t_n the readout system reads out a value Q_n for the meter coordinate, and using Eq. (C.20a) the experimenter infers a value

$$\xi_n = \alpha_{n-1} - (2L/K\tau^2)Q_n \tag{C.21}$$

for X_1. The probability distribution of ξ_n, obtained directly from the probability distribution of Q (Eqs. C.17), is given by

$$P(\xi_n) = (2\pi\sigma^2)^{-1/2} \int d\xi |\chi_{n-1}(\xi)|^2 \exp[-(\xi-\xi_n)^2/2\sigma^2] \quad , \tag{C.22}$$

where

$$\sigma \equiv (4\cancel{\hbar}L/K^2\tau^3)^{1/2} \quad . \tag{C.23}$$

This probability distribution refers to an ensemble of identical systems which begin the n^{th} measurement in the same state. The mean and variance of ξ_n (averages over this ensemble) are

$$\bar{\xi}_n = \alpha_{n-1} - (2L/K\tau^2)\langle\hat{Q}\rangle(t_n) = \langle X_1\rangle_{n-1} \quad , \tag{C.24a}$$

$$\Delta\xi_n = [\sigma^2 + (\Delta X_1)^2_{n-1}]^{1/2} \quad . \tag{C.24b}$$

Note that if $|\chi_{n-1}(\xi)|^2$ is a Gaussian, then $P(\xi_n)$ is also a Gaussian.

Equations (C.24) tell us that the n^{th} measurement can determine the expectation value $\langle X_1 \rangle_{n-1}$ with probable error $\Delta\xi_n$. The error is minimized when $|\chi_{n-1}(\xi)|^2$ is highly peaked about its mean value [$(\Delta X_1)_{n-1} \ll \sigma$]; in this situation it makes sense to talk about X_1 having a particular value--a value which can be determined with error

$$\Delta\xi_n \simeq \sigma = (4\hbar L/K^2\tau^3)^{1/2} \quad . \tag{C.25}$$

Since $(\Delta X_1)_{n-1}$ can be arbitrarily small, <u>σ is the fundamental measure of the accuracy of X_1-measurements of duration τ, made with a meter of "mass" L which is perfectly coupled to X_1 with coupling constant K.</u>
No matter how small τ may be, σ can be made as small as one wishes (in principle) by choosing K^2/L large enough; the measurements of X_1 can be arbitrarily quick and arbitrarily accurate.

This situation is to be contrasted with, for example, a measurement of the position of a free mass. There the feedback of momentum uncertainty onto position prevents a measurement of duration τ from having an accuracy better than $(\hbar\tau/m)^{1/2}$ (standard quantum limit for free-mass position; Eq. 3.2).

A useful dimensionless characterization of the accuracy of X_1-measurement is provided by the ratio η of the standard quantum limit for amplitude-and-phase measurement (Eq. 2.16) to σ:

$$\eta \equiv \frac{1}{\sigma}\left(\frac{\hbar}{2m\omega}\right)^{1/2} \quad , \qquad \eta^2 = \frac{K^2\tau^3}{8mL\omega} \quad ; \tag{C.26}$$

η^{-1} is the factor by which measurements with given K, L, and τ beat this standard quantum limit.

When the readout determines a value Q_n for the meter coordinate at time t_n, it localizes the meter at $Q = Q_n$. This localization is described formally by projecting the state vector $|\psi_{n-1}(t_n)\rangle$ onto the eigenstate corresponding to the measured value (reduction of the wave function). We define a projection operator

$$\hat{\theta}(Q) \equiv |Q\rangle\langle Q| = \int d\xi |\xi,Q;t_n\rangle\langle\xi,Q;t_n| \quad , \tag{C.27}$$

which projects the meter onto the eigenstate $|Q\rangle$. The state vector of the oscillator-meter system immediately after the readout is

$$\begin{aligned} |\psi_a\rangle &= \alpha\hat{\theta}(Q_n)|\psi_{n-1}(t_n)\rangle \\ &= \left[\alpha\int d\xi |\xi,t_n\rangle\, \psi_{n-1}(\xi,Q_n;t_n)\right] \otimes |Q_n\rangle \end{aligned} \tag{C.28}$$

[wave function $\psi_a(\xi,Q) = \alpha\psi_{n-1}(\xi,Q_n;t_n)\ \delta(Q-Q_n)$], where α is a normalization constant. (α also contains an unknown, but irrelevant, phase factor which we shall ignore.) The state vector (C.28) splits cleanly into oscillator and meter states. The oscillator state after the measurement becomes the initial state $|\chi_n\rangle$ for the $(n+1)^{\text{th}}$ measurement; its wave function is

$$\chi_n(\xi) = \alpha\psi_{n-1}(\xi,Q_n;t_n) \quad . \tag{C.29}$$

This wave function can be put in the form

$$\chi_n(\xi) = \beta\chi_{n-1}(\xi)\ \exp\left\{-\frac{\xi^2 - 2\xi_n\xi}{4\sigma^2} + \frac{i}{\hbar}\, m\omega\eta^2\left[(3\xi_n - \tfrac{4}{3}\alpha_{n-1})\xi - \tfrac{5}{6}\,\xi^2\right]\right\} \tag{C.30}$$

(Eqs. C.16, C.19, C.21, C.23, C.26), where β is another normalization constant.

Equation (C.30) is the fundamental equation of our analysis. It tells us how the oscillator wave function changes from one measurement to the next, and from it all our results will flow. One immediate consequence of Eq. (C.30) is the following: If the oscillator begins the n^{th} measurement in an eigenstate of $\hat{X}_1$ [$|\chi_{n-1}\rangle = |\xi',t\rangle$, $\chi_{n-1}(\xi) = \delta(\xi - \xi')$], then it remains in an eigenstate of $\hat{X}_1$ with the same eigenvalue after the measurement. As is discussed in Sec. IV, this is the essential feature of quantum nondemolition measurement.

5. Analysis of a Sequence of Measurements

Having completed our analysis of a single measurement, we turn next to analyzing a sequence of measurements and, in particular, to investigating the behavior of X_1 and X_2 during a sequence of measurements. To do so requires specifying a particular form for $\chi_{n-1}(\xi)$. The form we choose is

$$\chi_{n-1}(\xi) = [2\pi(\Delta X_1)^2_{n-1}]^{-1/4} \exp\left[-\frac{(\xi - \langle X_1\rangle_{n-1})^2}{4(\Delta X_1)^2_{n-1}} + \frac{i}{\hbar} m\omega(a_{n-1}\xi - \mu_{n-1}\xi^2)\right], \tag{C.31}$$

where a_{n-1} and μ_{n-1} are real constants. If $\mu_{n-1} = 0$, $\chi_{n-1}(\xi)$ is a minimum-uncertainty wave packet. Using the fact that in the ξ-representation $\hat{X}_2$ is equivalent to $(\hbar/im\omega)(\partial/\partial\xi)$, one can readily evaluate the expectation value and variance of $\hat{X}_2(t_{n-1})$ associated with the wave function (C.31):

$$\langle X_2\rangle_{n-1} = a_{n-1} - 2\mu_{n-1}\langle X_1\rangle_{n-1} \quad , \tag{C.32a}$$

$$(\Delta X_2)^2_{n-1} = (\hbar/2m\omega)^2 (\Delta X_1)^{-2}_{n-1} + 4\mu^2_{n-1}(\Delta X_1)^2_{n-1} \quad . \tag{C.32b}$$

The reason for the choice (C.31) should be clear. As a glance at Eq. (C.30)

shows, the form (C.31) for the initial oscillator wave function is preserved from one measurement to the next in a sequence; the only things that change are the constants characterizing the wave function:

$$(\Delta X_1)_n^{-2} = (\Delta X_1)_{n-1}^{-2} + \sigma^{-2} \quad , \tag{C.33a}$$

$$\frac{\langle X_1 \rangle_n}{(\Delta X_1)_n^2} = \frac{\langle X_1 \rangle_{n-1}}{(\Delta X_1)_{n-1}^2} + \frac{\xi_n}{\sigma^2} \quad , \tag{C.33b}$$

$$a_n = a_{n-1} + \eta^2 (3\xi_n - \frac{4}{3}\alpha_{n-1}) \quad , \tag{C.33c}$$

$$\mu_n = \mu_{n-1} + \frac{5}{6}\eta^2 \quad . \tag{C.33d}$$

The first of these equations has a couple of immediate consequences. The first is that $(\Delta X_1)_n \leq (\Delta X_1)_{n-1}$; hence, as a sequence of measurements proceeds, $|\chi_n(\xi)|^2$ becomes more and more highly peaked. The second is that if the oscillator is in a state with $\Delta X_1 >> \sigma$, one measurement is sufficient to prepare it in a state with $\Delta X_1 \simeq \sigma$.

By manipulating Eqs. (C.33) with the help of Eqs. (C.24), one can show that the change in the expectation value of $\hat{X}_1$ in the n^{th} measurement is

$$\langle X_1 \rangle_n - \langle X_1 \rangle_{n-1} = [(\Delta X_1)_{n-1}/\Delta\xi_n]^2 \, (\xi_n - \overline{\xi}_n) \quad . \tag{C.34}$$

This expression for the change in $\langle X_1 \rangle$ is exact, but it depends on the value actually measured in the n^{th} measurement. More useful for discussing the behavior of X_1 would be some sort of expected value for the change in $\langle X_1 \rangle$. Indeed, throughout the rest of this Appendix, we shall want to deal with such expected changes between measurements and with expected changes over an entire sequence of measurements.

Defining such expected changes requires introducing a new type of average, which we shall denote by a superposed bar. A superposed bar was used previously in Eq. (C.24a) to denote the mean value of ξ_n. There it meant an average over an ensemble of identical oscillators which began the n^{th} measurement in the same state; such an average is, of course, equivalent to an expectation value. In all <u>other</u> applications throughout the rest of this Appendix, a superposed bar will denote an average over an ensemble of identical oscillators which begin in the same state before the <u>initial</u> measurement in a sequence; this "barred average" is a generalization of the usual notion of expectation value.

One must keep in mind that the mean value $\overline{\xi}_n$ is <u>not</u> an average over this second type of ensemble; rather, each oscillator in the ensemble has its own value of $\overline{\xi}_n$ --a value which depends on the results of previous measurements for that particular oscillator (see Eq. C.40 below). On the other hand, all oscillators in the ensemble do have the same set of values for the uncertainties $(\Delta X_1)_n$ (Eq. C.33a) and the measurement errors $\Delta\xi_n$ (Eq. C.24b). This makes it easy to apply the barred average to the differences $(\xi_n - \overline{\xi}_n)$; these differences are statistically independent quantities with mean zero and with correlation matrix

$$\overline{(\xi_k - \overline{\xi}_k)(\xi_\ell - \overline{\xi}_\ell)} = (\Delta\xi_k)^2\, \delta_{k\ell} \quad . \tag{C.35}$$

We can now return to Eq. (C.34) and apply the concept of a barred average. We first note that the mean change of $\langle X_1 \rangle$ in a given measurement is zero ($\overline{\langle X_1\rangle_n - \langle X_1\rangle_{n-1}} = 0$). However, the change does have an rms-value, which can be thought of as the expected magnitude of the change in $\langle X_1 \rangle$:

$$(\delta X_1)_n \equiv \left[\overline{(\langle X_1\rangle_n - \langle X_1\rangle_{n-1})^2}\right]^{1/2} = (\Delta X_1)_{n-1}\left[1 + \frac{\sigma^2}{(\Delta X_1)^2_{n-1}}\right]^{-1/2} \qquad (C.36)$$

(cf. Eq. C.24b). Note that $(\delta X_1)_n \leq (\Delta X_1)_{n-1}$ — i.e., the expected change in $\langle X_1\rangle$ is always less than or equal to the variance of $\hat{X}_1$ at the beginning of the measurement. If $(\Delta X_1)_{n-1} \gtrsim \sigma$, then $(\delta X_1)_n \sim (\Delta X_1)_{n-1}$; however, if $(\Delta X_1)_{n-1} \ll \sigma$, then $(\delta X_1)_n \simeq (\Delta X_1)^2_{n-1}/\sigma \ll (\Delta X_1)_{n-1}$.

To make further progress, we must specify the oscillator state $|\chi_0\rangle$ before the initial (n = 1) measurement in the sequence. We choose a state of the form (C.31): a minimum-uncertainty state with $\langle X_2\rangle_0 = 0$ ($a_0 = \mu_0 = 0$), with $(\Delta X_1)_0 \gg \sigma$, and with $\langle X_1\rangle_0$ arbitrary. A good example of such a state is a coherent state [$(\Delta X_1)_0 = (\Delta X_2)_0 = (\hbar/2m\omega)^{1/2} \gg \sigma$ if $\eta \gg 1$]. The oscillator can be prepared in a coherent state using high-precision "amplitude-and-phase" techniques (see discussion in Sec. II.B). Throughout the following we neglect terms of order $\sigma/(\Delta X_1)_0$.

The first measurement in the sequence serves essentially as a "state-preparation measurement." Its result is highly uncertain, but it leaves the oscillator in a state with $\langle X_1\rangle_1 = \xi_1$ and $(\Delta X_1)_1 = \sigma$ (Eqs. C.33). We assume there is no feedback during the first measurement ($\alpha_0 = 0$).

Subsequent measurements are the ones of real interest. Equations (C.33) can be iterated to obtain the constants describing the oscillator state after the n^{th} measurement:

$$(\Delta X_1)_n = \sigma/\sqrt{n} \quad , \qquad (C.37a)$$

$$\langle X_1\rangle_n = \frac{1}{n}\sum_{k=1}^{n} \xi_k \quad , \qquad (C.37b)$$

$$a_n = \eta^2 \sum_{k=1}^{n} (3\xi_k - \tfrac{4}{3}\alpha_{k-1}) \quad , \qquad (C.37c)$$

$$\mu_n = \tfrac{5}{6}\eta^2 n \qquad (C.37d)$$

($n \geq 1$); Eq. (C.24b), together with (C.37a), gives the likely error of the n^{th} measurement:

$$\Delta\xi_n = \sigma\left(\frac{n}{n-1}\right)^{1/2} \quad , \qquad n \geq 2 \quad ; \tag{C.38}$$

and Eqs. (C.37) applied to Eqs. (C.32) give the expectation value and variance of $\hat{X}_2$ after the n^{th} measurement:

$$\langle X_2 \rangle_n = \frac{4}{3}\eta^2 \sum_{k=1}^{n} (\xi_k - \alpha_{k-1}) \quad , \tag{C.39a}$$

$$(\Delta X_2)_n = \frac{\sqrt{34n}}{3}\,\eta\left(\frac{\hbar}{2m\omega}\right)^{1/2} \tag{C.39b}$$

($n \geq 1$).

6. Discussion of Results

Equations (C.37)-(C.39) provide a complete description of the sequence of measurements; our task now is to discuss their implications.

We first note that the variances of $\hat{X}_1$ and $\hat{X}_2$ change in a completely deterministic way, independent of the actual measured values. On the other hand, the changes in the expectation values are entirely dependent on the measured values. Indeed, the expectation value of $\hat{X}_1$ after a given measurement is simply the arithmetic mean of all previously measured values. This last statement means that the experimenter knows in advance the expected result of each measurement after the first--i.e.,

$$\overline{\xi}_n = \langle X_1 \rangle_{n-1} = \frac{1}{n-1} \sum_{k=1}^{n-1} \xi_k \quad . \tag{C.40}$$

This is the finite-coupling analog of the situation analyzed in Sec. IV.A. There we assumed infinite coupling, and the experimenter could predict exactly

the result of each measurement after the first. Here we have finite coupling, the experimenter knows the expected result of each measurement, but the actual result is likely to differ from the expected by an amount $\Delta\xi_n \simeq \sigma$. Equation (C.40) also describes the situation one wants for measuring a classical force, because one detects the force by looking at the difference between the actual measured value and the (known) expected result (cf. Sec. III.B).

Given a set of measured values, one can calculate the changes in the expectation value of $\hat{X}_1$ using Eq. (C.37b). Exact this may be, but enlightening it is not. To gain insight we look at expected changes in $\langle X_1 \rangle$, and to do that we begin by writing Eq. (C.34) in the form

$$\langle X_1 \rangle_n - \langle X_1 \rangle_{n-1} = (\xi_n - \overline{\xi}_n)/n \quad . \tag{C.41}$$

The expected change in $\langle X_1 \rangle$ is

$$(\delta X_1)_n = \Delta\xi_n/n = \sigma/\sqrt{n(n-1)} \quad . \tag{C.42}$$

The expectation value of $\langle \hat{X}_1 \rangle$ "jumps" at each measurement. The "jumps" add randomly, but their expected size decreases so rapidly that after many measurements $\langle X_1 \rangle$ is likely to have wandered only a distance $(\Delta X_1)_1 = \sigma$ from its value after the first measurement--i.e.,

$$\left[\overline{(\langle X_1 \rangle_n - \langle X_1 \rangle_1)^2}\right]^{1/2} = \left[\sum_{k=2}^{n} (\Delta\xi_k)^2/k^2\right]^{1/2} = \sigma\left(1 - \frac{1}{n}\right)^{1/2} \tag{C.43}$$

(cf. Eqs. C.41, C.35, and C.38). This means that the results of all measurements after the first cannot determine $\langle X_1 \rangle_1$ more accurately than $(\Delta X_1)_1$. [One can easily show that the jumps prevent measurements after the n^{th} from determining $\langle X_1 \rangle_n$ more accurately than $(\Delta X_1)_n$.]

This behavior of X_1 can be summarized as follows: After the first measurement the oscillator is in a state with $\langle X_1\rangle_1 = \xi_1$ and $(\Delta X_1)_1 = \sigma$. For the next few measurements $\langle X_1\rangle$ jumps around within a region $\xi_1 \pm$ (a few) $\times\, \sigma$, while ΔX_1 gets smaller at each measurement. As the sequence proceeds the jumps of $\langle X_1\rangle$ become smaller and smaller, $\langle X_1\rangle$ "zeros in" on some particular value $\langle X_1\rangle_\infty$, ΔX_1 goes to zero, and the probability distribution $|\chi(\xi)|^2$ approaches a delta-function at $\langle X_1\rangle_\infty$. The final value $\langle X_1\rangle_\infty$ is likely to be within the region $\xi_1 \pm$ (a few) $\times\, \sigma$.

We now turn to the behavior of X_2, and we begin by noting that one can associate with X_2 a characteristic "quantum step size" $\sim \sigma^{-1}(\hbar/2m\omega) = \eta(\hbar/2m\omega)^{1/2}$, obtained from the basic accuracy σ of X_1-measurement and the uncertainty principle (2.9a).

The expectation value of $\hat{X}_2$ changes at each measurement, and the change is given by

$$\langle X_2\rangle_n - \langle X_2\rangle_{n-1} = \frac{4}{3}\eta^2(\xi_n - \alpha_{n-1}) \quad . \tag{C.44}$$

These "kicks" to X_2 are essentially classical. Indeed, Eq. (C.44) is precisely the classical displacement of X_2, which our measurement system would produce in a classical oscillator with $X_1 = \xi_n$, during the time interval between t_{n-1} and $t_n = t_{n-1} + \tau$; cf. Eqs. (C.1) viewed classically, together with $Q(t_{n-1}) = \Pi(t_{n-1}) = 0$, and Eq. (C.26). In the absence of feedback, the kicks (C.44) accumulate and $\langle X_2\rangle$ runs away. However, feedback can eliminate this "classical runaway of X_2," because the measured value ξ_n of X_1 tells one precisely the kick given $\langle X_2\rangle$ during the n^{th} measurement. The simplest feedback is to let $\alpha_n = \xi_n$; then the feedback between t_n and t_{n+1} cancels the kick given X_2 in the n^{th} measurement.

One can do much better by choosing the feedback so that at each measurement it not only cancels the previous kick but also attempts to cancel the current kick. The feedback cannot cancel the current kick precisely, because to

do so would require knowing the result of the measurement. However, one can try to guess the result, and the best guess is the expected result (C.40). The resulting feedback has the form

$$\alpha_1 = 2\xi_1 \quad ,$$
$$\alpha_n = \xi_n - \frac{1}{n-1}\sum_{k=1}^{n-1}\xi_k + \frac{1}{n}\sum_{k=1}^{n}\xi_k \quad , \qquad n > 1 \quad . \tag{C.45}$$

With this feedback the expectation value of $\hat{X}_2$ after n measurements is

$$\langle X_2\rangle_n = \frac{4}{3}\eta^2(\xi_n - \bar{\xi}_n) \quad , \tag{C.46}$$

a displacement with mean zero and with rms value

$$\left[\overline{\langle X_2\rangle_n^2}\right]^{1/2} = \frac{4}{3}\eta^2\,\Delta\xi_n = \frac{4}{3}\left(\frac{n}{n-1}\right)^{1/2}\eta\left(\frac{\hbar}{2m\omega}\right)^{1/2} \quad , \qquad n \geq 2 \quad . \tag{C.47}$$

The effectiveness of the feedback is evident from its ability to keep $\langle X_2\rangle$ within one "quantum step" of zero.

Effective though the feedback may be, it cannot prevent the huge, unpredictable, quantum mechanical kicks given X_2 by precise measurements of X_1. As Eq. (C.39b) shows, the effect of these kicks appears in the variance of $\hat{X}_2$, which grows as $\sqrt{n}$ — behavior which suggests that of a classical random-walk variable. The step size is $(\sqrt{34}/3)\eta(\hbar/2m\omega)^{1/2}$, in agreement with what one predicts from the uncertainty principle. This "random walk of X_2" means that the energy in the oscillator grows as the sequence proceeds:

$$\langle \hat{H}_o\rangle_n \simeq \frac{1}{2}m\omega^2(\Delta X_2)_n^2 = \frac{17}{18}\eta^2 n\hbar\omega \tag{C.48}$$

(Eqs. 2.2 and 2.6). The source of the energy is the generator. Interaction

with the generator can add energy to or remove energy from the oscillator, but on the average energy is added. Practical implications of the random walk of X_2 are considered in Paper II.

The analysis in this Appendix has emphasized the possibility of making quick measurements of X_1, but nothing restricts the analysis to this case. It applies equally well to measurements of X_1 which, because of weak coupling, require a long time to achieve good accuracy. This point is made clear by introducing a new constant

$$\varepsilon^2 \equiv \eta^2(\omega\tau)^{-3} = K^2/8mL\omega^4 \quad , \tag{C.49}$$

which is a dimensionless measure of the coupling strength. Written in terms of ε, the fundamental accuracy becomes

$$\sigma = \varepsilon^{-1}(\omega\tau)^{-3/2}\,(\hbar/2m\omega)^{1/2} \quad . \tag{C.50}$$

If $\varepsilon \gg 1$, a measurement much shorter than a period can beat the standard quantum limit (2.16);[13] but if $\varepsilon \ll 1$, beating the standard limit requires a measurement many periods long. Regardless of how small ε may be, the basic accuracy (C.50) can be made as small as one desires (in principle) by choosing τ large enough. Long measurement times yield arbitrarily good accuracy because $\hat{X}_1$ is completely isolated from noise in the measuring apparatus (cf. Sec. IV.B). The constant ε plays an important role in Appendix D, and it and its relatives are considered extensively in Paper II.

7. Analysis of Imprecise Readout Systems

One possible objection to the above analysis is its treatment of the readout system. We have assumed that when the readout determines a value

for the meter coordinate, it localizes the meter coordinate precisely at the measured value. Of course, no real readout system can achieve such arbitrarily good precision. One way to handle this difficulty is to do a better job of analyzing the readout: Specify in detail the design of a realistic readout system, and include all or part of the readout in the exact quantum mechanical analysis. The resulting analysis is likely to be difficult, if not impossible.

Fortunately, there is an easier and more general approach. In this approach the imprecision of the readout system is described by a (classical) conditional probability distribution $W(Q|Q_n)$. The distribution $W(Q|Q_n)$ can be thought of as giving the probability $W(Q|Q_n)dQ$ that, when the readout determines a value Q_n for the meter coordinate, the meter is actually located between Q and Q+ dQ.

The introduction of $W(Q|Q_n)$ can be justified by considering a simple model for the readout system. The first three-quarters of this section (through Eq. C.59) will present that model and will show how it gives rise to $W(Q|Q_n)$. The last one-quarter will assume a simple form for $W(Q|Q_n)$, and from it will derive results for the measurement errors and variances in a sequence of measurements with an imprecise readout system.

In our simple model for the readout system, the first stage is a "readout meter": a one-dimensional, quantum mechanical "free mass" with generalized coordinate $\hat{Q}$, generalized momentum $\hat{\mathcal{P}}$, and generalized mass M. The readout meter is coupled to the meter by coordinate-coordinate coupling; hence, the total Hamiltonian for the oscillator, the meter, and the readout meter is

$$\hat{H}_T = \hat{H}(\text{Eqs. C.1}) + k\hat{Q}\hat{\mathcal{Q}} + \hat{\mathcal{P}}^2/2M \quad , \tag{C.51}$$

where k is a coupling constant. We shall include the readout meter in the

quantum mechanical analysis. The readout meter is coupled to subsequent stages of the readout system in such a way that, at designated moments of time, the subsequent stages can "read out" a value for the readout-meter coordinate. We shall idealize these readouts of $\mathcal{Q}$ as arbitrarily precise, essentially instantaneous measurements. Then we need not treat the subsequent stages of the readout system quantum mechanically — i.e., we can place the quantum-classical cut of our analysis between the readout meter and the subsequent stages of the readout system.

The scenario envisioned for the n^{th} measurement divides neatly into two parts. During the first part, lasting from t_{n-1} to $t_{n-1}+\tau$, the oscillator and meter interact via the interaction Hamiltonian $K(\hat{X}_1 - \alpha_{n-1})\hat{Q}$ (Eq. C.1d) just as in the previous analysis. During the second part, lasting from $t_{n-1}+\tau$ to $t_n = t_{n-1}+\tau+\tilde{\tau}$ (note that t_n is defined differently than in the previous analysis), the meter and the readout meter interact via the interaction Hamiltonian $k\hat{Q}\hat{\mathcal{Q}}$ (Eq. C.51). (The coupling "constants" have the following functional form for the n^{th} measurement: $K = k = 0$ for $t < t_{n-1}$ and $t > t_n$; $K =$ constant $\neq 0$, $k = 0$ for $t_{n-1} < t < t_{n-1}+\tau$; $K = 0$, $k =$ constant $\neq 0$ for $t_{n-1}+\tau < t < t_n$.) At time t_n the subsequent stages of the readout system read out a value of $\mathcal{Q}$, from which the experimenter infers a value of Q (and X_1). The three operations of (i) interaction between meter and readout meter, (ii) readout of $\mathcal{Q}$, and (iii) inference of a value for Q, together constitute what was called the "readout of the meter coordinate" in the previous analysis. After the n^{th} measurement the meter is thrown away; a new meter is used for the next measurement.

The discarding of the meter at the end of each measurement is an important feature of our analysis. Unless we keep track of the states of the

meters discarded in previous measurements, it will turn out that the entire system cannot be described by a pure state; instead it must be described by a mixed state. Thus the analysis is most conveniently carried out using density operators. During the n^{th} measurement the state of the total system — oscillator, meter, and readout meter — is specified by a density operator $\hat{\rho}_T(t)$ with associated density matrix $\rho_T(\xi,\xi';Q,Q';\mathcal{Q},\mathcal{Q}';t) \equiv \langle \xi,Q,\mathcal{Q};t|\hat{\rho}_T(t)|\xi',Q',\mathcal{Q}';t\rangle$, where the states $|\xi,Q,\mathcal{Q};t\rangle$ are the obvious generalization of the states $|\xi,Q;t\rangle$. The density matrix has the interpretation that $\rho_T(\xi,\xi;Q,Q;\mathcal{Q},\mathcal{Q};t)\, d\xi\, dQ\, d\mathcal{Q}$ is the probability at time t of simultaneously finding the readout meter between $\mathcal{Q}$ and $\mathcal{Q}+d\mathcal{Q}$, the meter between Q and $Q+dQ$, and the oscillator with X_1 between ξ and $\xi+d\xi$. The total density operator evolves according to $\hat{\rho}_T(t) = \hat{U}_T(t,t_0)\hat{\rho}_T(t_0)\hat{U}_T^{\dagger}(t,t_0)$, where $\hat{U}_T(t,t_0)$ is the time-development operator for the total Hamiltonian (C.51).

During the first part of the n^{th} measurement ($t_{n-1} < t < t_{n-1}+\tau$), we need only be concerned with the state of the oscillator and meter. Their state is specified by a density operator $\hat{\rho}_{n-1}(t)$, which evolves according to $\hat{\rho}_{n-1}(t) = \hat{U}(t,t_{n-1})\hat{\rho}_{n-1}(t_{n-1})\hat{U}^{\dagger}(t,t_{n-1})$ (cf. Eq. C.13), and which has density matrix $\rho_{n-1}(\xi,\xi';Q,Q';t) \equiv \langle \xi,Q;t|\hat{\rho}_{n-1}(t)|\xi',Q';t\rangle$.

We now analyze the components of the n^{th} measurement in greater detail. The oscillator begins the measurement (at time t_{n-1}) in a state with density matrix $\mathcal{T}_{n-1}(\xi,\xi')$, and the meter is prepared in the (pure) Gaussian state (C.18). The initial density operator $\hat{\rho}_{n-1}(t_{n-1})$ has density matrix $\rho_{n-1}(\xi,\xi';Q,Q';t_{n-1}) = \mathcal{T}_{n-1}(\xi,\xi')\ \Phi(Q)\ \Phi^*(Q')$. The oscillator and meter interact as in the previous analysis for a time τ; the evolution of ρ_{n-1} during this time can be inferred from the evolution of the corresponding wave function (Eqs. C.16 and C.19).

At time $t_{n-1}+\tau$ the readout meter is prepared in a (pure) state with wave function $\Theta(\mathcal{Q})$, which has $\langle\hat{\mathcal{Q}}\rangle = \langle\hat{\mathcal{P}}\rangle = 0$. For the moment we leave the precise form of $\Theta(\mathcal{Q})$ unspecified. The total density matrix at time $t_{n-1}+\tau$ is $\rho_T(\xi,\xi';Q,Q';\mathcal{Q},\mathcal{Q}';t_{n-1}+\tau) = \rho_{n-1}(\xi,\xi';Q,Q';t_{n-1}+\tau)\,\Theta(\mathcal{Q})\,\Theta^*(\mathcal{Q}')$. The expectation value and variance of $\hat{Q}$ at time $t_{n-1}+\tau$ are denoted $\langle\hat{Q}\rangle_i$ and $(\Delta Q)_i$; they are given by Eqs. (C.20). During the subsequent interval of duration $\tilde{\tau}$ ($t_{n-1}+\tau < t < t_n = t_{n-1}+\tau+\tilde{\tau}$), the meter and the readout meter interact; the total Hamiltonian is given by Eq. (C.51) with $K = 0$. We make three assumptions about the evolution of the system during this time:

Assumption 1. $\tilde{\tau} \ll \tau$;

Assumption 2. $k^2\tilde{\tau}^4/LM \ll 1 \quad [(\hbar M/k^2\tilde{\tau}^3)^{1/2} \gg (\hbar\tilde{\tau}/L)^{1/2}]$;

Assumption 3. $(\hbar\tilde{\tau}/M)^{1/2} \lesssim (\Delta\mathcal{Q})_i \ll (\hbar\tilde{\tau}/M)^{1/2}[(LM/k^2\tilde{\tau}^4)(\tau/\tilde{\tau})]^{1/2}$,

$(\Delta\mathcal{P})_i \ll (\hbar M/\tilde{\tau})^{1/2}[(LM/k^2\tilde{\tau}^4)(\tau/\tilde{\tau})]^{1/2}$.

Here the subscript "i" denotes the value at $t_{n-1}+\tau$. These assumptions guarantee that the meter coordinate remains essentially undisturbed by the evolution of the entire system during the time $\tilde{\tau}$. Assumption 1 guarantees that the meter does not evolve significantly under the influence of its own Hamiltonian. Assumptions 2 and 3 guarantee that the "back-action" of the readout meter onto the meter coordinate is negligible.

Assumptions 2 and 3 can be viewed in another way. They imply that the readout meter does not do a very good job of measuring the meter coordinate — i.e., the readout meter is far from being a "quantum-limited measuring device." Assumption 2 guarantees that, in measuring Q, the best accuracy the readout meter can achieve is far worse than the standard quantum limit $(\hbar\tilde{\tau}/L)^{1/2}$ (cf. Eq. 3.2). Assumption 3 allows $(\Delta\mathcal{Q})_i$ and $(\Delta\mathcal{P})_i$ to be much greater than

the optimum uncertainties for a measurement of duration $\tilde{\tau}$. Thus we do not place stringent demands on the performance of the readout meter. That this is intimately connected with the absence of back-action onto Q should not be surprising.

With assumptions 1-3, the evolution of the total system is precisely analogous to the evolution of the meter coupled to $\hat{X}_1$ of the oscillator (Eqs. C.16). The total density matrix is given by

$$\rho_T(\xi,\xi';Q,Q';\mathcal{Q},\mathcal{Q}';t) = \rho_{n-1}(\xi,\xi';Q,Q';t_{n-1}+\tau) \times$$
$$\times \exp\{-\frac{i}{\hbar}[f(Q,\mathcal{Q},t) - f(Q',\mathcal{Q}',t)]\} \times$$
$$\times \Theta_{free}\left(\mathcal{Q} + \frac{kv^2}{2M} Q, t\right) \Theta^*_{free}\left(\mathcal{Q}' + \frac{kv^2}{2M} Q', t\right), \quad (C.52a)$$

$$f(Q,\mathcal{Q},t) \equiv \frac{k^2v^3}{6M} Q^2 + kvQ\mathcal{Q} \quad , \quad (C.52b)$$

where $v \equiv t - t_{n-1} - \tau$, and where $\Theta_{free}(\mathcal{Q},t)$ gives the evolution of a free readout meter with initial state $\Theta(\mathcal{Q})$ (analogue of Eqs. C.16b,c).

During the interval $\tilde{\tau}$ the readout meter "swings" due to its interaction with the meter. At time t_n the expectation value and variance of $\hat{\mathcal{Q}}$ become

$$\langle\hat{\mathcal{Q}}\rangle(t_n) = -(k\tilde{\tau}^2/2M)\langle\hat{Q}\rangle_i \quad , \quad (C.53a)$$

$$\Delta\mathcal{Q}(t_n) = \left[(\Delta\mathcal{Q})^2_{free}(t_n) + (k\tilde{\tau}^2/2M)^2(\Delta Q)^2_i\right]^{1/2} \quad , \quad (C.53b)$$

where $(\Delta\mathcal{Q})_{free}(t_n)$ is the variance of a free readout meter.

At time t_n the subsequent stages of the readout system read out a value $\mathcal{Q}_n$ for the readout-meter coordinate. Using Eq. (C.53a) the experimenter infers a value

$$Q_n = -(2M/k\tilde{\tau}^2)\mathcal{Q}_n \quad (C.54)$$

for the meter coordinate. In the terminology of the previous analysis, Q_n is the result of the "readout of the meter coordinate." From Q_n the experimenter infers a value ξ_n for X_1 just as before (Eq. C.21). The probability distribution of ξ_n (referred to an ensemble of identical systems which begin the n^{th} measurement in the same state) is easily obtained from the probability distribution of $\mathcal{Q}$:

$$\begin{aligned} P(\xi_n) &= (k\tilde{K\tau}^2\tau^2/4ML) \int d\xi\, dQ\; \rho_T(\xi,\xi;Q,Q;\mathcal{Q}_n,\mathcal{Q}_n;t_n) \\ &= (2\pi\sigma^2)^{-1/2} \int d\xi\, dQ\, T_{n-1}(\xi,\xi)\; \times \\ &\qquad \times \exp\left\{-\left[\xi - \alpha_{n-1} + (2L/K\tau^2)Q\right]^2/2\sigma^2\right\} W(Q|Q_n) \end{aligned} \tag{C.55}$$

(cf. Eq. C.22), where the conditional probability distribution $W(Q|Q_n)$ is defined by

$$W(Q|Q_n) \equiv \frac{k\tilde{\tau}^2}{2M} \left| \Theta_{\text{free}}\left(\frac{k\tilde{\tau}^2}{2M}(Q - Q_n),\; t_n\right)\right|^2 \quad . \tag{C.56}$$

$W(Q|Q_n)$ has mean Q_n and variance $\sigma_W = (2M/k\tilde{\tau}^2)(\Delta\mathcal{Q})_{\text{free}}(t_n)$.

The mean and variance of ξ_n (averages over the ensemble) are

$$\bar{\xi}_n = \langle X_1\rangle_{n-1} \quad , \tag{C.57a}$$

$$\Delta\xi_n = \left[(2L/K\tau^2)^2\, \sigma_W^2 + \sigma^2 + (\Delta X_1)^2_{n-1}\right]^{1/2} \tag{C.57b}$$

(cf. Eqs. C.24). The measurement error $\Delta\xi_n$ is the same as in the previous analysis, except that it is augmented by a term which accounts for the imprecision of the readout meter. Even if the readout meter is extremely

imprecise [$\sigma_W \gg (\hbar\tau/L)^{\frac{1}{2}}$], it is still true that the measurement of X_1 can be arbitrarily accurate when K is made arbitrarily large.

When the subsequent stages of the readout system read out the value Q_n, they localize the readout meter precisely at Q_n. This "reduction of the wave function" means that immediately after the readout the density matrix of the oscillator-meter system is

$$\rho_a(\xi,\xi';Q,Q';t_n) = \mathcal{C}\,\rho_T(\xi,\xi';Q,Q';Q_n,Q_n;t_n) \quad , \tag{C.58}$$

where $\mathcal{C}$ is a normalization constant. After the readout we throw the meter away, and we prepare a new meter for use in the next measurement. Throughout all subsequent measurements in the sequence, we shall not be interested in computing any expectation values which involve observables of the discarded meter. To compute any other expectation value we must "take the trace" of the density matrix on Q. Therefore, insofar as any future expectation values of interest are concerned, we can take the trace on Q now — i.e., we can replace the density matrix (C.58) with a density matrix that describes only the oscillator:

$$\begin{aligned} \mathcal{T}_n(\xi,\xi') &= \int \rho_a(\xi,\xi';Q,Q;t_n)\, dQ \\ &= \mathcal{A} \int W(Q|Q_n)\, \rho_{n-1}(\xi,\xi';Q,Q;t_{n-1}+\tau)\, dQ \quad , \end{aligned} \tag{C.59}$$

where $\mathcal{A}$ is another normalization constant. Equation (C.59) gives the initial oscillator state for the $(n+1)^{\text{th}}$ measurement (cf. Eq. C.29).

The key results of our analysis of an imprecise readout system are Eqs. (C.55) and (C.59). They justify our claim that the imprecision of the readout can be described by a classical probability distribution:

Eq. (C.55) shows how the readout imprecision contributes to the measurement error, and Eq. (C.59) shows how the readout imprecision "smears out" the "reduction of the wave function." In the limit that the readout meter is arbitrarily precise [$W(Q|Q_n) = \delta(Q - Q_n)$], Eqs. (C.55) and (C.59) reduce to the corresponding equations of the previous analysis (cf. Eqs. C.22 and C.29). Indeed, this analysis justifies our previous treatment of an arbitrarily precise readout system — i.e., it justifies the procedure of "reducing the wave function" after each arbitrarily precise readout.

Two features of this analysis deserve special emphasis. The first is that we have made assumptions which guarantee that the meter coordinate is essentially undisturbed by the interaction with the readout meter. Formally, this means that the total density matrix (C.52) splits cleanly into a product of two terms: (i) a density matrix for the free oscillator-meter system; and (ii) a function which depends only on the meter coordinate and the readout meter coordinate. The second feature is that we throw away the meter after each measurement. Both these features are necessary for defining $W(Q|Q_n)$; and it is the loss of information that occurs when the meter is discarded which allows us to identify the oscillator state after the measurement, and which converts an initial, pure oscillator state into a mixed state.

We must specify a particular form for $W(Q|Q_n)$ in order to use Eq. (C.59) to analyze a sequence of measurements. A reasonable form is a Gaussian with mean Q_n and variance $\sigma_W = \gamma(1-\gamma^2)^{-1/2}\,(\hbar\tau/L)^{1/2}$ $(0 \le \gamma < 1)$. This is the form $W(Q|Q_n)$ would have if $\Theta(Q)$ were a Gaussian wave packet. When $\gamma^2 \simeq 0.5$ the readout imprecision contributes about the same amount to the measurement error as the meter uncertainty (cf. Eq. C.57b). Using

this Gaussian for $W(Q|Q_n)$, we have integrated Eq. (C.59) to obtain

$$\mathcal{T}_n(\xi,\xi') = \mathcal{B}\,\mathcal{T}_{n-1}(\xi,\xi')\,\exp\Bigg\{-\frac{1}{4\sigma^2}\Big[(1+4\gamma^2)(\xi^2+\xi'^2) - 10\gamma^2\xi\xi' - 2(1-\gamma^2)\xi_n(\xi+\xi')\Big] + \frac{i}{\hbar}\,m\omega\eta^2\Big[3\xi_n(1-\gamma^2)(\xi-\xi') - \frac{4}{3}\,\alpha_{n-1}(\xi-\xi') - \frac{5}{6}\,(1-\frac{9}{5}\,\gamma^2)(\xi^2-\xi'^2)\Big]\Bigg\}\quad, \tag{C.60}$$

where $\mathcal{B}$ is a normalization constant. This equation is a generalization of the fundamental equation (C.30); it simplifies to (C.30) when $\gamma = 0$.

Equation (C.60) can be used to analyze a sequence of measurements. In particular, it can be used to analyze a sequence in which the oscillator begins in the same (pure) state as in the previous analysis. The results for the expectation values $\langle X_1\rangle_n$ and $\langle X_2\rangle_n$ are the same as before (Eqs. C.37b and C.39a); but Eq. (C.38) for the measurement error becomes

$$\Delta\xi_n = \frac{\sigma}{(1-\gamma^2)^{\frac{1}{2}}}\left(\frac{n}{n-1}\right)^{\frac{1}{2}} \qquad \text{for } n \geq 2\quad, \tag{C.61}$$

and Eqs. (C.37a) and (C.39b), which give the evolution of ΔX_1 and ΔX_2, are changed to

$$(\Delta X_1)_n = \sigma/[n(1-\gamma^2)]^{\frac{1}{2}}\quad, \tag{C.62a}$$

$$(\Delta X_2)_n = \frac{\sqrt{34n}}{3}\,\eta\left(\frac{\hbar}{2m\omega}\right)^{1/2}\left[(1-\frac{9}{17}\,\gamma^2)/(1-\gamma^2)\right]^{1/2} \tag{C.62b}$$

$(n \geq 1)$. For reasonable values of γ ($\gamma^2 \simeq 0.5$), the decrease of ΔX_1 and the growth of ΔX_2 are not markedly different from the results of the previous analysis.

APPENDIX D

SINGLE-TRANSDUCER, BACK-ACTION-EVADING MEASUREMENTS OF X_1: A FULLY QUANTUM MECHANICAL ANALYSIS[14]

1. Introduction

In this Appendix we give a fully quantum mechanical analysis of a single-transducer, back-action-evading measurement of the X_1 of a harmonic oscillator (see Sec. II.F.3). We consider a simplified version of a real measuring apparatus, analyze the measurement process quantum mechanically, and thereby demonstrate that in principle such single-transducer measurements can beat the standard quantum limit $\Delta X_1 = (\hbar/2m\omega)^{1/2}$ (Eq. 2.16).

Single-transducer, back-action-evading measurements are considered extensively in Paper II, where they are analyzed using semiclassical techniques. Those semiclassical analyses are to be preferred in almost every way over the analysis given here: They are more realistic and more adaptable, and they provide more detailed information. However, the reader might harbor lingering doubts about the validity of applying semiclassical techniques to measurements which purport to beat the standard quantum limit. The purpose of this Appendix is to remove such doubts by analyzing quantum mechanically a simple example of a single-transducer, back-action-evading measurement.

The analysis we give here is similar to the analysis in Sec. III.B and Appendix C. In particular, the measuring apparatus is the same. It consists of a generator, which provides the time-dependence in the interaction Hamiltonian; a meter, which is a one-dimensional quantum mechanical "free mass" coupled to the oscillator by the generator; and a readout system, which reads out the position of the meter. Only the meter will be treated quantum mechanically.

The difference between here and Sec.III.B lies in the way the meter is coupled to the oscillator. In Sec. III.B the meter was perfectly coupled to $\hat{X}_1$; here the meter is coupled to $\hat{X}_1$ only in a time-averaged sense. The total Hamiltonian for the oscillator coupled to the meter via the classical generator is given by Eqs. (3.16), except that in the interaction Hamiltonian the momentum coupling is omitted:

$$\hat{H}_I = K\hat{Q}\hat{x} \cos \omega t = \frac{1}{2} K\hat{Q}[\hat{X}_1(1+\cos 2\omega t) + \hat{X}_2 \sin 2\omega t] \tag{D.1}$$

(cf. Eq. 2.42a). Systems which in principle are governed by the Hamiltonian (3.16) are considered in Appendix B. They can be modified easily to have the Hamiltonian considered here; essentially, the modification consists of deleting the momentum transducer.

The motivation for considering single-transducer, back-action-evading measurements is the problem of weak coupling. In Sec. III.B and in Appendix C we showed that back-action-evading measurements with perfect $\hat{X}_1$-coupling can achieve arbitrarily good accuracy in an arbitrarily short time. However, such quick measurements (short compared to an oscillator period) require that the measuring apparatus be strongly coupled to the oscillator. In Appendix C we introduced a constant

$$\varepsilon^2 \equiv K^2/8mL\omega^4 \tag{D.2}$$

(cf. Eq. C.49), which provides a dimensionless measure of coupling strength for a simple "free-mass" meter coupled to an oscillator. Quick measurements require $\varepsilon >> 1$. If $\varepsilon \lesssim 1$, beating the standard quantum limit (2.16) requires a measurement time longer than a period.

In real experiments it is often quite difficult to achieve strong coupling. If one is stuck with weak coupling ($\varepsilon << 1$), then the required long

measurement time allows one to avoid coupling perfectly to $\hat{X}_1$ and permits one instead to couple to $\hat{X}_1$ in a time-averaged sense. In particular, one can omit one of the two transducers (position or momentum) required for perfect coupling, with a consequent simplification in the design and construction of the measuring apparatus. One modulates the output of the remaining transducer so that at some frequency the modulated output carries the desired information about X_1 with very little contamination from X_2, and one then runs the modulated output through a filter which picks out the desired frequency. (See Paper II for details; and see Thorne et al., 1979, for a semi-realistic example.) The Hamiltonian (3.16a-c), with interaction term (D.1), is the simplest example of this procedure: The momentum transducer is omitted, the modulation of the position transducer is a sinusoid at the oscillator frequency, the desired X_1-signal is at zero frequency, and the meter — a zero-frequency harmonic oscillator — serves as a filter at zero frequency.

Since single-transducer measurements are useful only in the case of weak coupling, we assume $\varepsilon << 1$ throughout this Appendix.

2. The Analysis

The analysis proceeds by solving for the evolution of the appropriate operators in the Heisenberg picture. The Hamiltonian (3.16a-c), with interaction term (D.1), yields the following Heisenberg equations of motion:

$$d\hat{X}_1/dt = (K/2m\omega)\hat{Q} \sin 2\omega t \quad , \tag{D.3a}$$

$$d\hat{X}_2/dt = -(K/2m\omega)\hat{Q}(1+\cos 2\omega t) \quad , \tag{D.3b}$$

$$d\hat{Q}/dt = \hat{\Pi}/L \quad , \tag{D.3c}$$

$$d\hat{\Pi}/dt = -\frac{1}{2} K[\hat{X}_1(1+\cos 2\omega t) + \hat{X}_2 \sin 2\omega t] \quad . \tag{D.3d}$$

The crucial difference between these equations and those for perfect $\hat{X}_1$-coupling (Eqs. 3.17) is that $\hat{X}_1$ is not completely isolated from the measuring apparatus.

Equations (D.3) cannot be solved exactly with any ease, but when ε is small a good approximate solution can be obtained. The key to the approximation is the realization that the operators of Eqs. (D.3) are nearly periodic with period π/ω. We implement the approximation by writing $\hat{X}_1$, $\hat{X}_2$, and $\hat{Q}$ as "Fourier series" with slowly-varying "Fourier coefficients":

$$\hat{X}_1(t) = \sum_{n=-\infty}^{\infty} \hat{b}_n(t)\, e^{2in\omega t} \quad , \tag{D.4a}$$

$$\hat{X}_2(t) = \sum_{n=-\infty}^{\infty} \hat{c}_n(t)\, e^{2in\omega t} \quad , \tag{D.4b}$$

$$\hat{Q}(t) = \sum_{n=-\infty}^{\infty} \hat{d}_n(t)\, e^{2in\omega t} \quad . \tag{D.4c}$$

Of course, these expansions are "quasi-unique" only for times greater than an oscillator period ($\omega t \gtrsim 2\pi$), but we are interested in the solutions only for such times. Hermiticity of $\hat{X}_1$, $\hat{X}_2$, and $\hat{Q}$ implies that $\hat{b}_{-n} = \hat{b}_n^\dagger$, etc., and as we show below, the assumption of slowly varying Fourier coefficients is satisfied because $d\hat{b}_n/dt \sim \varepsilon\omega\hat{b}_n$, etc. (see Eqs. D.7).

To proceed, we plug the expansions (D.4) into Eqs. (D.3) and equate terms with the same rapid time dependence. The result is a set of coupled differential equations for the Fourier coefficients. We then simplify these equations by neglecting time derivatives in all equations except the $n = 0$ equations—a step justified by the slowly varying character of the Fourier coefficients. The resulting coupled equations are all algebraic, except the $n = 0$ equations.

Little would be gained by the expansions (D.4) if we had to consider all terms in the expansions. Fortunately, we need not do so. We are interested only in the largest terms in each expansion; and beyond the first term or two, each expansion becomes a power series in the small quantity ε. Indeed, using the coupled equations for the Fourier coefficients, one can easily show that, for $n \geq 1$ and for $\omega\tau \gg 1$, $\hat{b}_n \sim \varepsilon^{n-1} \hat{b}_0$, $\hat{c}_n \sim \varepsilon^n \hat{c}_0$, and $\hat{d}_n \sim \varepsilon^n \hat{d}_0$. Consequently, the only coefficients of interest are those with $n = 0$ and $n = 1$; and the $n = 1$ terms can be neglected in the expansions for $\hat{X}_2$ and $\hat{Q}$, but they must be retained in the expansions for $\hat{X}_1$ and $\hat{\Pi}$. The $n = 1$ equations can then be used to write the remaining $n = 1$ coefficients in terms of $n = 0$ coefficients. Putting all this together, one finds that, at this level of approximation,

$$\hat{X}_1 = \hat{b}_0 - (K/4m\omega^2)\hat{d}_0 \cos 2\omega t \quad , \tag{D.5a}$$

$$\hat{X}_2 = \hat{c}_0 \quad , \tag{D.5b}$$

$$\hat{Q} = \hat{d}_0 \quad , \tag{D.5c}$$

$$\hat{\Pi}/L = (d\hat{d}_0/dt) + (K/4L\omega)\hat{c}_0 \cos 2\omega t \quad , \tag{D.5d}$$

where the operators $\hat{b}_0$, $\hat{c}_0$, and $\hat{d}_0$ satisfy the coupled equations

$$d\hat{b}_0/dt = \frac{1}{4}\varepsilon^2\omega\hat{c}_0 \quad , \tag{D.6a}$$

$$d\hat{c}_0/dt = -(K/2m\omega)\hat{d}_0 \quad , \tag{D.6b}$$

$$d^2\hat{d}_0/dt^2 = \varepsilon^2\omega^2\hat{d}_0 - (K/2L)\hat{b}_0 \quad . \tag{D.6c}$$

In Eqs. (D.5d), (D.6b), and (D.6c) terms proportional to $\hat{b}_0$ and $\hat{d}_0$ have been omitted because they are negligible.

Equations (D.6) can be solved easily. When the solutions are written in terms of appropriate initial values at $t = 0$, they have the form

$$\sqrt{3}\,\hat{b}_0 = \hat{X}_1(0)(\nu_2^2 \cosh \nu_1 u + \nu_1^2 \cos \nu_2 u) + \tfrac{1}{4}\varepsilon \hat{X}_2(0)(\nu_1 \sinh \nu_1 u + \nu_2 \sin \nu_2 u)$$

$$+ (K/8m\omega^2)\,\hat{Q}(0)[(2\nu_2^2 - 1)\cosh \nu_1 u + (2\nu_1^2 + 1)\cos \nu_2 u]$$

$$- (K/8mL\omega^3)\,\varepsilon^{-1}\hat{\Pi}(0)(\nu_1^{-1}\sinh \nu_1 u - \nu_2^{-1}\sin \nu_2 u) \quad , \qquad \text{(D.7a)}$$

$$\sqrt{3}\,\hat{c}_0 = 4\varepsilon^{-1}\hat{X}_1(0)(\nu_1\nu_2^2 \sinh \nu_1 u - \nu_2\nu_1^2 \sin \nu_2 u) + \hat{X}_2(0)(\nu_1^2 \cosh \nu_1 u + \nu_2^2 \cos \nu_2 u)$$

$$+ (K/2m\omega^2)\varepsilon^{-1}\,\hat{Q}(0)[\nu_1(2\nu_2^2 - 1)\sinh \nu_1 u - \nu_2(2\nu_1^2 + 1)\sin \nu_2 u]$$

$$- (K/2mL\omega^3)\varepsilon^{-2}\,\hat{\Pi}(0)(\cosh \nu_1 u - \cos \nu_2 u) \quad , \qquad \text{(D.7b)}$$

$$\sqrt{3}\,\hat{d}_0 = -(4m\omega^2/K)\,\hat{X}_1(0)(\cosh \nu_1 u - \cos \nu_2 u) - (2m\omega^2/K)\varepsilon\hat{X}_2(0)(\nu_1^3 \sinh \nu_1 u - \nu_2^3 \sin \nu_2 u)$$

$$+ \hat{Q}(0)(\nu_2^2 \cosh \nu_1 u + \nu_1^2 \cos \nu_2 u) + \varepsilon^{-1}[\hat{\Pi}(0)/L\omega](\nu_1 \sinh \nu_1 u + \nu_2 \sin \nu_2 u) \quad , \qquad \text{(D.7c)}$$

where $u \equiv \varepsilon\omega t$, and where

$$\nu_1 \equiv (\sqrt{3} + 1)^{1/2} / \sqrt{2} \quad , \qquad \nu_2 \equiv (\sqrt{3} - 1)^{1/2} / \sqrt{2} \quad . \qquad \text{(D.8)}$$

Note that the characteristic time scale of these solutions is $(\varepsilon\omega)^{-1}$, so the Fourier coefficients do indeed vary slowly in time. The reader might be bothered by the exponential instability of these solutions, but she should not be. As we show below, any real measurement will not last longer than a time $\tau \sim (\varepsilon\omega)^{-1}$.

Equations (D.5) and (D.7) give the free evolution of the coupled oscillator-meter system, and they can be applied to analyzing a measurement. The measurement process we consider is similar to that described in Sec. III.B and Appendix C. The measurement begins at $t = 0$; the oscillator and meter interact via the interaction Hamiltonian (D.1) for a time τ; and at the end of this time the readout system reads out a value for the meter coordinate, from which the experimenter infers a value for X_1.

To analyze the measurement, we must first specify the initial ($t = 0$) states of the oscillator and meter. Our objective in this Appendix is to find the best possible performance of single-transducer, back-action-evading measurements, so we shall choose the initial states to optimize the measurement accuracy. We assume that at $t = 0$ the oscillator is in a Gaussian (minimum-uncertainty) wave-packet state (in X_1) with $\langle\hat{X}_1(0)\rangle = \xi_o$ and $\langle\hat{X}_2(0)\rangle = 0$. The meter is prepared in a Gaussian wave packet (in Q) with $\langle\hat{Q}(0)\rangle = \langle\hat{\Pi}(0)\rangle = 0$. The initial variances $(\Delta X_1)_o$ and $(\Delta Q)_o$ are chosen to minimize the variance of the meter coordinate at $t = \tau$:

$$(\Delta X_1)_o^2 = \varepsilon(\hbar/4m\omega)CD^{-1} \quad , \tag{D.9a}$$

$$(\Delta Q)_o^2 = \varepsilon^{-1}(\hbar/2L\omega)AB^{-1} \quad , \tag{D.9b}$$

where

$$A \equiv \nu_1 \sinh \varepsilon\omega\nu_1\tau + \nu_2 \sin \varepsilon\omega\nu_2\tau \quad , \tag{D.10a}$$

$$B \equiv \nu_2^2 \cosh \varepsilon\omega\nu_1\tau + \nu_1^2 \cos \varepsilon\omega\nu_2\tau \quad , \tag{D.10b}$$

$$C \equiv \nu_1^3 \sinh \varepsilon\omega\nu_1\tau - \nu_2^3 \sin \varepsilon\omega\nu_2\tau \quad , \tag{D.10c}$$

$$D \equiv \cosh \varepsilon\omega\nu_1\tau - \cos \varepsilon\omega\nu_2\tau \tag{D.10d}$$

(Eqs. D.5c and D.7c).

The oscillator and meter interact for a time τ, during which the expectation value of the meter coordinate gets displaced to

$$\langle \hat{Q}(\tau) \rangle = - (4m\omega^2/K\sqrt{3})\xi_o D \quad , \tag{D.11a}$$

and the variance of the meter coordinate grows to

$$\Delta Q(\tau) = \varepsilon^{-1/2}(\hbar/3L\omega)^{1/2} \ (AB + CD)^{1/2} \tag{D.11b}$$

(Eqs. D.5c, D.7c, D.9, and D.10). At time τ the readout system reads out a value Q_m for the meter coordinate. Using Eq. (D.11a) the experimenter infers a value

$$\xi_m = -(K\sqrt{3}/4m\omega^2)Q_m D^{-1} \tag{D.12a}$$

for X_1. In a set of measurements on an ensemble of identical systems, the mean of this inferred value is ξ_o, and its variance is

$$\Delta\xi_m = \varepsilon^{1/2}(\hbar/2m\omega)^{1/2}(ABD^{-2} + CD^{-1})^{1/2} \quad . \tag{D.12b}$$

The measurement can determine ξ_o with probable error $\Delta\xi_m$. In Eqs. (D.11b) and (D.12b) the first term on the right comes from the initial uncertainty in the meter coordinate and the second from the initial uncertainty in X_1.

3. Discussion

Interpretation of Eqs. (D.11) and (D.12) is obscured by their complicated dependence on τ. Their meaning is made a great deal clearer by looking at their form for short and long measurement times. For short measurement times ($\varepsilon\omega\tau \ll 1$ but $\omega\tau \gg 2\pi$) the meter displacement (D.11a) and the probable error (D.12b) are

$$\langle \hat{Q}(\tau) \rangle = -(K\tau^2/4L)\xi_o \quad , \tag{D.13a}$$

$$\Delta\xi_m = 2\varepsilon^{-1}(\omega\tau)^{-3/2}(\hbar/2m\omega)^{1/2} = (16\hbar L/K^2\tau^3)^{1/2} \quad . \tag{D.13b}$$

(One can verify from Eqs. D.3 that these expressions are also valid to within factors of order unity when $\omega\tau \sim 2\pi$.) The probable error (D.13b) is due entirely to uncertainties in the meter; for short measurement times minimization of the uncertainty due to the initial oscillator variances is unimportant. Indeed, as long as $(\Delta X_1)_o^2$ is somewhat greater than its optimum value $[(\Delta X_1)_o > (\omega\tau)^{-1/2}(\hbar/2m\omega)^{1/2}$; cf. Eq. D.9a], the probable error has the form

$$\Delta\xi_m \simeq [(16\hbar L/K^2\tau^3) + (\Delta X_1)_o^2]^{1/2} \quad . \tag{D.13c}$$

If this measurement of X_1 is to be repeatable to within the error $\Delta\xi_m$, then the condition $\Delta X_1(\tau) \lesssim \Delta\xi_m$ must be satisfied; otherwise, at the time of the readout of Q, the expectation value of $\hat{X}_1$ will "jump" an unknown distance greater than $\Delta\xi_m$. That this condition holds for $\tau \lesssim (\varepsilon\omega)^{-1}$ can be easily verified using Eqs. (D.5a) and (D.7).

The important feature of Eqs. (D.13a) and (D.13c) is that they are virtually identical to the comparable equations for measurements with perfect coupling to $\hat{X}_1$ (cf. Eqs. 3.19a and 3.20b). The only difference is a factor of two in each equation; and this factor can be traced to the fact that, with the momentum coupling omitted, the mean force on the meter is cut in half (cf. Eqs. 3.17d and D.3d). Just as in the case of perfect $\hat{X}_1$-coupling,

single-transducer, back-action-evading measurements beat the standard quantum limit when $\omega\tau \gtrsim \varepsilon^{-2/3}$. Conclusion: For short measurement times $\tau \ll (\varepsilon\omega)^{-1}$ (but $\tau \gtrsim \omega^{-1}$) the imperfection of coupling to $\hat{X}_1$ has no significant effect on the measurement accuracy, because there has not been time for "noise" in the measuring apparatus to "feed back" onto $\hat{X}_1$ and disturb it significantly.

The difference between single-transducer and perfectly coupled two-transducer, back-action-evading measurements shows up at long measurement times ($\varepsilon\omega\tau \gg 1$), when the meter displacement (D.11a) and measurement error (D.12b) become

$$\langle\hat{Q}(\tau)\rangle = -(2m\omega^2/K\sqrt{3})\,\xi_o\, e^{\varepsilon\omega\nu_1\tau} \quad , \tag{D.14a}$$

$$\Delta\xi_m = (\varepsilon\nu_1\sqrt{3})^{1/2}\,(\hbar/2m\omega)^{1/2} \quad . \tag{D.14b}$$

In the case of a perfectly coupled measurement, one can choose the initial variance of $\hat{X}_1$ as small as desired (in principle); then the measurement becomes more and more accurate as τ increases (Eq. 3.20b). However, for a single-transducer measurement, the accuracy does not continue to improve; instead it hits a "floor" at approximately $\varepsilon^{1/2}(\hbar/2m\omega)^{1/2}$ for times $\tau \gtrsim (\varepsilon\omega)^{-1}$, because $\hat{X}_1$ no longer successfully evades "back-action" noise from the measuring apparatus. Note that for long measurement times $\tau \gg (\varepsilon\omega)^{-1}$, the measurements are not repeatable because $\Delta X_1(\tau) \gg \Delta\xi_m$ (cf. Eqs. D.5a and D.7).

The dependence of the measurement accuracy (D.12b) on τ can be conveniently summarized by using only the small and large τ forms:

$$\Delta\xi_m \simeq \begin{cases} \varepsilon^{-1}(\omega\tau)^{-3/2}\,(\hbar/2m\omega)^{1/2} & , \quad \varepsilon \lesssim \varepsilon\omega\tau \lesssim 1 \quad , \qquad \text{(D.15a)} \\ \varepsilon^{1/2}(\hbar/2m\omega)^{1/2} & , \quad \varepsilon\omega\tau \gtrsim 1 \quad . \qquad \text{(D.15b)} \end{cases}$$

This behavior is similar to what one expects for amplitude-and-phase measurements. The accuracy of an amplitude-and-phase measurement should improve as τ increases, but it must eventually hit a floor at the standard quantum limit $(\hbar/2m\omega)^{1/2}$. The floor must be at the standard quantum limit because X_1 and X_2 are measured with equal precision, so they are equally affected by back-action noise. The accuracy floor for single-transducer, back-action-evading measurements is lower because X_1 is partially shielded from back-action noise.

Up to now we have operated under the assumption that the coupling constand ε is fixed, and we have investigated the dependence of the measurement error on τ for fixed ε. One can adopt a different point of view--that the coupling strength is under the control of the experimenter. Given this freedom, the experimenter will choose the value of ε (by choosing L) to optimize the measurement accuracy for a given measurement time τ ($\gtrsim \omega^{-1}$). The choice he will make is $\varepsilon \simeq (\omega\tau)^{-1}$, and the measurement error (D.15) will be

$$\Delta\xi_m \simeq (\omega\tau)^{-1/2}\ (\hbar/2m\omega)^{1/2} \quad . \tag{D.16}$$

This is the optimum performance for a single-sensor measurement of the simple type considered in this Appendix (cf. Eq. 2.43).

So far in this Appendix we have considered a meter with no "restoring force." In practice this is not usually the case; in a typical design such as that in Appendix B.1, the meter is an LC-circuit (term $\hat{Q}^2/2C$ added to meter Hamiltonian, where C is the total capacitance in the circuit including that associated with the position transducer). In this situation the analysis given in this Appendix will apply approximately for measurement times smaller than the characteristic time of the circuit -- i.e., $\tau \lesssim \tilde{\tau} \equiv (LC)^{1/2}$. If $\tilde{\tau} \gtrsim (\varepsilon\omega)^{-1}$, i.e., $K^2C/8m\omega^2 \gtrsim 1$, the effect of the capacitor can essentially be ignored, because the preceding analysis applies for times long

enough to hit the accuracy floor. However, in practice it may be difficult to make the capacitance large enough, and one may be stuck with the case $\tilde{\tau} \ll (\varepsilon\omega)^{-1}$, i.e., $K^2C/8m\omega^2 \ll 1$.

To analyze this case in detail requires a more sophisticated model for the measuring apparatus than we have used here. We consider more sophisticated measuring systems in Paper II, and we analyze their performance using semiclassical techniques. However, we can get a good idea of the potential performance from the preceding analysis.

A measurement of duration $\tilde{\tau}$ has accuracy $\simeq \varepsilon^{-1}(\omega\tilde{\tau})^{-3/2}(\hbar/2m\omega)^{1/2}$. A measurement of duration $\tau \gtrsim \tilde{\tau}$ can be regarded as a sequence of measurements of duration $\tilde{\tau}$. Before the initial measurement in the sequence, the oscillator is prepared in a Gaussian wave-packet state (in X_1). Appendix C analyzed a sequence of measurements with perfect coupling to $\hat{X}_1$. In that analysis the variance of $\hat{X}_1$ always decreased during the sequence. Here, with imperfect coupling, we expect the variance of $\hat{X}_1$ to decrease until it is approximately equal to the optimum value for measurements of duration $\tilde{\tau}$: $(\Delta X_1)_o \simeq (\omega\tilde{\tau})^{-1/2}(\hbar/2m\omega)^{1/2}$ (cf. Eq. D.9a). Thus we shall choose the initial variance of $\hat{X}_1$ to be this optimum value; then the variance should not change significantly during the sequence.

The results of all the measurements in the sequence are used to determine the <u>initial</u> expectation value of $\hat{X}_1$. The accuracy of this determination improves as the square root of the number of measurements. Thus the measurement error for a sequence of total duration $\tau \gtrsim \tilde{\tau}$ is given approximately by

$$\Delta\xi \simeq \varepsilon^{-1}(\omega\tilde{\tau})^{-3/2}(\hbar/2m\omega)^{1/2}(\tilde{\tau}/\tau)^{1/2} \simeq (\beta\omega\tau)^{-1/2}(\hbar/2m\omega)^{1/2} \quad , \qquad (D.17)$$

where β is a dimensionless coupling constant defined by

$$\beta \equiv (\varepsilon\omega\tilde{\tau})^2 = K^2C/8m\omega^2 \quad . \qquad (D.18)$$

The improvement in accuracy of Eq. (D.17) does not continue forever, because the expectation value of $\hat{X}_1$ changes during the sequence. In particular, the expectation value of $\hat{X}_1$ "jumps" at the time of each readout; the detailed analysis in Appendix C suggests that the expected magnitude of each jump is approximately $(\Delta X_1)_o^2/[\varepsilon^{-1}(\omega\tilde{\tau})^{-3/2}(\hbar/2m\omega)^{1/2}] \simeq \varepsilon(\omega\tilde{\tau})^{1/2}(\hbar/2m\omega)^{1/2}$ (see Eq. C.36 and accompanying discussion). [The expectation value of $\hat{X}_1$ also changes <u>during</u> each measurement in the sequence because of the imperfect coupling to $\hat{X}_1$ (Eqs. D.5a and D.7); but these changes are negligible for $\tilde{\tau} \ll (\varepsilon\omega)^{-1}$, provided that one uses a "feedback force" on the meter like that in Appendix C.] The jumps add randomly, so that after a time $\tau \gtrsim \tilde{\tau}$, the expectation value of $\hat{X}_1$ will have wandered a distance $\simeq \varepsilon(\omega\tau)^{1/2}(\hbar/2m\omega)^{1/2}$. The measurement accuracy improves as in Eq. (D.17) only until the distance wandered becomes comparable to the measurement error. Thus the accuracy hits a floor at approximately $(\omega\tilde{\tau})^{-1/2}(\hbar/2m\omega)^{1/2}$ for measurement times $\tau \gtrsim \tilde{\tau}/\beta$. The accuracy floor is approximately equal to the initial variance of $\hat{X}_1$ — i.e., the entire sequence allows one to determine the initial expectation value of $\hat{X}_1$ with an error of order the initial variance.

The dependence of measurement error on τ can be summarized as follows:

$$\Delta\xi \simeq \begin{cases} (\beta\omega\tau)^{-1/2}(\tilde{\tau}/\tau)(\hbar/2m\omega)^{1/2} & , \quad \tau \lesssim \tilde{\tau} \qquad \text{(D.19a)} \\ (\beta\omega\tau)^{-1/2}(\hbar/2m\omega)^{1/2} & , \quad \tilde{\tau} \lesssim \tau \lesssim \tilde{\tau}/\beta \quad . \qquad \text{(D.19b)} \\ (\omega\tilde{\tau})^{-1/2}(\hbar/2m\omega)^{1/2} & , \quad \tau \gtrsim \tilde{\tau}/\beta \qquad \text{(D.19c)} \end{cases}$$

Note that Eqs. (D.19) simplify to Eqs. (D.15) when $\beta \simeq 1$.

Just as in the previous case ($\beta \gtrsim 1$), so in this case ($\beta \lesssim 1$), the optimum performance is achieved by adjusting $\tilde{\tau}$ (adjusting L) to obtain the best accuracy for a given τ. The optimum choice is $\beta\tau \lesssim \tilde{\tau} \lesssim \tau$, and the resulting optimum accuracy is

$$\Delta\xi \simeq (\beta\omega\tau)^{-1/2}\ (\hbar/2m\omega)^{1/2} \quad . \tag{D.20}$$

It should now be clear that β is the really important measure of coupling strength for this type of single-transducer, back-action-evading measurement. For $\beta \gtrsim 1$ the optimum performance is given by Eq. (D.16); for $\beta \lesssim 1$, by Eq. (D.20).

The constant β is an example of a Gibbons-Hawking (1971) coupling constant. In Paper II we give an exact definition of the Gibbons-Hawking constant for an arbitrary measuring system coupled to an oscillator; we present a semiclassical derivation of the limiting accuracy (D.20) for such a system; and we generalize that accuracy to the case where the system contains an amplifier with noise temperature greater than the quantum limit ($\hbar \to kT_n/\omega$); cf. Thorne et al. (1979).

REFERENCES

Allen, M. A., Z. D. Farkas, H. A. Hogg, E. W. Hoyt, and P. B. Wilson, 1971, IEEE Trans. Nucl. Sci. 18, 168.

Aharanov, Y., and D. Bohm, 1961, Phys. Rev. 122, 1649.

Aharanov, Y., and D. Bohm, 1964, Phys. Rev. 134, B1417.

Aharanov, Y., and A. Petersen, 1971, in Quantum Theory and Beyond, edited by T. Bastin (Cambridge University Press, Cambridge), p. 135.

Bagdasarov, Kh. S., V. B. Braginsky, V. P. Mitrofonov, and V. S. Shiyan, 1977, Vestnik Moskovskovo Universiteta, seriya Fiz. Astr. 1, 98; see also lecture by Braginsky in Bertotti (1977).

Bertotti, B. ed., 1977, Gravitazione Sperimentale, Proceedings of an international conference held at Pavia, Italy, 17-20 September 1976 (Accademia Nazionale dei Lincei, Rome).

Bohm, D., 1951, Quantum Theory (Prentice-Hall, Englewood Cliffs, NJ), esp. Chapters 6 and 22.

Bohr, N., 1928, Die Naturwissenschaften 16, 245.

Braginsky, V. B., 1970, Physical Experiments with Test Bodies (Nauka, Moscow) [English translation published as NASA-TT F672, National Technical Information Service, Springfield, VA]; esp. Eqs. (3.17) and (3.25).

Braginsky, V. B., 1974, in Gravitational Radiation and Gravitational Collapse, Proceedings of IAU Symposium No. 64, edited by Cécile DeWitt-Morette (Reidel, Dordrecht-Holland), p. 28.

Braginsky, V. B., 1977, in Topics in Theoretical and Experimental Gravitation Physics, edited by V. De Sabbata and J. Weber (Plenum Press, London and New York), p. 105.

Braginsky, V. B., C. M. Caves, and K. S. Thorne, 1977, Phys. Rev. D 15, 2047.

Braginsky, V. B., L. P. Grishchuk, A. G. Doroshkevich, Ya. B. Zel'dovich, I. D. Novikov, and M. V. Sazhin, 1973, Zh. Eksp. Teor. Fiz. 65, 1729 [English translation in Sov. Phys.—JETP 38, 865 (1974)].

Braginsky, V. B., V. I. Panov, V. G. Petnikov, and V. D. Popel'nyuk, 1977, Pribori i Tekhnika Eksperimenta 20 (No. 1), 234 [English translation in Instruments and Experimental Techniques 20, 269 (1977)].

Braginsky, V. B., and V. N. Rudenko, 1978, Physics Reports 46, 165.

Braginsky, V. B., and Yu. I. Vorontsov, 1974, Usp. Fiz. Nauk 114, 41 [English translation in Sov. Phys.—Uspekhi 17, 644 (1975)].

Braginsky, V. B., Yu. I. Vorontsov, and F. Ya. Khalili, 1977, Zh. Eksp. Teor. Fiz. 73, 1340 [English translation in Sov. Phys.—JETP 46, 705 (1977)].

Braginsky, V. B., Yu. I. Vorontsov, and F. Ya. Khalili, 1978, Pis'ma v Zh. Eksp. Teor. Fiz. 27, 296 [English translation in JETP Lett. 27, 276 (1978)].

Braginsky, V. B., Yu. I. Vorontsov, and V. D. Krivchenkov, 1975, Zh. Eksp. Teor. Fiz. 68, 55 [English translation in Sov. Phys.—JETP 41, 28 (1975)].

Carruthers, P., and M. M. Nieto, 1965, Phys. Rev. Lett. 14, 387.

Caves, C. M., 1979, Physics Lett. 80B, 323.

Douglass, D. H., and V. B. Braginsky, 1979, in Gravitational Theories Since Einstein, edited by S. W. Hawking and W. Israel (Cambridge University Press, Cambridge, England).

Drever, R. W. P., J. Hough, W. A. Edelstein, J. R. Pugh, and W. Martin, 1977, pp. 365-369 of Bertotti (1977).

Epstein, R., and J. P. A. Clark, 1979, in Sources of Gravitational Radiation, edited by L. Smarr (Cambridge University Press, Cambridge, England).

Fock, V., 1962, Zh. Eksp. Teor. Fiz. 42, 1135 [English translation in Sov. Phys. — JETP 15, 784 (1962)].

Gibbons, G. W., and S. W. Hawking, 1971, Phys. Rev. D 4, 2191.

Giffard, R., 1976, Phys. Rev. D 14, 2478.

Grishchuk, L. P., and M. V. Sazhin, 1975, Zh. Eksp. Teor. Fiz. 68, 1569 [English translation in Sov. Phys.—JETP 41, 787 (1975)].

Heffner, H., 1962, Proc. IRE 50, 1604.

Hollenhorst, J. N., 1979, Phys. Rev. D in press; also available as a Stanford University preprint.

McGuigan, D. F., C. C. Lam, R. Q. Gram, A. W. Hoffmann, D. H. Douglass, and H. W. Gutche, 1978, J. Low Temp. Phys. 30, 621.

Merzbacher, E., 1970, Quantum Mechanics, second edition (Wiley, New York), esp. Secs. 15.8-15.10.

Misner, C. W., K. S. Thorne, and J. A. Wheeler, 1973, Gravitation (W. H. Freeman, San Francisco).

Pauli, W., 1958, in Handbuch der Physik (Vol. V, Part 1): Principles of Quantum Theory I, edited by S. Flügge (Springer-Verlag, Berlin), esp. pp. 73-74.

Pegoraro, F., E. Picasso, and L. A. Radicati, 1978, J. Phys. A 11, 1949.

Pfister, H., 1976, Cryogenics 16, 17.

Robinson, F. N. H., 1974, Noise and Fluctuations in Electronic Devices and Circuits (Clarendon Press, Oxford).

Serber, R., and C. H. Townes, 1960, in Quantum Electronics, a Symposium, edited by C. H. Townes (Columbia University Press, New York).

Smagin, A. G., 1974, Pribori i Tekhnika Eksperimenta 17 (No. 6), 143 [English translation in Instruments and Experimental Techniques 17, 1721 (1974)].

Takahasi, H., 1965, Adv. in Comm. Systems 1, 227, esp. Sec. XI.

Thorne, K. S., 1978, in Theoretical Principles in Astrophysics and Relativity, edited by N. R. Lebovitz, W. H. Reid, and P. O. Vandervoort (University of Chicago Press, Chicago), esp. pp. 163-174.

Thorne, K. S., R. W. P. Drever, C. M. Caves, M. Zimmermann, and V. D. Sandberg, 1978, Phys. Rev. Lett. 40, 667.

Thorne, K. S., C. M. Caves, V. D. Sandberg, M. Zimmermann, and R. W. P. Drever, 1979, in Sources of Gravitational Radiation, edited by L. Smarr (Cambridge University Press, Cambridge, England).

Tyson, J. A., and R. P. Giffard, 1978, Ann. Rev. Astron. Astrophys. 16, 521.

Unruh, W. G., 1977, preprint from University of British Columbia; published in revised form as Unruh (1978).

Unruh, W. G., 1978, Phys. Rev. D 18, 1764.

Unruh, W. G., 1979, Phys. Rev. D, in press.

Von Neumann, J., 1932, Mathematische Grundlagen der Quantenmechanik (Julius Springer: Berlin). [English translation: Mathematical Foundations of Quantum Mechanics (Princeton University Press, Princeton, NJ, 1955)].

Wagoner, R. V., C. M. Will, and H.-J. Paik, 1978, Stanford University preprint.

Weber, J., 1959, Rev. Mod. Phys. 31, 681, see esp. Sec. V.

Weiss, R., 1972, Progress Report 105, Res. Lab. Electron., MIT, p. 54.

Wyler, J. A., 1974, J. Gen. Rel. and Grav. 5, 175.

FOOTNOTES

1. "Less is more" is an aphorism popularized in this century by architect Ludwig Mies van der Rohe. It appears earlier in Robert Browning's poem Andrea del Sarto (1855), l. 78. Wyler (1974) has used "less is more" and related ideas as fundamental conceptual tools for exploring the frontiers of modern physics and cosmology.

2. Hollenhorst (1979) has suggested that the idea of such back-action-evading measurements has been known at least since the analysis by Takahasi (1965) of the degenerate parametric amplifier. We do not understand Hollenhorst's suggestion: A degenerate parametric amplifier takes the input signal Real $\{(V_1 + iV_2)e^{-i\omega t}\}$ from an ideal voltage source, and preferentially amplifies the real part of the complex amplitude while attenuating the imaginary part; the amplifier's output is $AV_1 \sin\omega t - (V_2/A)\cos\omega t$. While this is analogous to a back-action-evading measurement of the real part X_1 of the complex amplitude $X_1 + iX_2$ of an oscillator, it is by no means the same. For example, if one simply attaches a capacitive position transducer to a mechanical oscillator, and follows it by a degenerate parametric amplifier, the amplifier will act back on the oscillator through the transducer to drive directly the X_1 oscillations which it seeks to measure. Such a measurement, instead of evading the amplifier's back action, actually enhances the back action! On the other hand, this enhancement is of a nonstochastic nature, and one might therefore be able to find a way to compensate for it. For comments on the related issue of "phase-sensitive detection" and its relationship to "back-action evasion," see Sec. II.F.3.

3. A more careful discussion would pay attention to the back-action kick (2.10b) which occurs during the initial quick measurement of x. That

kick modifies the initial measurement error (2.10a) to read

$$\delta x_o \simeq \left[\frac{S_Q}{2\tau} + \left(\frac{\delta p_o}{m}\tau\right)^2\right]^{1/2}$$

$$\simeq \left[\frac{S_Q}{2\tau} + \frac{S_V\tau^3}{8m^2}\right]^{1/2} .$$

The discussion in the text implicitly assumes that the second term is much smaller than the first.

Later (Sec. III.A.1) we shall discuss the case where the two terms are of comparable size. This case leads to an absolute minimum value for the error in our initial quick measurement:

$$\delta x_o \gtrsim \left[\frac{(S_Q S_V)^{1/2}}{2m}\tau\right]^{1/2} \gtrsim \left(\frac{\hbar\tau}{m}\right)^{1/2}$$

(cf. Eq. 2.11).

4. For a discussion of difficulties with making rigorous the quantum mechanical concept of the oscillator's phase ψ see, e.g., Carruthers and Nieto (1965). We circumvent these difficulties by working with the real and imaginary parts of the complex amplitude, $\hat{X}_1$ and $\hat{X}_2$, instead of the amplitude and the phase.

5. Relativistic quantum theory is not so kind. It places firm constraints on the precision with which certain observables can be measured. For example, the position of a particle (or the X_1 of a harmonic oscillator) cannot be measured with a precision better than the Compton wavelength $\hbar/mc$. Roughly speaking, the reason for this constraint is the following: If one tries

to localize a particle within a region smaller than its Compton wavelength, then its momentum uncertainty will be so large that its kinetic energy will be of order its rest mass, and particle-antiparticle pairs will be created. For the X_1 of an oscillator the situation is similar: If one tries to localize X_1 within a Compton wavelength (2×10^{-43} cm if m = 1 ton), then X_2 will be so uncertain that the oscillator's energy will be of order its rest mass. Clearly, this constraint is completely irrelevant for the macroscopic systems considered in this paper.

6. These two requirements on the measuring apparatus — precise coupling to the measured observable and arbitrarily strong coupling — are also the basic assumptions behind a controversial general "theorem" which asserts, "Nonrelativistic quantum theory permits arbitrarily accurate, instantaneous (often called impulsive) measurements of the first kind for any observable." [A measurement of the first kind (Pauli, 1958) is one for which, if the system is in an eigenstate of the measured observable at the instant of the measurement, the result of the measurement is equal to the eigenvalue, with arbitrary accuracy; and regardless of the system's initial state, the measurement leaves it in an eigenstate of the measured observable with the measured eigenvalue.] For a concise review of the literature on this "theorem," see Aharanov and Petersen (1971).

This "theorem" is implicit in the viewpoint of Bohr, and it has been championed in recent years by David Bohm. Bohm discusses and gives a proof of the "theorem" in his textbook; see Sec. 22.5 of Bohm (1951). He regards the "theorem" as an immediate consequence of the two requirements on the measuring apparatus. However, one can question the generality of Bohm's proof because of his neglect of the measured system's free Hamiltonian $\hat{H}_o$ during the course of the measurement. In particular, by means of strong

forces embodied in the interaction Hamiltonian, the measuring apparatus acts back on variables which do not commute with the measured observable $\hat{A}$. These variables then drive $\hat{A}$ via $\hat{H}_o$, and the resulting disturbance of $\hat{A}$ might preclude (for some observables) arbitrarily accurate measurements even in the limit of zero measurement time.

To prove the "theorem" in a particular case, one must include the effects of $\hat{H}_o$ and one must show that the measurement error goes to zero in an appropriate limit where the coupling strength goes to infinity and the measurement time goes to zero. In general, the error can be made to go to zero only in the limit of an instantaneous measurement. Fortunately, for the observables considered in this paper (such as the position of a free particle or harmonic oscillator) the theorem is undoubtedly true. Indeed, for "quantum nondemolition observables" the theorem holds in the stronger form given in the text for $\hat{X}_1$ (arbitrarily accurate measurements even for nonzero measurement times).

The "theorem" has long been controversial because it implies (in its stronger form) that the energy of a system can be measured arbitrarily quickly and accurately, in violation of a common misinterpretation of the energy-time uncertainty relation. [For a specific gedanken experiment that proves the possibility of arbitrarily quick and accurate energy measurements, see Aharanov and Bohm (1961, 1964). The latter is a valid special case of Bohm's (1951) proof of the general "theorem."] The misinterpretation of $\Delta E\, \Delta t \gtrsim \hbar$ has generated so much confusion in the physics community that even Von Neumann (1932; Sec. V.1) regarded it as a counter-example to the "theorem."

7. To achieve a Hamiltonian of the form (3.16), the measuring systems described in Appendix B must incorporate a negative capacitor or a negative spring,

which converts a velocity sensor into a momentum sensor (cf. Sec. III.A.2). For these systems the free meter is a "mass on a negative spring"; the coupling to the oscillator converts the meter into a "free mass."

8. The ideas and prose of this section are due entirely to Carlton M. Caves, and constitute a portion of the material submitted by him to the California Institute of Technology in partial fulfillment of the requirements for the Ph.D. degree.

9. One might wish to require that there exist a one-to-one correspondence between the possible measured values at $t = t_0$ and $t = t_1$, in which case f_1 must be invertible.

10. The assumption about the nature of $\hat{H}_I$ is sufficient, but it is not always necessary. For example, if $\hat{A}$ is conserved in the absence of interactions, $\hat{H}_I$ can depend on any observable of the system which commutes with $\hat{A}$.

11. In our original Physical Review Letter (Thorne et al., 1978), we discussed a gedanken experiment for an arbitrarily quick and accurate back-action-evading measurement of the X_1 of an electromagnetic oscillator (cf. Appendix B.2 of this paper). In that discussion we asserted that a torque Γ in the sensing system could be read out with precision $\Delta\Gamma \simeq (I\hbar/\tau^3)^{1/2}$. We had invented the required "torque-balance readout system" at the time of our Letter (though we did not describe it in the Letter). Our viewpoint on that torque balance was the third viewpoint described above; and we were unaware that our balance was functioning, in effect, like a negative spring.

The reason we presented in Thorne et al. (1978) a gedanken experiment for measuring an electromagnetic oscillator, rather than a mechanical oscillator, was that we had not yet invented the "negative-capacitor" readout system of Fig. 7.

12. The ideas and prose of this Appendix are due entirely to Carlton M. Caves, and constitute a portion of the material submitted by him to the California Institute of Technology in partial fulfillment of the requirements for the Ph.D. degree.

13. For quick measurements ($\tau \lesssim \omega^{-1}$) it is more reasonable to compare the accuracy σ to $(\hbar\tau/m)^{1/2}$, the standard quantum limit for measurements of free-mass position (Eq. 3.2). Beating this standard limit requires even stronger coupling than is required to beat the standard quantum limit for amplitude-and-phase measurements.

14. The ideas and prose of this Appendix are due entirely to Carlton M. Caves, and constitute a portion of the material submitted by him to the California Institute of Technology in partial fulfillment of the requirements for the Ph.D. degree.

FIGURE CAPTIONS

Fig. 1. The "error box" in the phase plane for a quantum mechanical oscillator. This error box is an ellipse, with centroid at the expectation value $(\langle\hat{x}\rangle, \langle\hat{p}/m\omega\rangle)$ of the position and momentum. The principal axes of the error ellipse are the eigendirections of the variance matrix

$$\begin{Vmatrix} (\Delta x)^2 & \sigma_{xp} \\ \sigma_{xp} & (\Delta p/m\omega)^2 \end{Vmatrix} ,$$

and the principal radii are the square roots of the corresponding eigenvalues. Here $\sigma_{xp} \equiv (1/2m\omega) \langle(\hat{x} - \langle\hat{x}\rangle)(\hat{p} - \langle\hat{p}\rangle) + (\hat{p} - \langle\hat{p}\rangle)(\hat{x} - \langle\hat{x}\rangle)\rangle$. This error box has the property

$$\Delta x \cdot \frac{\Delta p}{m\omega} \geq \frac{1}{\pi} (\text{area of box}) \geq \frac{\hbar}{2m\omega} ,$$

$$\Delta X_1 \cdot \Delta X_2 \geq \frac{1}{\pi} (\text{area of box}) \geq \frac{\hbar}{2m\omega}$$

(as one can verify by elementary calculations). Here X_1 and X_2 are the real and imaginary parts of the complex amplitude, and the (X_1, X_2) coordinates of the phase plane are related to the $(x, p/m\omega)$ coordinates by a simple time-dependent rotation

$$x + ip/m\omega = (X_1 + iX_2)e^{-i\omega t} .$$

Fig. 2. A simple example of an oscillator coupled to an amplifier. Part (a) (to left of dashed line) is the oscillator, an LC circuit; part (b) (to right of dashed line) is a zero-impedance charge amplifier whose "Thevenin equivalent circuit" is shown in the figure. See text for discussion.

Fig. 3. Error boxes for various types of measurements of a harmonic oscillator. (a) The error box characterizing the results of a "quick measurement" of position. After the measurement the error box rotates clockwise in the phase plane with angular velocity ω, which means that it remains fixed as seen in the "rotating" (X_1,X_2) coordinates. (b) The error box for "amplitude-and-phase measurements" as seen in the (X_1,X_2) coordinate system. (c) The error annulus ($\delta N \equiv 1$) for "quantum-counting measurements." (d) The error box for a "back-action-evading measurement" of X_1.

Fig. 4. A harmonic oscillator, initially in an energy eigenstate with N = 30 quanta, is driven by a classical force for a time τ. The integrated strength of the force is characterized by the dimensionless number $|\alpha(\tau,0)|$ (Eqs. 2.20b and 2.22b). Here we show the probability $P(30 \to N';\tau)$ that after the force acts the oscillator is in an eigenstate with N' quanta (Eq. 2.26). The various probability distributions are labeled by the strength $|\alpha(\tau,0)|$ of the wave. Notice that, if one makes a quantum-counting measurement and discovers a transition from N = 30 to N' = 29, one cannot with confidence determine the strength of the force that acted. One can only conclude that $0.05 \lesssim |\alpha(\tau,0)| \lesssim 0.3$.

Fig. 5. (a) A classical harmonic oscillator is described by a single "system point," which moves about in the complex amplitude plane in response to an external driving force (Eq. 2.21). (b) A quantum mechanical oscillator in a coherent state is described by a minimum-uncertainty wave packet. In the absence of measurements the center of that wave packet moves about in the complex amplitude plane, in response to

an external driving force, with precisely the same motion as the system point of the classical oscillator (Eq. 2.21'). However, it is impossible to measure that motion more precisely than $\Delta X_1 = \Delta X_2 = (\hbar/2m\omega)^{1/2}$. (c) Two quantum mechanical oscillators, one in an eigenstate of $\hat{X}_1$, the other in an eigenstate of $\hat{X}_2$, are described by two orthogonal error lines in the complex amplitude plane. Under the action of an external driving force the intersection of the two error lines moves in exactly the same manner as the system point of a classical oscillator. In principle, this motion can be measured with complete precision, and without perturbing the error lines, by means of back-action-evading measurements.

Fig. 6. (a) An idealized velocity sensor. The "free mass" m has a wire (dark vertical bar) rigidly attached to it. The wire is hooked up to an LC circuit; and it passes through a region of uniform magnetic field (stippled region). The velocity $\dot{x}$ of the mass produces an emf $Ba\dot{x}/c$ in the LC circuit. During a measurement one either attaches a voltage amplifier in parallel with the capacitance C (dashed part of figure) and makes C as small as possible (open circuit), or one attaches a charge or current amplifier in series (not shown) and makes C as large as possible (short circuit). In any case, to achieve minimum noise one makes the stray inductance L as small as possible. As discussed in Sec. III.A.2, one can turn this velocity sensor into a momentum sensor by inserting a negative capacitance $-C_K = -1/mK^2 = -mc^2/(aB)^2$ at the location indicated by a dotted arrow. (b) Equivalent circuit for the velocity sensor of Fig. (a); see text for discussion.

Fig. 7. (a) A model of a spring-based capacitor with negative capacitance. (b) A model for the perfect, noiseless batteries that appear in part (a). For details see text.

Fig. 8. (a) A model of an amplifier-based capacitor with negative capacitance. (b) The Thevenin equivalent circuit for this model negative capacitor. For details see text.

Fig. 9. Idealized physical realization of a system for measuring the $\hat{X}_1$ of a mechanical oscillator arbitrarily quickly and accurately. See text for discussion.

Fig. 10. Idealized physical realization of a system for measuring the $\hat{X}_1$ of an electromagnetic oscillator arbitrarily quickly and accurately. See text for discussion.

Fig. 11. An idealized example of a negative spring attached to a torsion pendulum. A DC bias voltage $-V_o$ is applied to the upper plate P, and a voltage $+V_o$ to the lower plate P', of a parallel-plate capacitor. The middle plate R is held at ground potential by the wavy wire, and is physically attached by a lever arm of length b to the central shaft S of the torsion pendulum. When the shaft rotates through a small angle Q from equilibrium, plate R moves upward by a distance bQ; and the batteries V_o drive a charge $q = (bQ/d)CV_o$ onto R. (Here $C = 2\alpha/4\pi d$ is the capacitance of plates P - P' relative to plate R, and we assume $bQ \ll d$.) The charge q couples to the electric field V_o/d in the capacitor, producing an anti-restoring torque

$$\Gamma = bqV_o/d = (b/d)^2 \, CV_o^2 Q.$$

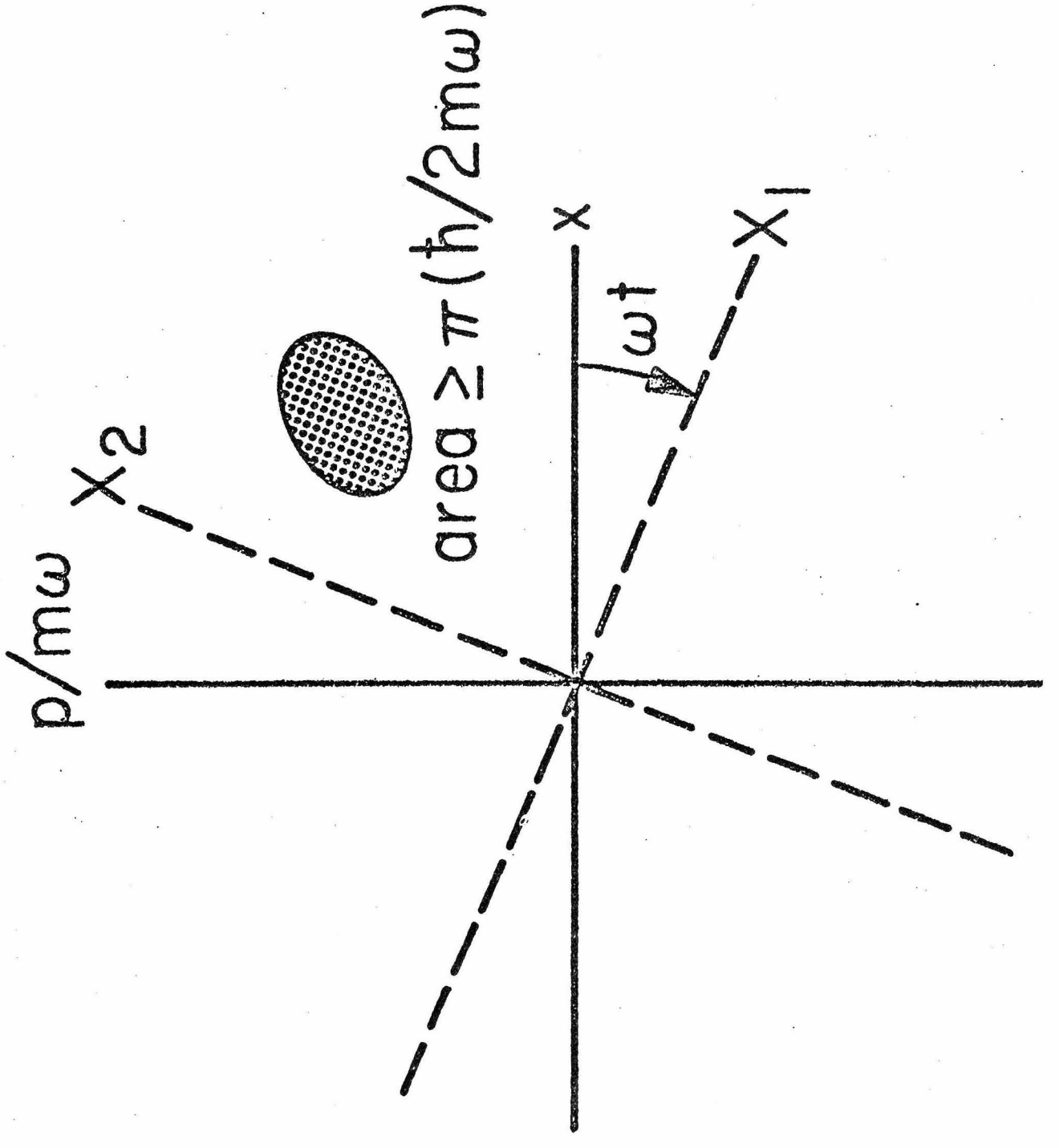

Fig. 1

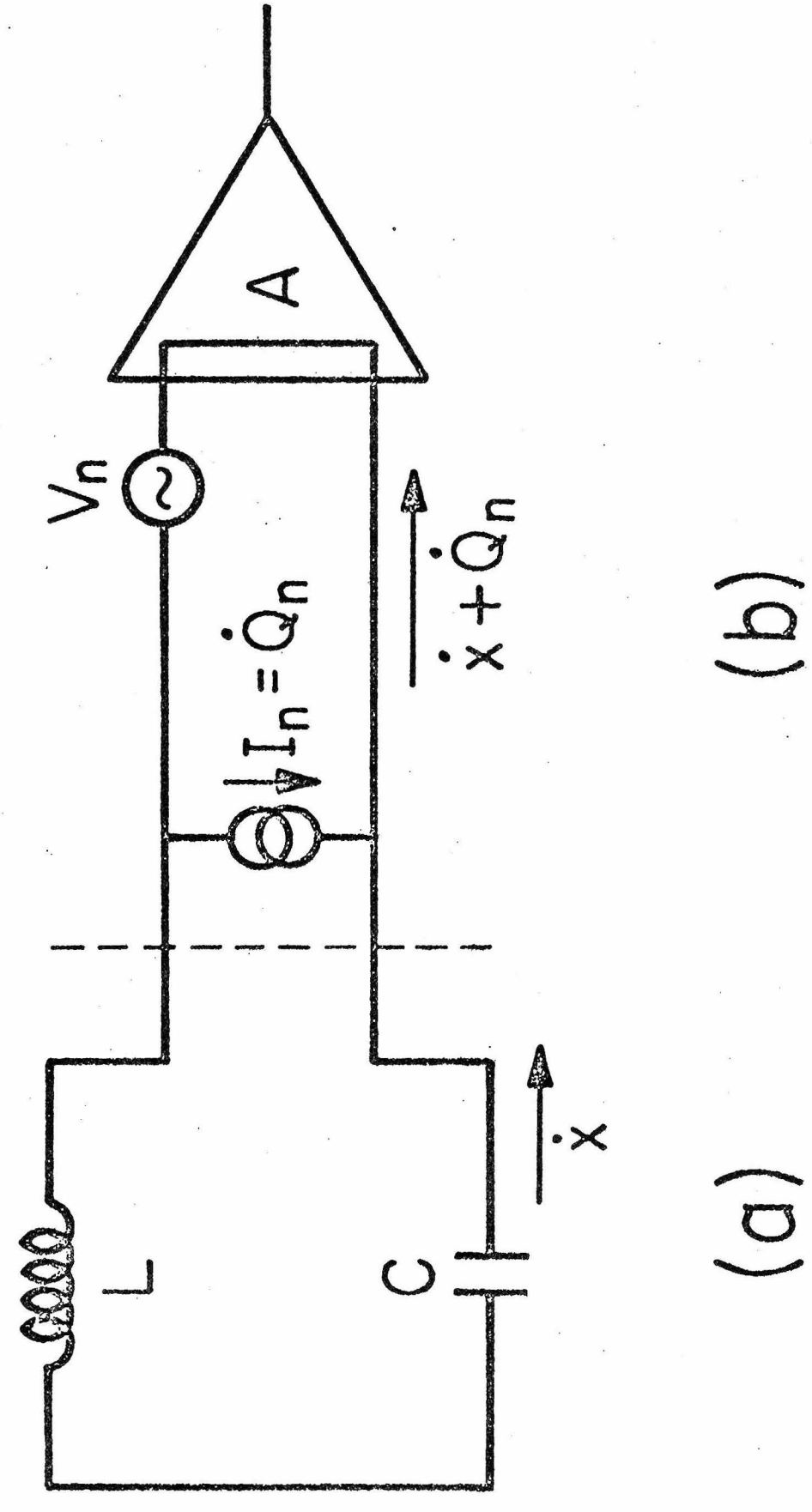

Fig. 2

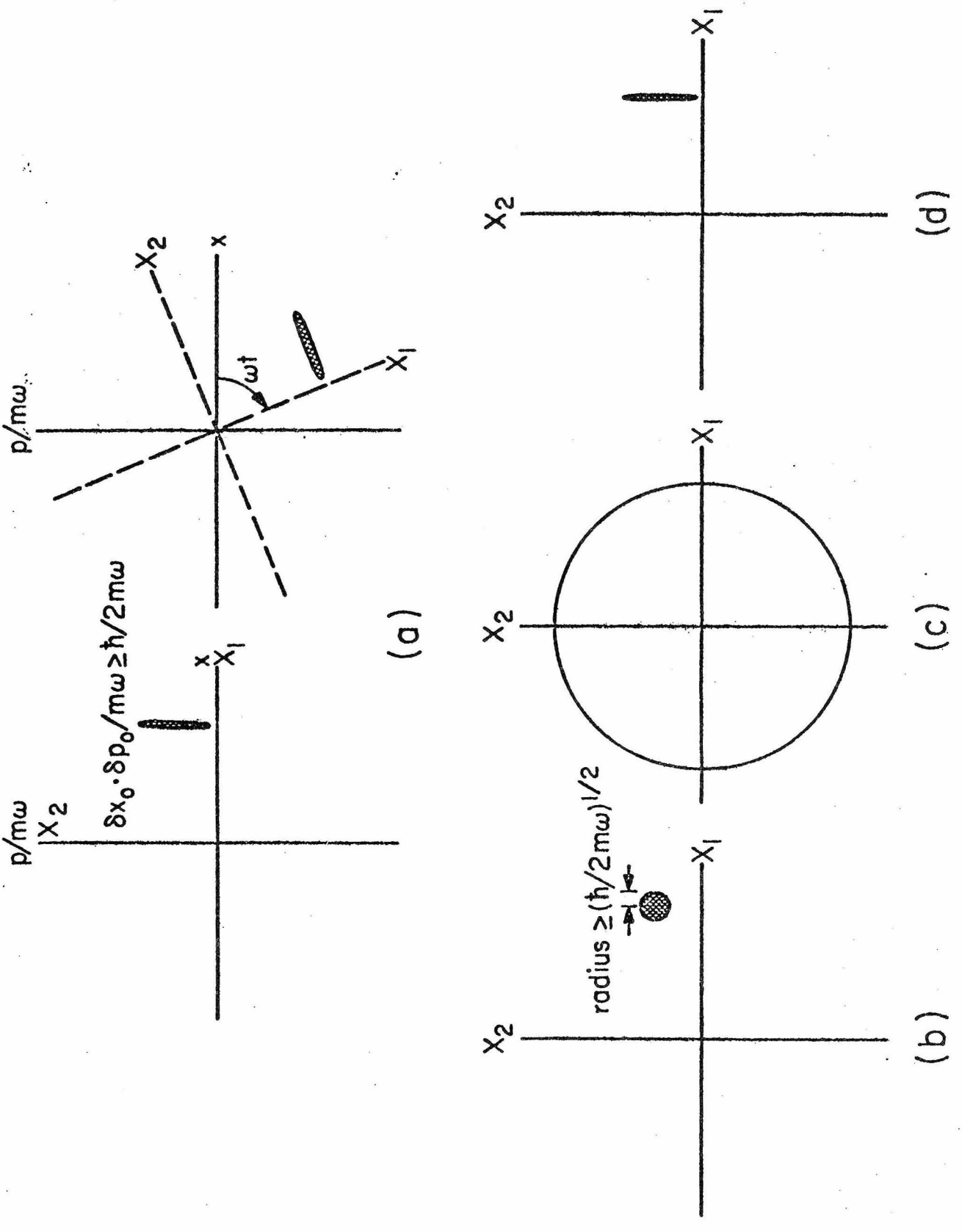
p/mω
X2
x
X1
ωt
(a)
p/mω
X2
x
X1
δx₀·δp₀/mω ≥ ħ/2mω
X2
X1
radius ≥ (ħ/2mω)^1/2
(b)
X2
X1
(c)
X2
X1
(d)

Fig. 3

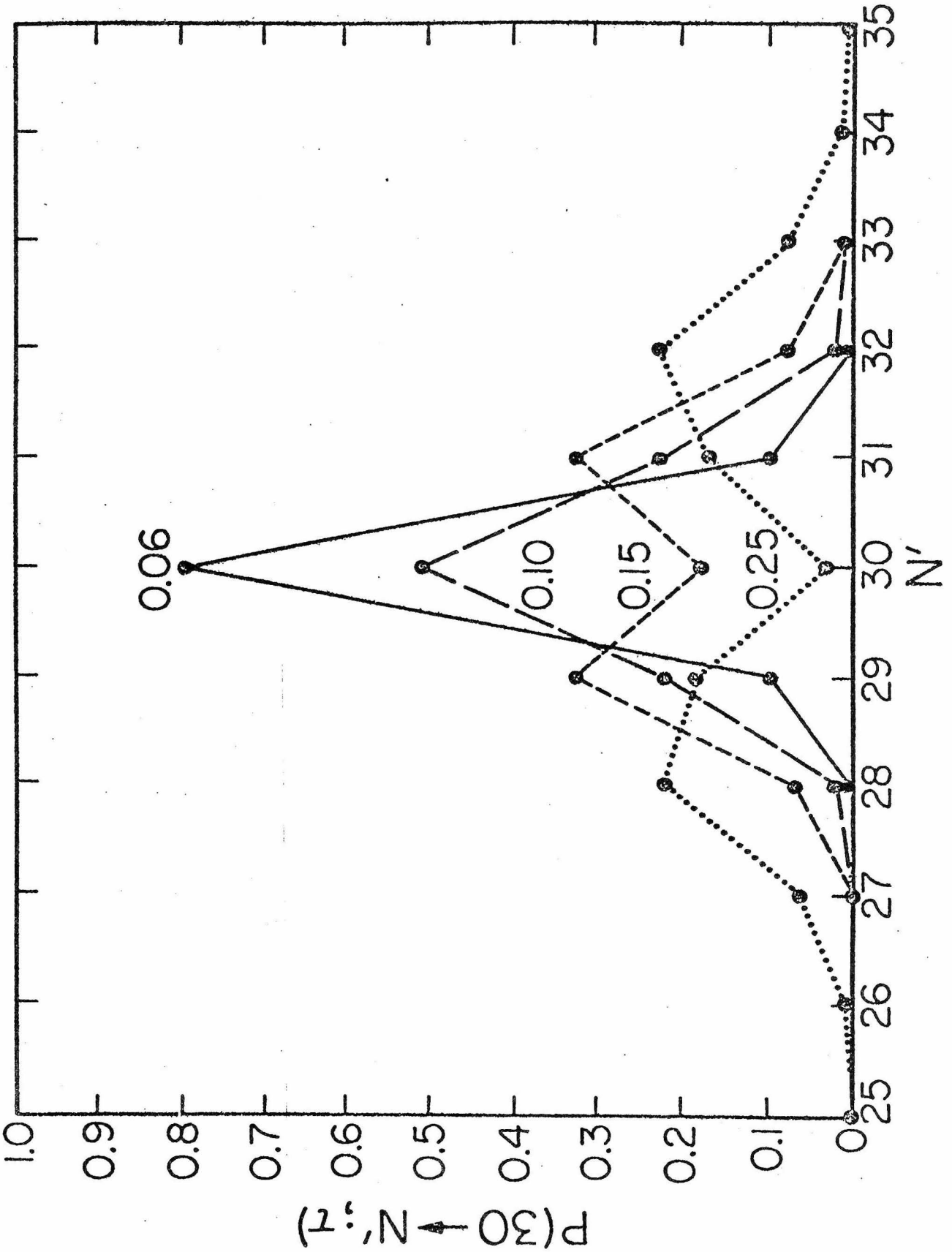
P(30 → N';τ)
N'
0.06
0.10
0.15
0.25
1.0
0.9
0.8
0.7
0.6
0.5
0.4
0.3
0.2
0.1
0
25
26
27
28
29
30
31
32
33
34
35

Fig. 4

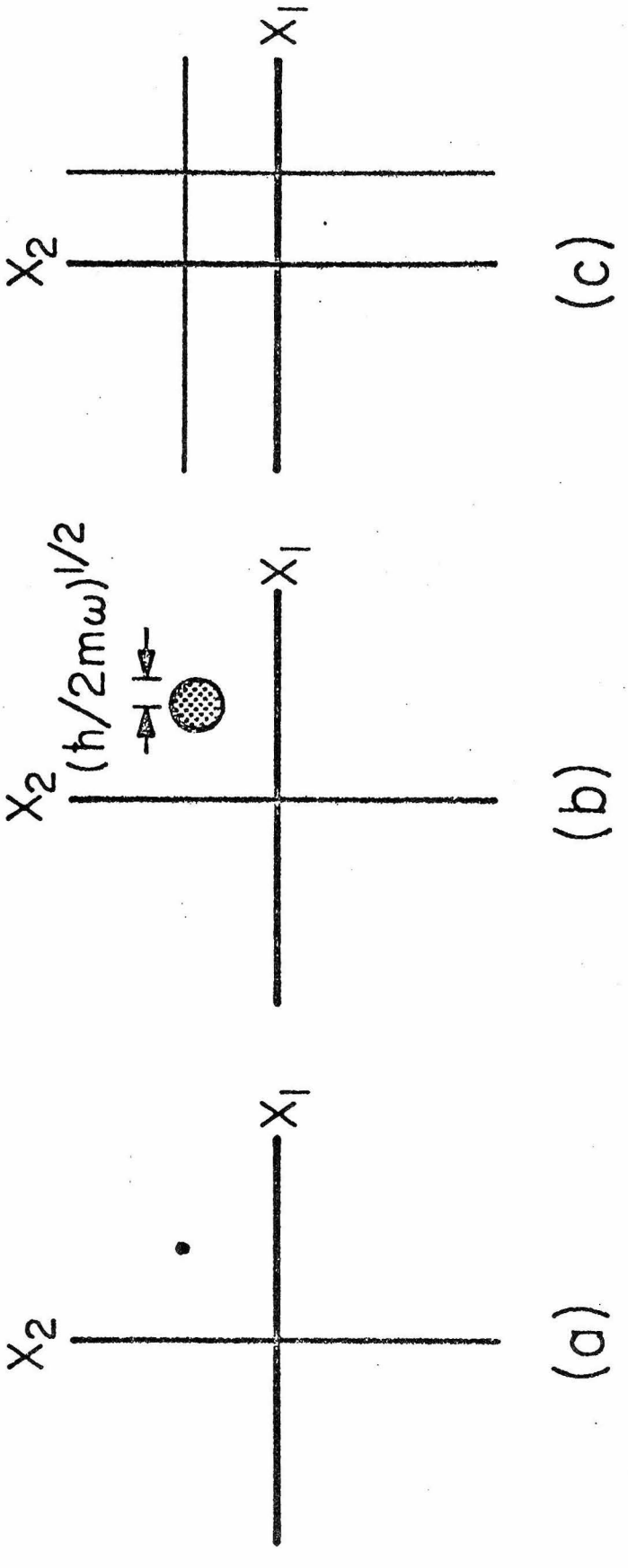

Fig. 5

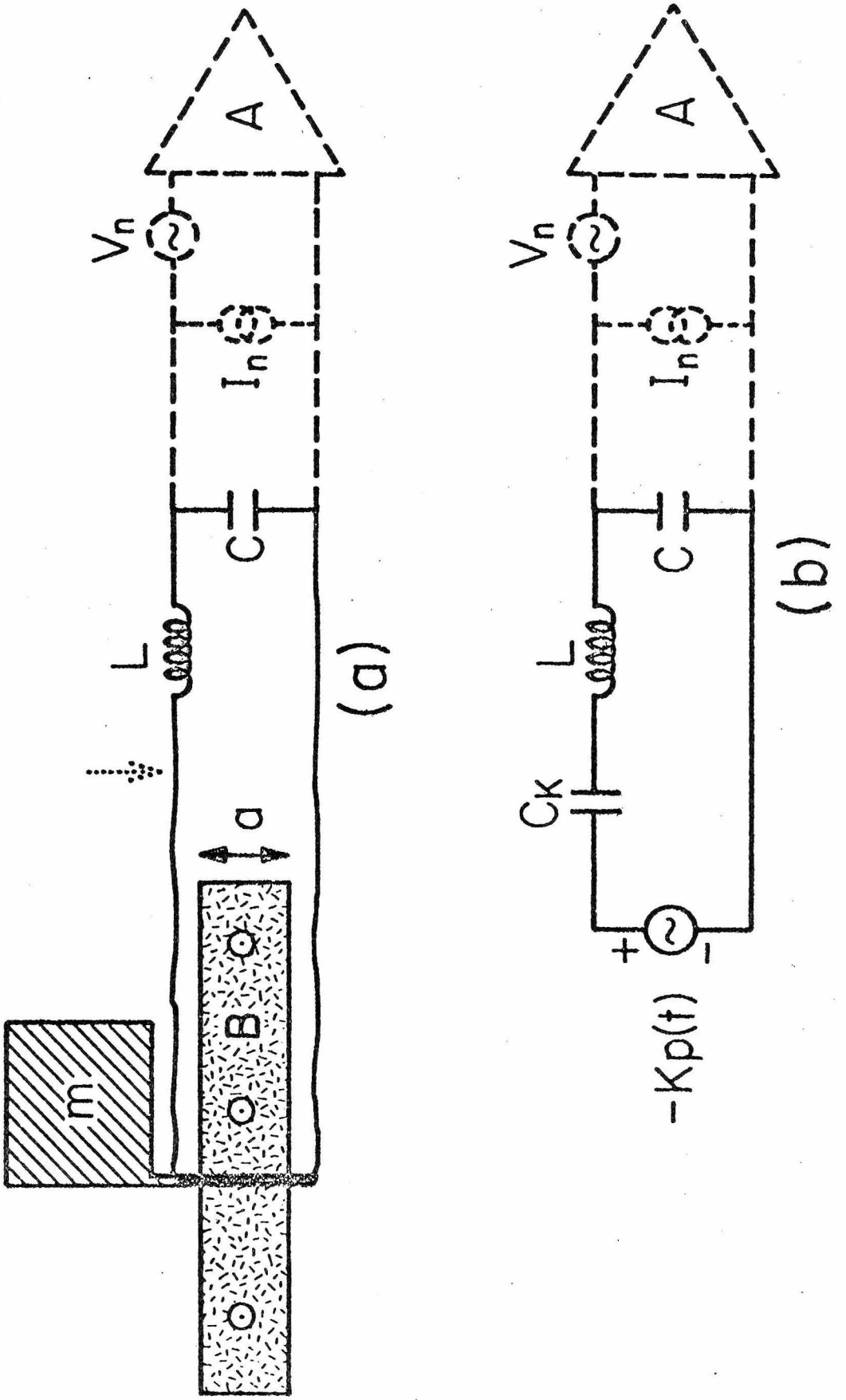

Fig. 6

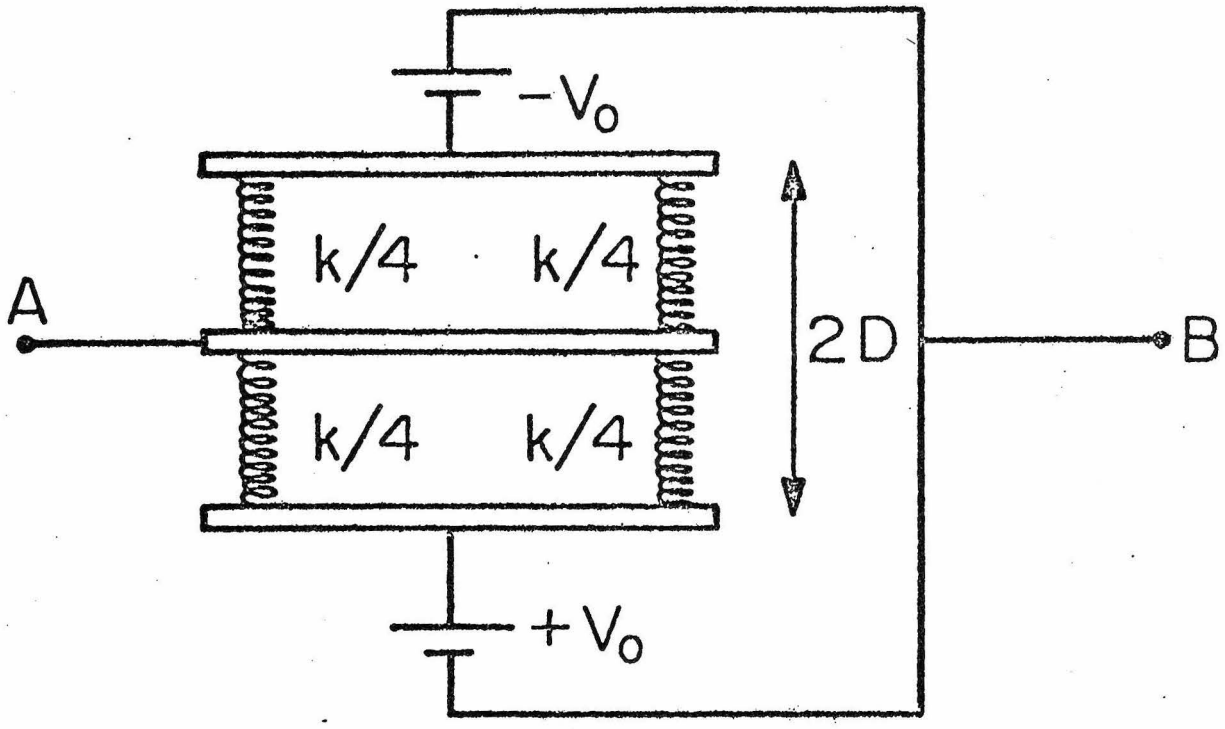

(a)

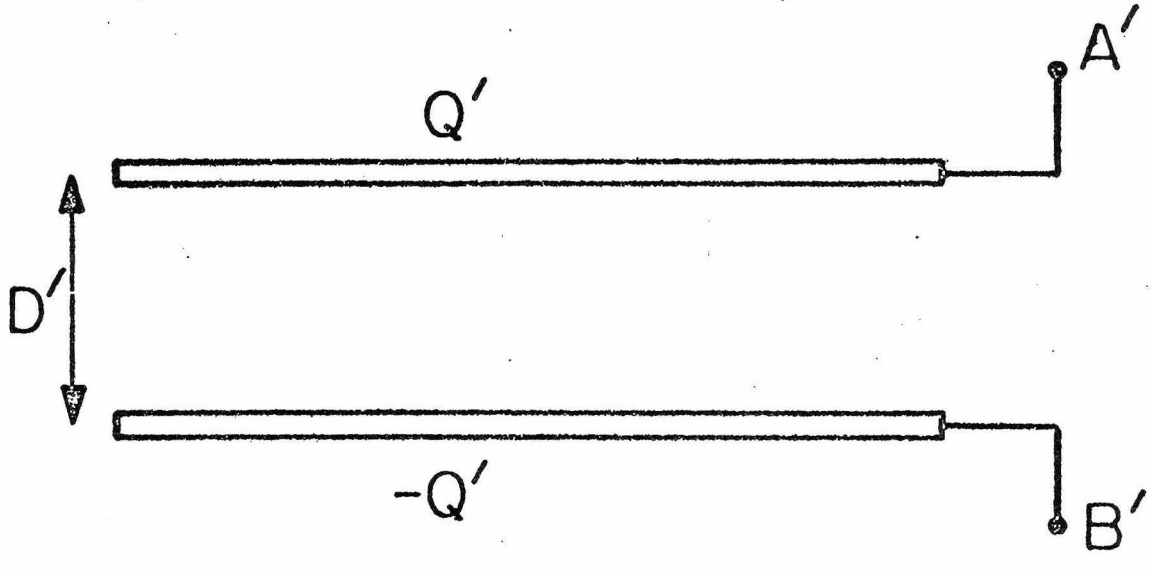

(b)

Fig. 7

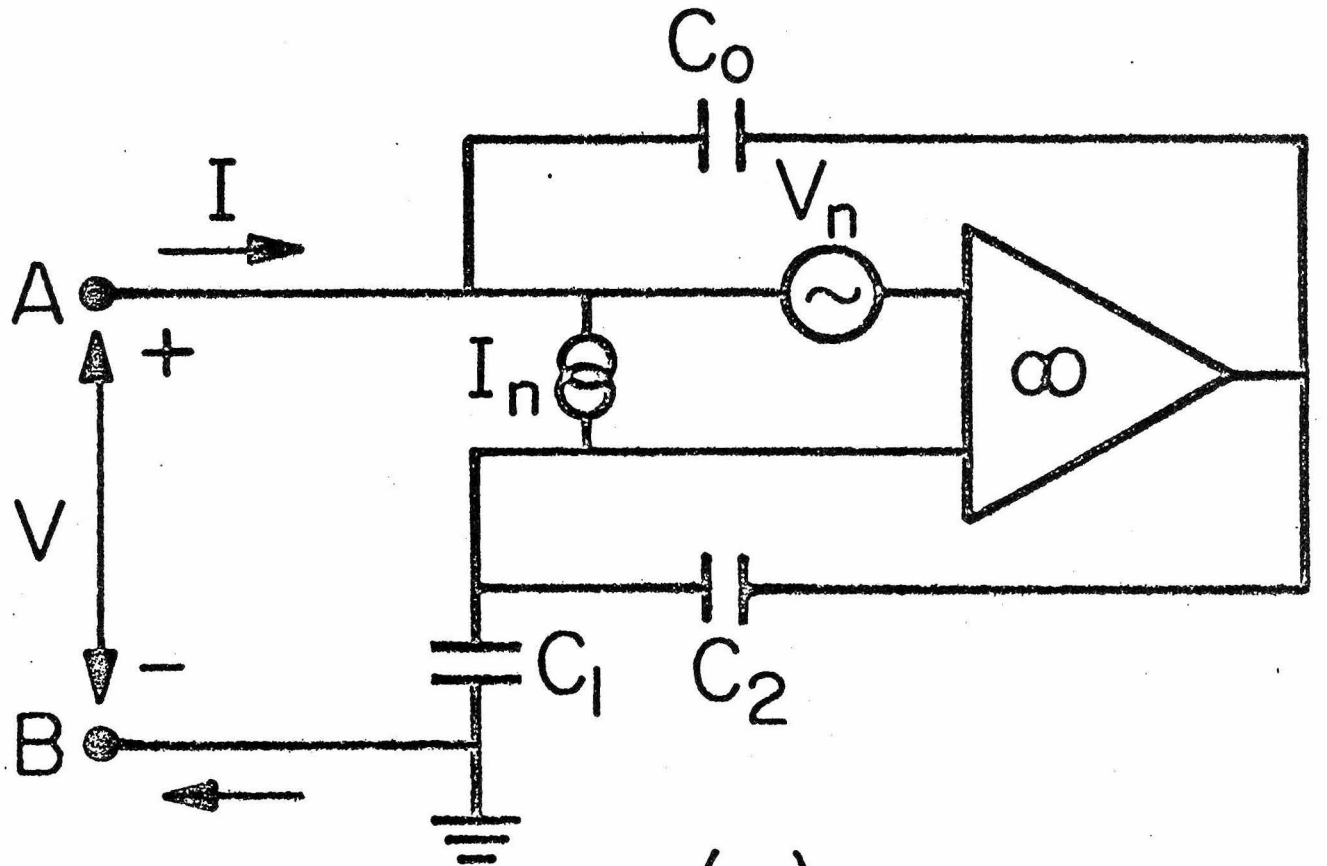

(a)

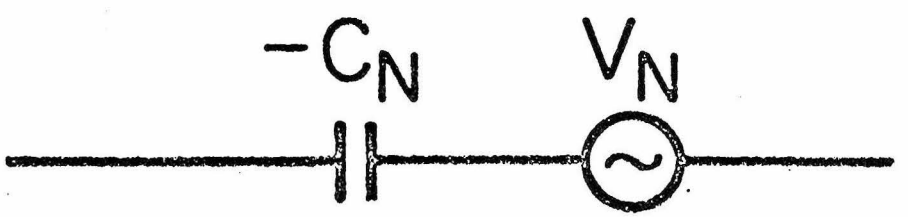

(b)

Fig. 8

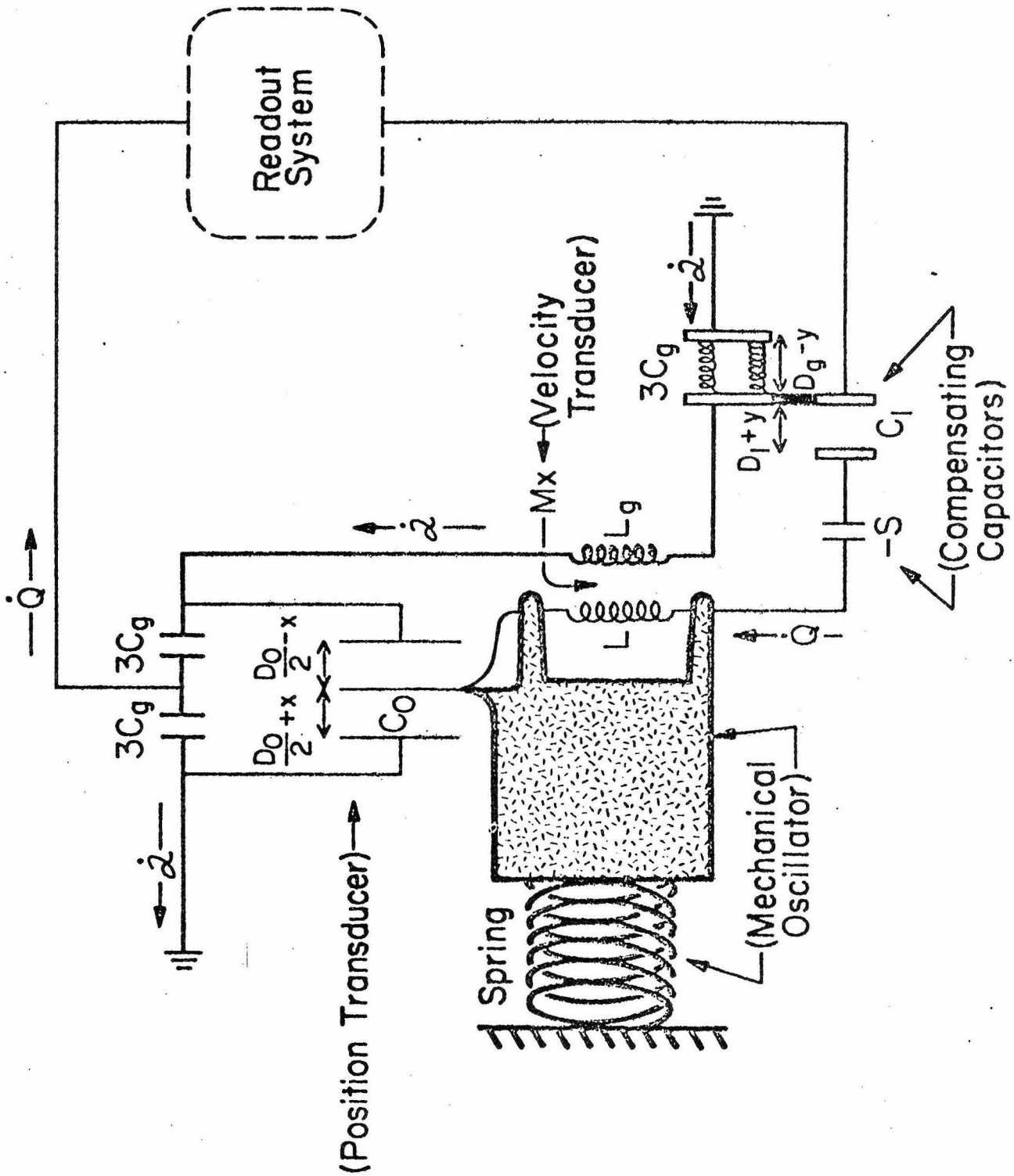
Readout System
(Velocity Transducer)
Mx
$3C_g$
$D_g - y$
$D_1 + y$
C_1
(Compensating Capacitors)
-S
L_g
L
$\dot{Q}$
$\dot{\lambda}$
$\frac{D_0}{2} - x$
$\frac{D_0}{2} + x$
C_0
(Position Transducer)
Spring
(Mechanical Oscillator)

Fig. 9

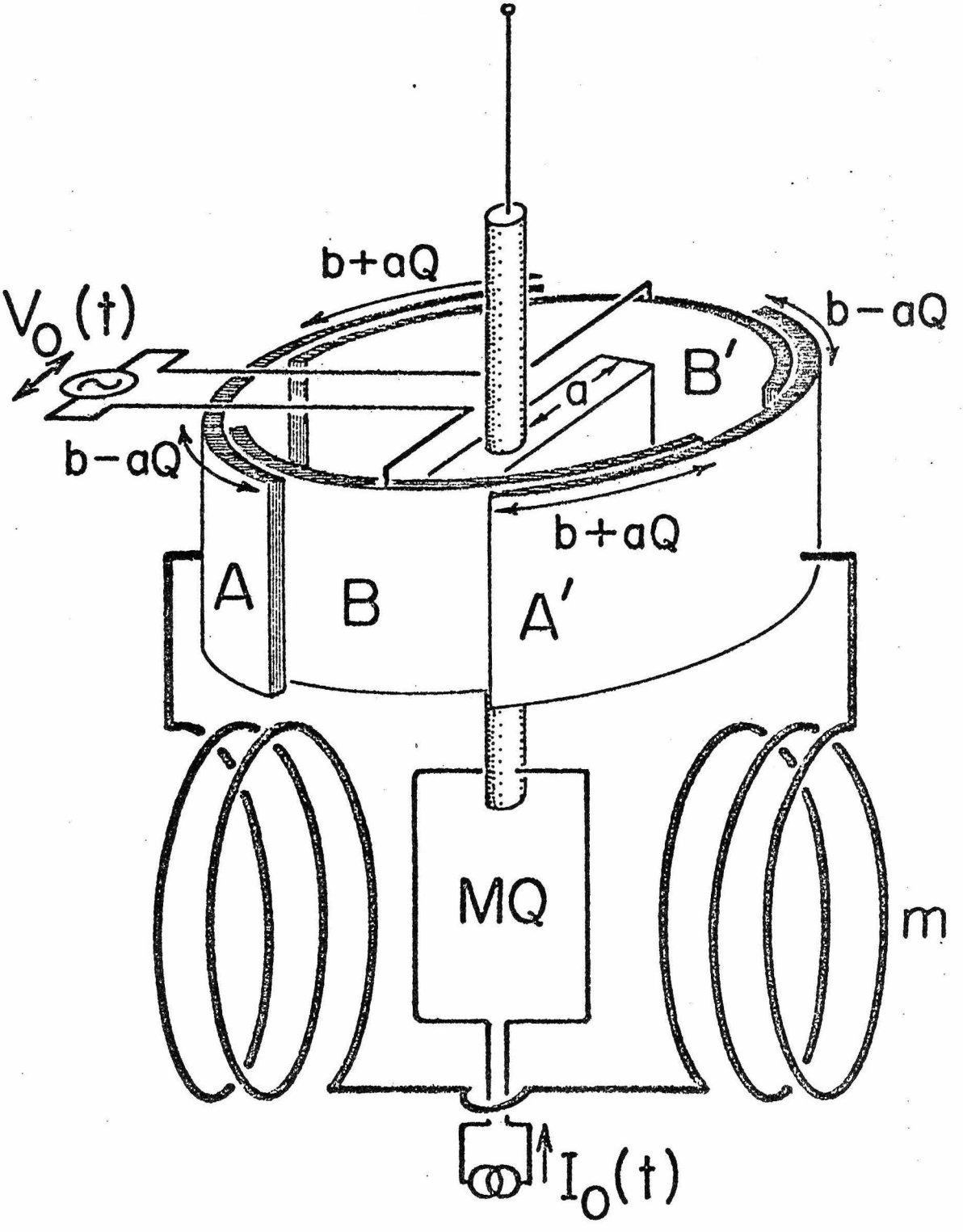

Fig. 10

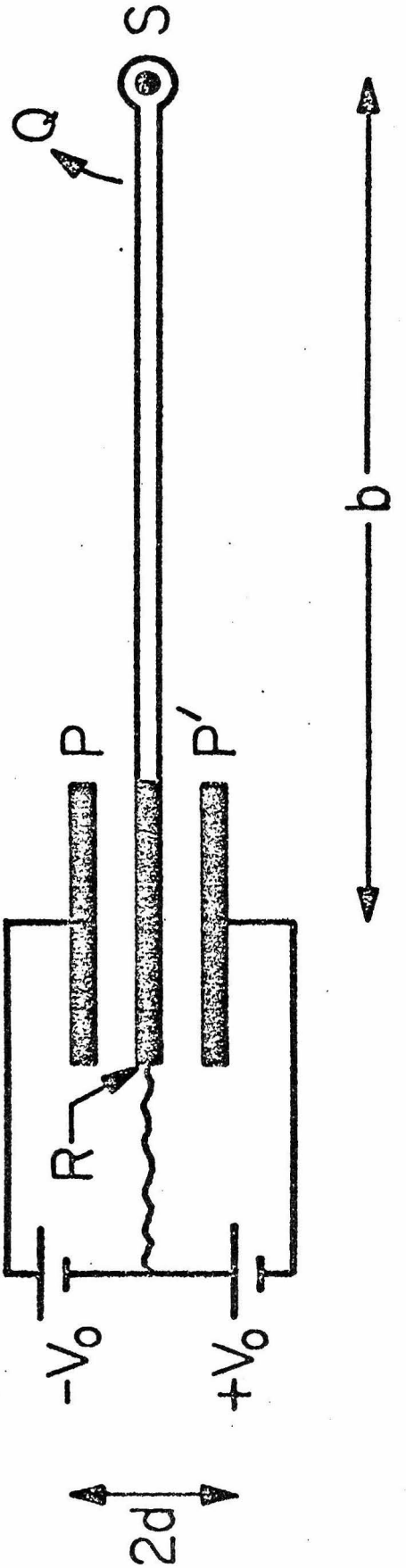

Fig. 11

CHAPTER 4

GRAVITATIONAL RADIATION AND THE ULTIMATE SPEED IN ROSEN'S BIMETRIC THEORY OF GRAVITY

This chapter is a paper which has been submitted for publication to Annals of Physics. It was supported in part by the National Science Foundation [AST76-80801] and the National Aeronautics and Space Administration [NGR05-002-256].

1. INTRODUCTION

Several years ago Nathan Rosen [1] proposed a new theory of gravity, the "bimetric" theory -- the two metrics being the physical metric $g_{\mu\nu}$ and a flat, "background" metric $\eta_{\mu\nu}$.[1] The theory is perhaps better described as a two-tensor, metric theory (see [2] for discussion). It is a metric theory in the sense that the physical metric obeys the Einstein Equivalence Principle: in the local, freely falling frames of $g_{\mu\nu}$ the nongravitational laws of physics reduce to those of special relativity. One immediate consequence is local conservation of nongravitational stress-energy $T_{\mu\nu}$ -- the matter-response equation:

$$T^{\mu\nu}{}_{;\nu} = 0 \quad . \tag{1.1}$$

The auxiliary, symmetric two-tensor $\eta_{\mu\nu}$ can be thought of as a second metric; it is constrained to be flat and is used in constructing the field equations for the physical metric (see Section 2B). In a series of papers Rosen and others have analyzed various consequences of the theory, including the maximum mass of neutron stars [3], cosmological models [4], equations of motion [5], gravitational radiation [6], and other topics [7].

The traditional testing ground for such a theory is the solar system, where observations at today's accuracies probe the theory's predictions to post-Newtonian order (see [8] for a review). Lee et al. [9] have calculated the post-Newtonian limit of Rosen's theory and shown that it is the same as that of general relativity, except for the preferred-frame PPN parameter α_2. [For a discussion of the Nordtvedt-Will Parametrized Post-Newtonian (PPN) Formalism and a description of the meaning of the PPN parameters, see chapter 39 of [10]; in particular, Box 39.5.] The values of α_2 and the Newtonian

gravitational "constant" G are determined by the distant matter in the Universe, which reaches into the solar system through boundary conditions applied far outside it. An appropriate adjustment of the cosmological boundary values brings the theory into agreement with present limits on α_2 and on the time rate of change of G. Put the other way around, these limits place constraints on the possible boundary values. One way to test the viability of the theory is to construct cosmological models and ask whether the models can be made consistent with these constraints. In this paper I point out a new set of observations which yield particularly stringent constraints on the cosmological models in Rosen's theory.

The two metrics in Rosen's theory play different roles. Gravitational radiation propagates along "light" cones of the flat metric, while light propagates along "light" cones of the physical metric. The two "light" cones need not coincide, so the speed of gravitational radiation is, in general, different from the speed of light. Lee et al. [9] showed that the speed of gravitational radiation, as measured by an observer at rest in the universal rest frame far from any local concentration of matter, is determined solely by the cosmological boundary values. This speed v_{gc} is related to α_2 by

$$v_{gc}^2 = (1 + \alpha_2)^{-1} \quad . \tag{1.2a}$$

In the vicinity of a local source of gravity with (dimensionless) Newtonian potential $U \ll 1$ $(U > 0)$, the speed of gravitational radiation increases to

$$v_g = v_{gc}(1 + 2U) \tag{1.2b}$$

(see Section 2B). It is possible for v_g to be less than the speed of light.

I show here (Section 3B) that as a particle of nonzero rest mass is accelerated through the gravitational "light" cone, it emits an infinite amount of energy in gravitational radiation. It follows that, if $v_g < 1$, the speed of gravitational radiation is the ultimate speed for such particles; they cannot escape the gravitational "light" cone. As a result, observation of a relativistic particle with Lorentz factor γ provides a lower bound for v_g at the point of observation:

$$1 - v_g < \frac{1}{2}\gamma^{-2} \quad . \tag{1.3a}$$

If the Newtonian potential at the point of observation is known, one also obtains a lower bound for v_{gc}. This lower bound can be re-expressed as an upper bound on the value of $\alpha_2 \simeq 2(1 - v_{gc})$:

$$\alpha_2 < \gamma^{-2} + 4U \quad . \tag{1.3b}$$

Equations (1.3) are the basis for obtaining observational constraints on v_g and α_2 (see Section 4).

In this paper I analyze the gravitational radiation emitted by particles moving at speeds near the speed of gravitational radiation. This analysis leads to the conclusion that, in Rosen's theory, particles of nonzero rest mass cannot exceed the speed of gravitational radiation. This conclusion is likely to have far wider applicability than just to Rosen's theory. The detailed analysis presented here does not depend critically on any special feature of Rosen's theory; one can make a strong case that a similar analysis holds in any theory of gravity which permits the speed of gravitational radiation to differ from the speed of light (see [11] for a brief review of such theories). Indeed, it seems likely that the "gravitational speed limit" is a feature of all such theories.

Another crucial test of Rosen's theory comes from observations of the

change in orbital period of the binary pulsar [12]. Unless the two components of the binary system have identical ratios of gravitational binding energy to inertial mass, Rosen's theory predicts that the system will emit dipole gravitational radiation and that the radiation will carry away negative energy [13]. Observations of the binary pulsar are now good enough that Rosen's theory can be ruled out -- unless the two ratios are the same to within less than a percent [14].

Section 2 develops the formalism for analyzing gravitational radiation emission from weak-field systems in Rosen's theory. Section 3 builds upon this foundation to justify the claim that a particle of finite rest mass cannot exceed the speed of gravitational radiation. Section 3A calculates the energy spectrum of gravitational Cherenkov radiation emitted by a particle moving with uniform velocity $v > v_g$, and Section 3B analyzes the energy emitted as a particle is accelerated through the gravitational "light" cone. The result of these considerations is Eqs. (1.3), which Section 4 uses to obtain observational limits on v_g and $\alpha_2 (v_{gc})$. Section 5 argues that these constraints apply to any theory of gravity with a variable speed of gravitational radiation.

2. FOUNDATION FOR ANALYZING EMISSION OF GRAVITATIONAL RADIATION

This section lays the foundation for analyzing emission of gravitational radiation from weak-field, linearized systems in Rosen's theory. The foundation will be laid in two pieces: the first piece is construction of coordinates which take into account matching to boundary values provided by an external gravitational field; the second piece is construction of equations governing generation of gravitational radiation and specifying the amount of energy the radiation carries.

A. Isolated Sources and Preferred Coordinates

Below I shall deal with "isolated" sources of gravity, such as the solar system or one of the ultrarelativistic particles of Section 3. Since such sources are not actually alone in the Universe, it is necessary to describe briefly what is meant by an "isolated" source.

The key feature of an isolated source is that the gravitational field can be split into two pieces: the field of the isolated source (the local field), which applies near the source; and the field of the rest of the matter in the Universe (the external field), which applies far from the source.

To understand the conditions necessary for such a split, consider the length scales characteristic of the source and the external field. The source is characterized by two lengths: its physical size R and the length Gm corresponding to its mass m. The external field is also characterized by two lengths: a typical radius of curvature a and the length L over which the external field varies appreciably. Let r_o be the distance from the source at which the curvature produced by the source becomes comparable to the external curvature:

$$r_o \equiv (Gma^2)^{1/3} \quad . \tag{2.1}$$

To get a clean split between the local and external fields, the source must be buried deep inside r_o ($R \ll r_o$), and r_o must be much smaller than the external scales ($r_o \ll \min\{a,L\}$). These two conditions translate into

$$Gm/R^3 \gg a^{-2} \quad , \tag{2.2a}$$

$$Gm \ll \min\{a\ ,\ L(L/a)^2\} \quad . \tag{2.2b}$$

The curvature produced by the isolated source is a large, but small-scale "bump" in the large-scale external curvature.

When Eqs. (2.2) are satisfied, the region around the source can be broken up into three parts, which provide a natural split of the gravitational field:

(i) the local-field region, in which the curvature of the isolated source dominates:

$$r \lesssim r_o \quad , \tag{2.3a}$$

where r is distance from the source;

(ii) the transition region, in which the external curvature dominates, but which is small enough that the external field is nearly homogeneous:

$$r_o \lesssim r \lesssim r_1 \equiv \varepsilon \cdot \min\{a,L\} \quad , \tag{2.3b}$$

where ε is a suitably chosen factor less than one;

(iii) the external-field region:

$$r \gtrsim r_1 \quad . \tag{2.3c}$$

The nearly flat transition region splits the gravitational field into local and external fields. The only connection between the two fields is the requirement that they match smoothly in the transition region; from the point of view of the local field, the external field establishes boundary conditions in the transition region.

The boundary conditions are made explicit by choosing a specific coordinate system. A particularly convenient set of coordinates can be constructed as follows. Consider the external gravitational field in the absence of the isolated source. Let an observer falling freely in this field construct Fermi normal coordinates $\{x^\alpha\} \equiv \{t,x^j\}$ in the vicinity of his world line [15]. In these coordinates the two metrics can be expanded about the observer's world line:

$$g_{\alpha\beta} = g^{(B)}_{\alpha\beta} + [\text{terms of order } R_{\alpha j\beta k}x^j x^k \sim (r/a)^2] + \cdots , \qquad (2.4a)$$

$$\eta_{\alpha\beta}(t,x^j) = \eta_{\alpha\beta}(t,x^j=0) + \eta_{\alpha\beta,k}(t,x^j=0)x^k + \cdots , \qquad (2.4b)$$

where $g^{(B)}_{\alpha\beta}$ is Minkowskian, i.e., $\| g^{(B)}_{\alpha\beta} \| = \text{diag}(-1,+1,+1,+1)$, and $R_{\alpha\beta\gamma\delta}$ is the Riemann tensor derived from the physical metric. Now introduce the isolated source in the vicinity of the fiducial world line and use these coordinates to solve for its local field. The flat metric retains the form (2.4b), and the physical metric retains the form (2.4a) in the transition region outside the source.

Equations (2.4) display explicitly the boundary conditions to be applied in the transition region. In general relativity, which has only a physical metric, the external field influences the isolated source only through the Riemann and higher-order terms in Eq. (2.4a), which represent tidal and higher-order multipole forces on the isolated source. The situation is different in Rosen's theory because of the presence of the flat metric. Although the region around the source has been split cleanly into local and external parts, $\eta_{\alpha\beta}$ cannot be adjusted independently in the two regions; rather, the external field determines the form of $\eta_{\alpha\beta}$ in the transition region, and a particular choice of coordinates together with its flatness then determines $\eta_{\alpha\beta}$ in the local-field region. (The above choice of coordinates insures that $\eta_{\alpha\beta}$ is nearly constant in the local field region.) In general, the external field prohibits finding coordinates such that both $g_{\alpha\beta}$ and $\eta_{\alpha\beta}$ are nearly Minkowskian in the transition region. This lack of "meshing" allows the external field to reach into the vicinity of the isolated source and affect local gravitation physics. (Will [2, Section 5.3] gives a general discussion of the manner in which auxiliary tensor fields in metric theories of gravity

couple local gravitation physics to an external field.)

Gravitational radiation emitted by the source is analyzed in the transition region. In order to separate the radiation from the external curvature, the wavelength λ of the radiation must be much smaller than external scales:

$$\lambda \ll \min\{a,L\} \quad , \tag{2.5}$$

a requirement which also guarantees that the wave zone of the radiation extends into the transition region. In Section 3 I will be interested in calculating gravitational radiation emission in the linear approximation. In this limit another consequence of (2.5) is that, in Eqs. (2.4), one can ignore both the tidal terms in $g_{\alpha\beta}$ and the spatial and temporal derivatives of $\eta_{\alpha\beta}$; these terms cannot affect radiation at wavelengths much smaller than their own characteristic lengths.

As a result, in calculating the gravitational radiation emitted by an isolated source in the linear approximation, one can always use coordinates with the following two properties:

Property 1. The physical metric $g_{\alpha\beta}$ is asymptotically Minkowskian in the transition region far from the source.

Property 2. The flat metric $\eta_{\alpha\beta}$ is a nearly constant matrix in the the local-field and transition regions; its slowly changing values are determined by the external field, and its temporal derivatives can be ignored.

I shall refer to a coordinate system which satisfies these two properties as a preferred coordinate system. Such coordinates are particularly useful for analyzing gravitational radiation emission: Property 1 insures that the coordinates provide a good reference frame for an observer in the transition

region monitoring the emitted radiation; and Property 2 insures that the field equations and gravitational stress-energy assume a particularly simple form (see Section 2B). Properties 1 and 2 do not uniquely specify the coordinates; instead, they specify a family of preferred coordinate systems, the members of which are related by arbitrary Lorentz transformations and translations. Throughout the following I shall use preferred coordinates.

Now restrict attention to the sources considered in Sections 3 and 4 -- ultrarelativistic particles moving in a typical astrophysical environment. For such sources, the external field must include both the smoothed-out cosmological solution and the fields of nearby, large-scale density enhancements. A typical source might be a cosmic-ray proton near the Earth; then the nearby density enhancements include the Virgo cluster, the Local Group, the Galaxy, the solar system, and the Earth. To sufficient accuracy the gravitational fields of the large-scale density enhancements can be treated in the weak-field, slow-motion approximation. If the Universe is homogeneous and isotropic (assumed henceforth), the solution for the full external field — including the cosmological boundary values and nearby density enhancements — is that given in reference [9]. In the universal rest frame — the frame in which the cosmological fluid is at rest — the two metrics are given by

$$g_{00} = -1 + 2U \quad , \tag{2.6a}$$

$$g_{0j} = 0 \quad , \tag{2.6b}$$

$$g_{jk} = \delta_{jk}(1 + 2U) \quad , \tag{2.6c}$$

$$||\eta_{\alpha\beta}|| = \mathrm{diag}(-c_0^{-1}, c_1^{-1}, c_1^{-1}, c_1^{-1}) \quad , \tag{2.6d}$$

where c_0 and c_1 are determined by the cosmological solution, and U is the Newtonian potential due to those nearby density enhancements which produce a significant deviation from the cosmological solution. The g_{0j} components have been neglected, since they are much smaller than U for slow-motion sources.

The external field (2.6) is used to construct preferred coordinates appropriate for analyzing an isolated source. For many purposes the most convenient set of preferred coordinates is obtained by using a (freely falling) fiducial observer who is initially at rest in the universal rest frame. In the resulting preferred coordinates $g_{\alpha\beta}$ is asymptotically Minkowskian in the transition region (Property 1), and $\eta_{\alpha\beta}$ is given by

$$\eta_{00} = - c_0^{-1}(1 + 2U) \quad , \tag{2.7a}$$

$$\eta_{0j} = 0 \quad , \tag{2.7b}$$

$$\eta_{jk} = c_1^{-1} \delta_{jk}(1 - 2U) \quad , \tag{2.7c}$$

where U (= constant) is evaluated in the vicinity of the isolated source. These preferred coordinates will be called the local universal rest (LURF); they will be used for all the calculations in Section 3.

B. Linearized Field Equations and Gravitational Stress-Energy

It is not necessary to give the full, nonlinear Rosen field equations here; only the linearized version will be needed. For the full equations the reader is referred to the original papers of Rosen [1] and to [9].

For a weak-field source, the physical metric in a preferred coordinate system is nearly Minkowskian in both the local-field and transition regions. In the usual way, define the metric perturbation $h_{\mu\nu}$ to be the deviation of $g_{\mu\nu}$ from Minkowskian:

$$g_{\mu\nu} = g^{(B)}_{\mu\nu} + h_{\mu\nu} \ , \quad g^{(B)}_{\mu\nu} \equiv \mathrm{diag}(-1,+1,+1,+1) \ ; \tag{2.8}$$

and let $\bar{h}_{\mu\nu}$ be the trace-reversed metric perturbation:

$$\bar{h}_{\mu\nu} \equiv h_{\mu\nu} - \frac{1}{2} g^{(B)}_{\mu\nu} h \quad , \tag{2.9}$$

where $h \equiv g^{(B)\mu\nu} h_{\mu\nu}$. The indices of $h_{\mu\nu}$ and $\bar{h}_{\mu\nu}$ are raised and lowered

using $g^{(B)}_{\mu\nu}$.

To linear order in the metric perturbation, the field equations in any preferred coordinate system are given by

$$\eta^{\alpha\beta}\bar{h}_{\mu\nu,\alpha\beta} = -16\pi\,(-g/-\eta)^{1/2}\,G_o T_{\mu\nu} \quad . \tag{2.10a}$$

Here $\eta^{\alpha\beta}$ is the inverse of $\eta_{\alpha\beta}$; g and η are the determinants of $g_{\mu\nu}$ and $\eta_{\mu\nu}$, respectively; and G_o is a coupling constant with dimensions of the Newtonian gravitational constant (see [9]). In LURF coordinates, Eq. (2.10a) becomes

$$\nabla^2\bar{h}_{\mu\nu} - (1/v_g^2)\,\bar{h}_{\mu\nu,00} = -16\pi\,GT_{\mu\nu} \quad . \tag{2.10b}$$

Here $G = (c_0c_1)^{1/2}G_o$ is the gravitational "constant" at the epoch of interest (as measured, e.g., by a Cavendish experiment performed far away from any local density enhancements), and v_g -- the speed of gravitational radiation in the LURF -- is given by Eqs. (1.2). Equation (1.2a) uses the results of [9] to relate v_{gc} to α_2 [$v_{gc}^2 = c_1/c_0 = (1 + \alpha_2)^{-1}$].

The linearized matter-response equations are obtained from Eq. (1.1):

$$T^{\mu\nu}{}_{,\nu} = 0 \quad . \tag{2.11}$$

Just as in general relativity or any other metric theory, gravitational effects disappear from the matter-response equations at linear order; the linear approximation is valid only so long as the motion of the source is governed by nongravitational forces.

To analyze gravitational radiation emitted by a source, one must be able to calculate the energy and momentum carried by the radiation. Rosen [1] has demonstrated the existence of a stress-energy complex $\Theta_\mu{}^\nu$ which is conserved with respect to the flat metric:

$$\Theta_{\mu}{}^{\nu}{}_{|\nu} = 0 \quad , \tag{2.12a}$$

$$\Theta_{\mu}{}^{\nu} = (-g/-\eta)^{1/2} \, (T_{\mu}{}^{\nu} + t_{\mu}{}^{\nu}) \quad . \tag{2.12b}$$

The tensor $t_{\mu}{}^{\nu}$ is interpreted as the gravitational stress-energy; it is a quadratic expression in first derivatives of $g_{\mu\nu}$ with respect to $\eta_{\mu\nu}$ $(g_{\mu\nu|\alpha})$. To lowest order in the metric perturbation, it is given in any preferred coordinate system by

$$t_{\mu}{}^{\nu} = \frac{1}{32\pi G_o} (-\eta/-g)^{1/2} \left(\delta_{\mu}{}^{\alpha} \eta^{\nu\beta} - \frac{1}{2} \delta_{\mu}{}^{\nu} \eta^{\alpha\beta} \right) \left(\bar{h}^{\gamma\delta}{}_{,\alpha} \bar{h}_{\gamma\delta,\beta} - \frac{1}{2} \bar{h}_{,\alpha} \bar{h}_{,\beta} \right) \quad , \tag{2.13}$$

where $\bar{h} \equiv g^{(B)\mu\nu} \bar{h}_{\mu\nu}$.

Equations (2.12) can be integrated to obtain conservation laws for the total 4-momentum. In a preferred coordinate system, the 4-momentum P_{α} of the source is defined by

$$P_{\alpha} \equiv \int (-g)^{1/2} (T_{\alpha}{}^{0} + t_{\alpha}{}^{0}) \, d^3x \quad . \tag{2.14}$$

P_{α} transforms like a 4-vector under Lorentz transformations among the preferred coordinates, and its indices are raised and lowered using $g^{(B)}_{\mu\nu}$. Now surround the source with a closed 2-surface S which lies in the transition region, and let $\underset{\sim}{n}$ be the unit outward normal (with respect to $g^{(B)}_{\mu\nu}$) to S . The conservation law (2.12) relates the change of 4-momentum inside S to a flux of 4-momentum through S :

$$\frac{dP^{\alpha}}{dt} = - \int_{S} (T^{\alpha j} + t^{\alpha j}) n_j \, dA \quad . \tag{2.15}$$

Here the first index of $t_{\mu}{}^{\nu}$ has been raised using $g^{(B)}_{\mu\nu}$.

The important quantity for calculating energy loss due to gravitational radiation is t^{0j}, the energy flux in the radiation. Its form (to lowest

order in the metric perturbation) is particularly simple in LURF coordinates:

$$t^{0j} = -\frac{1}{32\pi G}\left(\bar{h}^{\gamma\delta}{}_{,0}\,\bar{h}_{\gamma\delta,j} - \bar{h}_{,0}\,\bar{h}_{,j}\right) \quad . \tag{2.16}$$

Note that the field equations (2.10a) and the gravitational stress-energy (2.13) are not invariant under infinitesimal coordinate (gauge) transformations. This lack of invariance reflects the fact that a gauge transformation destroys Property 2 of the preferred coordinates, i.e., $\eta_{\alpha\beta}$ does not remain constant on local scales. In such coordinates, $g^{(B)}_{\alpha\beta|\gamma} \neq 0$ and terms containing $g^{(B)}_{\alpha\beta|\gamma}$ and $g^{(B)}_{\alpha\beta|\gamma\delta}$ appear in the linearized field equations and in the gravitational stress-energy.

3. GRAVITATIONAL RADIATION AND THE GRAVITATIONAL SPEED LIMIT

In Rosen's theory the speed of gravitational radiation is determined by the combined effects of the cosmological gravitational field and the gravitational fields of nearby, local concentrations of matter [Eqs. (1.2)]. Although the latter always tend to increase v_g, the cosmological field can force v_g to be less than the speed of light. It is this case -- $v_g < 1$ -- that I consider in this section; in particular, I investigate the gravitational radiation emitted by particles moving at speeds near v_g.

The motivation for doing so is provided by an analogy with electromagnetism. A charged particle, moving through a material medium at a speed faster than the speed of light in the medium, emits electromagnetic Cherenkov [16] radiation. In any real medium dispersion restricts the radiation to a finite range of frequencies; however, for an idealized, dispersionless medium, the energy emitted diverges. Similarly, in Rosen's theory, a particle which exceeds the speed of gravitational radiation ought to emit gravitational

Cherenkov radiation. Moreover, the gravitational "medium" is dispersionless (at least at high frequencies), so the electromagnetic analogy suggests that the energy emitted ought to diverge. If so, this result would suggest that particles cannot exceed the speed of gravitational radiation.

These ideas were first considered in a different context by Aichelburg, Ecker, and Sexl [17]. They considered a particle whose equation of motion apparently allows it to exceed the speed of light, but which is coupled to a field that propagates at the speed of light. They argued that radiation reaction prohibits accelerating the particle to speeds greater than the speed of light. They showed, for example, that if such a particle is charged, the electromagnetic radiation it emits diverges as it is accelerated through the light cone. The situation considered here is similar, and the analysis is patterned after their work. I shall first consider the gravitational Cherenkov problem and then analyze the power radiated in gravitational radiation as a particle is accelerated through the gravitational "light" cone.

A. Gravitational Cherenkov Radiation

Consider a particle with rest mass m_o moving with uniform velocity $\underset{\sim}{v}$ relative to the LURF; let $v > v_g$. In the case of interest, v_g is very close to the speed of light. Adopt LURF coordinates and solve for the gravitational field in the linear approximation. The solution of the field equations (2.10b) proceeds exactly as in the analogous electromagnetic problem (see, e.g., [18], Section 14.9). The metric perturbation $h_{\mu\nu}$ forms a shock front along a cone which extends back from the instantaneous position of the particle (see Fig. 1); the angle θ_C between the velocity $\underset{\sim}{v}$ and the normal to

the cone is given by $\cos\theta_C = (v_g/v)$. Outside the cone $\bar{h}_{\mu\nu}$ vanishes; inside the cone,

$$\bar{h}_{00}(\underset{\sim}{x},t) = \frac{8G\gamma m_o}{|\underset{\sim}{x} - \underset{\sim}{v}t|[1 - (v/v_g)^2\sin^2\alpha]^{1/2}} \quad , \tag{3.1a}$$

$$\bar{h}_{0j} = -\bar{h}_{00}\, v^j \quad , \tag{3.1b}$$

$$\bar{h}_{jk} = \bar{h}_{00}\, v^j v^k \quad , \tag{3.1c}$$

where α is the angle between the observation point $\underset{\sim}{x}$ and the velocity $\underset{\sim}{v}$, and $\gamma \equiv (1-v^2)^{-1/2}$ is the particle's Lorentz factor. The field (3.1) represents gravitational Cherenkov radiation propagating in the direction normal to the Cherenkov cone. By evaluating the energy flux using (2.16) and then following the procedure used for electromagnetic Cherenkov radiation, one obtains the energy d^2E radiated into an angular frequency interval $d\omega$ as the particle moves a distance $d\ell$:

$$\frac{d^2E}{d\omega d\ell} = Gm_o^2\omega(v^{-2} - 1) \qquad \text{for} \quad v > v_g \quad . \tag{3.2}$$

This expression is similar to the Frank-Tamm [19] result for electromagnetic Cherenkov radiation.

Equation (3.2) does not, of course, hold for all frequencies, and it is important to determine its region of validity. In using the formalism of Section 2, the above analysis neglects variations in the external gravitational field. However, since the particle is assumed to radiate for an infinite amount of time, these variations cannot be ignored; their effect is to modify Eq. (3.2) at low frequencies. To estimate the frequency at which such modification becomes important, consider a particle which radiates for

only a finite time $T \sim (r_1/v)$ [see Eq. (2.3b)]. Then the particle's motion and the radiation it emits can be analyzed within the transition region, where the formalism developed in Section 2 is applicable. The emitted radiation is a pulse which lies just inside the Cherenkov cone (see Fig. 1). It is easy to show that, when the radiation is analyzed at a distance $\sim r_1$ from the particle's trajectory, the pulse has a duration $\Delta t \sim [(v/v_g) - 1](T/8)$. Thus the energy spectrum will be given by Eq. (3.2) for frequencies $\omega \gtrsim \omega_c \equiv (1/\Delta t)$. The wavelength corresponding to the critical frequency ω_c is

$$\lambda_c \sim \varepsilon(v_g^{-1} - v^{-1}) \cdot \min\{a,L\} \simeq \frac{1}{2}\,\varepsilon\,(\gamma_g^{-2} - \gamma^{-2}) \cdot \min\{a,L\} \quad , \qquad (3.3)$$

where $\gamma_g \equiv (1 - v_g^2)^{-1/2}$. I have confirmed this result by a detailed analysis of the radiation emitted by a particle which moves faster than v_g for only a finite time.

Variations in the external gravitational field can be regarded as producing "dispersion" in the propagation of gravitational radiation. This dispersion modifies the Cherenkov spectrum at frequencies below ω_c. Note that, as v approaches v_g, ω_c increases and dispersion affects more of the spectrum. Even when γ is not close to γ_g, the critical wavelength λ_c is typically rather small. For example, for a particle near the earth, the relevant external scale is of order the radius of the earth: $L \sim 10^9$cm. Using the smallest value of v_g allowed by the limits obtained in Section 4 [see Eq. (4.2b)] and choosing $\varepsilon = 10^{-2}$, one finds $\lambda_c \sim (10^{-11}\text{cm})[1 - (\gamma_g/\gamma)^2]$.

The importance of the preceding analysis lies not so much in estimating the size of λ_c, but rather in demonstrating that, as long as $v > v_g$, there is a <u>finite</u> critical frequency above which the gravitational "medium" is

dispersionless and Eq. (3.2) applies. In the purely classical analysis given above, the validity of Eq. (3.2) extends to arbitrarily high frequencies, and the spectrum diverges as $\omega \to \infty$. However, quantum mechanics often eliminates classical divergences, and one might expect a proper quantum-mechanical treatment to modify the classical spectrum at very high frequencies. In particular, conservation of energy might seem to require that the spectrum be cut off at a frequency $\omega_{max} = (\gamma m_o/\hbar)$ corresponding to emission of a graviton whose energy is equal to the particle's energy. Applying this cutoff to Eq. (3.2) (and assuming $\omega_{max} >> \omega_c$), one finds an energy loss rate

$$\frac{dE}{d\ell} = \frac{Gm_o^4}{2v^2\hbar^2} \sim 10^{-16} \text{ eV - cm}^{-1} \quad \text{for protons .} \tag{3.4}$$

This energy loss rate is so small that, if there is a cutoff at ω_{max}, the effects of gravitational Cherenkov radiation are negligible even on galactic distance scales.

However, the existence of the cutoff is by no means certain. The uncertainty arises because it is not clear that Rosen's theory, even in its linearized version, can be quantized; the linearized field equations (2.10a) are not those of a canonical field theory. The difficulties that thereby arise are perhaps most apparent in an examination of plane gravitational waves in Rosen's theory:

(i) The Riemann tensor derived from an arbitrary plane wave has six independent polarizations — the most general polarization structure allowed in a metric theory. Even in the case $v_g = 1$, where the theory is Lorentz-invariant, these six polarizations form a nonunitary representation of the inhomogeneous Lorentz group; they cannot be associated with massless quanta of definite, Lorentz-invariant helicity (see [20] for a general discussion of these issues).

(ii) The time-averaged energy density in an arbitrary plane wave ($v_g \neq 1$), evaluated using (2.13), can be regarded as a quadratic form in the amplitudes of the ten independent potentials $\bar{h}_{\mu\nu}$. (None of these ten potentials can be removed from the energy density by a gauge transformation; see Section 2B.) When this quadratic form is diagonalized, one finds that four of the eigenvalues are negative. In other words, four of the ten degrees of freedom in the wave carry negative energy. The presence of negative-energy radiation has been noted previously in analyses of radiation emitted by binary systems in Rosen's theory [13]. In a theory with such negative-energy radiation, the stability of the vacuum is uncertain.

Any attempt to quantize Rosen's theory must confront these two problems. Even if they can be overcome, the presence of negative-energy radiation removes the raison d'etre for a cutoff at ω_{max}. The classical Cherenkov radiation (3.1) is made up of both positive- and negative-energy parts, the total energy emitted being a balance between the two. Quantum-mechanically, this Cherenkov emission might well be represented by multi-graviton processes in which both positive- and negative-energy gravitons are emitted. In such processes, conservation of energy imposes no restrictions on the frequency of the emitted gravitons.

Another potential quantum-mechanical cutoff is the Planck frequency $\omega_p \equiv (G\hbar)^{-1/2}$. If the Cherenkov spectrum (3.2) is cut off at ω_p, the energy loss rate becomes

$$\frac{dE}{d\ell} \simeq \frac{\gamma m_o}{2\gamma^3(\hbar/m_o)} \sim \frac{\gamma m_o}{\gamma^3(5\times 10^{-14}\,\text{cm})} \qquad \text{for protons .} \tag{3.5}$$

Just as for the cutoff at ω_{max}, it is not clear that this cutoff should be imposed. However, even if it is, the loss rate (3.5) is large enough that

the limits obtained in Section 4 are not affected.

The classical analysis of gravitational Cherenkov radiation hints at a serious problem in Rosen's theory. The divergence of the spectrum as $\omega \to \infty$ means that the energy emitted is infinite (and positive). This result strongly suggests that particles cannot exceed the speed of gravitational radiation. It is not clear that a quantum-mechanical treatment will eliminate the divergence, nor indeed that such a treatment can be given. Even as a purely classical analysis, the above calculation has serious difficulties: it is clearly inconsistent and, just as clearly, the linear approximation is not valid. However, there is little point in trying to patch up these difficulties. If particles cannot exceed the speed of gravitational radiation, a consistent calculation of gravitational Cherenkov radiation is not possible. More realistic and more relevant would be an examination of what happens as a particle is accelerated up to the speed of gravitational radiation.

Before turning to this problem, it is interesting to ask about the Cherenkov radiation emitted by photons and other zero rest-mass particles. The best that can be done using the above calculation is to model a free photon as the limit $v \to 1$, $\gamma \to \infty$, $\gamma m_o \to$ constant. Applying this limit to Eq. (3.2), one finds that free photons apparently do not produce any gravitational Cherenkov radiation.

B. Acceleration through the Gravitational "Light" Cone

Now consider a particle with rest mass m_o which has velocity $\underset{\sim}{v}(t)$ in LURF coordinates. The particle is being accelerated by interactions with other matter and nongravitational fields. The objective is to evaluate, in the linear approximation, the energy emitted in gravitational

radiation as v approaches v_g. In doing so, one must remember that the total stress-energy is conserved [Eq. (2.11)]. This means that one cannot, in general, neglect the radiation emitted by the matter and nongravitational fields as they "recoil" from the interaction. However, I shall argue that in the case of interest here, this "recoil" radiation can be neglected.

Imagine the following scenario for accelerating the particle -- a scenario similar to those often envisioned for accelerating cosmic rays [21]. The particle is accelerated by a series of "collisions" with local concentrations of stress-energy. These "blobs" of stress-energy have masses much larger than m_o, and their velocities -- both center-of-mass and internal -- relative to the LURF are small. In each collision, the momentum exchanged is small compared to the particle's momentum. The subsequent motion of the "blob" occurs on time scales much longer than the collision time; clearly, the radiation emitted by the "blob" does not diverge. Now consider the final stage of the acceleration process, when after many collisions the particle has attained a velocity so close to v_g that one more collision can push its velocity above v_g. From the point of view of the particular "blob" involved, this collision is no different from the preceding ones. However, the radiation produced by the particle in this collision is beamed in the direction of its velocity, and the radiation diverges in that direction as v approaches v_g. Therefore, in analyzing the final stage of the acceleration process, one can neglect the "recoil" motion and calculate the radiation emitted by considering only the particle's motion. The results obtained will be valid when v is very close to v_g.

The field equations (2.10b) for a single-particle source can be solved in the same way as in electromagnetism (see, e.g., [18], Sec. 14.1). The $\bar{h}_{\mu\nu}$ have the same form as the Liénard-Wiechert potentials. The energy

flux is evaluated using Eq. (2.16), and an integral over a sphere in the transition region gives the power radiated:

$$\frac{dE}{dt} = \frac{1}{3}\frac{Gm_o^2 v_g^3}{(1-\mu^2)^4}\left[\gamma^6(\underset{\sim}{v}\cdot\dot{\underset{\sim}{v}})^2(-11+26\mu^2-9\mu^4) + \gamma^4\dot{\underset{\sim}{v}}^2(1-\mu^2)(-11+12\mu^2)\right]$$

$$\longrightarrow Gm_o^2 v_g^3\left[2\gamma^6(\underset{\sim}{v}\cdot\dot{\underset{\sim}{v}})^2(1-\mu^2)^{-4} + \frac{1}{3}\gamma^4\dot{\underset{\sim}{v}}^2(1-\mu^2)^{-3}\right] \quad , \qquad (3.6)$$

where $\mu \equiv \gamma/\gamma_g$, and where the last expression contains the leading-order terms in the limit $v \to v_g$. As anticipated, the power radiated diverges. In a real situation, of course, the power radiated cannot diverge; instead, radiation reaction diverges and prevents the particle from exceeding the speed of gravitational radiation.

This calculation suffers from some of the same difficulties as the Cherenkov calculation. The particle radiates substantial amounts of energy only at very high frequencies where quantum corrections might well be important. For the reasons given earlier, the effect of these corrections is uncertain, and I shall ignore them. A perhaps more serious objection is that the linear approximation is not valid; however, it seems unlikely that the nonlinear terms in the field equations can eliminate the divergences that have cropped up in both the preceding problems.

Despite its uncertainties, the analysis of Rosen's theory in this section leads one to the following tentative conclusion: if $v_g < 1$, the speed of gravitational radiation is the ultimate speed for particles of nonzero rest mass -- a "speed limit" enforced by the emission of gravitational radiation. Hence, observations of relativistic particles can be used to place limits on the speed of gravitational radiation [Eq. (1.3a)] and on the cosmological boundary values [Eq. (1.3b)].

4. OBSERVATIONAL CONSTRAINTS

The highest-energy particles in the vicinity of the earth are ultra-high-energy cosmic rays, which have been detected at energies exceeding 10^{20} eV (see [22] for a review of the observations). At these very high energies, cosmic rays are not observed directly; rather, they are detected by the air shower they produce as they enter the atmosphere. The energy assigned to the primary particle in a given event is somewhat uncertain, since it is derived from a model for the shower. However, an energy of 3×10^{19} eV seems reasonably firm.

This energy estimate, even if correct, is not a measurement of velocity. One obtains a velocity by using the familiar relation $E = \gamma m_o$. However, one might expect this relation to fail in Rosen's theory, because a particle's gravitational binding energy might diverge as v approaches v_g. Indeed, an analysis using the linear approximation suggests that the energy of a particle, as measured by an observer at rest in the LURF, diverges logarithmically:

$$E = \gamma m_o + \gamma q \, \Omega_o \log\{2v_g[1 - (\gamma/\gamma_g)^2]^{-1/2}\} \quad , \tag{4.1}$$

where Ω_o is the gravitational binding energy when the particle is at rest in the LURF, and q is a dimensionless quantity which depends on the structure of the particle. This divergence is one more reason why particles cannot exceed the speed of gravitational radiation.

The logarithmic divergence (4.1) is slow enough that it does not interfere with interpretation of the cosmic-ray observations. If a particle's speed is so close to v_g that the binding-energy term in (4.1) dominates, then Eq. (3.6) predicts that the particle will radiate away almost all its

energy as gravitational radiation. It will not produce the observed shower of particles.

A more serious uncertainty results from the inability to identify the primary particle. The most likely candidates are protons or, perhaps, alpha particles; however, the possibility of heavier nuclei -- perhaps nuclei near iron -- has not been ruled out. For a proton at 3×10^{19} eV, the limit (1.3a) on the speed of gravitational radiation near the earth today is

$$1 - v_g \lesssim 5\times10^{-22} \quad . \tag{4.2a}$$

For an iron nucleus at the same energy, the limit is a bit weaker:

$$1 - v_g \lesssim 1\times10^{-18} \quad . \tag{4.2b}$$

Since v_g increases toward the galactic center, these limits also apply at any point closer to the galactic center than the earth.

Equations (4.2) actually hold not only at the earth but also in those regions traversed by the cosmic rays after their initial acceleration. Unfortunately, the point of origin of ultra-high-energy cosmic rays is uncertain. Their Larmor radii in the galactic magnetic field are much larger than the thickness of the galactic disk. This, together with the lack of anisotropy in the observed events [23], means that, if they are galactic in origin, they must come from a distance less than the thickness of the disk ($\sim$ 200 pc). It seems more likely that they are extragalactic, in which case Eqs. (4.2) probably apply out to a distance of at least 100 Mpc.

Earth-based observations of relativistic particles also provide an upper bound on the value of α_2 (v_{gc}) today [Eq. (1.3b)]. This limit is considerably less stringent than the limit on v_g because it is determined by the Newtonian potential at the earth, which is dominated by the galactic

potential U_{gal}. Any particle with $\gamma \gtrsim 10^3$ -- a medium-energy cosmic-ray proton or electron, a positron or electron produced in a high-energy collision at Fermi Lab or CERN or circulating in a storage ring at SLAC or DESY -- yields the same limit:

$$\alpha_2\Big|_{\text{today}} \lesssim 4U_{gal} \sim 3 \times 10^{-6} \quad . \tag{4.3}$$

Here I have used a galactic mass of $1.4 \times 10^{11} M_\odot$ at a distance of 10 kpc. For positive values of α_2, this limit (valid only in Rosen's theory) is almost three orders of magnitude better than the best previous limit, obtained by searching for anomalous earth tides [24].

There is a possibility that the Newtonian potential of the Virgo cluster at the earth is as large as the galactic potential. However, there is considerable uncertainty in estimating the mass of the Virgo cluster, and the two potentials are comparable only for the largest estimates. In any case, including the potential of the Virgo cluster is not likely to degrade the limit (4.3) by more than a factor of two.

Compact radio sources at substantial red shifts provide information about the speed of gravitational radiation in the past. They emit a power-law radio spectrum which is thought to be incoherent electron-synchrotron radiation; the spectrum has a low-frequency turnover attributed to synchrotron self-absorption. The Lorentz factor of the electrons can be estimated from the brightness temperature T_b at the turnover frequency: $\gamma \sim (kT_b/m_e)$, where m_e is the rest mass of an electron. Jones, O'Dell, and Stein [25] have developed a detailed model for compact, nonthermal sources, including the effects of synchrotron self-absorption and synchrotron self-Compton radiation. Burbidge, Jones, and O'Dell [26] have applied the model to

several compact sources, some of which have more than one component (see their Tables 1-3). For nine of the ten sources in their sample, they provide (for one or more of the components) a red shift, an angular diameter determined by VLBI, a size determined from the angular diameter by placing the source at its red-shift distance, and a Lorentz factor determined by the model. To estimate a Newtonian potential for each component, I have assumed a mass of $10^9 M_\odot$ — a mass larger than or of order those usually thought to be associated with active galactic nuclei; and I have assumed a constant (nonevolving) gravitational constant G. As an example, consider the source with the largest red shift in their sample — PKS 2134 + 00.4 at $z = 1.936$. The estimates for one of its two components are $\gamma \sim 590$ and $U \sim 1 \times 10^{-5}$, which implies $\alpha_2 < 4 \times 10^{-5}$ [Eq. (1.3b)]. Similar considerations for the other sources provide upper bounds on α_2 at a variety of red shifts; considering all these limits together, one can conclude that

$$\alpha_2 \lesssim 5 \times 10^{-4} \qquad \text{for} \qquad 0 \lesssim z \lesssim 2 \quad . \tag{4.4}$$

No other observation provides information about the value of α_2 (v_{gc}) in the past.

There are considerable uncertainties in estimating the Newtonian potentials which go into the limit (4.4). The masses and radii of the sources are uncertain; in addition, the gravitational "constant" does evolve in Rosen's theory, so that its value in the past depends on the cosmological model. Because of these uncertainties, the limit (4.4) has been chosen conservatively; with the above assumptions, all but one of the six sources at $z > 0.1$ provide a limit at least an order of magnitude stronger than (4.4).

5. CONCLUSION

Rosen [27] has recently modified his "bimetric" theory. In the modified version, the "background" metric $\eta_{\mu\nu}$ is no longer required to be flat;

instead, it is required to be a space of constant curvature. Cosmological models are affected by this modification, but local gravitation physics is not, except insofar as it is influenced by cosmological boundary values. The analysis in Sections 2 and 3 remains the same, and the limits obtained in Section 4 apply to the new version of the theory.

The analysis in this paper has been restricted to Rosen's theory, but the results obtained are likely to have far wider applicability. There are numerous metric theories of gravity which predict different speeds for gravitational radiation and light. Typically in such theories, the difference in speed is produced just as in Rosen's theory: light propagates along "light" cones of the physical metric, while gravitational radiation propagates along "light" cones of a flat, "background" metric. In all such theories, one expects the speed of gravitational radiation to have a form similar to that in Rosen's theory: $v_g = v_{gc}(1 + 2\xi U)$, where v_{gc} is determined by cosmological boundary values and ξ is a constant of order unity. The important question is whether emission of gravitational radiation restricts particles to speeds less than v_g. Although detailed calculations are necessary in each theory, one can give a general argument, based on the analysis in Rosen's theory, for the existence of the "gravitational speed limit."

Whenever a particle exceeds the speed of propagation of a "radiation" field to which it is coupled, one expects a shock wave to form. One can think of numerous examples, such as the shock wave produced by supersonic motion in an acoustic medium and electromagnetic Cherenkov radiation. In these familiar examples, the radiation does not diverge because the shock front is not absolutely sharp; it is spread out over some length d characteristic of the medium through which the radiation is propagating. This

"blurring" of the shock front cuts off the radiation at frequencies $\gtrsim v_{wave}/d$. In the gravitational case, the "medium" is spacetime itself, or more accurately, the "background" structure on spacetime which determines the speed of gravitational radiation. The gravitational "medium" has no small-scale structure to blur the shock front. Thus, there is no high-frequency cutoff (unless quantum mechanics introduces one), and the radiation does diverge.

This argument makes it seem quite likely that any theory with a variable speed of gravitational radiation must confront the limits obtained in Section 4. If so, Eqs. (4.3) and (4.4) can be used to constrain the cosmological boundary values in any such theory. [In general, the α_2 of these limits is not a PPN parameter; it is simply a parameter related to v_{gc} by Eq. (1.2a).] In addition, Eqs. (4.2) provide a general, theory-independent lower bound on the speed of gravitational radiation near the earth.

ACKNOWLEDGMENTS

I thank Kip S. Thorne and Mark Zimmermann for frank and productive discussions. I also acknowledge the support of a Feynman Fellowship at Caltech during part of the time this research was being carried out.

FOOTNOTES

[1]Throughout I use the summation convention, Greek indices running from 0 to 3 and Latin indices from 1 to 3. The signatures of the metrics are +2. A semicolon (;) denotes a covariant derivative with respect to $g_{\mu\nu}$, a vertical bar (|) a covariant derivative with respect to $\eta_{\mu\nu}$, and a comma an ordinary partial derivative. Units are chosen so that the speed of light c = 1.

REFERENCES

1. N. ROSEN, J. Gen. Rel. and Grav. 4 (1973), 435; Ann. Phys. (N.Y.) 84 (1974), 455.
2. C. M. WILL, The Theoretical Tools of Experimental Gravitation, in "Experimental Gravitation: Proceedings of Course 56 of the International School of Physics 'Enrico Fermi'" (B. Bertotti, Ed.), p. 1, Academic Press, New York, 1974.
3. J. ROSEN and N. ROSEN, Astrophys. J. 202 (1975), 782; 212 (1977), 605; I. GOLDMAN and N. ROSEN, Astrophys. J. 225 (1978), 708.
4. D. BABALA, J. Phys. A 8 (1975), 1409; I. GOLDMAN and N. ROSEN, J. Gen. Rel. and Grav. 7 (1976), 895; Astrophys. J. 212 (1977), 602.
5. M. ISRAELIT, J. Gen. Rel. and Grav. 7 (1976), 623; 7 (1976), 857.
6. I. GOLDMAN, J. Gen. Rel. and Grav. 9 (1978), 575.
7. I. GOLDMAN, J. Gen. Rel. and Grav. 7 (1976), 681; I. GOLDMAN and N. ROSEN, J. Gen. Rel. and Grav. 8 (1977), 617; D. FALIK and R. OPHER, Astron. and Astrophys. 71 (1979), 332; J. Gen. Rel. and Grav. 10 (1979), 227.
8. C. M. WILL, The Confrontation between Gravitation Theory and Experiment, in "Gravitational Theories Since Einstein" (S. W. Hawking and W. Israel, Eds.), Cambridge University Press, Cambridge, 1979.
9. D. L. LEE, C. M. CAVES, W.-T. NI, and C. M. WILL, Astrophys. J. 206 (1976), 555.
10. C. W. MISNER, K. S. THORNE, and J. A. WHEELER, "Gravitation," Freeman, San Francisco, 1973.
11. K. S. THORNE, How to Test Gravitation Theories by Means of Gravitational-Wave Experiments, in "Colloques Internationaux C.N.R.S. No. 220 — Ondes et Radiations Gravitationelles," p. 213, Institut Henri Poincare, Paris, 1974.

12. R. A. HULSE and J. H. TAYLOR, Astrophys. J. (Letters) 195 (1975), L51.

13. C. M. WILL and D. M. EARDLEY, Astrophys. J. (Letters) 212 (1977), L91; C. M. WILL, Astrophys. J. 214 (1977), 826.

14. J. H. TAYLOR, L. A. FOWLER, and P. M. McCULLOCH, Nature 277 (1979), 437.

15. F. K. MANASSE and C. W. MISNER, J. Math. Phys. 4 (1963), 735; W.-T. NI and M. ZIMMERMANN, Phys. Rev. D 17 (1978), 1473.

16. P. A. CHERENKOV, Dokl. Akad. Nauk. SSSR 2 (1934), 451.

17. P. C. AICHELBURG, G. ECKER, and R. U. SEXL, Nuevo Cimento 2B (1971), 63.

18. J. D. JACKSON, "Classical Electrodynamics," 1st ed., Wiley, New York, 1962.

19. I. FRANK and I. TAMM, Dokl. Akad. Nauk. SSSR 14 (1937), 109.

20. D. M. EARDLEY, D. L. LEE, A. P. LIGHTMAN, R. V. WAGONER, and C. M. WILL, Phys. Rev. Letters 30 (1973), 884; D. M. EARDLEY, D. L. LEE, and A. P. LIGHTMAN, Phys. Rev. D 8 (1973), 3308.

21. E. FERMI, Phys. Rev. 75 (1949), 1169.

22. A. A. WATSON, Proc. 14th Int. Cosmic Ray Conf. 11 (1975), 4019.

23. A. M. HILLAS, Phil. Trans. R. Soc. London A 277 (1974), 413.

24. K. NORDTVEDT, JR., and C. M. WILL, Astrophys. J. 177 (1972), 775. R. J. WARBURTON and J. M. GOODKIND, Astrophys. J. 208 (1976), 881.

25. T. W. JONES, S. L. O'DELL, and W. A. STEIN, Astrophys. J. 188 (1974), 353.

26. G. R. BURBIDGE, T. W. JONES, and S. L. O'DELL, Astrophys. J. 193 (1974), 43.

27. N. ROSEN, J. Gen. Rel. and Grav. 9 (1978), 339.

FIGURE CAPTION

Figure 1. A "snapshot", taken at time t, of the Cherenkov cone produced by a particle moving with uniform velocity $v = 2v_g$ along the z-axis. The particle is at the apex of the cone. The angle θ_C between the normal to the cone and the z-axis is given by $\cos \theta_C = (v_g/v)$. The shaded region is the pulse of Cherenkov radiation produced by a particle which radiates from $t = 0$ to $t = T$.

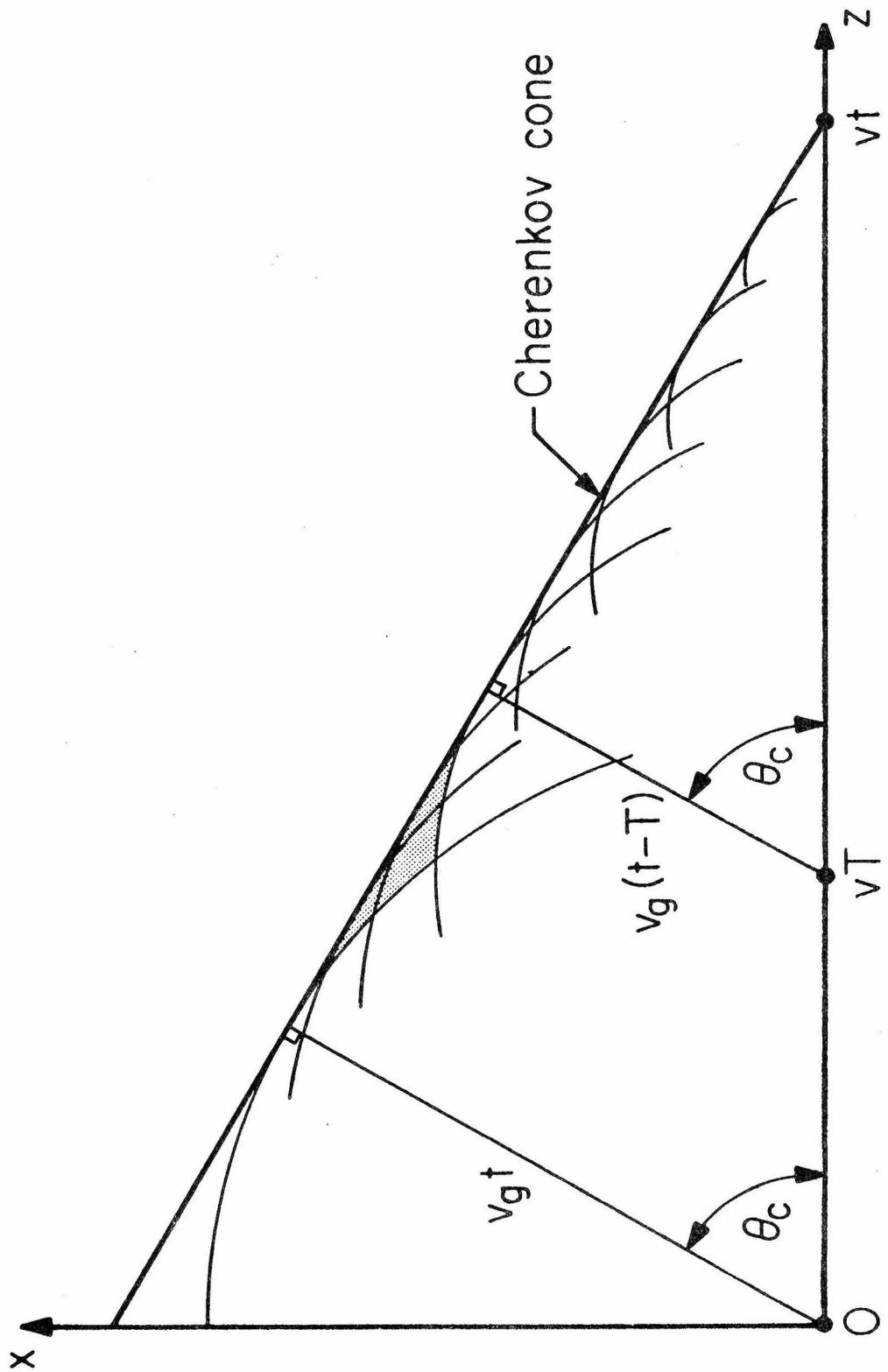

Fig. 1